Topical meeting on Condensed-matter Chemistry on Actinides

The Kumatori meeting 2021

CCA, KURNS, Kyoto University

Mar. 31, 2021

The originating Section of this publication in the KURNS, Kyoto University was: The CCA lab. (The laboratory in the field of Condensed-matter Chemistry on Actinides) 2, Asashiro-Nishi, Kumatori-cho, Sennan-gun, Osaka 590-0494 JAPAN

Topical meeting on Condensed-matter Chemistry

on Actinides

The Kumatori meeting 2021

Institute for Integrated Radiation and Nuclear Science (KURNS),

Kyoto University

Published by CCA, KURNS, Kyoto Univ. in Japan

Mar. 31, 2021

Preface

This workshop was co-organized by Prof. Yamagami (Kyoto Sangyo Univ.), who is a theoretical researcher of condensed matter physics of actinides, to provide a basis for current and future research activities in a wide range of fields. The actinide science stems from basic research on condensed matter physics and chemistry, to research on nuclear fuel cycle and radioactive waste as its application, and recently to basic research on 1F debris and nuclear medicine.

This year, many international conferences have been postponed, and domestic conferences have been also postponed or held online because of the worldwide spread of the COVID-19 virus. On the other hand, by focusing on the advantages of online conferences, we have felt that we could make a conference even much better for young researchers and busy domestic researchers to have encouraging discussions with other professionals, and for all of us to have great discussions with prominent foreign researchers. Online meeting technology is particularly suitable for promoting flat scientific discussions. Since we have held many extended seminars within our laboratory and strongly feel the advantages of this technology, we discussed with some of researchers in this community about holding an online conference this time. Fortunately, we received positive feedback from everyone and were able to hold this conference.

Our institute (KURNS, Kyoto University) has decided to shut down the KUR reactor in 2026. Based on discussions in Japan, a new research reactor will be built at Fukui, and the institute will participate in its construction and operation of cooperative researches among universities. On the other hand, the future of the Kumatori site, where the institute is currently located, is currently being discussed. Among the discussions, the core of the Kumatori site has gradually been recognized as the hot laboratory, which is expected to play an important role in basic research on actinides, radioactive wastes, and cancer treatments as nuclear research in a broad sense.

This report is published to preserve the discussions of “the Kumatori 2021” conference

held on Feb. 10, 2021. As a background of this conference, we had preceding 13 domestic conferences and we have published the meeting reports for all of them. This time is the third conference since T. Yamamura has moved to Kyoto Univ. from Tohoku Univ. Since last year, based on the suggestion from Prof. H. Yamagami, we have registered the report in the Kyoto University Academic Repository KURENAI to make it available to a wider audience and to preserve it permanently. We hope that the publication of this book in the repository will attract more people, especially young people, to the field of condensed matter chemistry of actinides and its applications.

March, 2021

Tomoo Yamamura

Professor, KURNS, Kyoto Univ.

Preface to the First Publication of the Report of the Topical Meeting on "Topical meeting on Condensed-matter Chemistry on Actinides"

This workshop was organized by Prof. Tomoo Yamamura and many others at the Institute for Integrated Radiation and Nuclear Science, Kyoto University, and was held on February 7, 2020 (Friday). This booklet is a report of the meeting, and is the first publication. Although the new coronavirus infection spread worldwide in the following month, it was fortunate that 42 researchers from a wide range of fields in basic research of actinide science, both domestic and overseas, participated in the meeting and that the meeting was successfully held.

I would like to express my thoughts on the purpose of establishing this workshop. The main focus of this group is "basic research and its application in actinide science" in a broad perspective, and we will deal with a wide range of research topics with an interest in experiment and theory, basics and applications. It is also a research group where researchers from various research fields such as physics, chemistry, biology, engineering, and medicine come together. The main participants are joint users of the Institute for Integrated Radiation and Nuclear Science, but many other researchers are also attracted by the activities of the group.

I hope that this workshop will provide an opportunity to learn about the latest research results from different fields, to understand each field with new eyes, and to get feedback for our own research. Furthermore, it would be great if we could create new research themes and collaborations that are cross-cutting and complementary among the fields. In order to achieve this, it is necessary for the meeting to be a place for open academic exchange and discussion, and I hope that you will continue to actively participate. In addition, due to the unique nature of the field of actinide science, there is an urgent need to pass on sustainable technologies and skills and to develop young human resources, and we welcome student-level participation in this workshop.

We look forward to your continued cooperation in making this a successful and open forum for active discussion.

March 23, 2020

Hiroshi Yamagami,

Kyoto Sangyo University

Contents

Chapter 1 Program

（Listed on the next page）

Topical meeting on Condensed-matter Chemistry on Actinides : The Kumatori meeting 2021

Oral Session, Feb. 10th, 2021@Zoom

Chair	JST	Presenter	Title
A. Sunaga	10:00	T. Yamamura (KURNS, Kyoto Univ.)	Opening Remarks
	10:05	H. Yamagami (Kyoto Sangyo Univ.)	Objectives of this meeting
S. Kambe	10:15	Y. Haga (ASRC, JAEA)	Uranium-based intermetallics with layered structure: characterization and magnetism
	10:35	K. Ishida (Dept. Phys., Kyoto Univ.)	Superconducting Spin Susceptibility of UTe_2
	10:55	T. Yaita (SPring-8, JAEA)	Recent activities of Actinide Chemistries in the Materials Sciences Rsearch Center of JAEA
	11:15	(Intermission)	
Y. Haga	11:25	N. Ishikawa (Dept. Chem., Osaka Univ.)	Observation of interaction between 5f electronic system and photo-excited cyclic π system
	11:45	T. Suzuki (Nagaoka Univ. Tech.)	Fundamental Study for Precise Analysis of Actinides in Hardly Soluble Substances Containing Uranium Oxides
	12:05	K. Washiyama (Fukushima Medical University)	Current status and prospects of domestic supply of alpha-emitting radionuclides
C. Tabata		Group photo (Capturing on Zoom)	
	12:25	(Lunch)	
M. Hino	13:00	Y. Kawabata (KURNS, Kyoto Univ.)	Current status and future plans of our institute
	13:15	T. Yamamura (KURNS, Kyoto Univ.)	Actinide researches using KUR hot-lab
T. Yamamura	13:30	M. Suzuki (KURNS, Kyoto Univ.)	The Future of Cyclotron-Based BNCR Research
	13:50	Break Session 1	
K. Shirasaki	14:50	T. Kitazawa (Dept. Chem., Toho Univ.)	Synthesis and Crystal Structures of Three New Complexes Constructed with Uranyl(VI)-acetylacetonate and Uranyl(VI)-nitrate
	15:10	T. Yoshimura (IRS, Osaka Univ.)	Preparation of guidelines for evaluation to ensure safety in the use of short-lived unsealed radioisotopes
	15:30	(Intermission)	
K. Ishida	15:40	H. Amitsuka (Hokkaido Univ.)	Odd Parity Multipole Ordering in Uranium Compounds
	16:00	T. Yanagisawa (Hokkaido Univ.)	Electric Quadrupolar Contributions in the Magnetic Phases of UNi_4B
	16:20	Break Session 2	
H. Tanaka	17:20	M. Manjum (Dept. Appl. Chem., Keio Univ.)	Electrochemical Formation of Samarium and Samarium-Cobalt Nanoparticles in a Pyrrolidinium-based Ionic Liquid
	17:40	T. Nomoto (Tokyo Inst. Tech.)	Drug delivery using functional polymer-conjugates
	18:00	(Intermission)	
H. Amitsuka	18:10	A. P. Goncalves (Universidade Lisboa, Portugal)	On the U-Fe-Ge system and its compounds
M. Abe	18:40	A. S. P. Gomes (Universite de Lille, France)	Electronic structure of actinide systems from relativistic correlated and quantum embedding approaches
Y. Haga	19:10	R. Caciuffo (EU JRC, Karlsruhe, Germany)	Radioisotopes for medical applications
A. Sunaga	19:40	S. Kambe (ASRC, JAEA)	Concluding Remarks 1
	19:50	H. Yamagami (Kyoto Sangyo Univ.)	Concluding Remarks 2
C. Tabata		Group photo (Capturing on Zoom)	

Topical meeting on Condensed-matter Chemistry on Actinides : The Kumatori meeting 2021

Break Sessions, Feb. 10th, 2021@Zoom

Break Session 1 (13:50 - 14:50)				13:50 - 14:20	14:20 - 14:50
Room	Presenter	Afilation	Title	Chair 1	Chair 2
1	H. Shishido	Tohoku Univ.	Proposals for the advanced nuclear fuel cycle by introducing a fusion reactor	M. Hino	T. Suzuki
2	M. Nakase	Tokyo Inst. Tech.	Development and characterization of phthalocyanine-derivatized ligands for recognition and complexation of light Actinide elements	K. Nagata	A. Kawaguchi
3	H. Nakai	Kindai Univ.	Development of ligands for new actinide complexes	T. Yamamura	T. Yaita
4	C. Tabata	Kyoto Univ.	Crystal structure and magnetic property of uranium phthalocyanine complexes	N. Ishikawa	Y. Haga
5	Y. Kasamatsu	Osaka Univ.	Co-precipitation experiment of group 2 elements with barium hydrosulfate toward chemical study of No	T. Kitazawa	A. Sunaga
6	K. Shirasaki	Tohoku Univ.	Extraction of strontium from aqueous solutions into HFC using dicyclohexano-18-crown-6 and perfluorinated polyethylene glycol derivative	M. Nogami	T. Kobayashi
7	Y. Sekiguchi	CRIEPI	Thermodynamic estimation of vaporization of CsI dissolved in LiF-NaF-KF molten salt	Y. Katayama	M. Yokota
8	F. Kon	Hokkaido Univ.	Observation of Antiferromagnetic Order in the Heavy-Fermion Compound UIr_2Ge_2 – Resonant X-ray Scattering	K. Ishida	T. Oda
9	A. Sato	Tokyo Met. Univ.	Theoretical study on isotope fractionation in uraninite	H. Yamagami	A. Toyoshima
10	Y. Kitawaki	Kyoto Sangyo Univ.	Orbital magnetization in many-electron systems described by spin-orbital-polarized coupled Dirac equation	M. Abe	T. Yanagisawa
Break Session 2 (16:20 - 17:20)				16:20 - 16:50	16:50 - 17:20
Room	Presenter	Afilation	Title	Chair 1	Chair 2
1	T. Fukuda	JAEA	Present status of the study on energy conversion using actinides in radioactive wastes	T. Yoshimura	K. Kakinoki
2	T. Oda	Kyoto Univ.	Slow dynamics study by neutron resonance spin echo spectrometer	H. Amitsuka	H. Shishido
3	A. Sunaga	Kyoto Univ.	Theoretical study of the linearity of uranyl molecule based on relativistic correlation method	H. Yamagami	S. Kambe
4	M. Nogami	Kindai Univ.	Change in precipitation ability of treated cyclic urea compounds for selective precipitation of U(VI) species	H. Nakai	K. Maeda
5	Y. Homma	Tohoku Univ.	Mössbaure spectroscopy of the Eu-based skyrmion compounds EuPtSi and $EuAl_4$	H. Takeuchi	T. Kitazawa
6	K. Nagata	Osaka Univ.	Synthesis of Actinium Complex with a Macrocycle Having Pyridine Phosphonate Pendant Arms	M. Abe	M. Suzuki
7	T. Yamane	Nagaoka Univ. Tech.	Electrochemical method of minor actinide recovery from nitric acid solution using Ga liquid electrode and ionic liquid	T. Shimada	Y. Katayama
8	M. Yokota	Kindai Univ.	Adsorptivity of monoamide polymer adsorbent impregnated with PPTPT to metal ions in neutral aqueous solutions for recovery of uranium in seawater	K. Shirasaki	M. Iizuka
9	K. Mori	Kyoto Univ.	Introduction of Versatile Compact Neutron Diffractometer (VCND) at B-3 Beam Port of KUR	Y. Haga	F. Kon
10	T. Kobayashi	SPring-8, JAEA	XAFS study on the the aged deterioration of a simulated fuel debris	T. Tadokoro	C. Tabata

Chapter 2 Opening Remarks

The meeting is linked to our Projective Research at KURNS, named as “Condensed-matter Chemistry on Actinides and its applications”. Our objectives are characteristic chemical and electronic properties of Actinides due to the intermediate shielding of the 5f orbitals. Importance of this fields lies in the coexistence of superconductivity and ferromagnetism, alpha-emitter nuclear medicine, and managements of radioactive wastes from nuclear power plants. However, it is not easy for usual universities to have sufficient experimental research environments due to many regulations for nuclear fuel materials and radioisotope materials.

This project can be defined in terms of the multidisciplinary methods, the substances investigated, and the platform-like research sites. The researchers in chemistry, condensed matter physics, and nuclear medicine join this project, who are interested in the properties of actinides as the 5f-intratransition elements. Also, they include excellent researchers both of experiments and theoretical calculations to start corroborative works. Substances investigated are the actinide mixed oxides, actinide complexes, and uranium intermetallic compounds.

At the present, eco system of actinides research includes following three institutes: Tohoku Univ. IMR Hot Laboratories (Sendai, Oarai), JAEA (Tokai, SPring-8), and KEK-PF. A g-scale research experiment can be provided in collaboration with these institutes. By using starting materials provided by IMR and JAEA, users can complete preparations and basic measurements based on the platform-like equipment systems which our community had built during past 20 years. After the basic measurements, the users can send other facilities for specialized experiments, such as synchrotron radiation experiment.

This year, we have invited three prominent researchers from abroad. First is Prof. Roberto G. Caciuffo (EU-JRC Karlsruhe), who in fact, has planned to have a talk at our last meeting (2020/2/7), but it was postponed due to the corona-virus matter. The second is Dr. Antonio Goncalves (Universidade Lisboa), who had been a visiting researcher of KURNS in 2019. The third is Dr. A. S. P. Gomes (Universite de Lille).

This is the first online meeting on Zoom. However, we have a large audience, i.e. 60 attendees, 39 speakers including 3 foreign speakers. We have planned a special session: "(Coffee) Break Sessions", where two chairs are assigned as audiences who help cultivate fruitful scientific discussions. Please have a coffee and enjoy discussions!

KYOTO UNIVERSITY

KURNS

Topical meeting on Condensed-matter Chemistry on Actinides
(The Kumatori meeting 2021)

Opening remark

Tomoo Yamamura, KURNS, Kyoto Univ.
10:00-10:05, Feb. 10, 2021

The meeting is linked to:
Our **Projective Research** at KURNS
Condensed-matter Chemistry on Actinides and its applications:

- Objectives:
  - Characteristic chemical and electronic properties of Actinides:
    - due to the intermediate shielding of the 5f orbitals
  - Importance of this fields lies in:
    - **the coexistence of superconductivity and ferromagnetism**
    - **alpha-emitter nuclear medicine**
    - **managements of radioactive wastes** from nuclear power plants.
  - Difficulty of research environments in universities due to regulations.

Objectives (continued)

- Methods:
  - **in** chemistry, condensed matter physics, and nuclear medicine who are interested in these properties of actinides
  - **Collaborations of experiments and theoretical calculations**
  - **Substances**: actinide mixed oxides, actinide complexes, and uranium intermetallic compounds.
- Research environment for g-scale research in collaboration with:
  - Universities
  - IMR Hot Laboratories (Sendai, Oarai)
  - JAEA Tokai
  - SPring-8 Beamline BL22XU of JAEA
  - KEK PF

Eco system of Actinides research

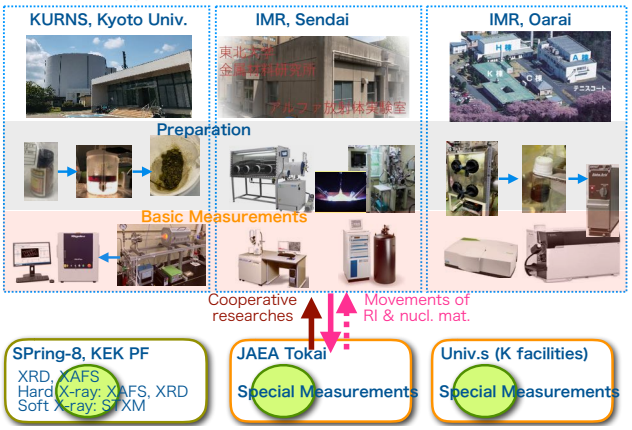

Our Projective Research: Members

Representative	Afilation
Y. Haga	ASR, JAEA
H. Amitsuka	Hokkaido Univ.
T. Suzuki	Nagaoka Univ. Tech.
K. Shirasaki	IMR, Tohoku Univ.
M. Nogami	Kindai Univ.
M. Abe	Tokyo Met. Univ.
H. Shishido	Tohoku Univ.
M. Nakase	Tokyo Inst. Tech.
T. Yamamura	KURNS
H. Nakai	Kindai Univ.
T. Kobayashi	SPring-8, JAEA

Copyright protected content

Our meeting background:
Proceeding 13 domestic and 1 international mtgs

Fiscal Year	Classification	Conference Name
2008	IMR, Oarai meeting (Tohoku Univ.)	Actinide element lab. user's meeting
2009		Oarai user's meeting (Actinides)
2008	IMR LARE meeting (Tohoku Univ., Sendai)	Sci. Res. Grants Fundamental Research(S) meeting
2009		Sci. Res. Grants Fundamental Research(S) meeting (No.2)
2010		Oarai user's meeting including LARE
2011		Collaboration of LARE user's mtg with Sci. Res. Grants Fundamental Research(S) mtg.
2013		Collaboration of LARE user's mtg with Sci. Res. Grants Fundamental Research(S) mtg.
2014		Collaboration of LARE user's mtg with Sci. Res. Grants Fundamental Research(S) mtg.
2015		7th LARE user's meeting
2016		8th LARE user's meeting
2017		Collaboration of Workshop "Science and Technology of Actinide Elements" IMR, Tohoku Univ. with 9th LARE user's mtg.
2017	International Conf.	Actinides-2017 (Sendai)
2018	Kumatori mtg.	Topical meeting on Condensed-matter Chemistry on Actinides
2019	Official mtg.	
2020	Kumatori mtg.	

* mtg in FY 2012 was not planned because of the damages due to the Tohoku earthquake (March 11, 2011)

Invitation of prominent researchers from abroad:

- As an alternative to the visit that was cancelled due to coronavirus
  - The remote meeting has enabled us to hold this international meeting.
- **Prof. Roberto G. Caciuffo** (EU-JRC Karlsruhe)
  - Planned to have a talk at our last meeting (2020/2/7)
  - T.Y. had a plan to visit him during this fiscal year.
- **Prof. Antonio Goncalves** (Universidade Lisboa)
  - Prof. C. Tabata had a plan to visit him during this fiscal year.
- **Prof. A. S. P. Gomes** (Universite de Lille)

Welcome to the meeting

- **The first remote meeting** on Zoom to prevent the spread of coronavirus.
- 60 attendees, 39 speakers including 3 foreign speakers
- "(Coffee) **Break Sessions**" are planned:
  - To cultivate the fruitful sciences in this field
  - **Two chairs as assigned audiences.** The repeated talk but no more than twice.
  - Please have a coffee and enjoy discussions!

Chapter 3 Presentation Materials

With the permission of the speakers, the materials of their presentations are included here.

3.1 H. Yamagami（Kyoto Sangyo Univ.）

Objectives of this meeting

10 February, 2021 ZOOM meeting

Topical meeting of
Condensed-matter Chemistry on Actinides
The Kumatri Meeting 2021

- Department pf Physics, Faculty of Science, Kyoto-Sangyo University, JAPAN
- Electronic-Structure Research Group, JAEA, Harima, JAPAN

Hiroshi Yamagami

First Meeting: 2020年2月7日　京大複合研　事務棟大会議室　9:35-9:50

「アクチノイドの物性化学とその応用」の開催趣旨

- 京都産業大学　理学部　物理科学科
- 日本原子力研究開発機構　電子構造物性研究グループ　グループリーダ

山上　浩志

参加者皆様へのお詫び：

本研究会の外部委員で、専門研究会の趣旨説明をするべきところ、本務大学の「入学センター長」を補職として兼務している関係で、大学入試期間中で本日の研究会には出席できなくなってしまいました。
大変申し訳ありません。新型肺炎ウィールスが流行していますので、予防と体調管理にはご注意いただき、オープンで活発な議論をよろしくお願いします。

Objectives of this meeting：

2019　A selection for public offering of the meeting in Institute for Integrated Radiation and Nuclear Science, Kyoto University　(複合原子力科学研究所)

Host：T. Yamamura and outside：H. Yamagami

Objective：This meeting will hold as a part of shared use in the Institute, and the meeting theme is about a research in this Institute and a nuclear reactor.

「professional research meeting」= A general meeting independent of the theme including a meeting for discussing on a research subject to a project.

Sugestion: (1) As a research theme, a basic science of condensed-matter chemistry on Actinides, as a wide meaning
(2) Experimental and theoretical research, basic and application-oriented research
(3) cosse-sectional and complemental research between some different fields of science, physics, chemistry, biology, engineering, medical science and so on.
(4) Scheme and framework toward human resource development and devolution for engineering skill
(5) Open meeting through a scholarly exchange and an academic discussion

---

Meeting Schedule

Chair	JST	Presenter	Title
A. Sasaga	10:00	T. Yamamura (KURNS, Kyoto Univ.)	Opening Remarks
	10:05	H. Yamagami (Kyoto Sangyo Univ.)	Objectives of this meeting
S. Kambe	10:15	Y. Haga (ASRC, JAEA)	Uranium-based intermetallics with layered structure: characteristics and magnetism
	10:55	K. Ishida (Dept. Phys., Kyoto Univ.)	Superconducting Spin Susceptibility of UTe_2
	10:55	T. Yaita (SPring-8, JAEA)	Recent activities of Actinide Chemistry in the Materials Science Research Center of JAEA
	11:15	(Intermission)	
Y. Haga	11:25	N. Ishikawa (Dept. Chem., Osaka Univ.)	Observation of interaction between 5f electronic system and photo-excited cyclic π system
	11:45	T. Suzuki (Nagaoka Univ. Tech.)	Fundamental Study for Precise Analysis of Actinides in Hardly Soluble Substances Containing Uranium Oxides
	12:05	K. Washiyama (Fukushima Medical University)	Current status and prospects of domestic supply of alpha-emitting radionuclides
C. Ishida		Group photo (Capturing on Zoom)	
	12:25	(Lunch)	
M. Hino	13:00	Y. Kawchura (KURNS, Kyoto Univ.)	Current status and future plans of our institute
	13:15	T. Yamamura (KURNS, Kyoto Univ.)	Actinide researches using KUR hot lab
T. Yamamura	13:30	M. Suzuki (KURNS, Kyoto Univ.)	The Future of Cyclotron-Based BNCR Research
	13:50	(Break Session 1)	
K. Shimazu	14:50	T. Kimuro (Dept. Chem., Tokyo Univ.)	Synthesis and Crystal Structures of Three New Complexes Constructed with Uranyl(VI) carbylcarbonate and Uranyl(VI) nitrate
	15:10	Y. Yoshimura (IRS, Osaka Univ.)	Preparation of pozzolans for evaluation to ensure safety in the use of short-lived unsealed radioisotopes
	15:30	(Intermission)	
K. Ishida	15:40	H. Amitsuka (Hokkaido Univ.)	Odd Parity Multipole Ordering in Uranium Compounds
	16:00	T. Yanagisawa (Hokkaido Univ.)	Electric Quadrupolar Contributions in the Magnetic Phases of UO_2,R
	16:20	(Break Session 2)	
H. Tanaka	17:20	M. Manjiro (Dept. Appl. Chem., Keio Univ.)	Electrochemical Formation of Samarium and Samarium-Cobalt Nanoparticles in a Pyrrolidinium-based Ionic Liquid
	17:40	T. Nomoto (Tokyo Inst. Tech.)	Drug delivery using functional polymer-conjugate
	18:00	(Intermission)	
H. Amitsuka	18:10	A. P. Gonçalves (Universidade Lisboa, Portugal)	On the U-Fe-Ge system and its compounds
M. Abe	18:30	A. S. P. Gomes (Université de Lille, France)	Electronic structure of actinide systems from relativistic correlated and quantum embedding approaches
Y. Haga	19:10	R. Castillo (FEI JRC, Karlsruhe, Germany)	Radioisotopes for medical applications
A. Sasaga	19:40	S. Kambe (ASRC, JAEA)	Concluding Remarks 1
	19:50	H. Yamagami (Kyoto Sangyo Univ.)	Concluding Remarks 2
C. Ishida		Group photo (Capturing on Zoom)	

Finally

Thank you for your attention!
And enjoy the Kumatri meeting!

3.2 Y. Haga（ASRC, JAEA）

Uranium-based inter metallics with layered structure: characterization and magnetism

Uranium-based inter metallics with layered structure: characterization and magnetism

Yoshinori Haga
Advanced Science Research Center, Japan Atomic Energy Agency

Introduction

Actinide intermetallic compounds

5f electrons characterize physical properties
Located in the boundary between localized/itinerant
Sensitivity to external condition (pressure, magnetic field, chemical environment)

Example of actinides intermetallic compounds consisting of several building blocks — arrangements controlled artificially

Designing a material with desired functions ?

Uranium "2-6-15" known as $Sr_{0.6}Fe_2Si_{4.9}$-type

- 2-6-15: hexagonal. common for actinide and lanthanide compounds

	Fe	Ni	Pd	Pt
Al	1-2-10	3-5-19	2-6-15	2-6-15
Ga	1-1-5	1-1-5	1-1-5	2-6-15
Si	2-6-15			

Compounds found in An-(Ni,Pd,Pt)-X system (X-rich region)

- UPd_2Al_3, UNi_2Al_3 heavy fermion antiferromagnetic superconductor
- Binary : UAl_2, UPd_3, UPt_3, etc.
- AFM 115 compounds: $UTGa_5$
- Heavy Fermion SC **$NpPd_5Al_2$** and *An/Ln* analogues

$Sr_{0.6}Fe_2Si_{4.9}$-type crystal structure

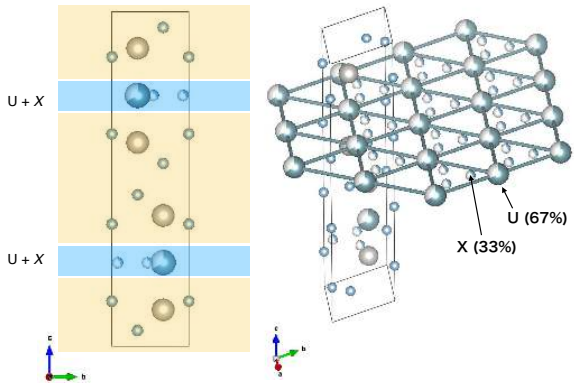

Atomic arrangement in the basal plane

U-X "mono layer" is stacked on the T-X buffer layer
Looks nice !

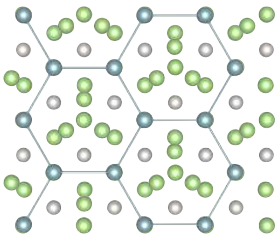

However, the next U-X layer (8 Å apart) has (±1/3, ±2/3, 0) displacement.
Therefore, the "actual" local symmetry is orthorhombic or lower.

Structure model

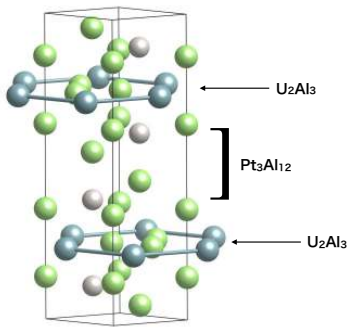

Experimental signature of ordered structure

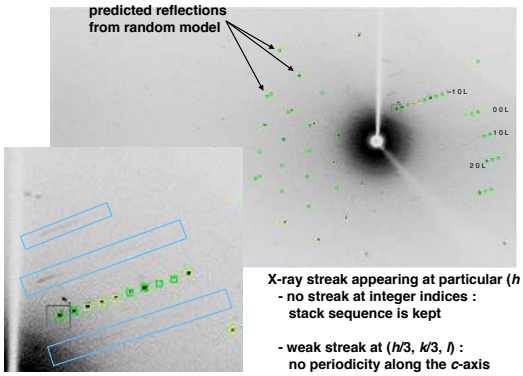

X-ray streak appearing at particular (*h k l*)
- **no streak at integer indices : stack sequence is kept**
- **weak streak at (*h*/3, *k*/3, *l*) : no periodicity along the *c*-axis**

$U_2Pt_6Ga_{15}$

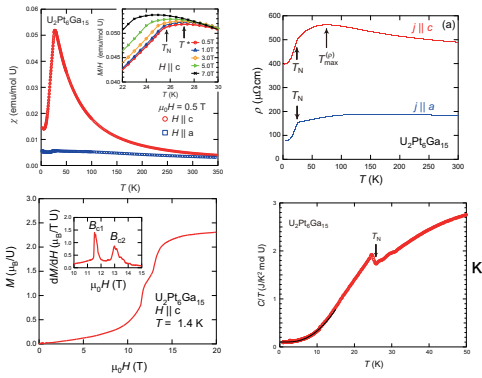

$U_2Pt_6Ga_{15}$

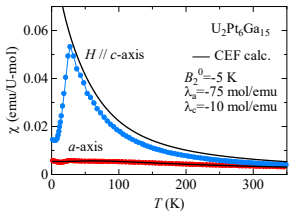

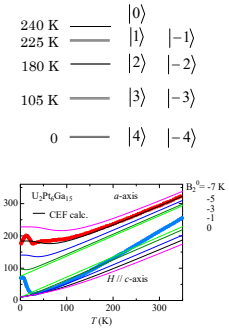

基底状態:Jz=4 第１励起状態:105 K

B20で異方性を再現。
100K付近の電気抵抗異常もおそらく対応

ただし、高温のeffective momentは再現できない。
基底状態はJz=4となるが、飽和磁化は実験値より大きい。

Summary and Outlook

2-6-15 structure

Previously reported as random atomic arrangements
X-ray diffraction detects streak signal
Consists from stacking of ordered layers shifting arbitrary within the basal plane
- uranium nearest neighbor interaction is quite regular
- consistent with well-defined antiferromagnetic transition

Robustness of U-X layer

A possible playground for naturally occurring multi-layer
- substituting U-X layers ?
- insertion of more buffer layers ? (to kill U-X interlayer coupling - pure 2D uranium)

U-X can be substituted by U-X' (preliminary)
- leading to physical property modification

3.3 K. Ishida（Dept. Phys., Kyoto Univ.）

Superconducting Spin Susceptibility of UTe_2

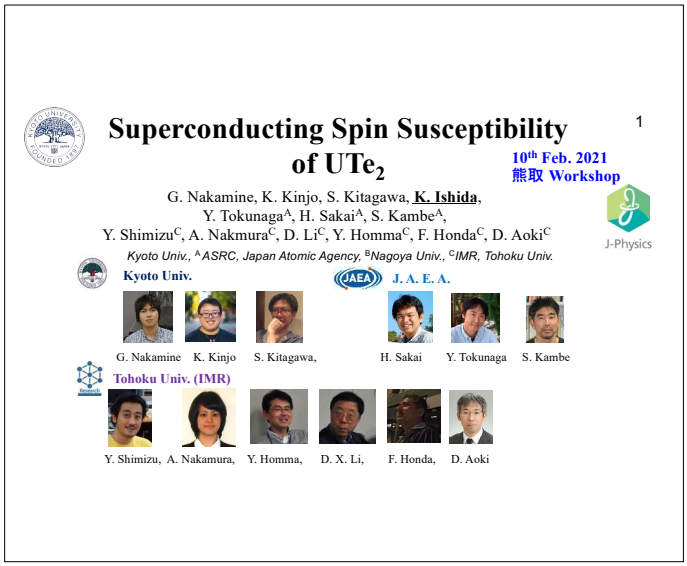

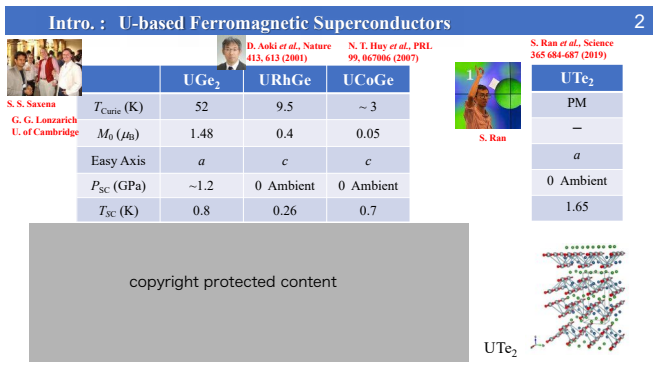

	UGe_2	URhGe	UCoGe
T_{Curie} (K)	52	9.5	~ 3
M_0 (μ_B)	1.48	0.4	0.05
Easy Axis	a	c	c
P_{SC} (GPa)	~1.2	0 Ambient	0 Ambient
T_{SC} (K)	0.8	0.26	0.7

UTe_2
PM
–
a
0 Ambient
1.65

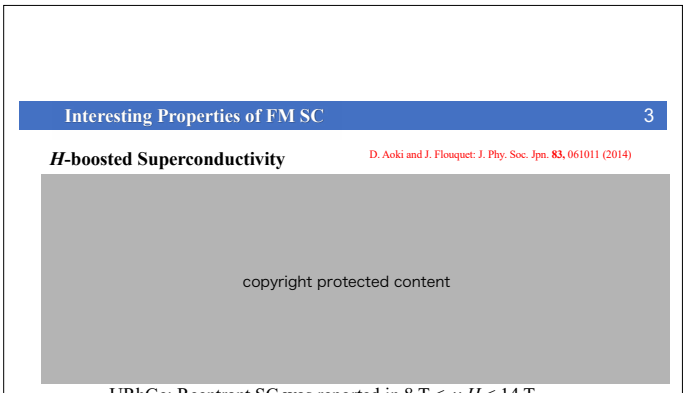

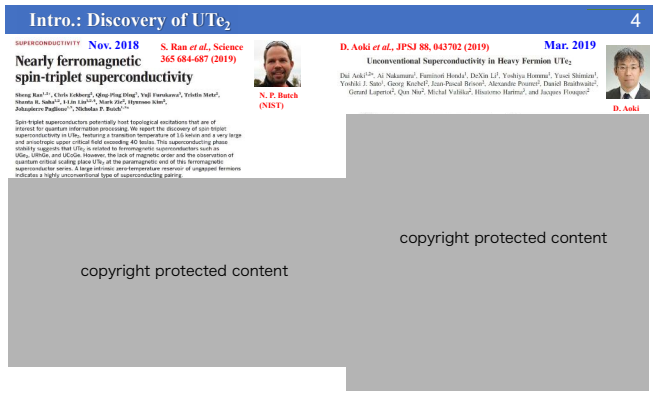

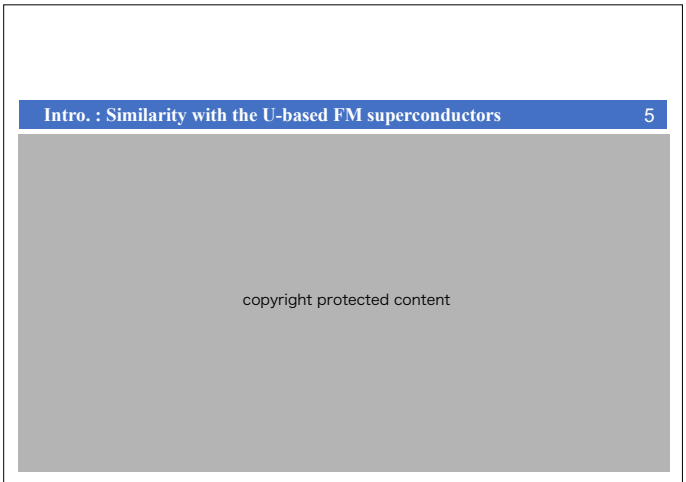

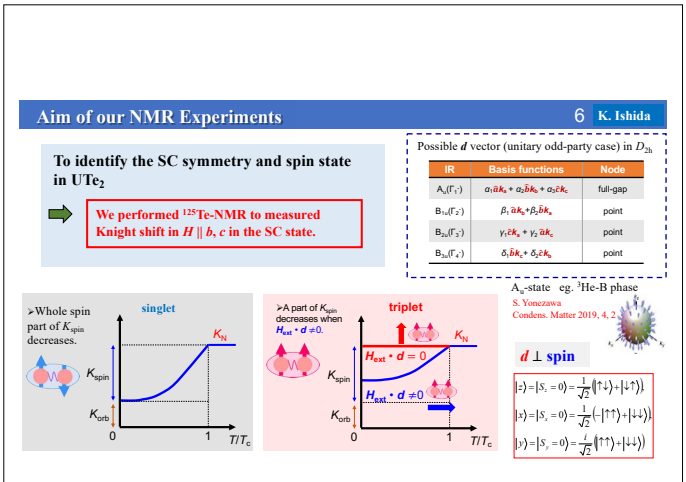

Experiment 7

➢The sample was provided by D. Aoki group. (*IMR, Tohoku University*)

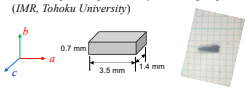

➢^{125}Te (99.9%) enriched sample

N. A. of ^{125}Te : 7 %

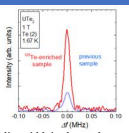

➢The linewidth is almost the same as that of the previous sample.

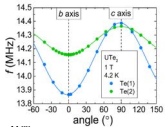

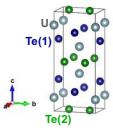

^{125}Te-NMR
$I = 1/2$
$\gamma = 13.454$ MHz/T

$$\mathcal{H} = \mathcal{H}_Z + \mathcal{H}_Q$$

$$\mathcal{H} = -\gamma\hbar\, \boldsymbol{I}\cdot(1+K)\boldsymbol{H}_0$$

$$K = \frac{A_{hf}}{N_A\mu_B}\chi$$

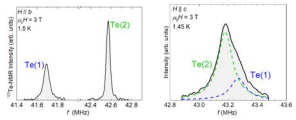

➢ Knight shift was determined at the peak of the spectrum.

Results: NMR spectrum in the SC state in $H \parallel b$ 8

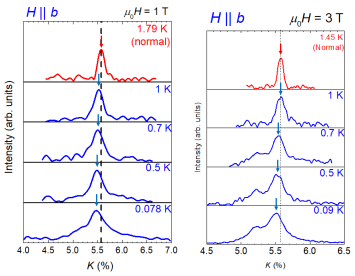

➢ A small Knight-shift decrease was observed.

⇒ **The signal arises from the SC region.**

➢ The spectrum was broadened and shoulder peak appears at low temperatures.

⇒ **Magnetic SC state !?**

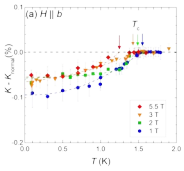

Results: NMR spectrum in the SC state in $H \parallel c$ 9

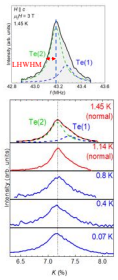

➢For H ∥ c, signals from both sites are overlapped.

➢We focused on the peak position

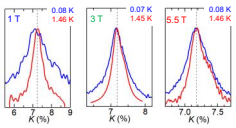

➢The decrease in Knight shift becomes smaller by applying H.

➢K is almost unchanged at 5.5 T (μ_0H_{c2} =11 T).

Spin-triplet pairing is strongly suggested.

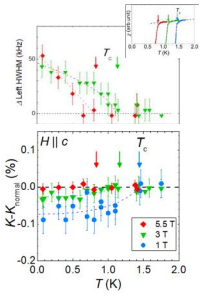

Result: H-dep. of spin part of Knight shift 10

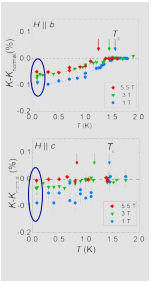

$$\Delta K = \Delta K_{\rm spin} + \Delta K_{\rm dia}$$

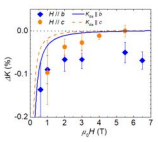

$$\Delta K_{dia} = \frac{H_{dia}}{H} = \frac{H_{c1}}{H}\frac{\ln\left(\frac{\beta d}{\sqrt{e}\xi}\right)}{\ln\kappa}$$

$\left(\frac{\sqrt{3}}{2}d^2(\mu_0H) = \phi_0\right)$ ϕ_0: flux quantum

d: distance between the vortices

used Parameters	∥ c
μ_0H_{c2} (T)	11
μ_0H_{c1} (mT)	1.2
κ	159
ξ (nm)	5.38

$\mu_0H_c \sim 49$ mT

$H_{c2}^{\rm orb} = \phi_0/2\pi\xi^2$ $\quad H_{c1} = \frac{H_c}{\sqrt{2}\kappa}(\ln\kappa + 0.497)$ $\quad \kappa = \frac{H_{c2}}{\sqrt{2}H_c}$

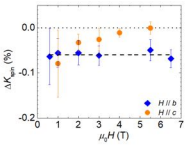

$\Delta K_{\rm spin} \sim 0.06$ %

Discussion: Estimation of spin part of Knight shift 11

$$K_{spin} = \frac{A_{hf}}{N_A\mu_B}\chi^{qp} = \frac{A_{hf}}{N_A\mu_B}\frac{\gamma_{el}(\mu_{eff})^2}{\pi^2k_B^2}R_w$$

→ Wilson ratio H. Tou *et al.*, J. Phys. Soc. Jpn. **74**, 1245 (2005.)

$(\mu_{eff})^2 = g^2j(j+1)\mu_B^2 = 3\mu_B^2$, assuming $g = 2$, $j = 1/2$

$$\Delta K_{\rm spin} = \frac{A_{hf}}{N_A\mu_B}\frac{3\mu_B^2}{\pi^2k^2}R_w\Delta\gamma_{el} = 149\times10^{-3}\times R_w$$

⟹ 0.71 $\times R_w$ (%)

$\Delta K_{cal} >> \Delta K_{exp} \sim 0.06$ % 1∼2

$\Delta K_{\rm spin}^{\rm SC} / K_{\rm spin} \sim 4$ %

copyright protected content

➢In URu_2Si_2 and UPd_2Al_3 with spin-singlet pairing, $\Delta K_{cal} \sim \Delta K_{exp}$ was reported.

Obviously, this relation does not hold in UTe_2, rather

Unchanged K_c in the SC state at 5.5T suggests the **spin-triplet pairing**.

Tiny decrease is consistent with the spin-triplet model by Prof. Fujimoto's group

j=5/2 multi-orbital band model with the magnetization anisotropy

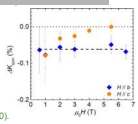

K. Hiranuma and S. Fujimoto, arXiv 2010.05112(2020).

Discussion: H-dep. of spin part of Knight shift 12

Possible $\boldsymbol{d}$ vector (unitary odd-party case) in D_{2h}

IR	Basis functions	Node
$A_u(\Gamma_1^-)$	$\alpha_1\hat{a}k_a + \alpha_2\hat{b}k_b + \alpha_3\hat{c}k_c$	full-gap
$B_{1u}(\Gamma_2^-)$	$\beta_1\ \hat{a}k_a + \beta_2\hat{b}k_b$	point
$B_{2u}(\Gamma_3^-)$	$\gamma_1\hat{c}k_a + \gamma_2\hat{a}k_c$	point
$B_{3u}(\Gamma_4^-)$	$\delta_1\hat{b}k_a + \delta_2\hat{c}k_b$	point

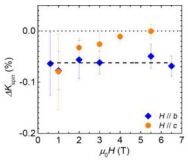

H = 0

➢reduction of Knight shift ∥ b, c ⇒ $\boldsymbol{d} \ni \hat{b}, \hat{c}$,

A_u: $\boldsymbol{d} = \alpha_1\hat{a}k_a + \alpha_2\hat{b}k_b + \alpha_3\hat{c}k_c$ is expected.

B_{3u}: $\boldsymbol{d} = \delta_1\hat{b}k_c + \delta_2\hat{c}k_b$ (easy axis ∥ a)

H ∥ c

➢$\boldsymbol{d}$ vector has c component at low fields.

➢The amount of $\Delta K_{\rm spin}$ decreases by applying $\boldsymbol{H}$ and is almost unchanged at 5.5 T (< H_{c2} ~ 11 T).

⇨ $\boldsymbol{d}$ vector is rotated in $H \parallel c$.

H ∥ b

➢$\Delta K_{\rm spin}$ is almost constant up to 6.5 T.

⇨ **Some $\boldsymbol{d}$ vector pinning mechanism?**

B_{3u}: 0 T

$\boldsymbol{d} = \delta_1\hat{b}k_c + \delta_2\hat{c}k_b$

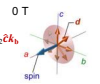

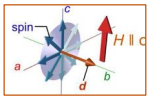

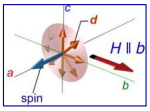

Discussion: *H*-dep. of spin part of Knight shift

13

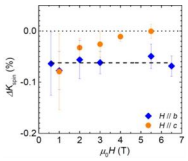

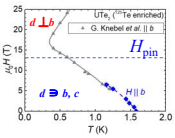

$H \parallel b$

E_{pin} : $-\frac{1}{2}\mu_0 \Delta\chi_{spin} H_{pin}^2$ $(\Delta\chi_{spin} = \Delta K_{spin}/A_{hf})$

E_{SC} : $\frac{1}{2}\mu_0 H_c^2$

When $H_{ext} = \boldsymbol{H}_{pin}$, $E_{SC} = E_{pin}$

$$-1/2\mu_0 H_c^2 = -1/2\mu_0 \Delta\chi_{spin} \boldsymbol{H}_{pin}^2$$

$\mu_0 \boldsymbol{H}_{pin} = \mu_0 H_c / \sqrt{\Delta\chi_{spin}}$ ~ **13 T**

Exp. ΔK_{spin} = - 0.06 %

A_{hf} = 5.18 T/ μ_B

Related to upturn behavior of T_c?

◆ ***d*** vector is rotated away to the *b* axis.

***d*-vector in high-*H* SC : *d* ⊥ *b* ?**

B_{3u}:
$\boldsymbol{d} = \delta_1 \hat{b} k_c + \delta_2 \hat{c} k_b$

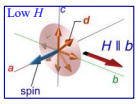

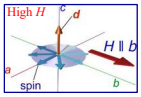

Summary

14

➢We measured NMR Knight shift in $H \parallel b$ and $H \parallel c$

➢Tiny decrease was observed in both K_b and K_c in low H. ⇒ $\boldsymbol{d} \ni \hat{b}, \hat{c}$,

Possible SC state A_u: $\boldsymbol{d} = \alpha_1 \hat{a} k_a + \alpha_2 \hat{b} k_b + \alpha_3 \hat{c} k_c$

B_{3u}: $\boldsymbol{d} = \delta_1 \hat{b} k_c + \delta_2 \hat{c} k_b$

➢ K_c is unchanged in the SC state at 5.5 T.

⇒ **spin-triplet superconductivity**

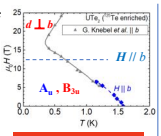

$H \parallel b$

➢ΔK_{spin} is constant up to 6.5 T :

⇨ ***d* vector is pinned along the *b* axis?**

ΔK_{spin} ~ 0.06 %

$\mu_0 \boldsymbol{H}_{pin} = H_c / \sqrt{\Delta\chi_{spin}}$ ~ 13 T

$(\Delta\chi_{spin} = \Delta K_{spin}/A_{hf})$

⇨ **Related to T_c upturn?**

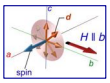

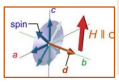

$H \parallel c$

➢ The $\hat{c}$ component is suppressed in $H \parallel c$.

⇨ ***d* vector is rotated in $H \parallel c$.**

➢ K_c is unchanged at 5.5 T.

⇨ ***d* ⊥ *c* at 5.5 T**

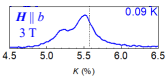

➢ Shoulder peak appears at low temperatures in $H \parallel b$.

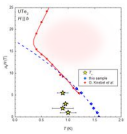

➢ A measurement at high H is needed.

Perspective

15

➢ Physics of spin-triplet superconductivity

- Understanding of the spin and orbital degrees of freedom
- Search of the collective mode in the SC state

➢ Playground of the topological superconductivity

Article

Chiral superconductivity in heavy-fermion metal UTe_2

Lin Jiao *et al.* Nature 579, 523 (2020)

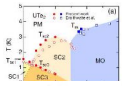

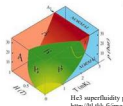

He3 superfluidity phase diagram
http://ltl.tkk.fi/images/overview/ab.jpg

Weyl Superconductivity in UTe_2

arXiv:2002.02539

Ian M. Hayes,[1,+] Di S. Wei,[2,3,+] Tristin Metz,[1] Jian Zhang,[4] Yun Suk Eo,[1] Sheng Ran,[1,5] Shanta R. Saha,[1,5] John Collini,[1] Nicholas P. Butch,[1,5] Daniel F. Agterberg,[6] Aharon Kapitulnik,[2,3,7,8,1] and Johnpierre Paglione[1,5,9,-]

Insulator-Metal Transition and Topological Superconductivity in UTe_2 from a First-Principles Calculation

PRL 123, 217001 (2019)

Jun Ishizuka, Shuntaro Sumita, Akito Daido, and Youichi Yanase
Department of Physics, Graduate School of Science, Kyoto University, Kyoto 606-8502, Japan

Kerr effect

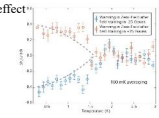

16

3.4 T. Yaita（SPring-8, JAEA）

Recent activities of Actinide Chemistries in the Materials Sciences Rsearch Center of JAEA

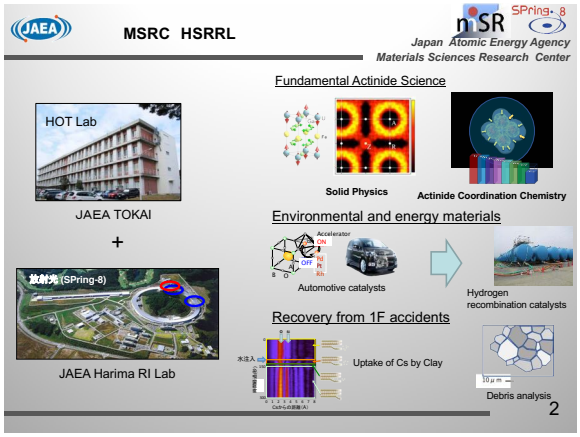

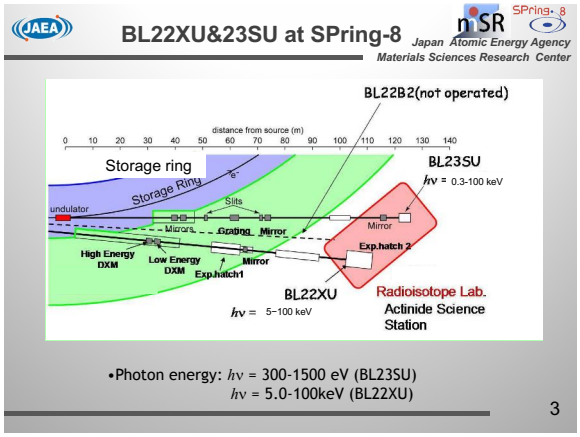

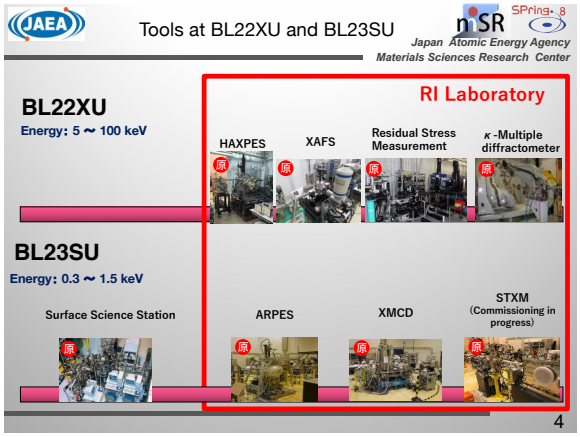

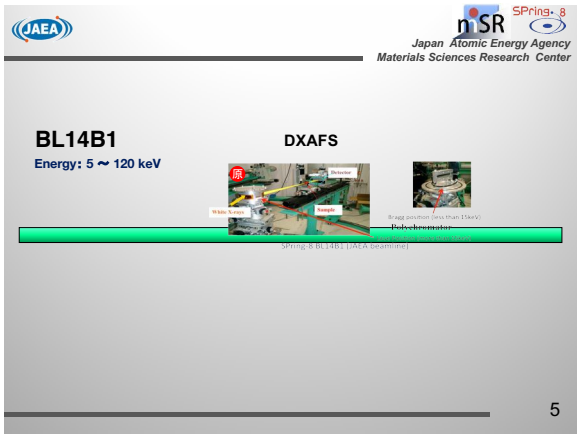

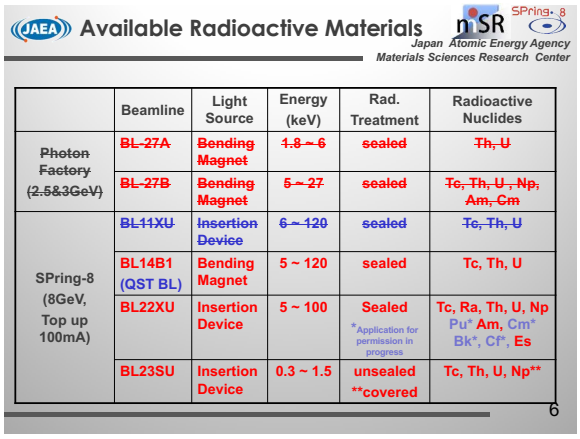

	Beamline	Light Source	Energy (keV)	Rad. Treatment	Radioactive Nuclides
~~Photon Factory (2.5&3GeV)~~	~~BL-27A~~	~~Bending Magnet~~	~~1.8 ~ 6~~	~~sealed~~	~~Th, U~~
	~~BL-27B~~	~~Bending Magnet~~	~~5 ~ 27~~	~~sealed~~	~~Tc, Th, U , Np, Am, Cm~~
SPring-8 (8GeV, Top up 100mA)	~~BL11XU~~	~~Insertion Device~~	~~6 ~ 120~~	~~sealed~~	~~Tc, Th, U~~
	BL14B1 (QST BL)	Bending Magnet	5 ~ 120	sealed	Tc, Th, U
	BL22XU	Insertion Device	5 ~ 100	Sealed *Application for permission in progress	Tc, Ra, Th, U, Np Pu* Am, Cm* Bk*, Cf*, Es
	BL23SU	Insertion Device	0.3 ~ 1.5	unsealed **covered	Tc, Th, U, Np**


Sealing test according to JIS standard
Japan Atomic Energy Agency
Materials Sciences Research Center
Holder & Tube
Seal Level Test
Impact & Punc test
Pin, weight
Pressure (Low)
Pressure (High)
High Temp.
Low Temp.
7

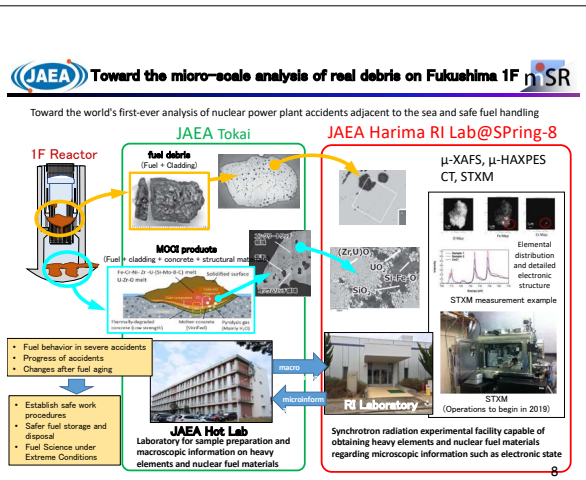
Toward the micro-scale analysis of real debris on Fukushima 1F
Toward the world's first-ever analysis of nuclear power plant accidents adjacent to the sea and safe fuel handling
JAEA Tokai
JAEA Harima RI Lab@SPring-8
1F Reactor
fuel debris
(Fuel + Cladding)
MOCI products
μ-XAFS, μ-HAXPES
CT, STXM
Elemental distribution and detailed electronic structure
STXM measurement example
STXM
(Operations to begin in 2019)
Fuel behavior in severe accidents
Progress of accidents
Changes after fuel aging
Establish safe work procedures
Safer fuel storage and disposal
Fuel Science under Extreme Conditions
macro
microinform
RI Laboratory
JAEA Hot Lab
Laboratory for sample preparation and macroscopic information on heavy elements and nuclear fuel materials
Synchrotron radiation experimental facility capable of obtaining heavy elements and nuclear fuel materials regarding microscopic information such as electronic state
8


Japan Atomic Energy Agency
Materials Sciences Research Center
Research Topics
9

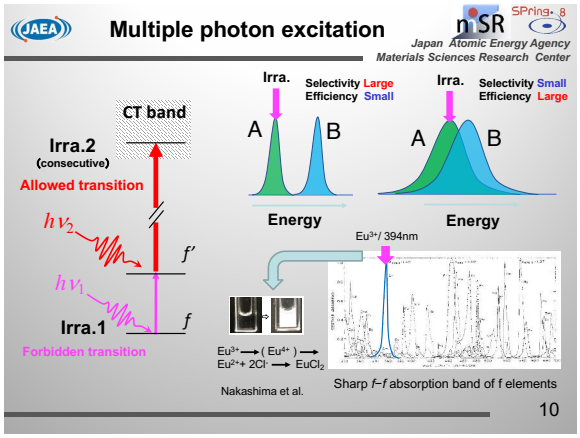
Multiple photon excitation
Japan Atomic Energy Agency
Materials Sciences Research Center
CT band
Irra.2
(consecutive)
Allowed transition
Irra.1
Forbidden transition
Irra.
Selectivity Large
Efficiency Small
Selectivity Small
Efficiency Large
A
B
Energy
Eu3+/ 394nm
Eu3+ → (Eu4+) →
Eu2++ 2Cl- → EuCl2
Nakashima et al.
Sharp f–f absorption band of f elements
10

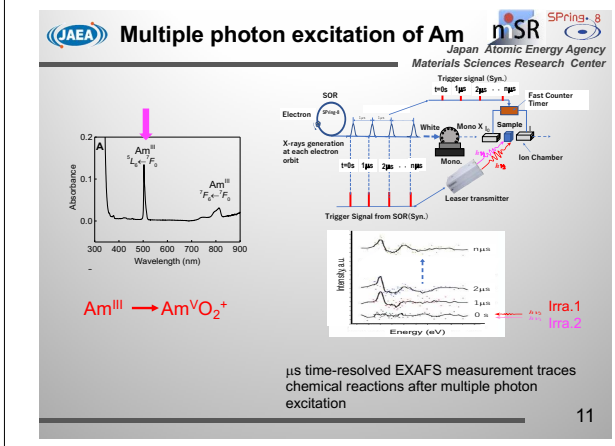
Multiple photon excitation of Am
Japan Atomic Energy Agency
Materials Sciences Research Center
Absorbance
Wavelength (nm)
AmIII → AmVO2+
Trigger signal (Syn.)
Fast Counter Timer
Electron
SOR
X-rays generation at each electron orbit
Mono X
Sample
Mono.
Ion Chamber
Leaser transmitter
Trigger Signal from SOR(Syn.)
Intensity a.u.
Energy (eV)
Irra.1
Irra.2
μs time-resolved EXAFS measurement traces chemical reactions after multiple photon excitation
11

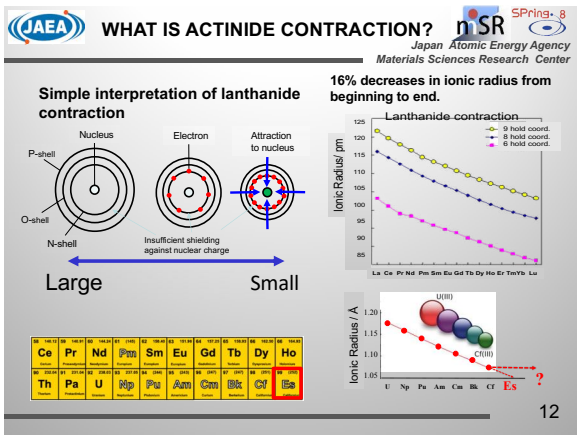
WHAT IS ACTINIDE CONTRACTION?
Japan Atomic Energy Agency
Materials Sciences Research Center
Simple interpretation of lanthanide contraction
Nucleus
Electron
Attraction to nucleus
P-shell
O-shell
N-shell
Insufficient shielding against nuclear charge
Large
Small
16% decreases in ionic radius from beginning to end.
Lanthanide contraction
Ionic Radius/ pm
9 hold coord.
8 hold coord.
6 hold coord.
Ionic Radius / Å
U(III)
Cf(III)
12

Einsteinium Break of Hydration bond distances

Japan Atomic Energy Agency
Materials Sciences Research Center

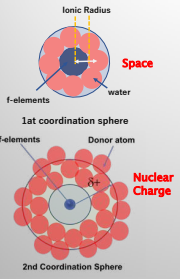

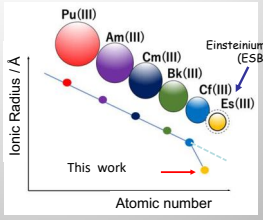

The ESB may have been caused by a change in the electron configuration.

13

Simulated Debris analysis

Kobayashi's Presentation

Japan Atomic Energy Agency
Materials Sciences Research Center

Experiments simulating environmental changes in the fuel picking-up process

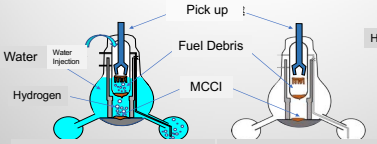

Picking up of uranium from water in a high radiation field

Picking up of uranium from dry envilonmnet in a high radiation field

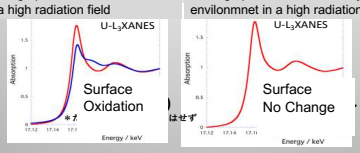

14

DXAFS application for Fukushima

Japan Atomic Energy Agency
Materials Sciences Research Center

Cs sorption on clay

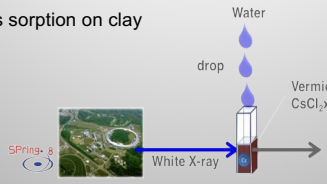

15

Interpretation for Cs Sorption

Japan Atomic Energy Agency
Materials Sciences Research Center

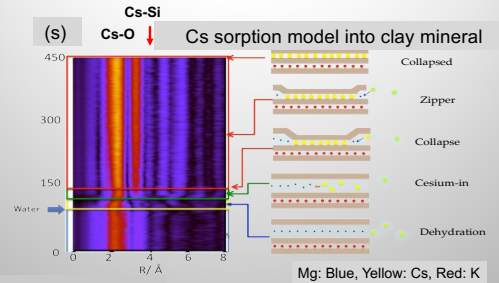

TR-RSF Image

Mg: Blue, Yellow: Cs, Red: K

Yaita et al., GER(2017)

16

Summary

Japan Atomic Energy Agency
Materials Sciences Research Center

1. Introduction of new structure of JAEA Beamline
2. Introduction of recent topics and plan using JAEA Beamline and Experimental station

17

3.5 N. Ishikawa（Dept. Chem., Osaka Univ.）

Observation of interaction between 5f electronic system and photo-excited cyclic π system

---

Observation of interaction between 5f electronic system and photo-excited cyclic π system.

５ｆ電子系と光励起環状π電子系の相互作用の観測

ISHIKAWA Naoto, Osaka University

大阪大学　理学研究科　石川直人

Introduction of myself 自己紹介

- Research field:
  coordination chemistry
  錯体化学
- Main interest:
  Molecular magnetism involving 4f systems
  ４ｆ電子系が関与する「分子磁性」
- Recent interest:
  Molecular magnetism involving 5f systems
  ５ｆ電子系が関与する「分子磁性」

Phthalocyanine Complexes

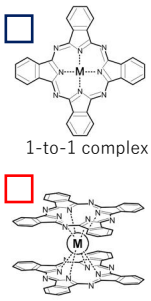

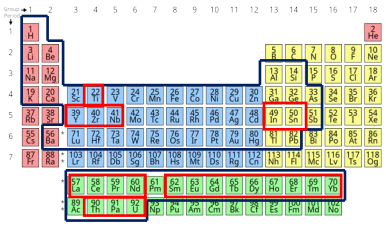

Lanthanide-Pc Double-Decker Complexes

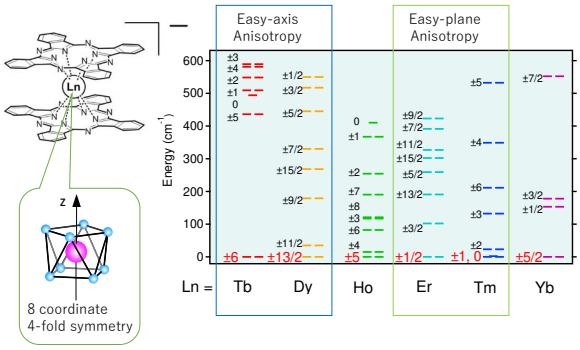

Ishikawa,et.al. *Inorg. Chem.* **2003**, 42, 2440-2446.

---

lanthanide SMM (Single Molecule Magnet)

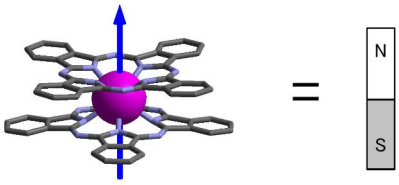

Tb complex　&　Dy complex　=　First lanthanide SMM
初の希土類「単分子磁石」

Ishikawa, Sugita, Ishikawa, Koshihara, Kaizu, *J.A.C.S.*, **2003**, *125* (29), 8694–8695

Interaction between 4f electronic system and photo-excited cyclic π system

4f電子系と光励起環状π電子系との相互作用

Doubly-degenerate π - π * excited state of Pc ligand

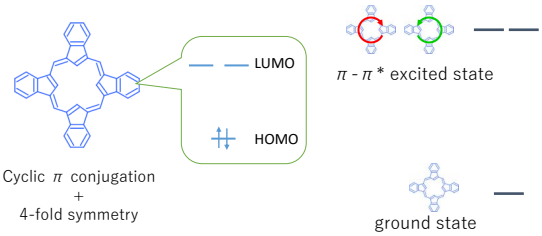

The doubly-degenerate π - π * excited states can have an orbital angular momentum ***L***
二重縮重したπ - π *励起状態は 軌道角運動量***L***を持つことができる

Two Angular momenta in Pc_2Tb^- & Pc_2Dy^-

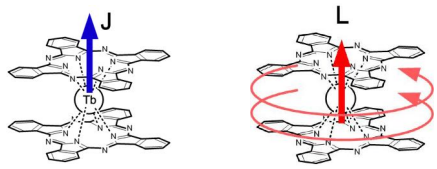

J of the 4f system **L** of the ligand in a π - π * state

Question: Does **J** interact with **L**? If so, how?

→ VTVH-MCD (温度・磁場可変磁気円二色性分光法) measurements have been conducted.

MCD spectrum of Pc_2Y^- ($4f^0$)

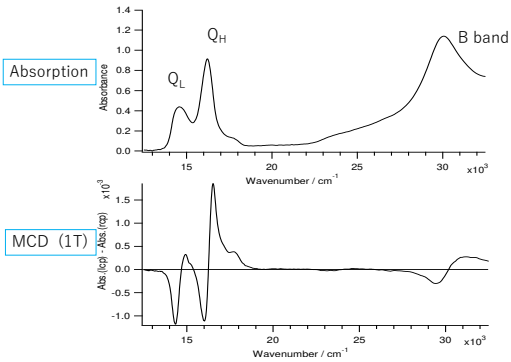

MCD spectrum of Pc_2Y^- ($4f^0$)

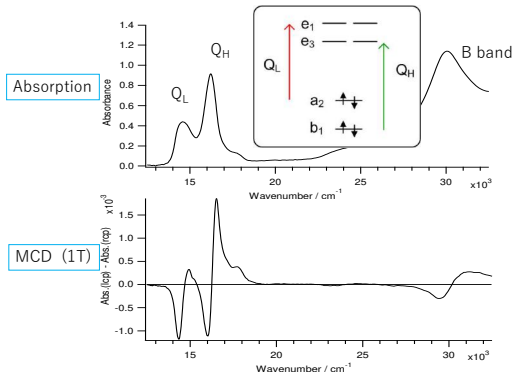

Derivative pattern = A term

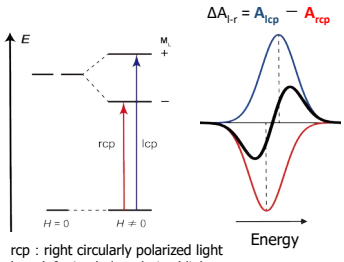

rcp : right circularly polarized light
lcp : left circularly polarized light

Appears when a degenerate state is split by Zeeman interaction

→ evaluation of angular momentum and magnetic moment

Q_L: $|L_z| = 2.0\hbar$ Q_H: $|L_z| = 2.2\hbar$

Temperature dependence of MCD

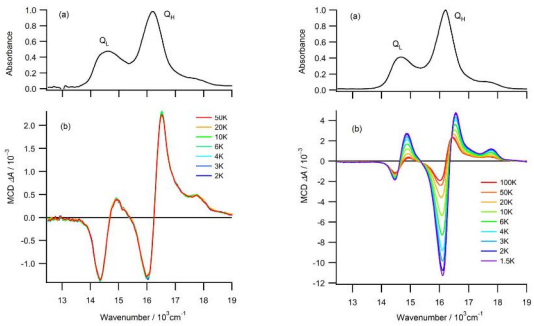

Pc_2Y^- (f^0) Pc_2Tb^- (f^8)

How can it be explained ?

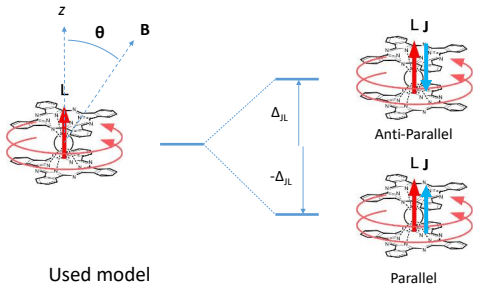

A term temperature dependence

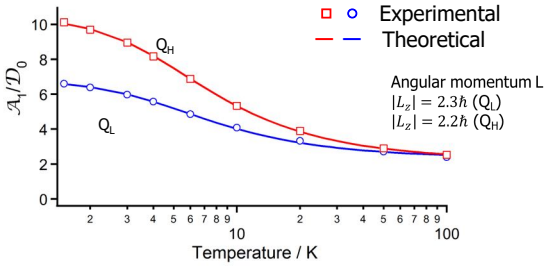

J-L interaction
$\Delta_{JL} = 1.4\ \mathrm{cm}^{-1}$ (Q_L)
$\Delta_{JL} = 2.6\ \mathrm{cm}^{-1}$ (Q_H)

J and **L** are coupled ferromagnetically

Chem. Commun. **2017**, *53*, 6168.

Interaction between 5f electronic system and photo-excited cyclic π system

5f電子系と光励起環状π電子系との相互作用

Pc_2U

U^{4+} ：$(5f)^2$ configuration
L=5, S=1, J=4 → $^3H_4$ term

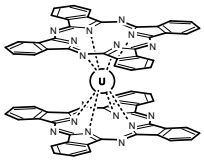

試料提供：山村朝雄先生　京都大学複合原子力科学研究所
白崎謙次先生　東北大学金属材料研究所

現在までに分かったこと

ウラン-フタロシアニン錯体で、5f電子系と光励起π電子系の間に相互作用があることがわかった。

希土類4f電子系で有効であった理論モデルが、5f電子系ではうまく機能しないことがわかった。

4fと5fの違いを考慮した理論モデルの構築が必要であることがわかった。

展望

より単純な構造を持つPc単層型のウラン錯体（$PcU(acac)_2$など）での実験を行う。

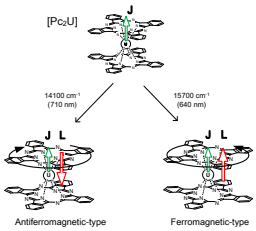

3.6 T. Suzuki（Nagaoka Univ. Tech.）

Fundamental Study for Precise Analysis of Actinides in Hardly Soluble Substances Containing Uranium Oxides

Topical meeting of
Condensed-matter Chemistry
on Actinides:
The Kumatori meeting 2021

Fundamental Study for Precise Analysis of Actinides in Hardly Soluble Substances Containing Uranium Oxides

Tatsuya Suzuki
Nagaoka University of Technology

1

Aim in our presented works

Quantitative analysis and Isotopic Ratio analysis of actinides (U, Np, Pu, Am, Cm), and lanthanides in UO_2 containing solid Substances, such as spent fuel, and nuclear debris. for Waste Management, Nuclear Forensics, and so on.

For this aim

Developments of
- Dissolution Methods
- Nuclide Separation
- Actinide Analysis methods

are required.

2

Diagram of Our Developing Methods

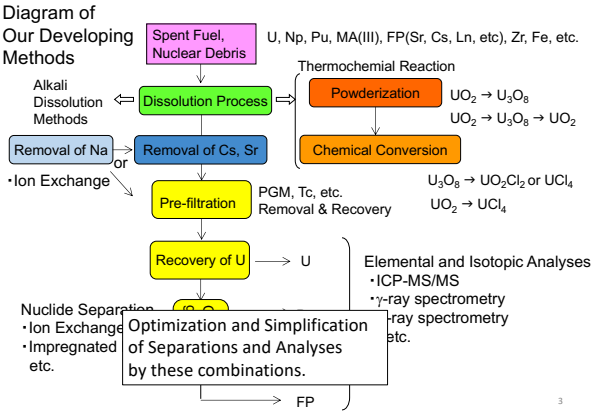

3

Dissolution Method（Pretreatment for Dissolution）

Chemical Conversion for Pretreatment of Dissolution

- Powderization

  Chemical Conversion of UO_2 by Oxidation to U_3O_8

  → Powderization occurred by Volume Expansion

  Embrittlement (Easy Mechanical Powderization)

- Chlorination

  Conversion to Chloride by Thermochemical Reaction using Carbon Chloride.

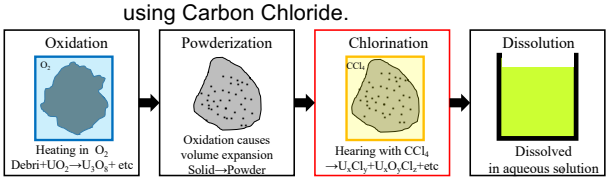

Chemical Conversion Experiment of UO_2 pellet.

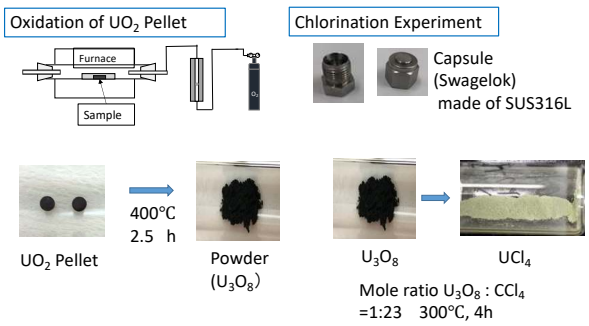

5

Investigation of Separation Process

Plan of Separation

(1) Removal of Cs and Sr
  Inorganic adsorbents, e.g. AMP, AWP, ZMP, etc.

(2) Selective Recovery of Uranium
  Pyrrolidone resin, TBP resin

(3) Separation and Recovery of Actinides and Rare Earths
  CMPO impregnated Resin (EiChrom TRU-resin or RE resin)

(4) Separation of Actinides from Rare Earths
  DGA-resin(EiChrom), Dipex-resin(EiChrom Actinide resin), Pyridine resin

(5) Mutual Separation of trivalent Actinides, or Rare Earths
  HDEHP impregnated Resin(EiChrom Ln-resin), Cation Exchange Resins, Anion Exchange Resins

6

Examples of Separation Methods, 1
Removal of Cs and Sr

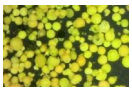

Synthesis of
AMP embedded in porous silica beads
(AMP-Silica, AWP-Silica)

Removal of Cs from simulant HLW in HCl system

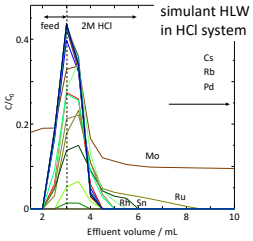

Removal of Cs from simulant HLW in HNO_3 system

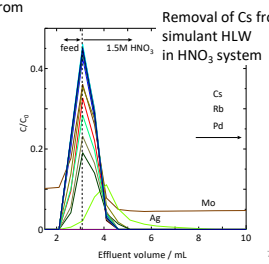

7

Example of Separation Methods, 2
Separation of Actinides from Rare Earths
and Mutual Separation of trivalent Actinides
by Pyridine resin (one kind of anion exchange resin)

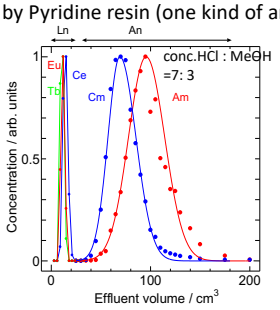

Separation of Actinides from Rare Earths

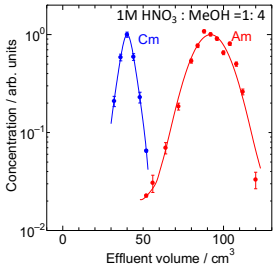

Mutual Separation of trivalent Actinides

Example of Separation Methods, 3
Separation of Actinides from Rare Earths
by DGA resin (TODGA Impregnated Resin, EiChrom)

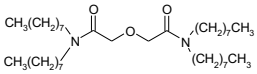

TODGA

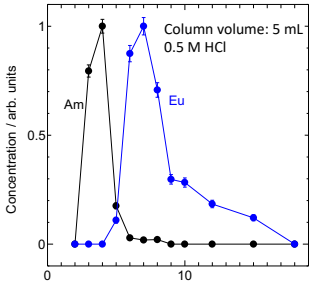

9

Actinide Analysis methods
・ICP-MS/MS analysis for Actinides

・Confirmation of Quantitative Actinide Analysis
by using Triple Quadrupole ICP-MS/MS (Agilent 8900)
+Obtaining the measurement condition for Actinides,
and their limitation of detection.
・Confirmation of Molecular Ion Formation in ICP-Ion Source
・Investigation of Interference Ion Removal
by Collision/Reaction Cell
+ Removal of Interference Molecular Ions by Collision Cell
+ Feasibility Study on Isobaric Interference Removal
by Mass Shifts

10

Triple Quadrupole ICP-MS/MS (Agilent 8900) was placed in
Building of Actinide Experiment,
Oarai center, Inst. Material Research, Tohoku Univ.
This facility is one of the important Japanese centers
of Inter-University Cooperation for Actinide Researches.

Agilent 8900 Triple Quadrupole ICP-MS/MS

11

Difference between normal ICP-MS and QQQ-ICP-MS/MS

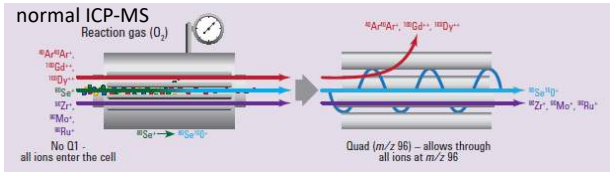

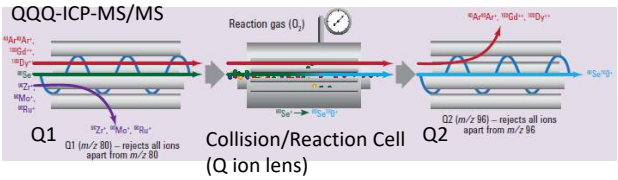

12

Mass Shift of Actinides by Reaction with Oxygen gas in Reaction Cell of ICP-MS/MS.

Yields of Actinide Ionic Species in Oxygen Cell Gas mode at Oxygen Gas flow rate of 30% (0.45mL/min).

%	M^+	MO^+	MO_2^+
^{238}U	0.0	0.2	99.8
^{237}Np	0.0	1.6	98.4
^{240}Pu	0.0	15.0	85.0
^{241}Am	0.2	98.6	1.2
^{244}Cm	0.1	99.9	---

13

O_2 Gas Flow Rate Effect on Intensity of Detected Ion Species

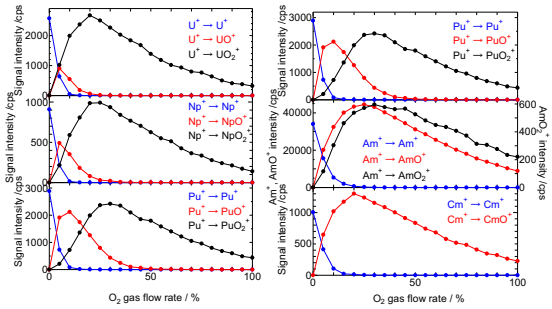

(T. Suzuki, et al., Journal of Radioanalytical and Nuclear Chemistry (2018) 318:221–225)

14

Summary

I introduced

Dissolution method of UO_2-containg materials,
Nuclide separation, Cs removal, Actinide separation,
Actinide analysis using ICP-MS/MS,
among our works.

15

Acknowledgements

This work was partly performed under the Inter-University Cooperative Research Program of the Institute for Materials Research, Tohoku University (Proposal Nos. 17F0018, 18F0023, 19F0021, 20F0026), and under the long training course of "Education Program on Separation & Analysis for Radioactive Waste Disposal (head: Tohoku University)" , and partially supported by the Grant-in-Aid for Scientific Research (B) (KAKENHI No. 16H04628) and the Nuclear Energy Science & Technology and Human Resource Development Project (through concentrating wisdom) from the Japan Atomic Energy Agency / Collaborative Laboratories for Advanced Decommissioning Science.

16

3.7 K. Washiyama（Fukushima Medical University）

Current status and prospects of domestic supply of alpha-emitting radionuclides

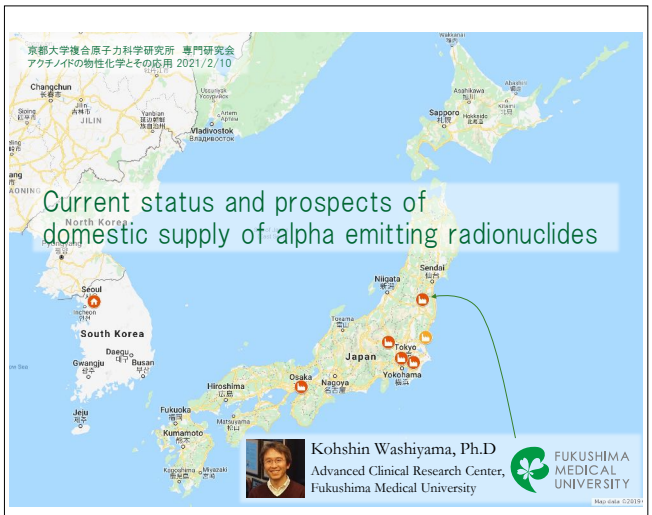

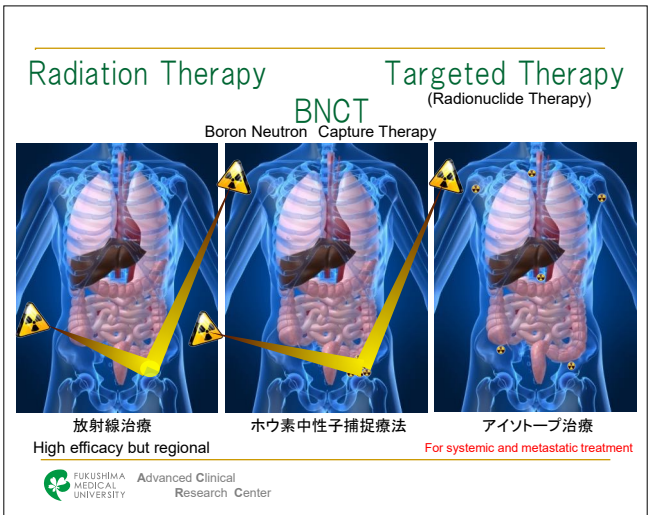

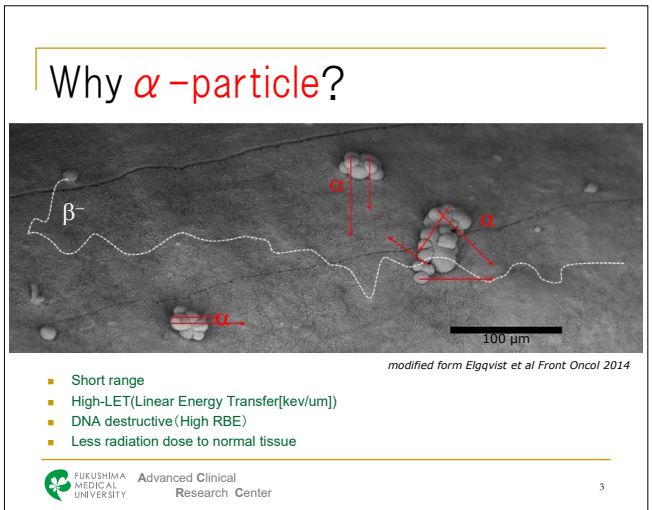

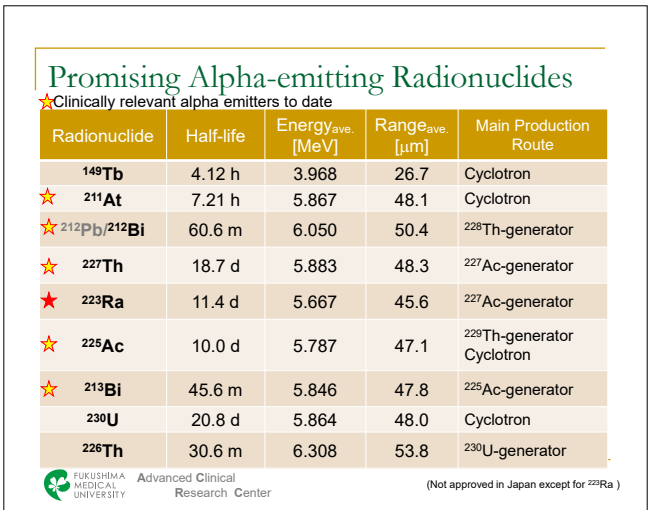

Radionuclide	Half-life	Energy$_{ave.}$ [MeV]	Range$_{ave.}$ [μm]	Main Production Route
^{149}Tb	4.12 h	3.968	26.7	Cyclotron
☆ ^{211}At	7.21 h	5.867	48.1	Cyclotron
☆ ^{212}Pb/^{212}Bi	60.6 m	6.050	50.4	^{228}Th-generator
☆ ^{227}Th	18.7 d	5.883	48.3	^{227}Ac-generator
★ ^{223}Ra	11.4 d	5.667	45.6	^{227}Ac-generator
☆ ^{225}Ac	10.0 d	5.787	47.1	^{229}Th-generator Cyclotron
☆ ^{213}Bi	45.6 m	5.846	47.8	^{225}Ac-generator
^{230}U	20.8 d	5.864	48.0	Cyclotron
^{226}Th	30.6 m	6.308	53.8	^{230}U-generator

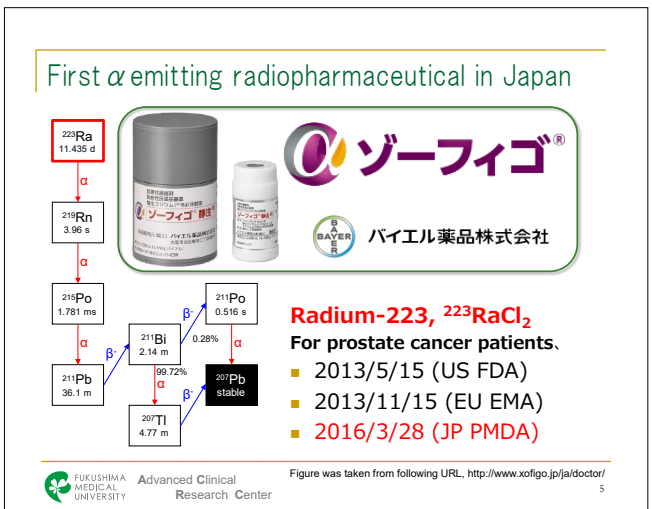

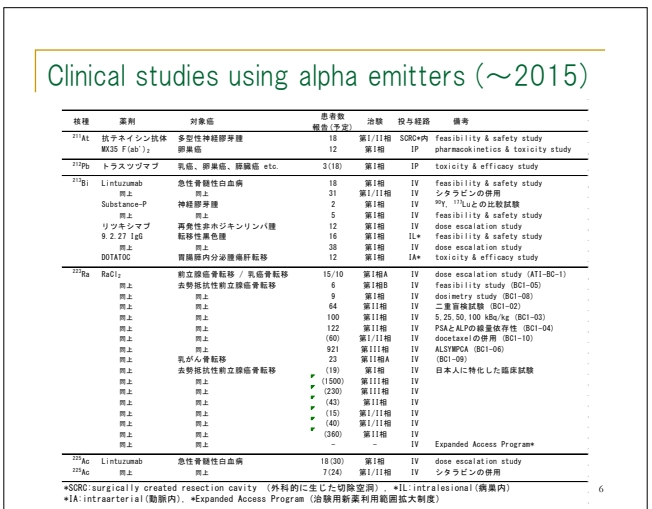

核種	薬剤	対象癌	患者数 報告(予定)	治験	投与経路	備考
^{211}At	抗チネイシン抗体	多型性神経膠芽腫	18	第I/II相	SCRC*内	feasibility & safety study
	MX35 F(ab')$_2$	卵巣癌	12	第I相	IP	pharmacokinetics & toxicity study
^{212}Pb	トラスツマブ	乳癌、卵巣癌、膵臓癌 etc.	3(18)	第I相	IP	toxicity & efficacy study
^{213}Bi	Lintuzumab	急性骨髄性白血病	18	第I相	IV	feasibility & safety study
	同上	同上	31	第I/II相	IV	シタラビンの併用
	Substance-P	神経膠芽腫	2	第I相	IV	^{90}Y, ^{177}Luとの比較試験
	同上	同上	5	第I相	IV	feasibility & safety study
	リツキシマブ	再発性非ホジキンリンパ腫	12	第I相	IV	dose escalation study
	9.2.27 IgG	転移性黒色腫	16	第I相	IL*	feasibility & safety study
	同上	同上	38	第I相	IV	dose escalation study
	DOTATOC	胃腸膵内分泌腫瘍肝転移	12	第I相	IA*	toxicity & efficacy study
^{223}Ra	RaCl$_2$	前立腺癌骨転移 / 乳癌骨転移	15/10	第I相A	IV	dose escalation study (ATI-BC-1)
	同上	去勢抵抗性前立腺癌骨転移	6	第I相B	IV	feasibility study (BCI-05)
	同上	同上	9	第I相	IV	dosimetry study (BCI-06)
	同上	同上	64	第II相	IV	二重盲検試験 (BCI-02)
	同上	同上	100	第II相	IV	5,25,50,100 kBq/kg (BCI-03)
	同上	同上	122	第II相	IV	PSAとALPの線量依存性 (BCI-04)
	同上	同上	(60)	第I/II相	IV	docetaxelの併用 (BCI-10)
	同上	同上	921	第III相	IV	ALSYMPCA (BCI-06)
	同上	乳がん骨転移	23	第I相A	IV	(BCI-09)
	同上	去勢抵抗性前立腺癌骨転移	(19)	第I相	IV	日本人に特化した臨床試験
	同上	同上	(1500)	第III相	IV	
	同上	同上	(230)	第III相	IV	
	同上	同上	(43)	第II相	IV	
	同上	同上	(15)	第I/II相	IV	
	同上	同上	(40)	第I/II相	IV	
	同上	同上	(360)	第III相	IV	
	同上	同上	-	-	IV	Expanded Access Program*
^{225}Ac	Lintuzumab	急性骨髄性白血病	18(30)	第I相	IV	dose escalation study
^{223}Ac	同上	同上	7(24)	第I/II相	IV	シタラビンの併用

Next Generation…

Journal of Nuclear Medicine, published on July 28, 2016 as doi:10.2967/jnumed.116.178673

^{225}Ac-PSMA-617 for PSMA-Targeted α-Radiation Therapy of Metastatic Castration-Resistant Prostate Cancer

Clemens Kratochwil[1*], Frank Bruchertseifer[2,3], Frederik L. Giesel[1], Mirjam Weis[2], Frederik A. Verburg[1], Felix Mottaghy[1], Klaus Kopka[4], Christos Apostolidis[2], Uwe Haberkorn[1], and Alfred Morgenstern[2]

[1]Department of Nuclear Medicine, University Hospital Heidelberg, Heidelberg, Germany; [2]European Commission, Joint Research Centre, Institute for Transuranium Elements, Karlsruhe, Germany; [3]Department of Nuclear Medicine, RWTH University Hospital Aachen, Aachen, Germany; and [4]Division of Radiopharmaceutical Chemistry, German Cancer Research Center, Heidelberg, Germany

TABLE 1
Overview of Pretreatments

Patient A	Patient B
Leuprorelin	Radical prostatectomy
Zoledronate	Radiotherapy of lymph node metastasis
Docetaxel (50 cycles)	Leuprorelin
Carmustine/epirubicin in hyperthermia	Leuprorelin plus bicalutamide, 150 mg/d
Abiraterone	Docetaxel (11 cycles)
Enzalutamide	Cabazitaxel (10 cycles)
^{223}Ra (6 cycles)	Abiraterone
Abiraterone reexposition	Enzalutamide (not tolerated)
Estramustine	

Copyright protected content

Figure 1: ^{68}Ga-PSMA-11 PET/CT-scans of patient A. Pre-therapeutic tumor spread (A), restaging 2 months after the third cycle of Ac-225-PSMA-617 (B) and 2 months after one additional consolidation therapy (C).

Copyright protected content

Figure 3: ^{68}Ga-PSMA-11 PET/CT-scans of patient B. In comparison to the initial tumor spread (A), restaging after 2 cycles of beta-emitting ^{177}Lu-PSMA-617 presented progression (B). In contrast, restaging after 2nd (C) and 3rd (D) cycle of alpha-emitting ^{225}Ac-PSMA-617 presented impressive response.

Actinium-225 is NOT approved in Japan

Clinical experience with ^{225}Ac and ^{213}Bi

Cancer type	Radio-conjugate	No. of patients	Hospitals
Leukemia	^{213}Bi-Lintuzmab	49	MSKCC (New York)
	^{225}Ac-Lintzumab	36	MSKCC (New York)
Lymphoma	^{213}Bi-Rituximab	12	Heidelberg, Dusseldorf
Melanoma	^{213}Bi-9.2.27-mab	16	Sydney
	^{213}Bi-9.2.27-mab	38	Sydney
Brain	^{213}Bi-Substance-P	67	Basel, Warsaw
	^{225}Ac-Substance-P	27	Warsaw
Neuroendocrine	^{213}Bi-DOTATOC	25	Heidelberg
	^{225}Ac-DOTATOC	39	Heidelberg
Bladder	^{213}Bi-Erbitux	12	Munich
Prostate	^{225}Ac-PSMA-617	> 400	Heidelberg, Munich, Pretoria, Warsaw, ….

Data from Dr. Morgenstern presentation @ ISTR-2019 (2019.10.30)

Chart of nuclides

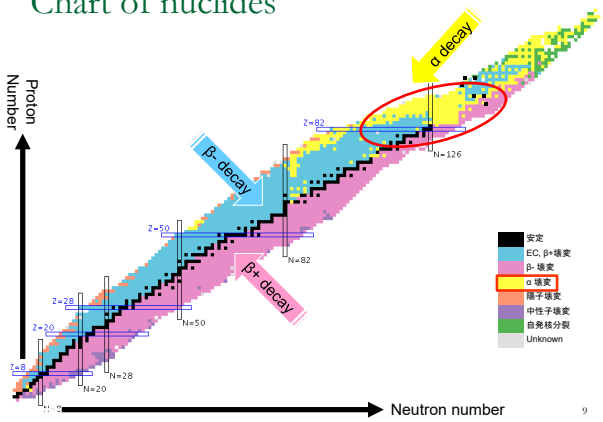

General production route for alpha emitters for TAT

Radionuclide	Production Method	Production Route
^{149}Tb	accelerator	^{152}Gd(p, 4n)^{149}Tb, ^{142}Nd(^{12}C, 5n)^{149}Dy→^{149}Tb
		^{141}Pr(^{12}C, 5n)^{149}Tb, ^{nat}Ta(p, spall)^{149}Tb
^{211}At	accelerator	^{209}Bi(α, 2n)^{211}At
	^{211}Rn/^{211}At generator	^{209}Bi(^{7}Li, 5n)^{211}Rn, ^{232}Th(p, spall)^{211}Rn
^{212}Pb/^{212}Bi	^{228}Th/^{212}Pb generator	Decay of ^{232}Th, ^{226}Ra multiple(n, γ)^{228}Th
^{227}Th, ^{223}Ra	^{227}Ac source	Decay of ^{235}U, ^{226}Ra(n, γ)^{227}Ra→^{227}Ac
	accelerator	^{232}Th(p, spall)^{223}Ra
^{225}Ac	^{229}Th source	Decay of ^{233}U, ^{226}Ra multiple(n, γ)^{229}Th
	accelerator	^{226}Ra(p, 2n)^{225}Ac, ^{226}Ra(d, 3n)^{225}Ac
		^{236}Ra(γ, n)^{225}Ra→^{225}Ac, ^{232}Th(p, spall)^{225}Ac
^{213}Bi	^{225}Ac/^{213}Bi generator	
^{230}U	^{230}Pa/^{230}U generator	^{232}Th(p, 3n)^{230}Pa
	accelerator	^{231}Pa(p, 2n)^{230}U, ^{231}Pa(d, 3n)^{230}U
^{226}Th	^{230}U/^{226}Th generator	

^{223}Ra availability: a simple calculation.

^{223}Ra (11.435d) is routinely separated from ^{227}Ac (22.7y) as a generator form.

- A HRPC patient who has bone metastases receive 50 kBq/kg (ex 3 MBq/ 1 injection for 60 kg body weight man) of ^{223}Ra 6 times every 4 wks
- 13.8 MBq/vial is delivered from Norway to global→ At the time of certification, it will be 6 MBq / 6 mL / 1 vial
- After ^{223}Ra separation from the parent nuclide ^{227}Ac, the next milking is possible again about 1 month (≒4wks) later the 3 half-life (3 x 11.435d) of ^{223}Ra.
- If ^{223}Ra is prescribed weekly to 100 patients worldwide, then approximately 15 MBq x 100 patients = 1.5 GBq is required. Note that the 1.5 GBq of ^{223}Ra should only be used for half a year for certain 100 patients. After 25 weeks (= half a year), the ^{223}Ra will be used for the next 100 patients. In fact, we need 1.5GBq of ^{223}Ra every week
- To get ^{223}Ra for 25 weeks for 50,000 (=100 x 25 x 2) patients, we need 25 times of 1.5GBq of ^{227}Ac, that is 37GBq.

PNNL separated 44GBq&5GBq of ^{227}Ac from ^{227}Ac/Be neutron source and sold to Bayer

In the United States, around 350,000 people die each year from bone metastasis (Weilbaecher KN, Guise TA, McCauley LK. Cancer to bone: a fatal attraction. Nat Rev Cancer 2011;11:411-25).

Current and potential production method of ^{225}Ac

	Production Method	Facility	Capabilities	Monthly ^{225}Ac Production [GBq (Ci)]
Current Sources	^{229}Th generator	ORNL	0.704 g (150 mCi) of ^{229}Th	2.2 (0.06)
		ITU	0.215 g (46 mCi) of ^{229}Th	1.1 (0.03)
		IPPE	0.704 g (150 mCi) of ^{229}Th	2.2 (0.06)
Potential Future Sources	^{232}Th(p,x)^{225}Ac (^{227}Ac co-produced)	TRIUMF	500 MeV, 120 μA	11266.5 (304.05)
		BNL	200 MeV, 173 μA	2675.84 (72.32)
		INR	160 MeV, 120 μA	1002.0 (27.08)
		Arronax	70 MeV, 2×375 μA	462.1 (12.49)
		LANL	100 MeV, 250 μA	12.00
		iThemba LABS	66 MeV, 250 μA	127.7 (3.45)
	^{226}Ra(p,2n)^{225}Ac	20 MeV, 500 μA cyclotron		3983.1 (107.65)
		15 MeV, 500 μA cyclotron		1157.4 (31.28)
	ISOL	TRIUMF (existing)		0.37 (0.01)
		TRIUMF (potential upgrades)		190.6 (5.15)
	^{226}Ra(γ,n)^{225}Ra	medical linac	18 MeV, 26 μA	48.1 (1.3)
		ALTO	50 MeV, 10 μA	55.5 (1.5)
	^{226}Ra(n,2n)^{225}Ra	fast breeder reactor		~37 (1)

^{229}Ra (15 d) → β→ ^{225}Ac (9.9d)

The table is taken from AKH Robertson, Ph.D thesis 2020 (Univ. British Columbia)

US Nuclear Science Advisory Committee - Isotopes [NSAC-I] Subcommittee Reports

U.S. DEPARTMENT OF ENERGY — Re-organizing the Isotope Program

The changes to the program have been substantial

- Created Research and Development Program for new and improved isotope production techniques
- Introduced peer review into mode of operations
- Restructured the federal organization of the program
- Created the National Isotope Development Center
- Charged NSAC to set priorities for research opportunities and to develop a long-term strategic plan for isotope production and development.

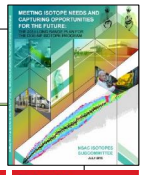

http://science.energy.gov/np/research/idpra/

^{225}Ac is the isotope that should be produced with the highest priority, followed by ^{211}At.

Production facilities of α-emitter in the US

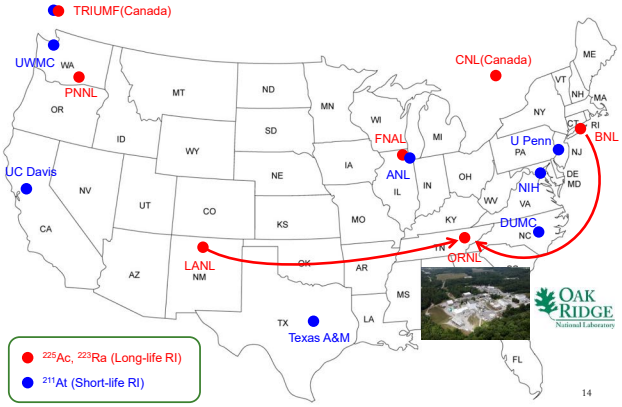

Domestic ^{225}Ac production Current status & future plan

- ^{229}Th→^{225}Ac : Tohoku Univ.
- Purchase from overseas (USDOE etc.)
- ^{226}Ra(p,2n) ^{225}Ac: QST, NMP, JRIA
- ^{226}Ra(g,n) ^{225}Ra→^{225}Ac : Hitachi, UTokyo

Not able to meet the demand at all!

http://www.aec.go.jp/jicst/NC/linkai/teirei/siryo2019/siryo22/1.pdf

https://www.nmp.co.jp/news/assets/files/pdf/press_release/Press%20Release_191011_Theranostics.pdf

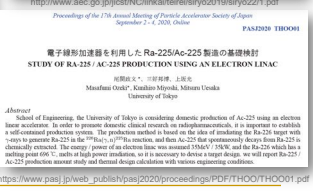

https://www.pasj.jp/web_publish/pasj2020/proceedings/PDF/THOO/THOO01.pdf

Target and projectile for production of alpha emitters

Target	Projectile	Product
^{209}Bi stable(2.01×10^{19} y)	^{4}He	^{211}At
	^{6}Li	^{211}Rn
	^{7}Li	^{211}Rn
^{226}Ra 1600 y	e	^{225}Ra→^{225}Ac
	n (thermal)	^{227}Ac, ^{228}Th, ^{229}Th
	n (fast)	^{225}Ra→^{225}Ac
	p (low)	^{225}Ac
	d	^{225}Ac
^{230}Th 7.54×10^{4} y	e	^{229}Th
	n (fast)	^{229}Th
	p (low)	^{229}Pa→^{229}Th, ^{230}Pa→^{230}U
	^{3}He	^{230}U
^{231}Pa 3.276×10^{4} y	n (fast)	^{230}Pa→^{230}U
	p (low)	^{230}U
	d	^{230}U
^{232}Th 1.40×10^{10} y	e (high)	^{211}At, ^{211}Rn, ^{223}Ra, ^{225}Ac, ^{227}Th, ^{230}Pa→^{230}U
	p (low)	^{230}Pa→^{230}U, ^{229}Pa→^{229}Th
	p (high)	^{211}At, ^{211}Rn, ^{223}Ra, ^{225}Ac, ^{227}Th, ^{230}Pa→^{230}U
	d	^{230}Pa→^{230}U, ^{229}Pa→^{229}Th

Astatine-211: a promising α-emitter

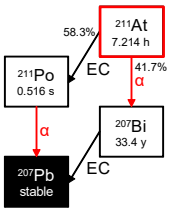

Decay scheme of ^{211}At

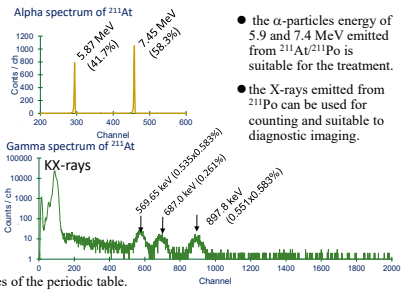

- the α-particles energy of 5.9 and 7.4 MeV emitted from ^{211}At/^{211}Po is suitable for the treatment.
- the X-rays emitted from ^{211}Po can be used for counting and suitable to diagnostic imaging.

- Belongs to Halogen series of the periodic table.
- its half-life is long enough for radiolabeling to make an Astatinated radiopharmaceuticals.
- its half-life is suitable for deposit an effective dose in vivo when the At labelled peptide or immunoconjugate used.

^{211}At is available in Japan

Manufacturing facilities	Production route and Separation metod	Production	The main contributor of ^{211}At manufacturing
Research Center for Nuclear Physics(RCNP), Osaka University	^{209}Bi(α,2n)^{211}At Dry distillation	More than Two decades	Dr. Atsushi Toyoshima Prof. Atsushi Shinohara
Takasaki Ion Accelerators for Advanced Radiation Application(TIARA), Takasaki Advanced Radiation Research Institute, National Institutes for Quantum and Radiological Science and Technology(QST)	^{209}Bi(α,2n)^{211}At Dry distillation	Since 2012	Dr. Shigeki Watanabe Dr. Noriko S. Ishioka
Quantum Medical Science Directorate, National Institute of Radiological Sciences(NIRS), National Institutes for Quantum and Radiological Science and Technology(QST)	^{209}Bi(α,2n)^{211}At Dry distillation	Sine 2013	Dr. Katsuyuki Minegishi Dr. Kotaro Nagatsu
Nishina Center for Accelerator-Based Science, Institute of Physical and Chemical Research(Riken)	^{209}Bi(α,2n)^{211}At Dry distillation	Since 2015	Dr. Hiromitsu Haba
Advanced Clinical Research Center(ACRC), Fukushima Medical University(FMU)	^{209}Bi(α,2n)^{211}At Dry distillation	Since 2016	Dr. Kohshin Washiyama Prof. Kazuhiro Takahashi
The tandem accelerator facility, Nuclear Science Research Institute, Japan Atomic Energy Agency(JAEA)	^{209}Bi(^{7}Li,5n)^{211}Rn/^{211}At Dry & Wet chemistry	Since 2011	Dr. Ichiro Nishinaka Dr. Kazuyuki Hashimoto

Production facilities of α-emitters in Japan

- ^{211}At production facilities (5 places)
- ^{211}Rn production facility (1 place)
- User facilities including production (more than 13 places)

Short-lived RI supply platform program (since 2016)

This program will provide stable supply of research radioisotopes throughout the year and technical support for safe handling.

1. Supply of short life isotopes that cannot be purchased from the commercial base.
2. A prompt and stable supply by the world's highest level of accelerator facility association.
3. Support for the promotion of basic research in a wide range of fields: ex. Development of probes for next generation PET, development of next generation therapeutic drugs, metabolic research of biological trace elements, etc.

- Research Center for Nuclear Physics[RCNP], Osaka University (Osaka)
- Nishina Center for Accelerator-Based Science, Riken (Tokyo)
- Cyclotron and Radioisotope Center [CYRIC], Tohoku University (Sendai)
- Research Center for ELectron PHoton Science (ELPH), Tohoku University (Sendai)
- TIARA, Takasaki QST (Takasaki)
- Quantum Medical Science Directorate,NIRS, QST (Chiba)

^{7}Be, ^{11}C, ^{18}F, ^{15}O, ^{24}Na, ^{28}Mg, ^{38,39}Cl, ^{38,42,43}K, ^{43,46,47}Sc, ^{44}Ti, ^{48}V, ^{55}Fe, ^{56,57,58}Co, ^{57}Ni, ^{61,64,67}Cu, ^{74}As, ^{83,84,86}Rb, ^{86,87,90}Y, ^{88,89,89m,95}Zr,….^{207}Bi, ^{207,210,211}At, ^{213}Fr, ^{238}Np, ^{255}Md

Fukushima Medical University

For the purpose of nurturing medical professionals who will contribute to the promotion of health, medical care and welfare of the citizen of Fukushima Prefecture. And to contribute to the community and the welfare of humanity through advances made in medicine, nursing and related areas.

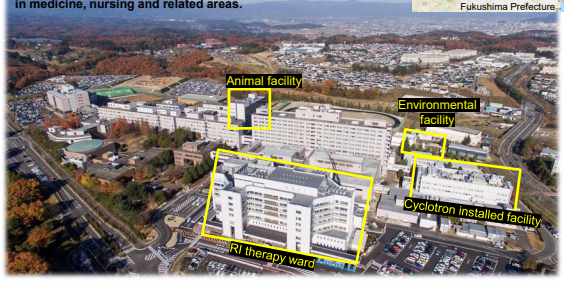

Monthly production of ^{211}At at FMU

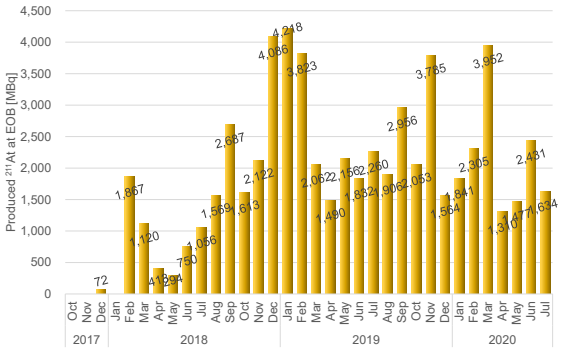

Clinical trials using ^{211}At planned in Japan

Osaka Univ.

- [^{211}At]-NaAt
- Phase-1
- Thyroid Cancer
- 2021~2023

Fukushima Medical Univ.

- meta-^{211}At-astato-benzylguanidine (^{211}At-MABG)
- Phase-1
- Pheochromocytoma
- 2022?~

How to choose the appropriate alpha emitters for Japanese TAT?

Nuclear Physician

- Evidenced based therapeutic effect
- Suitable pharmacokinetics for labelled compound

Radiochemist

- Target availability
- Modality or stockpile availability
- Easy handling
- Well-understood chemical characteristics

Summary

- With the development of medicine, TAT has attracted attention as a treatment potential method that can fully cure cancers.
- Clinical use of various α-emitters is being attempted worldwide.
- Most of the useful alpha emitters have no stable isotopes. Therefore, there have several ways to produce alpha emitters such as using Th-229 (U-233) and Ac-227 that have been stored so far, or using U and Th as starting materials for nuclear reactions.
- ^{225}Ac labeled with PSMA-617, which has been shown to be therapeutic in clinical trials, has often been isolated from 229Th, but cannot meet the increasing global demand.
- At DOE and TRIUMF in Canada, they try to manufacture by the Th spallation reaction to meet the demand.
- In Japan, the ^{226}Ra(p,2n)^{225}Ac and ^{226}Ra(g,n)^{225}Ra → ^{225}Ac reactions has been attempted at QST National Institutes for Quantum and Radiological Sciences, Nihon Medi-Physics, Hitachi, etc.
- ^{211}At is an alpha-emitting nuclide and its target is a Bi element that can be purchased easily. In Japan, manufacturing and basic research are underway at six facilities, including Fukushima Medical University.
- In accelerator manufacturing, it is important to avoid supply outages due to periodic inspections and accidental trouble of the accelerator, and the short-life RI supply platform is an attempt that has a complementary function.
- Clinical trials using At are scheduled to begin within a few years at the two facilities of Osaka University and Fukushima Medical University.
- The nuclear medicine side is demanding a drug (≠ RI) that has been shown to have a therapeutic effect.
- The RI manufacturing side is exploring manufacturing from the viewpoint of materials, accelerators, and separation and purification methods.

FUKUSHIMA MEDICAL UNIVERSITY Advanced Clinical Research Center

3.8　Y. Kawabata（KURNS, Kyoto Univ.）

Current status and future plans of our institute

3.9 T. Yamamura（KURNS, Kyoto Univ.）

Actinide researches using KUR hot-lab

Topical meeting on Condensed-matter Chemistry on Actinides
(The Kumatori meeting 2021)

Actinide researches using KUR hot-lab

Tomoo Yamamura, KURNS, Kyoto Univ.
13:15-13:30, Feb. 10, 2021

1. Scientific fields required in KUR-HL

Diversity required for Nuclear research

- **The role of research: Provide the public with choices**
  - Direct disposal, TRU burning in fast reactors, ADS, HTGR, Th fuel, etc.
  - Approach of the French radioactive waste law (Bataille law)
- **Broad technology as an option**
  - Direct Disposal, Advanced Reprocessing including MA management, ADS, Radiation Safety Research, Neutron Beam Science, Nuclear Medicine, MA for isotope battery

Power and neutron flux of Fukui reactor: beam reactor

ref. IAEA RRDB(Research Reactor Database)

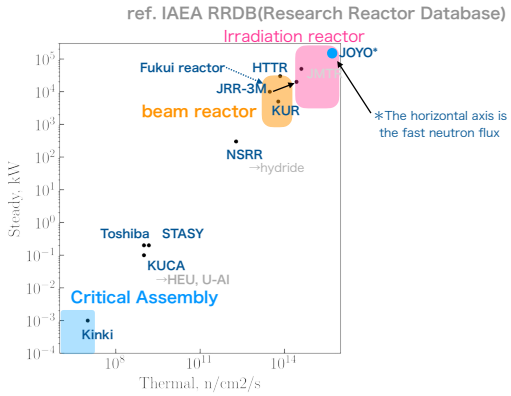

Thermal neutron flux and power of research reactors in Japan

The future of irradiation and research reactors

- **What can be done with a medium-sized reactor? (KUR→Fukui Reactor)**
  - 10 MW: Aiming to be an competitive neutron source
  - **Possible applications** :
    - **Neutron beam applications** (diffraction, scattering, reflection, radiography, etc. → crystal structure, magnetic structure, amorphous structure, dynamics, excitation, relaxation)
    - **RI production** (including medical use), **activation analysis**
    - **Neutron radiography** (flow visualization, etc.)
  - **Multipurpose reactors** (prior examples): OPAL (Australia, 20 MW) and BR2 (Belgium) are very actively used.
  - **Selection of fuel materials** (U_3Si_2, U-Mo, etc.) → Reprocessability is an issue
- **MA Research, Irradiation behavior of fuels and materials**
  - Promotion of fundamental research by complementing experimental and computational research, which is also possible with medium-sized reactors
  - **Possible experiments** :
    - Focus on **microscopic scales** and introduce **microscopic and spectroscopic methods**
    - Experiments to enable **highly radioactive** Pu-containing and irradiated samples

Time scenario to process MA

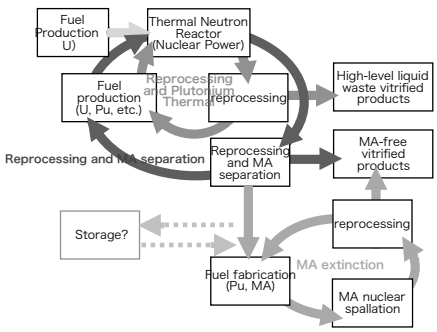

2. Possible plans in KUR-HL

Eco system around KUR-HL

	Domestic	KURNS	Abroad
Nucl. med.	IMR, Tohoku U. (Sendai, Oarai) ・Fukushima Medical U. ・National Cancer Center ・Grad. Sch. Sci., Osaka U. ・Inst. Rad. Sci., Osaka U.	・Particle Therapy Application Unit (Prof. M. Suzuki, et al.) ・LINAC, Cyclotron (Prof. H. Tanaka, Prof. K. Takamiya, et al.) ○RI production of nucl. med., pharmaceuticals, animal exp.	・EU JRC Karlsruhe ・→Hamburg U. Med. School ・Isotope (Russia)
Nucl. power Rad. waste Debris	・Nagaoka U. Tech. ・Tokyo Inst. Tech. ・Kinki U. ・Tohoku U. ・JAEA FMS	(Prof. K. Kurosaki) ○(Irradiation) exp. using nuclear fuel, MA	・Idaho NL (US) ・CEA
Condensed-matter phys.	・Hokkaido U. ・ASR, JAEA ・SPring-8 ・KEK	○Nuclear fuel sample prep.	・U. Lisbon, Portugal ・C2TN Nuclear Research Institute ・Charles U., Czeck
Relativistic quantum chem.	・Tokyo Met. U.	○Precise calc., theoretical support for heavy element systems	・Paul Sabatier Univ.

○Expectations to KURNS
○Items KURNS can offer

◎Human Resource Development
◎Experimental environment
◎Theoretical verification & discussions

Interactions-Scales Map: A Strategy of Condensed-matter Chemistry

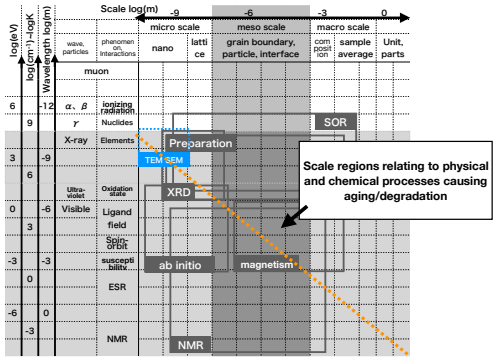

*Analysis is possible with probes of wavelengths below the scale (gray shading).

Nuclear medicine is the descendant of radionuclides in radioactive waste.

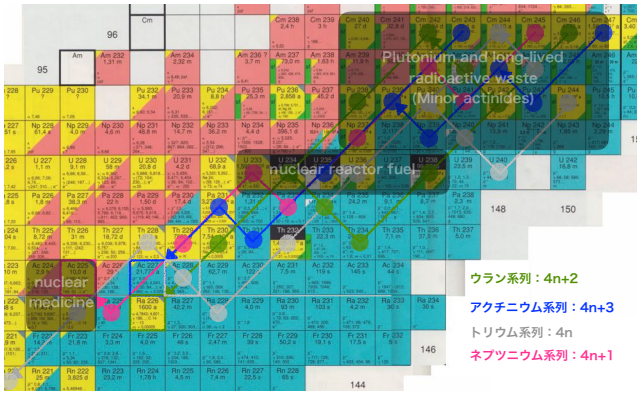

3. Activities required for TAT

Striking therapeutic effect of ^{225}Ac on primary prostate cancer

C. Kratochwil, et al., J. Nucl. Med., 57 (2016) 1941.

Humanitarian use for two terminally ill cancer patients (no other means available)

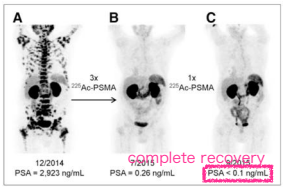

FIGURE 1. ^{68}Ga-PSMA-11 PET/CT scans of patient A. Pretherapeutic tumor spread (A), restaging 2 mo after third cycle of ^{225}Ac-PSMA-617 (B), and restaging 2 mo after one additional consolidation therapy (C).

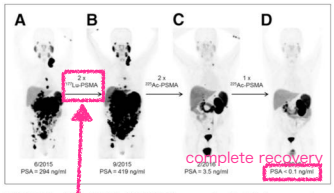

FIGURE 3. ^{68}Ga-PSMA-11 PET/CT scans of patient B. In comparison to initial tumor spread (A), restaging after 2 cycles of β-emitting ^{177}Lu-PSMA-617 presented progression (B). In contrast, restaging after second (C) and third (D) cycles of α-emitting ^{225}Ac-PSMA-617 presented impressive response.

Beta nuclides have no therapeutic effect.

The raw material for this 225Ac is 233U, a nuclear waste product of thorium reactor research. Supplied to the University of Heidelberg by the EU Joint Research Center, Germany.

Nuclear medicine: Practical application requires cooperation from various fields

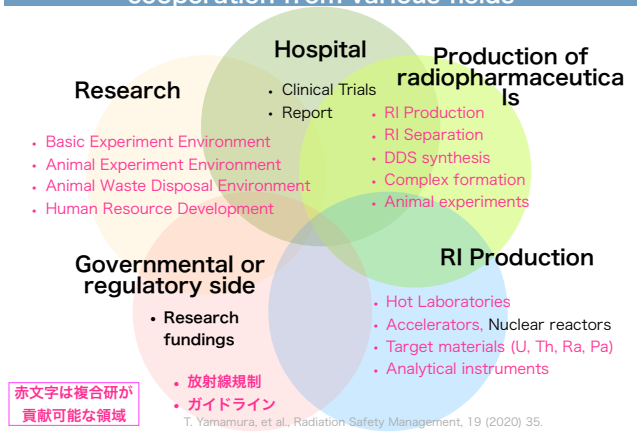

T. Yamamura, et al., Radiation Safety Management, 19 (2020) 35.

Foreign suppliers will go to large-scale manufacturing in a few years

Method	Reaction	Supplier	Country	Capacity	Productivity	Comment
Generator from ^{229}Th	^{229}Th→^{225}Ra→^{225}Ac	JRC	EU		11 GBq (300 mCi)/y	International Drug Development Center for Ac-225
		ORNL	US		140 mCi/y	
		Obrinsk	Rus		15.5 GBq/yだが、余り切れ	Th-232→Ra-228(n,γ)Ra-229→Ac-229→Th-229→Ra-225→Ac-
		CNL	Can	^{233}UO$_2$ 400g	^{229}Th 13mCi	
		TeraPower	US	^{229}Th 45g (370 GBq)		Founded by Bill Gates
^{226}Ra photonucl. reaction	Ra-226(γ,x)Ac-225	NIOWAVE	US	^{226}Ra several hundred mCi	2020年9月以降、370 GB/y目指す	
		TRIUMF	Can		理論的上限：74 TBq/m	
nuclear spallation	Th-232(p,x)Ac-225/Ac-227	Tri-Lab Team	US		Stage I (2016.6-2017.10): 50-60mCi	ORNL+BHNL+LANL+NIDC ^{227}Ac contamination be clearable
		TRIUMF	Can		将来、82Ci/m目指す	
		Inst. Nucl. Res.	Rus		2Ci/y を目指す	^{227}Ac removal is a challenge
		Northstar社	US		100mCi/y目指す	
^{226}Ra photonucl. reaction	Th-226(3n,2β)Th-229→Ra-225→Ac-225	ORNL (HFIR)	US			Inefficient, too much ^{228}Th, ^{227}Ac contamination.
^{226}Ra proton irr.	Ra-226(p,x)	JRC	EU			Patented, high yield, high
		SCK-CEN	Berg	226Ra 数百g	2019より1Ci/w	GMP grade
		ZAG Karlsruhe	Ger		400mCi/100h	
		KIRAMS	Korea			

Technical Meeting: Joint IAEA-JRC Workshop on the "Supply of Actinium-225"

Drug Delivery System for Targeted Alpha Ray Therapy

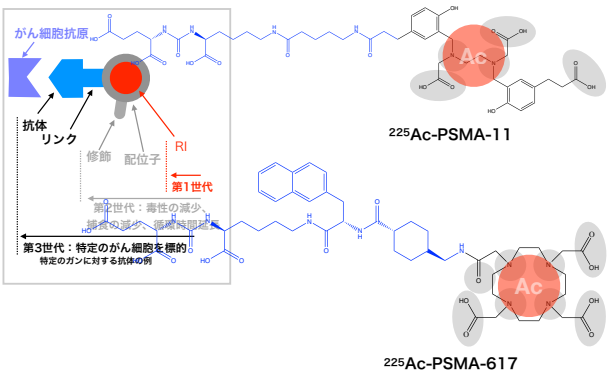

1F of the Innovation Building has a section designed as a chemistry laboratory

Copyright protected content

^{177}Lu（$T_{1/2}$=6.7 d）

- Purpose
  - Peptide receptor nuclear medicine internal use therapy (neuroendocrine tumor, prostate cancer)
- Production
  - Direct method：^{176}Lu(n, γ)^{177}Lu
    - Highly concentrated, products used as is = ready to use
    - 1e14 cm-2s-1、480 GBq for 30 days
  - Indirect method：^{176}Yb(n, γ)^{177}Yb→^{177}Lu
    - Highly concentrated raw material, requires advanced chemical purification（DGA、BioRad AG 50W-X8）
- Only reactors with high neutron flux are economically viable

^{64}Cu（$T_{1/2}$ = 12.7 h）

- 陽電子を放出
- 用途
  - 治療とPET
- 製造法
  - 原子炉：^{63}Cu(n, γ)^{64}Cu
  - LINAC：^{65}Cu(γ,n)^{64}Cu

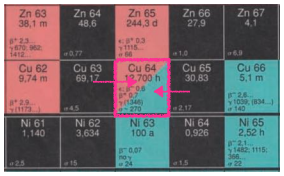

Recent trends

- Japan RI Association
  - Th-232→Th-228 → Ra-224
- IAEA Meeting (2019.12)
  - Nuclear Medicine of Th-227（Bayer）
  - Classified as nuclear fuel in Japan, but measures to make it usable are being considered.

4. Improvements of KUR-HL

Status of KUR Hot-lab

Copyright protected content

3.10 M. Suzuki（KURNS, Kyoto Univ.）

The Future of Cyclotron-Based BNCR Research

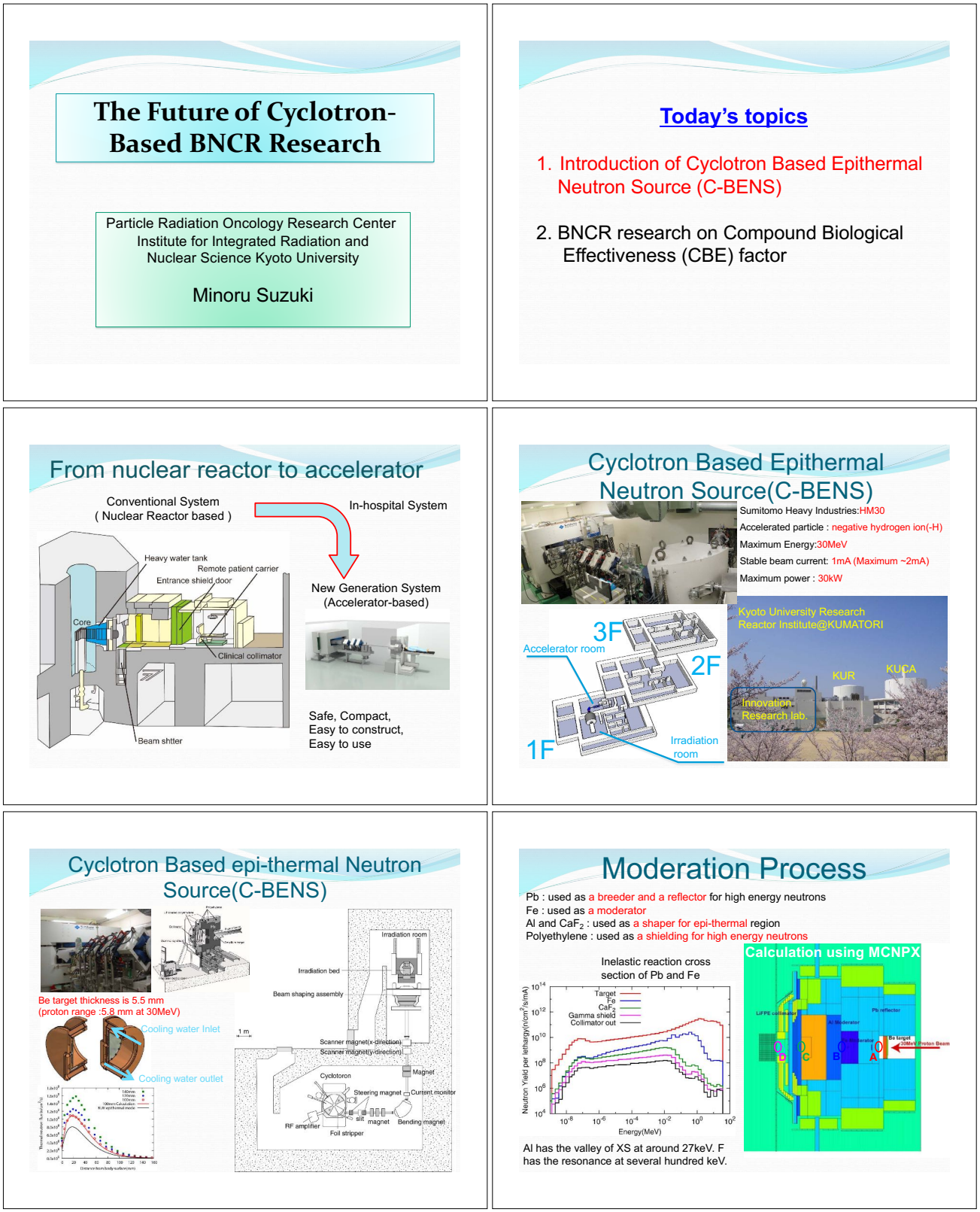

Kansai BNCT Medical Center
Southern TOHOKU BNCT Research Center

Osaka Medical College
Kansai BNCT Medical Center

http://southerntohoku-bnct.com/method.html

Pharmaceutical approval approach of C-BENS @KURNS

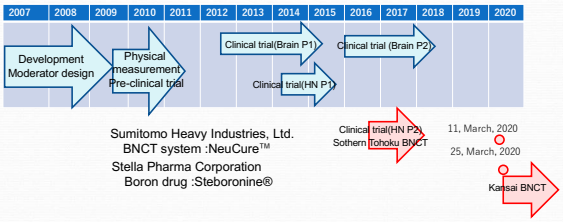

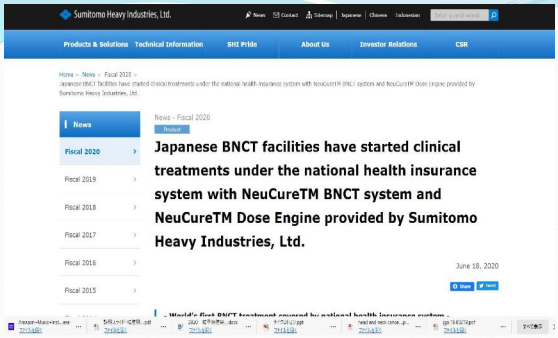

Sumitomo Heavy Industries, LTD HP

Today's topics

1. Introduction of Cyclotron Based Epithermal Neutron Source(C-BENS)

2. BNCR research on Compound Biological Effectiveness (CBE) factor

BNCR: Boron Neutron Capture Radiation (Reaction)

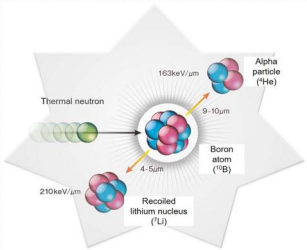

Fig.1 Boron capture neutron reaction（Boron neutron capture irradiation）
Nonradioactive isotope 10B atoms that absorb low-energy (<0.5 eV) neutrons (thermal neutrons) disintegrate into an alpha (4He) particle and a recoiled lithium nucleus (7Li). These particles deposit high energy along their very short path (<10 μm).

Normal tissues consist of three-type cells

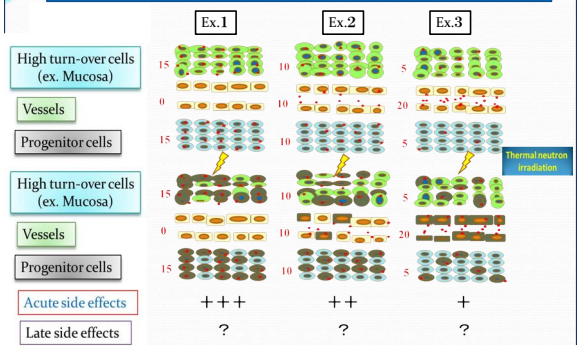

Dose estimation in BNCT

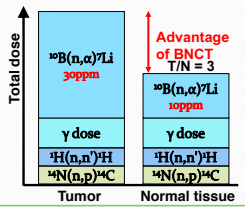

- Physical dose (Gy) = Dose[$^{10}B(n,\alpha)^7Li$] + Dose[γ dose] + Dose[$^1H(n,n')^1H$] + Dose[$^{14}N(n,p)^{14}C$]

- Physical dose (Gy) = Dose[$^{10}B(n,\alpha)^7Li$] + Dose[Thermal beam]

Tsubasa Watanabe et al. Cancer Letters 2016;370:27-32.cc

RBE: Relative Biological Effectiveness

$$RBE = \frac{D_x}{D_R}$$

$$D_x = RBE \times D_R$$

where D_X is a reference absorbed dose of radiation of a standard type X, and D_R is the absorbed dose of radiation of type R that **causes the same amount of biological damage.**

CBE: Compound Biological Effectiveness

$$CBE = \frac{D_x}{D^{10}_{B(n,\alpha)^7Li}}$$

$$D_x = CBE \times D^{10}_{B(n,\alpha)^7Li}$$

- Physical dose (Gy) in BNCT: Dose[$^{10}B(n,\alpha)^7Li$] + Dose[Thermal beam]

X-ray ED_{50} (Gy) = ($^{10}B(n, a)^7Li$ ED_{50} x CBE)+(Thermal beam ED_{50} x RBE) (Gy)

*ED50: Effective dose 50

$$\text{CBE factor} = \frac{\text{X-ray ED50- (Thermal beam ED50 x RBE)}}{^{10}B(n,\alpha)^7Li\ ED50}$$

Distribution of L-BPA and BSH

Introduction

GM Morris et al. Br J Cancer 2000;82:1764.

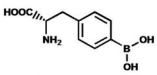

L-BPA (Boronophenylalanine)

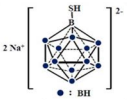

BSH ($Na_2B_{12}H_{11}SH$)

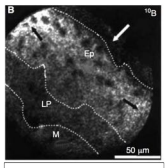

Distribution of L-BPA in tongue mucosa (L-BPA 500mg/kg i.v.)

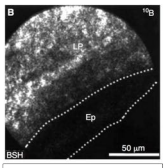

Distribution of BSH in tongue mucosa (BSH 100mg/kg i.v.)

CBE factor

	Brain	Skin	Mucosa	Lung	Hepatocyte
BPA	1.35	2.5	4.9	2.3	4.25
BSH	0.37	0.8	0.3	-	0.94

α–ray and β-ray in tissues

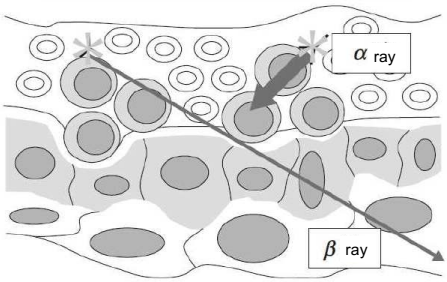

Hosono M. Isotope News 2013.7

BNCR research on CBE factor may bring about some insight in targeted alfa therapy research.

Ex) High-resolution alfa-autoradiography has been used in our laboratory.

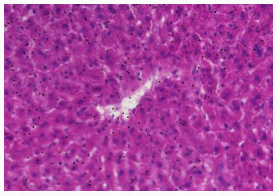


Thank you for your attention

3.11 T. Kitazawa（Dept. Chem., Toho Univ.）

Synthesis and Crystal Structures of Three New Complexes Constructed with Uranyl(VI)-acetylacetonate and Uranyl(VI)-nitrate

Synthesis and Crystal Structures of Three New Complexes Constructed with Uranyl(VI)-acetylacetonate and Uranyl(VI)-nitrate

Department of Chemistry, Faculty of Science, Toho University

Takafumi Kitazawa, Takeshi Kawasaki

Contents

Introduction

- The coordination chemistry of the actinides has potentially been linked to the reprocessing of nuclear fuels and treatment of actinide wastes in the backend chemistry for nuclear power plants.
- The fundamental investigation of the bonding and structure of actinide complexes provides important information on the field of backend chemistry.
- Actinide ions of high oxidation number X (≥ +5) tend to become liner structural actinyl(X) ion $An^{X}O_2^{X-2}$.
- The actinyl(X) ion's coordination geometry is often octahedral 6-coordination, pentagonal-bipyramidal 7-coordination or hexagonal-bipyramidal 8-coordination geometry.

octahedral pentagonal-bipyramidal hexagonal-bipyramidal

T. Kawasaki, T. Nishimura, T. Kitazawa, *Bull. Chem. Soc. Jpn.* **83**, 1528, 2010.

Introduction

- Uranyl(VI) *β*-diketonates with neutral donor ligands and uranyl(VI) complexes with multidentate *N*-heterocyclic ligands have been extensively studied due to their importance in the separation of uranium by solvent extraction.

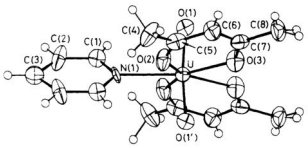

Example of uranyl *β*-diketonates with neutral donor ligands: $[UO_2(acac)_2py]$

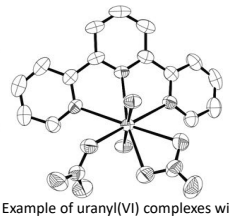

Example of uranyl(VI) complexes with multidentate *N*-heterocyclic ligands: $[UO_2(NO_3)_2(terpy)]$

N. W. Alcock, et al., *J. Chem. Soc. Dalton Trans.* 679, 1984.
N. W. Alcock, et al., *Acta Cryst. C***43**, 1476, 1987.

I. A. Charushnikova, et al., *Russ. J. Cood. Chem.* **30**, 511, 2004.

Introduction

- Np–O bond distance of the neptunium compounds is shorter by 0.01 Å than that of analogous uranium compounds.
- When discussing the structures of Np compounds, the 0.01 Å shorter difference has been used.
- However, single crystal data for $[UO_2(acac)_2py]$ reported in 1984 [1] may be strange.
  - The U=O_{yl} bond length in [1] is 1.83(1) Å, although the Np=O_{yl} length is 1.78(1) Å [2].
  - The O_{yl}=Np=O_{yl} bond angle of $[NpO_2(acac)_2py]$ is 176.5(19) [2], although [1] noted that the O_{yl}=U=O_{yl} for the large deviation from linearity of the O_{yl}=U=O_{yl} bond angle, 173.5(8).
- We had re-determined the crystal structure of $[UO_2(acac)_2py]$. The newly obtained U=O_{yl} bond length of 1.77 (1) Å was now reasonable, and the O_{yl}=U=O_{yl} linearity was similar to the O_{yl}=Np=O_{yl} in $[NpO_2(acac)_2py]$. [3]

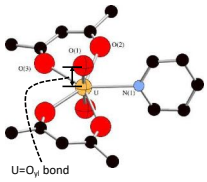

U=O_{yl} bond

Molecular Structure of $[UO_2(acac)_2py]$

[1] N. W. Alcock, et al., *J. Chem. Soc. Dalton Trans.* 679, 1984.
[2] N. W. Alcock, et al., *Acta Cryst. C***43**, 1476, 1987.
[3] T. Kawasaki, T. Kitazawa, et al., *Hyperfine Interact.* **166**, 417, 2005.

Background

Comparison of lattice parameter for $[UO_2(acac)_2py]$

	*Alcock et al.	*Kawasaki
Crystal system	orthorhombic	orthorhombic
Space group	Fdd2(#2)	Fdd2(#2)
a (Å)	29.702(4)	11.432(3)
b (Å)	11.433(2)	29.708(5)
c (Å)	10.593(2)	10.598(4)
V (Å^3)	3597.3(10)	3599(1)
U-O_{uranyl} av.(Å)	1.83	1.77
U-N (Å)	2.47(1)	2.602(3)
O-U-O (°)	173.5(8)	178.3(2)
py twist (°)	45	42

*N.W. Alcock et al. *J. Chem. Soc., Dalton Trans.* 679-681.(1984).

T. Kawasaki, T. Kitazawa, et al., *Hyperfine Interact.* **166**, 417, 2005

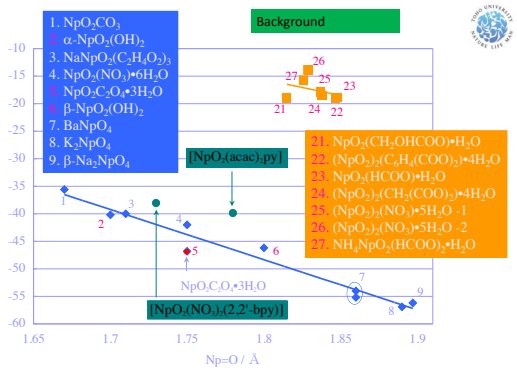

Plot of δ against Np=O bond distance for the neptunyl compounds

copyright protected content

Background

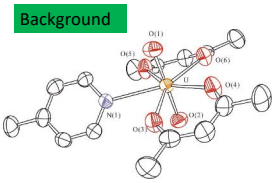

[UO_2(acac)$_2$(4-Mepy)]

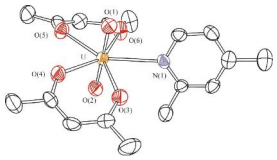

[UO_2(acac)$_2$(2,4-dmpy)]

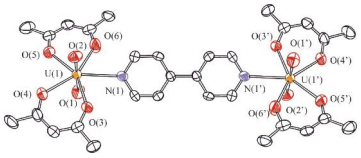

{[UO_2(acac)$_2$]$_2$(4,4'-bpy)}

Background

Bond lengths, angles, and pyridine twist for [UO_2(acac)$_2$L] complexes

	U-O_{uranyl} av. (Å)	U-O_{acac} av. (Å)	U-N (Å)	O=U=O (°)	py twist (°)
py[a)]	1.77	2.36	2.602(3)	178.3(2)	42
4-Mepy[a)]	1.78	2.35	2.614(6)	179.2(2)	42.5
2,4-dmpy[a)]	1.78	2.36	2.648(9)	179.2(4)	69.4
4,4'-bpy[a)]	1.77	2.34	2.66(1)	179.3(4)	41.7
4-Etpy	1.77	2.35	2.605(3)	179.1(1)	43
nic site-1	1.78	2.36	2.57(1)	178.1(4)	64
nic site-2	1.77	2.33	2.62(1)	177.5(4)	59

Introduction

- The vast majority of uranyl(VI) complexes feature a linear uranyl group (e.g., O_{yl}=U=O_{yl} : 180 °).
- However, there are a handful of complexes that feature much more acute O_{yl}=U=O_{yl} angles.

Example of uranyl(VI) complex with bent O_{yl}=U=O_{yl} angle

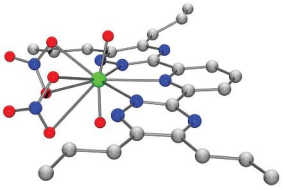

Molecular Structure of [$UO_2(NO_3)_2$(^{n}Pr-btp)]
O_{yl}=U=O_{yl} : 166.2(1) °

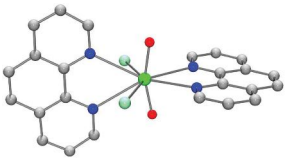

Molecular Structure of [UO_2Cl_2(phen)$_2$]
O_{yl}=U=O_{yl} : 161.8(1) °

* ●: uranium, ●: oxygen, ●: nitrogen, ●: carbon, ●: chlorine

T. W. Hayton, *Dalton Trans.* **47**, 1003, 2018.

Introduction

- ^{237}Np Mössbauer spectroscopy is a very powerful tool for structural studies, since the hyperfine parameters are significantly influenced by the electronic structure of the Np site.
- The ^{237}Np Mössbauer isomer shifts (δ) are range from +40 to -80 mm s^{-1} relative to $NpAl_2$ at 4.2 K, and are clearly correlated with the oxidation state of neptunium.
- The correlation between the δ value and coordination number (CN) of the Np atom has also been found for the Np(VI) compounds.

copyright protected content

T. Kawasaki, T. Kitazawa, et al., *Hyperfine Interact.* **166**, 417, 2005.
J. Wang, T. Kitazawa, et al., *J. Nucl. Sci. Tech.* suppl**3**, 429, 2002.

^{237}Np Mössbauer spectra of
(a) NpO_2, (b) $NpO_2(OH_2)$·xH_2O,
(c) $NH_4[NpO_2(NO_3)_3]$,
(d) $NpO_2C_2O_4$·$3H_2O$ at 10 K

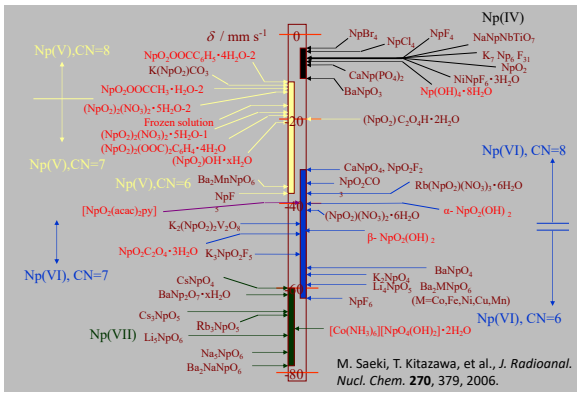

M. Saeki, T. Kitazawa, et al., *J. Radioanal. Nucl. Chem.* **270**, 379, 2006.

^{237}Np δ in various neptunium compounds from tri- to hepta-valent states. Relative to $NpAl_2$.
Red data are obtained by JAERI (Currently known as JAEA)

Introduction

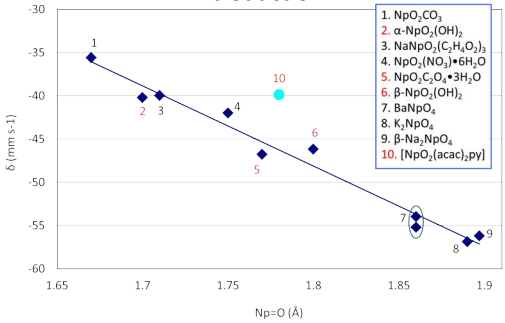

Plot of δ vs Np=O bond distance for the neptunyl(VI) compounds

T. Kawasaki, T. Kitazawa, et al., *Hyperfine Interact.* **166**, 417, 2005.

Introduction

- The strong correlation between the δ value and the mean of neptunyl $Np=O_{yl}$ bond lengths has been reported for the oxo-coordinated Np(VI) compounds, where the increase in the δ value, corresponding to the decrease in the s electron density at the Np nucleus follows an increase in the mean neptunyl $Np=O_{yl}$ bond lengths.
  - Because these $Np=O_{yl}$ bond lengths are shorter than that of other oxygen atoms of the ligand, the shielding effect of the 5f electron associated with the $Np=O_{yl}$ bonds has a link to the 6s electron density which governs the δ value.
- Neptunyl(VI) complex of $[NpO_2(acac)_2py]$ is coordinated by one nitrogen atom of pyridine-type ligand. These δ values are slightly more positive than the correlation line.
  - The electron donation of the nitrogen atom in the pyridine may have a larger effect on the Np 5f orbital than that of the oxygen atom in the acac.
  - These δ values has a positive trend due to the increase in the shielding effect of the 6s electron and the decrease in the total 6s electron density at the Np nucleus.

T. Kawasaki, T. Kitazawa, et al., *Hyperfine Interact.* **166**, 417, 2005.

Introduction

Reported uranyl(VI) complexes by our laboratory

T. Kawasaki, T. Nishimura, T. Kitazawa, *Bull. Chem. Soc. Jpn.* **83**, 1528, 2010.
- $[UO_2(acac)_2L]$ (※ L = 4-Mepy, 4-Etpy, 2,4-dmpy, nic, imH)
- $[\{UO_2(acac)_2\}_2(4,4'\text{-bpy})]$
- $(bpy)_2H[UO_2(acac)(NO_3)_2]$

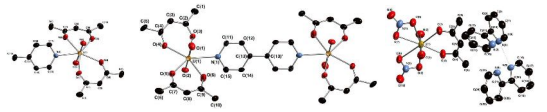

$[UO_2(acac)_2(4\text{-Mepy})]$ $[\{UO_2(acac)_2\}_2(4,4'\text{-bpy})]$ $(bpy)_2H[UO_2(acac)(NO_3)_2]$

T. Kawasaki, T. Kitazawa, *Acta. Cryst. E*, **64**, m673, 2008.
- $[UO_2(acac)_2(H_2O)]\cdot(pz)$

T. Kawasaki, T. Kitazawa, *Acta. Cryst. E*, **64**, m788, 2008.
- $[UO_2(acac)_2(4\text{-aldpy})]$

T. Kawasaki, T. Kitazawa, *Acta. Cryst. E*, **71**, m122, 2015.
- $[\{UO_2(NO_3)(terpy)\}_2O_2]$

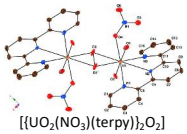

$[\{UO_2(NO_3)(terpy)\}_2O_2]$

Introduction

This study

Three uranyl(VI) complexes were synthesized using nitrogen-containing organic compounds, and were characterized crystallographically.

※Nitrogen-containing organic compounds

1,4-diazabicyclo[2.2.2]octane
(= DABCO)

2,3,5,6-tetramethylpyrazine
(= tmpz)

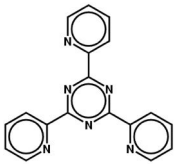

2,4,6-tris(2-pyridyl)-1,3,5-triazine
(= tptz)

Synthesis

Method 1

Hacac 3 mmol + N-comp 3 mmol
in solvent 5 ml

$UO_2(NO_3)_2\cdot6H_2O$ 1 mmol
in solvent 10 ml

slow evaporation at r.t.

Crystal

N-comp = DABCO
solvent = MeOH
↓
Complex I

tmpz
MeCN
↓
II

Method 2

tptz 0.5 mmol
in MeOH 10 ml

$UO_2(NO_3)_2\cdot6H_2O$ 0.5 mmol
in MeOH 10 ml

Crystal of complex III

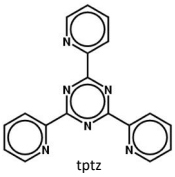

tptz

Crystal Data

complex	I	II	III
Empirical formula	$C_{15}H_{22}O_8U$	$C_{60}H_{96}N_{12}O_{24}U_3$	$C_{36}H_{28}N_{14}O_{10}U$
Formula weight	568.36	2083.58	1054.75
Temperature / K	253	298	90
Crystal system	Orthorhombic	Monoclinic	Triclinic
Space group	*Pnma*	*C2/m*	*P*-1
a / Å	18.087(3)	39.452(3)	8.1954(5)
b / Å	13.4746(19)	12.2398(8)	8.2338(5)
c / Å	7.9062(11)	8.8744(6)	14.4365(9)
α / °	90	90	83.9640(10)
β / °	90	100.913(3)	82.6810(10)
γ / °	90	90	84.7720(10)
V / Å^3	1926.9(5)	4207.8(5)	957.88(10)
Z	4	2	1
D_{calc} / g cm^{-3}	1.959	1.644	1.828
μ / mm^{-1}	8.458	5.830	4.315
F(000)	1072	2016	514
Reflections collected	13610	15693	7126
R_{int}	0.0567	0.0260	0.0115
Data / restraints / parameters	3006 / 0 / 221	5451 / 418 / 440	5311 / 0 / 285
GOF	1.187	1.068	1.099
R1, *wR2*	0.0410, 0.0933	0.0330, 0.1023	0.0198, 0.0520
$\Delta\rho_{max}$, $\Delta\rho_{min}$ e.Å^{-3}	2.496, -2.244	2.009, -0.558	1.490, -1.572

Crystal Structure of Complex I

Formula of Complex **I**: $[UO_2(acac)_2(Hacac)]$

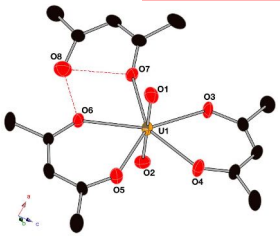

Asymmetric unit
(30 % probability level,
red dashed lines are hydrogen bonds,
H atoms are omitted)

U is pentagonal-bipyramidal 7-coordination

Selected bonds (Å) and angles (°)

U1-O1	1.785(10)
U1-O2	1.753(10)
U1-O3	2.355(9)
U1-O4	2.422(9)
U1-O5	2.377(9)
U1-O6	2.379(9)
U1-O7	2.361(9)
O1-U1-O2	178.4(5)

Hydrogen bonds (Å)

O8...O7	2.718(16)
O8...O6	3.136(15)

Crystal Structure of Complex I

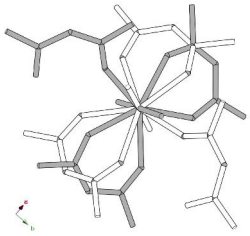

Disorder part (white) emerging from
asymmetric unit (gray) by symmetry operation _i

symmetry code _i : x,-y+1/2,z

Crystal Structure of Complex II

Formula of Complex **II**: $[UO_2(acac)_2(H_2O)]_2[UO_2(NO_3)_2(H_2O)_2]\cdot5(tmpz)$

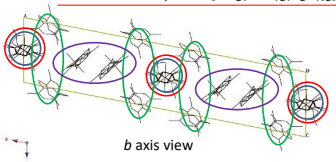

b axis view

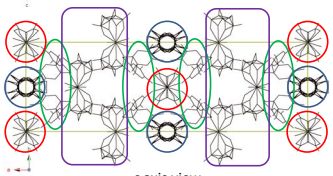

c axis view

Crystal structure of complex **II**

*
: $[UO_2(acac)_2(H_2O)]$
: $[UO_2(NO_3)_2(H_2O)_2]$
, : tmpz molecules

Crystal Structure of Complex II

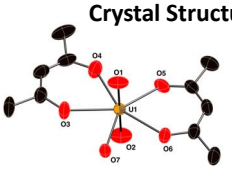

Asymmetric unit
(30 % probability level,
H atoms are omitted)

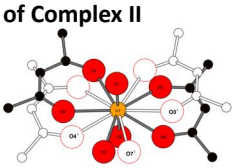

Disorder part (white) emerging
from asymmetric unit (gray)
by symmetry operation_i

symmetry code _i: x,-y,z

$[UO_2(acac)_2(H_2O)]$ molecule in complex **II**

U1 is pentagonal-bipyramidal 7-coordination

Selected bonds (Å) and angles (°) of $[UO_2(acac)_2(H_2O)]$ molecule

U1-O1	1.732(5)	U1-O5	2.317(7)
U1-O2	1.773(7)	U1-O6	2.327(6)
U1-O3	2.371(7)	U1-O7	2.446(6)
U1-O4	2.350(8)	O1-U1-O2	178.1(2)

Crystal Structure of Complex II

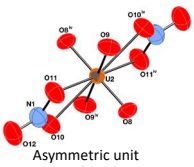

Asymmetric unit
(30 % probability level,
H atoms are omitted)

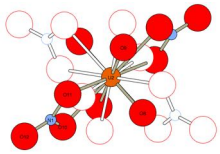

Disorder part (white) emerging
from asymmetric unit (gray)
by symmetry operations _ii and _iii

$[UO_2(NO_3)_2(H_2O)_2]$ molecule in complex **II**

U2 is hexagonal-bipyramidal 8-coordination

Selected bonds (Å) and angles (°) of $[UO_2(NO_3)_2(H_2O)_2]$ molecule

U2-O8	1.779(6)	U2-O11	2.525(7)
U2-O9	2.397(6)	O8-U2-O8_iv	180
U2-O10	2.502(6)		

symmetry codes _ii x,-y+1,z ; _iii -x+1,y,-z+1 ; _iv: -x+1,-y+1,-z+1

Crystal Structure of Complex II

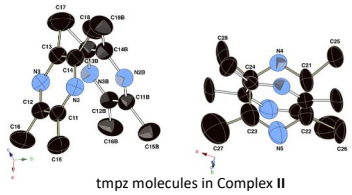

tmpz molecules in Complex **II**

molecular ratio in unit cell = 4 : 1

Hydrogen bonds (Å)	
O7…N3	2.788(10)
O7…N3_i	2.327(10)
O9…N2_v	2.726(11)

- The Complex **II** of formula $[UO_2(acac)_2(H_2O)]_2[UO_2(NO_3)_2(H_2O)_2]\cdot 5(tmpz)$ consists two crystallographically independent the tmpz molecules.
- These tmpz molecules are not coordinated to U atom.
- tmpz molecules are strongly disordered.

Crystal Structure of Complex III

Formula of Complex **III**: $[UO_2(NO_3)_2(H_2O)_2]\cdot 2(tptz)$ + solvent

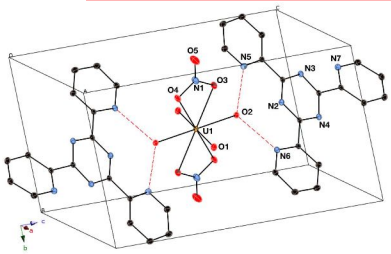

Selected bonds (Å)	
U1-O1	1.7687(16)
U1-O2	2.3667(15)
U1-O3	2.5305(17)
U1-O4	2.5332(17)

*U1 atom is located at inversion center in the unit cell;
O_{yl}=U=O_{yl} : 180 °

Hydrogen bonds (Å)	
O2…N5	2.737(3)
O2…N6	2.745(2)

Crystal structure of Complex **III** in unit cell
(30 % probability level, red dashed lines are hydrogen bonds, H atoms are omitted)
U is hexagonal-bipyramidal 8-coordination

- The tptz molecule is not coordinated to U atom, and is connected with aqua molecule by two hydrogen bonds.

Crystal Structure of Complex III

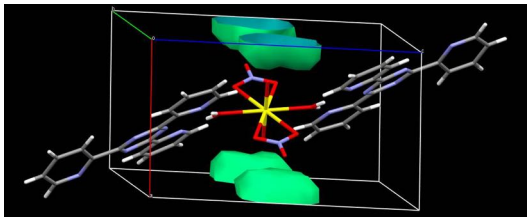

Void spaces (●) in unit cell of Complex **III**.
The voids were calculated by Mercury.

Summary

- We synthesized and characterized crystallographically three uranyl(VI) complexes, **I**, **II** and **III**.
- Complexes **I** and **II** were synthesized using $UO_2(NO_3)\cdot 6H_2O$, acetylacetone (= Hacac) and nitrogen-containing organic compound (DABCO or 2,3,5,6-tetramethylpyrazine (= tmpz)). Complex **III** was synthesized using $UO_2(NO_3)\cdot 6H_2O$ and 2,4,6-tris(2-pyridyl)-1,3,5-triazine (= tptz).
- Formula of complex **I** is a $[UO_2(acac)_2(Hacac)]$.
  - U atom is UO_7 pentagonal-bipyramidal 7-coordination geometry. Two uranyl-oxygen atoms are located at the axial positions, and, four oxygen atoms of two bidentate acac ligands and one oxygen atom of one monodentate Hacac ligand are located at the equatorial positions.
  - In the crystal, atoms except U atom are disordered.
- Formula of complex **II** is a $[UO_2(acac)_2(H_2O)]_2[UO_2(NO_3)_2(H_2O)_2]\cdot 5(tmpz)$.
  - Complex **II** contains two distinct uranyl(VI) molecules; $[UO_2(acac)_2(H_2O)]$ (= U1) and the other $[UO_2(NO_3)_2(H_2O)_2]$ (= U2) in a ratio of 2 : 1. U1 is UO_7 pentagonal-bipyramidal 7-coordination geometry and U2 is UO_8 hexagonal-bipyramidal 8-coordination geometry.
  - The tmpz molecules are not coordinated to U atoms.
- Formula of complex **III** is a $[UO_2(NO_3)_2(H_2O)_2]\cdot 2(tptz)$.
  - In complex **III**, U atom is UO_8 hexagonal-bipyramidal 8-coordination geometry.
  - The tptz molecule is not coordinated to U atom and connected with water ligand of $[UO_2(NO_3)_2(H_2O)_2]$ by hydrogen bonds.
- The DABCO, tmpz and tptz molecules are not coordinated to uranium(VI) atoms in this work.

Appendix

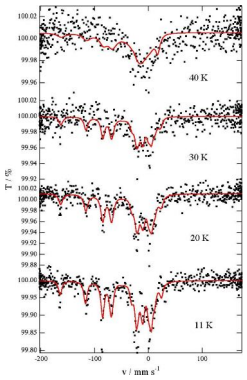

Temp / K	d (/$NpAl_2$) / mm s^{-1}	e^2qQ / mm s^{-1}	H_{eff} / T	t / ns
40	-39.6	190	220	0.23(5)
30	-39.6(5)	189(4)	220	0.7(3)
20	-39.5(3)	191(2)	220	2(1)
11	-39.9(2)	193(2)	220(1)	–

^{237}Np Mössbauer spectra and parameters of $[NpO_2(acac)_2(py)]$
T. Kawasaki, T. Kitazawa, et al., *Hyperfine Interact.* **166**, 417, 2005.

Molecular Structures of $[UO_2(acac)_2L]$ Type Complexes by Our Laboratory

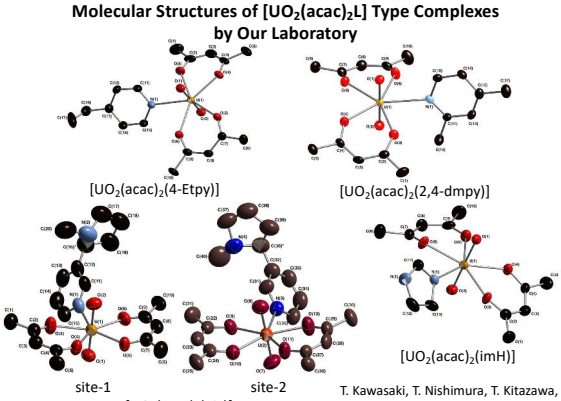

T. Kawasaki, T. Nishimura, T. Kitazawa, *Bull. Chem. Soc. Jpn.* **83**, 1528, 2010.

Selected Bond Lengths and Angles of $[UO_2(acac)_2L]$ Type Complexes by Our Laboratory

L	U=O / Å O=U=O / °	$U\text{-}O_{Nside}$ / Å	$U\text{-}O_{antiNside}$ / Å
4-Mepy	U(1)-O(1) 1.778(5) U(1)-O(2) 1.778(5) O(1)-U(1)-O(2) 179.2(2)	U(1)-O(3) 2.364(5) U(1)-O(5) 2.322(5)	U(1)-O(4) 2.357(5) U(1)-O(6) 2.353(5)
4-Etpy	U(1)-O(1) 1.772(3) U(1)-O(2) 1.769(3) O(1)-U(1)-O(2) 179.1(1)	U(1)-O(3) 2.323(3) U(1)-O(6) 2.361(3)	U(1)-O(4) 2.358(3) U(1)-O(5) 2.346(3)
2,4-dmpy	U(1)-O(1) 1.785(7) U(1)-O(2) 1.780(8) O(1)-U(1)-O(2) 179.2(4)	U(1)-O(3) 2.367(8) U(1)-O(6) 2.345(8)	U(1)-O(4) 2.350(8) U(1)-O(5) 2.380(8)
nic site-1	U(1)-O(1) 1.760(9) U(1)-O(2) 1.792(9) O(1)-U(1)-O(2) 178.5(4)	U(1)-O(3) 2.373(9) U(1)-O(6) 2.373(7)	U(1)-O(4) 2.327(8) U(1)-O(5) 2.323(9)
nic site-2	U(2)-O(7) 1.789(9) U(2)-O(8) 1.759(1) O(7)-U(2)-O(8) 177.4(4)	U(2)-O(9) 2.332(7) U(2)-O(12) 2.33(1)	U(2)-O(10) 2.35(1) U(2)-O(11) 2.338(9)
imH	U(1)-O(1) 1.76(1) U(1)-O(2) 1.73(1) O(1)-U(1)-O(2) 178.7(5)	U(1)-O(3) 2.32(1) U(1)-O(5) 2.32(1)	U(1)-O(4) 2.38(1) U(1)-O(6) 2.37(1)
4,4'-bpy	U(1)-O(1) 1.783(9) U(1)-O(2) 1.759(9) O(1)-U(1)-O(2) 179.3 (4)	U(1)-O(3) 2.341(8) U(1)-O(6) 2.34(1)	U(1)-O(4) 2.356(9) U(1)-O(5) 2.336(8)

T. Kawasaki, T. Nishimura, T. Kitazawa, *Bull. Chem. Soc. Jpn.* **83**, 1528, 2010.

Crystal Structure $[UO_2(acac)_2(H_2O)]\cdot(pz)$ (Already Reported Complex)

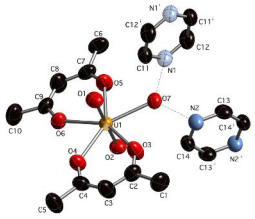

Molecular structure
(50 % probability level,
dashed lines are hydrogen bonds,
H atoms are omitted)

Selected bonds (Å) and angles (°)

U1-O1	1.777 (3)
U1-O2	1.774 (3)
U1-O3	2.352 (4)
U1-O4	2.348 (4)
U1-O5	2.361 (4)
U1-O6	2.353 (3)
U1-O7	2.409 (4)
O1-U1-O2	178.98 (14)

Hydrogen bonds (Å)

O7-N1	2.752 (5)
O7-N2	2.778 (6)

T. Kawasaki, T. Kitazawa, *Acta. Cryst. E*, **64**, m673, 2008.

Crystal Structure $(bpy)_2H[UO_2(acac)(NO_3)_2]$ (Already Reported Complex)

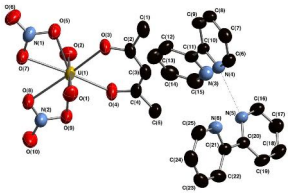

Molecular structure
(50 % probability level,
dashed lines are hydrogen bonds,
H atoms are omitted)

Selected bonds (Å) and angles (°)

U(1-)O(1) 1.759(2)
U(1)-O(2) 1.748(2)
U(1)-O(3) 2.341(2)
U(1)-O(4) 2.339(2)
U(1)-O(5) 2.544(2)
U(1)-O(7) 2.541(2)
U(1)-O(8) 2.561(2)
U(1)-O(9) 2.529(2)
O(1)-U(1-)O(2) 178.0(1)

T. Kawasaki, T. Nishimura, T. Kitazawa, *Bull. Chem. Soc. Jpn.* **83**, 1528, 2010.

It is reported that uranyl(VI) complexes coordinated by tptz ligand were obtained by solvo(hydro)thermal synthesis. [1-3]

[1] S. G. Thangavelu, et al., *CrystEngComm*, **17**, 6236, 2015.
[2] S. G. Thangavelu, et al., *Cryst. Growth Des.* **16**, 42, 2016.
[3] Z. Yue, et al., *CrystEngComm*, **21**, 5059, 2019.

3.12 T. Yoshimura（IRS, Osaka Univ.）

Preparation of guidelines for evaluation to ensure safety in the use of short-lived unsealed radioisotopes

Preparation of guidelines for evaluation to ensure safety in the use of short-lived unsealed radioisotopes

Radioisotope Research Center, Institute for Radiation Sciences, Osaka University

Takashi Yoshimura

Contents

Studies for safety handling of short-lived radioisotopes

- 2017—2019 Radiation Safety Regulation Research Strategic Promotion Project from Nuclear Regulation Authority, Japan
  「Development of safety management and radiation education by obtaining data for rational control of short-lived alpha particle emitters 」
  Determination of dispersal rates of ^{211}At, ^{223}Ra, ^{225}Ac, and their descendent nuclides
- 2019—2021 Radiation Safety Regulation Research Strategic Promotion Project from Nuclear Regulation Authority, Japan
  「Preparation of guidelines for evaluation to ensure safety in the use of short-lived unsealed radioisotopes」

Study for safety management of short-lived alpha particle-emitters

- In recent years, research for nuclear medicine applications of short-lived alpha particle emitters has been vigorously pursued. In the near future, medical applications of these nuclides are expected to be popular.
- Rational radiation control to support the research and development while ensuring the safety of workers and the public is important. For this purpose, obtaining data on the dispersal rate and development of safe handling method are required.

2017—2019 Radiation Safety Regulation Research Strategic Promotion Project from Nuclear Regulation Authority, Japan
「Development of safety management and radiation education by obtaining data for rational control of short-lived alpha particle emitters 」

Obtaining the dispersal rates of airborne ^{211}At, ^{223}Ra, ^{225}Ac and their descendent nuclides

Members

Osaka Univ.	A. Shinohara、K. Nakajima-Kaneda、Z. Zheng T. Yoshimura、A. Toyoshima、K. Nagata J. Hatazawa、T. Watabe、K. Ooe
Kyoto Univ.	T. Yamamura
Tohoku Univ.	K. Shirasaki、H. Kikunaga
RIKEN	H. Haba
Fukushima Medical Univ.	K. Washiyama

Summary (1)

Airborne dispersion of ^{211}At

- Dispersion of ^{211}At into the air is little from chloroform.
- The dispersal rate changes depending on the pH of the aqueous solution.
- When ascorbic acid is added to the solution of ^{211}At, dispersion of ^{211}At is lowered.

Airborne dispersion of ^{223}Ra

- There is no dispersion of ^{223}Ra from the aqueous $^{223}RaCl_2$.
- ^{211}Pb and ^{211}Bi were detected on the filters because of dispersion of ^{219}Rn.
- The dispersion of ^{219}Rn depends on the diameter of the vessel.
  → In radiopharmaceuticals, ^{223}Ra is sealed in a vial and dispensed by a syringe. Thus, ^{219}Rn is unlikely to be dispersed into the air.

Airborne dispersion of ^{225}Ac

- There is almost no dispersion of ^{225}Ac

- 2019—2021 Radiation Safety Regulation Research Strategic Promotion Project from Nuclear Regulation Authority, Japan
  「Preparation of guidelines for evaluation to ensure safety in the use of short-lived unsealed radioisotopes」

Purpose of Study

Preparation of guidelines for evaluation to ensure safety in the use of short-lived unsealed radioisotopes

Purpose
To prepare guidelines to summarize the new method of evaluation for license of short-lived radioisotopes at each radiation facility

Members

Chair：T. Yoshimura（Osaka Univ.）
PO：S. Furuta（PESCO）
Advisor：Y. Yonekura（Osaka Univ.）
J. Hatazawa（JRIA）

Assistant PO：
T. Nishio（NRA, Jpn）
M. Koga（NRA, Jpn）

Osaka Univ.
T. Todo
M. Tatsumi
K. Kaneda
T. Watabe
K. Yamaguchi
T. Kamiya
S. Kawaguchi
A. Shinohara
A. Toyoshima
K. Ooe
K. Nagata

Hiroshima Univ.
S. Nakashima

Hokkaido Univ.
Y. Kuge

QST
K. Nagatsu

Tohoku Univ.
H. Watabe
K. Shirasaki

Kyoto Univ.
T. Yamamura

RIKEN
H. Haba

Table of Contents of Guidelines

Title： guidelines for evaluation to ensure safety in the use of short-lived unsealed radioisotopes

Chapter1 Overview, Background, and Purpose of the Guidelines

Chapter2 Scope and Application of the Guidelines

Chapter3 Evaluation Method
Method for evaluating shielding, airborne RI concentration, exhaust air RI concentration, and RI concentration in waste water

Chapter4 Reliability assurance methods
Establishment of responsibility system, manuals to be equipped after approval

Chapter5 Education and Training
Subjects and contents of education and training

Outline of guidelines

○Purpose and necessity of the guidelines
In order to ensure safety of workers and the public, and implement rational radiation control, the guideline summarizes a method of evaluation for calculating the use quantity of short-lived nuclides at each radiation facility.

○Scope and application of the guidelines
The guidelines are applicable to the regulations based on the "Low Concerning the Regulation of Radioisotopes".

○Guideline of applicable nuclides
The guideline applies to short-lived radioactive nuclides with half-lives up to 15 days.

○Outline of the evaluation method for use
It is possible to apply values based on experiments to dispersal rate, etc. Furthermore, it is possible to be taken in account of decay of the nuclide for evaluation.

○Responsibility System
Each facility should establish a peer review system that include external experts to review the results of experiments.

Summary

Preparation of guidelines for evaluation to ensure safety in the use of short-lived unsealed radioisotopes

Many experts specializing in radiochemistry, nuclear medicine, and radiation safety management participate in the group to prepare the guidelines.

The guidelines have been prepared in consultation with relevant academic societies and the Nuclear Regulation Authority, Japan.

The prepared guidelines have been authorized by six academic societies.

Acknowledgement

Osaka Univ.
Prof. Atsushi Shinohara
Prof. Yoshiharu Yonekura
Prof. Jun Hatazawa
Prof. Takeshi Todo
Prof. Mitsuaki Tatsumi
Prof. Atsushi Toyoshima
Prof. Kazuko Kaneda
Prof. Yoshifumi Shirakami
Dr. Tadashi Watabe
Dr. Kazuhiro Ooe
Dr. Kojiro Nagata
Dr. Zijiang Zhang
Dr. Takashi Kamiya
Kazuya Yamaguchi
Syuhei Kawaguchi

QST
Dr. Kotaro Nagatsu

Tohoku Univ.
Prof. Hiroshi Watabe
Prof. Hidetoshi Kikunaga
Dr. Kenji Shirasaki

Hiroshima Univ.
Prof. Satoru Nakashima

Hokkaido Univ.
Prof. Yuji Kuge

RIKEN
Dr. Hiromitsu Haba

Kyoto Univ.
Prof. Tomoo Yamamura

Fukushima Medical Univ.
Prof. Kohshin Washiyama

This work was funded by the Radiation Safety Regulation Research Strategic Promotion Project from the Nuclear Regulation Authority, Japan (JP007057)

3.13 H. Amitsuka（Hokkaido Univ.）

Odd Parity Multipole Ordering in Uranium Compounds

Odd Parity Multipole Ordering in Uranium Compounds
– Resonant X-ray Scattering Study of UNi_4B

H. Amitsuka, **R. Murata**, **F. Kon**, Y, Kaneko, E, Hayasaka, **C. Tabata** [A],
H. Nakao [B], H. Saito [C], **Y. Shimizu** [D], D. Aoki [D], H. Hidaka, T. Yanagisawa

Grad. School of Sci., Hokkaido Univ., KURNS, Kyoto Univ. [A],
PF, IMSS, KEK. [B], *KENS, IMSS, KEK.* [C], *IMR, Tohoku Univ.* [D]

J-Physics 多極子伝導系の物理 Physics of Conductive Multipole Systems

J-Materials LAB. 強相関マテリアル研究室 Physics of Strongly Correlated Electron Systems

The Interest of Augmented Multipole

Multipole : Anisotropy of charge and magnetization distributions

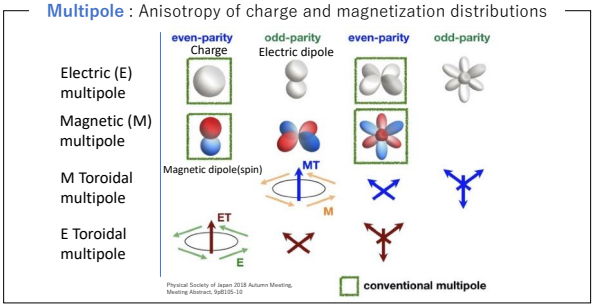

Hayami, Kusunose *et al.* derived the complete set of multipoles describing the electronic state.

Odd-parity multipoles are Active ➡ Cross correlation can be expected

Magnetoelectric(ME) effect etc…

What is UNi_4B

- Hexagonal ($P6/mmm$, D_{6h}^1, No. 191)
- Metallic component
- Antiferromagnetic (AFM) by 2/3 U T_N = 20.4 K
- AFM by 1/3 U T^* = 0.3 K

Crystal Structure

Copyright protected content

S.A.M. Mentink *et al.*, Phys. Rev. Lett. **73**, 1031 (1994)

Magnetic toroidal dipole order

Copyright protected content

S. Hayami, H. Kusunose, and Y. Motome Phys. Rev. B **90**, 024432 (2014)

Hayami *et al.* predicted

Copyright protected content

S.A.M. Mentink *et al.*, Phys. Rev. Lett. **73**, 1031 (1994)

ME effect can be generated in toroidal ordered metallic system UNi_4B

Current Induced Magnetization in UNi_4B

Theory

Current induced magnetization

consistent

Experiment

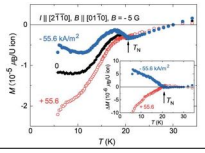

No current induced magnetization

inconsistent

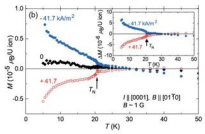

Both of results show current induced magnetizaiton

The reliability factor $R = 100\sum|I_{obs} - I_{calc}| / \sum I_{obs}$ *equals* ***11.2%***

S.A.M. Mentink *et al.*, Phys. Rev. Lett. **73**, 1031 (1994)

Magnetic toroidal dipole is tilted from c-axis ?

Either or both of crystal and magnetic structures are wrong ?

X-ray Crystal Analysis in UNi_4B

Orthorhombic ($Cmcm$, D_{2h}^{17}, No. 63)

$a_{ortho} = 6.943$ Å $\sim c_{hex}$

$b_{ortho} = 17.057$ Å $\sim 2\sqrt{3}a_{hex}$

$c_{ortho} = 14.807$ Å $\sim 3a_{hex}$

8f site : ordered at T_N 4c site : ordered at T^*

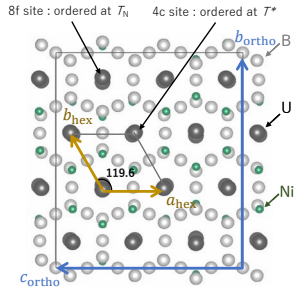

Y. Haga *et al.*, Physica B **403**, 900 (2008)
C. Tabata *et al.*, *Poster presentation, W6-08, in ICM, San Fransisco* (2018)

Previous

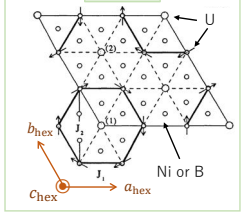

We have to check the **crystal** and **magnetic structures.**

High resolution
Polarization analysis
Can detect multipole orders

Resonant X-Ray Scattering

What is Resonant X-ray Scattering(RXS)

Consider the interaction between **electron** and **electromagnetic wave**

Two types of X-Ray scattering

$$f(\omega) = f_0 + f'(\omega) + if''(\omega)$$

Thomson scattering
Anytime occurs

Anomalous scattering
Enhanced at **absorption edge**

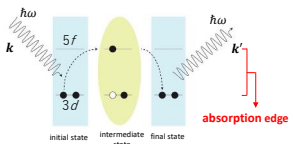

$$F_{E1}(\omega) = \sum_b \frac{1}{\hbar\omega - \hbar\omega_{ba} + i\Gamma_b} \times [(\varepsilon'^* \cdot \varepsilon)d_0 - i(\varepsilon'^* \times \varepsilon)\cdot \boldsymbol{u} d_1 + \{(\varepsilon'^* \cdot \boldsymbol{u})(\varepsilon \cdot \boldsymbol{u}) - (\varepsilon'^* \cdot \varepsilon)/3\}d_2]$$

ε : Polarization of incident X-ray
ε'^* : Polarization of reflected X-ray
$\boldsymbol{u}$: Unit vector in the main axis direction of the multipole
d_0 : Atom specific factor
d_1 : Dipole factor (no magnetic moment → $d_1 = 0$)
d_2 : Quadrupole factor (no quadrupole → $d_2 = 0$)

Anomalous factor becomes finite when the incident X-ray energy is near the absorption edge ➡ **Information on multipole ordering**

Polarization Analysis using RXS Method

Linear σ, π polarization and **magnetic moment** $\boldsymbol{u} = (u_x, u_y, u_z)$

$$F_{E1}(\omega) = \sum_b \frac{1}{\hbar\omega - \hbar\omega_{ba} + i\Gamma_b} \times [(\boldsymbol{\varepsilon}'^* \cdot \boldsymbol{\varepsilon})d_0 - i(\boldsymbol{\varepsilon}'^* \times \boldsymbol{\varepsilon}) \cdot \boldsymbol{u}d_1 + \{(\boldsymbol{\varepsilon}'^* \cdot \boldsymbol{u})(\boldsymbol{\varepsilon} \cdot \boldsymbol{u}) - (\boldsymbol{\varepsilon}'^* \cdot \boldsymbol{\varepsilon})/3\}d_2]$$

$$\begin{pmatrix} F_{\sigma\sigma'} & F_{\pi\sigma'} \\ F_{\sigma\pi'} & F_{\pi\pi'} \end{pmatrix} \propto \begin{pmatrix} 0 & u_y\cos\theta - u_z\sin\theta \\ -u_y\cos\theta - u_z\sin\theta & -u_x\sin 2\theta \end{pmatrix}$$

The method of Polarization Analysis in experiment

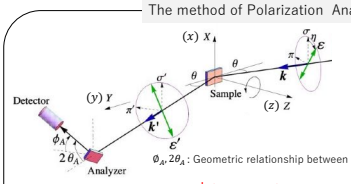

Analyzer = polarizer

$\phi_A = 0^\circ \longrightarrow F_{\sigma\sigma'}$, $F_{\pi\sigma'}$

$\phi_A = 90^\circ \longrightarrow F_{\sigma\pi'}$, $F_{\pi\pi'}$

Electric field vector of X-Ray: ⊥ (perpendicular), ∥ (parallel)

Scattering surface (YZ plane): = σ polarization X-ray, = π polarization X-ray

We can get the information of magnetic structure from the magnitude of each component.

Experimental Condition

Resonant X-ray Diffraction (RXD)

Diffraction

$2d\sin\theta = \lambda$

↓

Periodic structure

Lattice dipole quadrupole

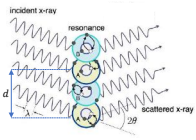

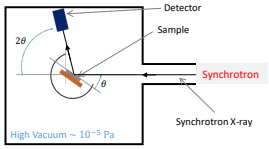

Experimental conditions

- BL-11B, Photon Factory, KEK
- X-ray energy E ~ 3720 eV (M_4-edge of U, E1 3d → 5f)
- Temperature : down to 7 K
- Incident X-ray : π polarization
- Using analyzer($SrLaAlO_4$) only polarization analysis

Top view

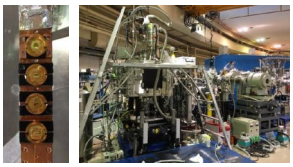

Sample

Single crystal grown by Czochralski method in Aoki Lab

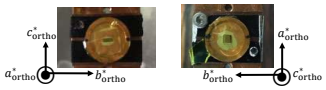

Sample Holder

Bragg and Magnetic Reflections (b^*_{ortho} - c^*_{ortho} plane)

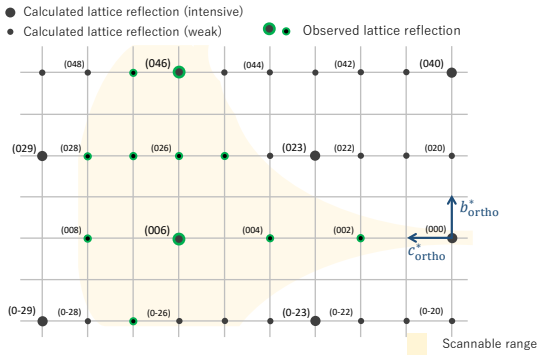

Crystal-lattice reflections can be assigned to theorthorhombic structure: *Cmcm*, D_{2h}^{17}, No. 63.

Bragg and Magnetic Reflections (b^*_{ortho} - c^*_{ortho} plane)

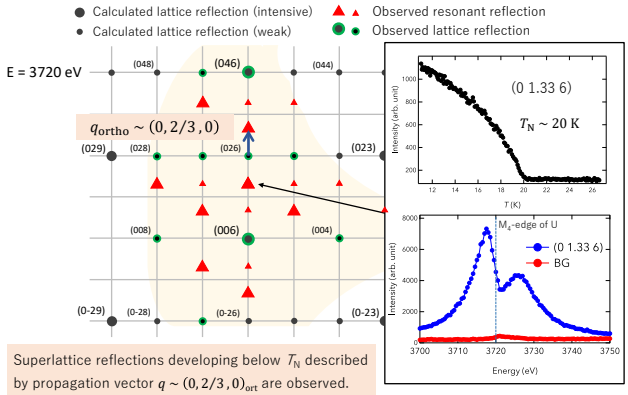

Superlattice reflections developing below T_N described by propagation vector $q \sim (0, 2/3, 0)_{ort}$ are observed.

Bragg and Magnetic Reflections (a^*_{ortho} - b^*_{ortho} plane)

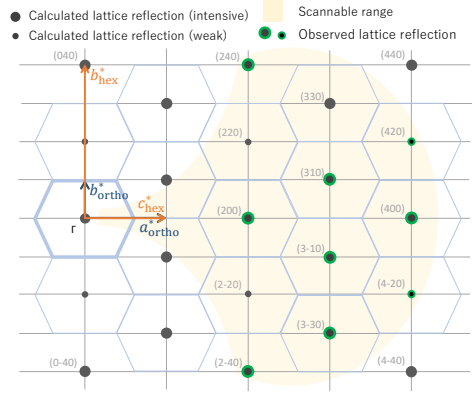

Bragg and Magnetic Reflections (a^*_{ortho} - b^*_{ortho} plane)

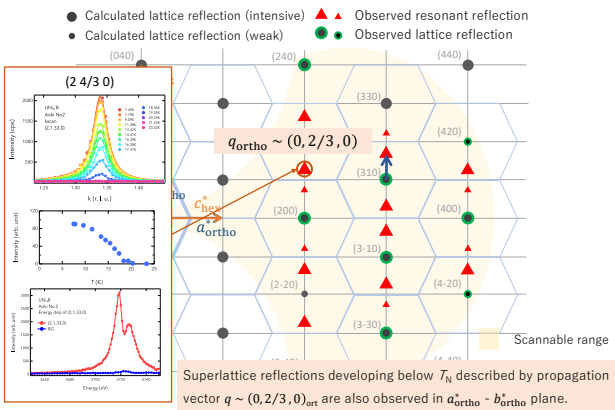

Superlattice reflections developing below T_N described by propagation vector $q \sim (0, 2/3, 0)_{ort}$ are also observed in a^*_{ortho} - b^*_{ortho} plane.

Discussion: Consideration of magnetic structure

Crystal structure : *Cmcm*

+

Ordering wave number $\boldsymbol{q}$ = (0, 2/3, 0)

Maximal magnetic space group

Cm'cm (#63.459)	*Cmcm* (#63.457)
Cm'c'm (#63.462)	*Cmc'm'* (#63.463)
Cm'c'm' (#63.465)	*Cmc'm* (#63.460)
Cm'cm' (#63.464)	*Cmcm'* (#63.461)
Magnetic moment only *b*, *c* components	Magnetic moment only *a* component

Copyright protected content

Discussion: Consideration of magnetic structure

4 sites

Magnetic moment of b_{ortho}, c_{ortho} components are arbitrary

○ possible

× impossible

Cm'cm AFM

Ferro magnetic toroidal dipole ○

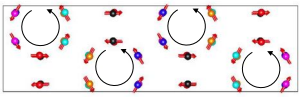

Cm'c'm' AFM

Ferro magnetic toroidal dipole ×

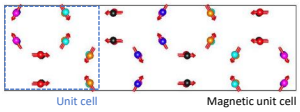

Cm'c'm AFM

Ferro magnetic toroidal × (Antiferro)

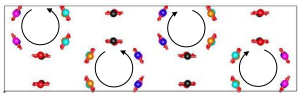

Cm'cm' FM

Ferro magnetic toroidal dipole ×

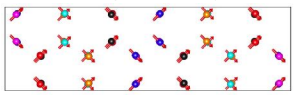

All magnetic structures are inconsistent with the results of current-induced magnetization for $I \parallel a$.

Discussion: Consideration of magnetic structure

● Lattice reflection (intensive)

• Lattice reflection (weak)

○ Observed magnetic reflection (NS)

▲ Observed resonant reflection

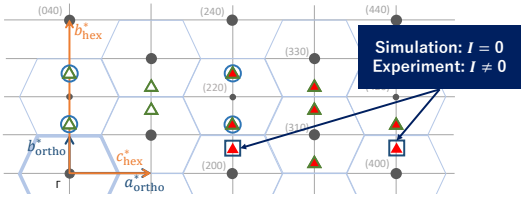

△ simulation

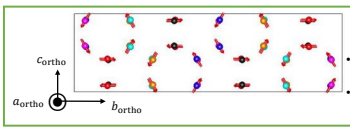

Magnetic space group: ***Cm'cm***

- The same magnitude of magnetic moments aligning **120°** rotation
- **Ferro magnetic toroidal dipole** ordering

Ideal Vortex-like magnetic structure can't explain all the results of RXS experiments.

Polarization Dependence of (0 2/3 7) Magnetic Reflection

(0 2/3 7) reflection

Incident X-ray: π Polarization

Analyzer = polarizer

$\phi_A = 0^\circ \longrightarrow F_{\pi\sigma'}$

$\phi_A = 90^\circ \longrightarrow F_{\pi\pi'}$

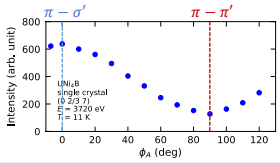

Resonant Scattering Amplitude (Magnetic Term)

$$\begin{pmatrix} F_{\sigma\sigma'} & F_{\pi\sigma'} \\ F_{\sigma\pi'} & F_{\pi\pi'} \end{pmatrix} = \begin{pmatrix} 0 & u_y \cos\theta - u_z \sin\theta \\ -u_y \cos\theta - u_z \sin\theta & -u_x \sin 2\theta \end{pmatrix}$$

u_y or u_z are finite

$$|F|^2_{obs} = |F_{\pi\sigma'} \cos\phi_A|^2 = |F_{\pi\sigma'}|^2 \cos^2\phi_A$$

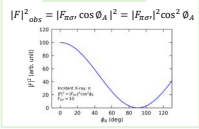

u_x is finite

$$|F|^2_{obs} = |F_{\pi\pi'} \sin\phi_A|^2 = |F_{\pi\pi'}|^2 \sin^2\phi_A$$

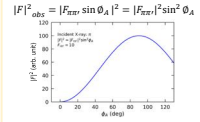

The component of magnetic moment is b_{ortho} and c_{ortho} ?

Discussion: Why $\pi - \pi$ component is finite

Ideal condition

Only σ X-ray is scattered

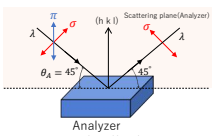

Our condition

π component mixes

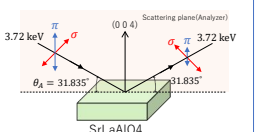

$$\frac{F_{\pi\pi'\,obs}}{F_{\pi\sigma'\,obs}} = \cos^2 2\theta_A = 0.1967$$

consistent

$$\frac{F_{\pi\pi'\,exp}}{F_{\pi\sigma'\,exp}} = \frac{152.3}{680.3} = 0.2238$$

Magnetic moment of UNi$_4$B likely has b_{ortho} and c_{ortho} component

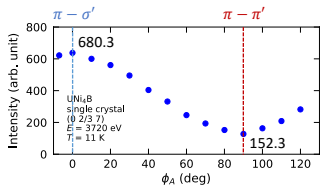

Temperature Dependence of Magnetic Reflection (b^*_{ortho} - c^*_{ortho} plane)

● Lattice reflection (intensive)

• Lattice reflection (weak)

▲ Observed resonant reflection

● Observed lattice reflection

○ nonlinear

○ linear

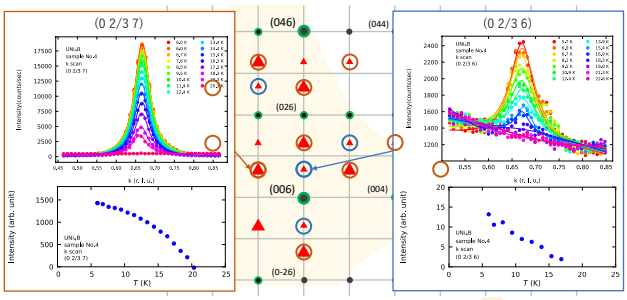

Scannable range

Two different types of magnetic reflection ware found

Temperature Dependence of Magnetic Reflection (a^*_{ortho} - b^*_{ortho} plane)

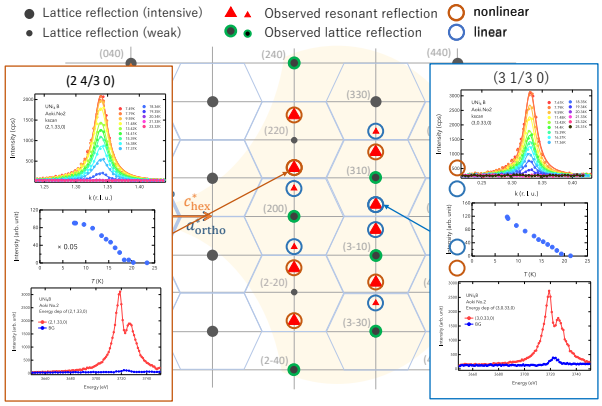

Examples ～ Coupled order parameters

$Ce_{0.7}La_{0.3}B_6$

Primary OP: **AF magnetic octupole**
Q = (½ , ½, ½)

Secondary OP: **Ferro quadrupole**
Q = 0

Resonant X-ray scattering

Copyright protected content

Mannix *et al.*,
Phys. Rev. Lett. **95**, 117206 (2005)

Thermal expansion || [111]

Copyright protected content

Akatsu *et al.*,
J. Phys. Soc. Jpn. **72**, 205 (2003)

Theory

$$\mathcal{F}_{\mathrm{GL}} = \frac{\alpha}{2}(T-T_\phi)\phi^2 + \frac{b}{4}\phi^4 + \frac{a}{2}\xi^2 + c\phi^2\xi + \cdots \; : \; \phi \equiv \bar{X}_{5u}(\boldsymbol{Q}), \quad \xi \equiv \bar{X}_{5g}(\boldsymbol{0})$$

primary secondary

$$\phi(T) = \sqrt{A(T_\phi - T)}, \quad \xi(T) = -\frac{c}{a}\left[\phi(T)\right]^2$$

Kusunose *et al.*, J. Phys. Soc. Jpn. **77**, 064710 (2008)

Examples ～ Coupled order parameters

$Cd_2Re_2O_7$

Harter *et al.*, Science **356**, 295 (2017).

Results of SHG experiments

Primary OP: **T_{2u} el.-nematic order**

Secondary OP: **E_u lattice distortion**

Copyright protected content

$$F = F_0 - \left(1 - \frac{T}{T_c}\right)(a_g\Psi_g^2 + a_u\Psi_u^2) + b\Phi_{E_u}^2 - g\Psi_g\Psi_u\Phi_{E_u} + \text{higher-order terms},$$

T_{2u}: $\Psi_u \propto \Psi_g \propto |1-T/T_c|^{1/2}$

E_u: $\Phi_{E_u} \propto \Psi_u\Psi_g \propto |1-T/T_c|$

Discussion: The Cause of Two types of temperature dependence

Same order parameter ←✕→ Two types of temperature dependence

⬇ Primary & Secondary

Magnetic moment × Higher order multipole ?

Magnetic moment × Crystal distortion ?

Example

$Ce_{0.7}La_{0.3}B_6$ in Resonant X-ray scattering & thermal expansion || [111]

Primary OP: **AF magnetic octupole** Q = (½ , ½, ½)

Secondary OP: **Ferro quadrupole** Q = 0

$Cd_2Re_2O_7$ in SHG experiments

Primary OP: **T_{2u} el.-nematic order**

Secondary OP: **E_u lattice distortion**

Recent study of UNi_4B

- Ultrasonic measurements

Electric quadrupolar degrees of freedom

Copyright protected content

Summary

- Crystal-lattice reflections can be indexed with orthorhombic structure (*Cmcm*, D_{2h}^{17}, No. 63).
- Superlattice reflections developing below T_N can be described by propagation vector $q \sim (0, 2/3, 0)_{\mathrm{ortho}}$.
- Based on *Cmcm* and $q \sim (0, 2/3, 0)_{\mathrm{ortho}}$, the results of current induced magnetization experiment cannot be explained because magnetic toroidal dipole is not tilted.
- Magnetic moment of UNi_4B likely has *b* and *c* component by polarization analysis.
- Two different types of magnetic reflections in a^*_{ortho} - b^*_{ortho} and b^*_{ortho} - c^*_{ortho} plane were found.

3.14 T. Yanagisawa（Hokkaido Univ.）

Electric Quadrupolar Contributions in the Magnetic Phases of UNi_4B

Symmetry, Elastic Constant, Strain, and Quadrupole

Symmetry	$\Gamma_1(A_{1g})$	$\Gamma_3(E_g)$		$\Gamma_5(T_{2g})$		
Elastic Const.	C_B	$(C_{11}-C_{12})/2$		C_{44}		
Symmetrized Strains	ε_B	ε_u	ε_v	ε_{yz}	ε_{zx}	ε_{xy}
E-Quadrupole Charge Distribution						
Stevens Op.	O_B	O_2^0	O_2^2	O_{yz}	O_{zx}	O_{xy}

Cubic → Hexagonal C_{66} (Γ_5: E_{2g})

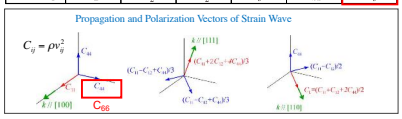

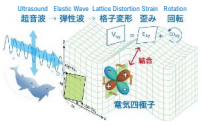

▶ Transverse ultrasound can detect each quadrupolar response spectroscopically.

Principle of Ultrasonic Measurements : Quadrupolar/Hexadecapolar Susceptibility

Conjugate Field	Multipole	Susceptibility
Magnetic Field $(T, P) = (-,+)$ H_{mag} — Coupling $\mathcal{H} = -g_J\mu_B \boldsymbol{J}\cdot\boldsymbol{H}_{mag}$	Magnetic Dipole $(-,+)$ $\boldsymbol{J}$	Magnetic Susceptibility χ
Strain Field $(T, P) = (+,+)$ ε_Γ — Coupling $\mathcal{H} = -g_\Gamma O_\Gamma \varepsilon_\Gamma$	Electric Quadrupole or Hexadecapole $(+,+)$ O_Γ	Multipolar Susceptibility χ_Γ

Hamiltonian

$$H = H_{CEF} + H_{QS} + H_{QQ}$$

$$H_{QS} = -\sum_{\Gamma} g_\Gamma O_\Gamma \varepsilon_\Gamma$$

$$H_{QQ}^{ad} = -\sum_{\Gamma} g_\Gamma^2 \langle O_\Gamma \rangle O_\Gamma$$

Elastic Constants

$$C_\Gamma(T) = \left.\frac{\partial^2 F}{\partial \varepsilon_\Gamma^2}\right|_{\varepsilon_\Gamma \to 0} = \underbrace{C_\Gamma^0}_{\text{Phonon B.G.}} - \frac{N g_\Gamma^2 \chi_\Gamma(T)}{1 - g_\Gamma^2 \chi_\Gamma(T)}$$

Multipolar Susceptibility

$$-g_\Gamma^2 \chi_\Gamma(T) = \underbrace{\left\langle \frac{\partial^2 E_\Gamma}{\partial \varepsilon_\Gamma^2} \right\rangle}_{\text{van Vleck term (Non-diagnal Element)}} - \underbrace{\frac{1}{k_B T}\left[\left\langle \left(\frac{\partial E_\Gamma}{\partial \varepsilon_\Gamma}\right)^2 \right\rangle - \left\langle \frac{\partial E_\Gamma}{\partial \varepsilon_\Gamma} \right\rangle^2\right]}_{\text{Curie term (Diagonal Element)}}$$

UNi_4B: Characteristics

Orthorhombic: *Cmcm*
D_{2h}^{17} (No.63) c/b ~ 0.8687(≒60.02°)

Hexagonal : *P6/mmm*
D_{6h}^{1} (No.191) c/b ~ 0.8660 (≒√3/2)

Y. Haga et al. (2008)
C. Tabata et al. (2016) → Re-confirmed by Synchrotron x-ray
S. A. M. Mentink et al. (1994)

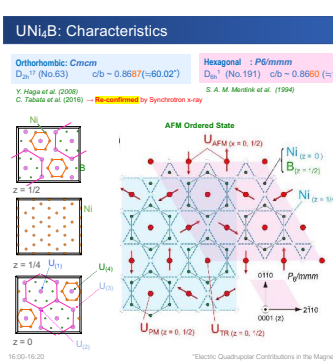

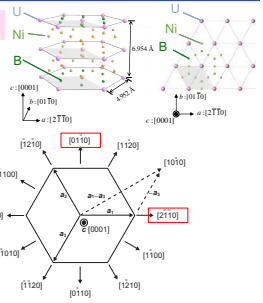

UNi_4B: Characteristics

T_N = 20.4 K AFM on U_{AFM} : 2/3 of U
$Q = (\frac{1}{2}, \frac{1}{2}, 0)$ (1.2 μB/U)
PM on $U_{(1)}$ &$U_{(2)}$: 1/3 of U
*Neutron diffraction of ^{11}B enriched sample by S. A. M. Mentink et al., Phys. Rev. Lett. **73**, 1031 (1994).*

$\chi_{\perp c}$ C/T $\rho \parallel c$ $\rho \parallel a$

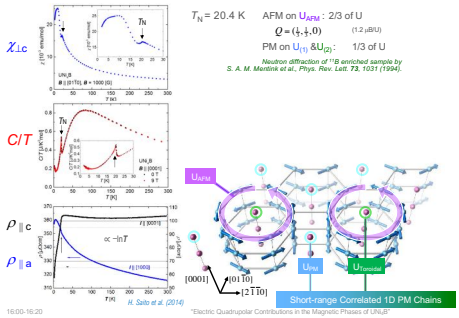

H. Saito et al. (2014)

UNi_4B: Characteristics

$\chi_{\perp c}$ C/T $\rho \parallel c$ $\rho \parallel a$

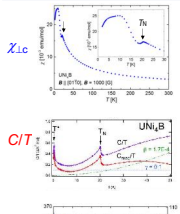

H. Saito et al. (2014)

T_N = 20.4 K AFM on U_{AFM} : 2/3 of U
$Q = (\frac{1}{2}, \frac{1}{2}, 0)$ (1.2 μB/U)
PM on $U_{(1)}$ &$U_{(2)}$: 1/3 of U
*Neutron diffraction of ^{11}B enriched sample by S. A. M. Mentink et al., Phys. Rev. Lett. **73**, 1031 (1994).*

T^* ~ 0.3 K Unidentified Order or Crossover?
Specific heat peak. Not observed in μSR and ACχ
*R. Movshovich et al., Phys. Rev. Lett. **83**, 2065 (1999).*

Magnetic structure and order parameters are both unknown

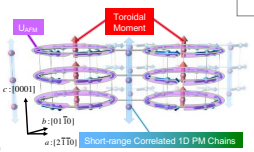

Definition of Toroidal Moment

Copyright protected content

$$\boldsymbol{t} = \frac{g\mu_B}{2}\sum_i \boldsymbol{r}_i \times \boldsymbol{S}_i$$

S. Hayami et al. PRB ■ (2014) 024432.

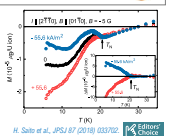

H. Saito et al., JPSJ 87 (2018) 033702. Editors' Choice

Open Issues and Motivation for UNi_4B

Open Issues

① UNi_4B shows peculiar non-collinear magnetic order.
② New magnetoelectric (ME) effect (confirmed).
③ Origin of T^* anomaly ~ 330 mK is unknown.

However, the information about higher-order multipoles in UNi_4B has not been investigated yet.

Motivation

▸ ① To obtain complementally information about electric quadrupoles by means of ultrasound. → Γ_ε quadrupole is active

✗ ② To check the ME effect by ultrasound →Not succeeded yet

▸ ③ To check the magnetic field-temperature phase diagram using pulsed-magnetic field and hybrid magnet system with DR.
→ T^* anomaly is clearly detected. *H-T* phase diagram is completed

Experimental Details : Ultrasonic Measurements

Sample: UNi_4B single crystal (CZ as cast)

for 28 T (Static): a × b × c = 3.94×1.96×1.33 mm³

for 17 T (Static) /60 T(Pulse): 2.23 x 1.67 x 1.80 mm³

Grown in Prague

LiNbO₃ Transducer

Ultrasonic Echo

Laue Picture of UNi_4B

Bottom of the Probe

Cryostat & SC Magnet:

³He-⁴He dilution fridge @ HZDR

Temperature: down to 40 mK

Magnetic Field: 17 T (static)

Phase Comparative Method

Signal Generator (100-500 MHz) → Chopper (500 ns, 30 kHz) → Power Amp. → Sample (w/ LN Transducers) → Gated Integrator → Phase Detector (DBM+BPF) → A/D converter

Feedback (Null detection)

Frequency

I (Cosine) Q (Sine)

CEF Analysis for Elastic Constant C_{66} in UNi_4B (PM phase)

A_{2g} and/or E_{2g} multipoles are active

CEF Analysis of C_{66} vs. T (PM)

$$C_\Gamma = C_\Gamma^0 - \frac{N g_\Gamma^2 \chi_\Gamma}{1 - g_\Gamma \chi_\Gamma} \rightarrow \Gamma_6$$ Quadrupolar Susceptibility

Previous CEF model does not Reproduce the softening of C_{66}

A. Oyamada et al., J. Phys. Conf. Ser. 145, 012044 (2009).

CEF Analysis for Elastic Constant C_{66} in UNi_4B (AFM phase)

CEF Analysis of C_{66} vs. T (PM)

$$C_\Gamma = C_\Gamma^0 - \frac{N g_\Gamma^2 \chi_\Gamma}{1 - g_\Gamma \chi_\Gamma} \rightarrow \Gamma_6$$ Quadrupolar Susceptibility

Previous CEF model can not Reproduce the C_{66} softening
→Possible origin of the softening
① New CEF model is required
② Coupling of Lattice and Augmented Multipole

A. Oyamada et al., J. Phys. Conf. Ser. 145, 012044 (2009).

Mag. Susceptibility

μ_{eff} = 2.5-2.8 μ_B
U^{3+} free 2.63μ_B
U^{4+} free 2.68μ_B

Copyright protected content

Matrix Elements (Scheme 0)

Ground State 0 K, 1st Ex-state 616 K

$E_{5/2} \otimes E_{5/2} = A_{1g} \oplus A_{2g} \oplus E_{1g}$

CEF Analysis for Elastic Constant C_{66} in UNi_4B (AFM phase)

Scheme 2 (Hex.): B_2^0 = 1 K, B_4^0 = -0.02 K, B_6^0 = -0.005 K, B_6^6 = 0.32 K

Scheme 1 (Ortho.): B_2^2 = 1 K, B_2^0 = 0.038 K, B_4^2 = -0.02 K, B_4^0 = 0.001 K, B_6^2 = -0.005 K, B_6^0 = 0 K, B_6^6 = 0.32 K

Matrix Elements (Scheme 2)

Ground State 0 K, 1st Ex-state 19.5 K

CEF Level Scheme 2: U^{4+} ($5f^2$) $J = 4$

$E_{2g} \otimes E_{2g} = A_{1g} \oplus A_{2g} \oplus E_{2g}$

CEF Analysis for Elastic Constant C_{66} in UNi_4B (AFM phase)

Scheme 2 (Hex.): B_2^0 = 1 K, B_4^0 = -0.02 K, B_6^0 = -0.005 K, B_6^6 = 0.32 K

Scheme 1 (Ortho.): B_2^2 = 1 K, B_2^0 = 0.038 K, B_4^2 = -0.02 K, B_4^0 = 0.001 K, B_6^2 = -0.005 K, B_6^0 = 0 K, B_6^6 = 0.32 K

Matrix Elements (Scheme 2)

Ground State 0 K, 1st Ex-state 19.5 K

Mag. Susceptibility

$E_{2g} \otimes E_{2g} = A_{1g} \oplus A_{2g} \oplus E_{2g}$

CEF Analysis for Elastic Constant C_{66} in UNi_4B (AFM phase)

Scheme 2 (Hex.): B_2^0 = 1 K, B_4^0 = -0.02 K, B_6^0 = -0.005 K, B_6^6 = 0.32 K

Scheme 1 (Ortho.): B_2^0 = 1 K, B_2^2 = 0.038 K, B_4^0 = -0.02 K, B_4^2 = 0.001 K, B_6^0 = -0.005 K, B_6^2 = 0 K, B_6^6 = 0.32 K

Two U-site Model

$$C_\Gamma = C_{bk}^{(PM)} - \frac{\frac{2}{3} N g_1^2 \chi_\Gamma}{1 - g_1 \chi_\Gamma} - \frac{\frac{1}{3} N g_2^2 \chi_\Gamma}{1 - g_2 \chi_\Gamma}$$

Site 1: U_{PM}, Site 2: U_{AFM}

$T < T_N$ $C_{bk}^{(AFM)} = const.$

Some of the U ions stay PM.

CEF Level Scheme 2: U^{4+} ($5f^2$) $J = 4$

CEF model calc. $T^* = \Delta/2.398 \sim 330$ mK

Possible Origin of T* (non-mag.)
(1) Schottky anomaly due to ortho.-distortion
(2) Glassy behavior caused by the frustration

UNi_4B: Experimental Details for High-magnetic Field Meas.

Dresden High-Mag. Field Lab.

Pulse: $H < 53$ T, $T > 1.5$ K
Dilution: $H < 18$ T, $T > 20$ mK

Sample prepared in Prague

Zherlitsyn *Wosnitza*

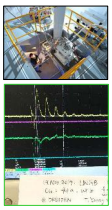

f = 117.5 MHz
τ_0 = 790 ns (@ 96 K)
v_{66} = 2771 m/s

IMR, Tohoku Univ.

Dilution: $H < 28$ T
$T > 30$ mK.
Sample prepared in Sapporo

Nakamura *Awaji*

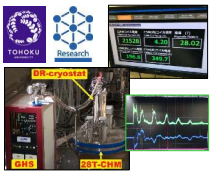

28 T with 32 mmϕ Hybrid Mag.+DR

f = 69.5 MHz

UNi_4B: Elastic Constant C_{66} vs. H || [01-10]

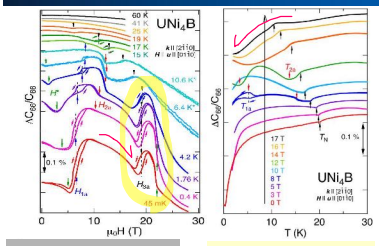

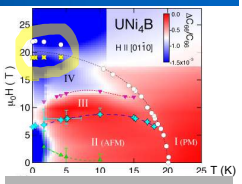

Copyright protected content

→ Recovery of Γ_1-type quadrupolar deg. of freedom in Phase IV?

Monthink et al. (1995)

Copyright protected content

H-T Phase Diagram of UNi_4B

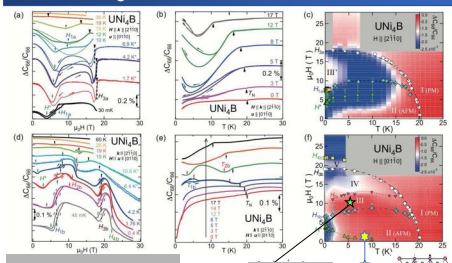

H || a: [2-1-10]
Specific Heat □△◇○
Magnetization △◇○
Magnetoresistance +
H || b: [01-10]
Magnetization ▲●

Previous H-T Phase Diag.

Copyright protected content

T (K) *Monthink et al. (1995)*

Phase IV
Γ_4 quadrupole is recovered

Phase III
Γ_4 quadrupole fluctuation is suppressed for H || [2-1-10] or enhanced for H || [01-10]

Phase II (AFM)
Γ_4 quadrupole is still active.

Copyright protected content

Phase III (SF) 12 T @ 4.2 K

Copyright protected content

Phase II (AFM) 0 T @ 4.2 K

Summary of Today's Talk

UNi_4B

The electric-quadrupole degrees of freedom play a crucial role in the low-temperature properties of UNi_4B.
→ Reading to anisotropic H-T phase diagrams and a newly revealed field-induced phase V.

C_{66} shows Curie-type softening in PM and AFM phases.
→ Γ_4 quadrupole is active
Some of the U ions stay disordered in the AFM ordered phase.

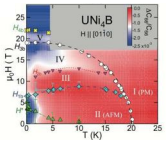

Thank you very much for your attentions.

3.15 M. Manjum（Dept. Appl. Chem., Keio Univ.）

Electrochemical Formation of Samarium and Samarium-Cobalt Nanoparticles in a Pyrrolidinium-based Ionic Liquid

2021/02/10

A meeting of Condensed-matter Chemistry on Actinides

Electrochemical Formation of Samarium and Samarium-Cobalt Nanoparticles in a Pyrrolidinium-based Ionic Liquid

Marjanul Manjum,[1] Naoki Tachikawa,[1] Nobuyuki Serizawa,[1] Adriana Ispas,[2] Andreas Bund,[1] and Yasushi Katayama[1]

[1]Keio University, Japan and [2]Technische Universität Ilmenau, Germany

General Introduction

ELECTROCHEMISTRY Department of Applied Chemistry Faculty of Science and Technology KEIO UNIVERSITY

Actinides and lanthanides

- ✓ Unique physicochemical properties due to f orbitals
- ✓ Radioactive actinides can be used as cardiac pacemakers
- ✓ Lanthanides are often considered as the simulated substance of actinides

Metal nanoparticles

- ✓ A large surface area
- ✓ Surface plasmon resonance
- ✓ High chemical activities and single-domain magnetic properties
- ✓ Drug delivery and cancer research in medical science

Importance of Sm

- ✓ Catalyst
- ✓ Magnet
- ✓ Lightweight electronic equipment (headphone, guitar, and iPod)

Importance of Sm-Co

- ✓ Catalyst
- ✓ Powerful magnet
- ✓ Automobile, military equipment
- ✓ High density magnetic storage
- ✓ Micro electro mechanical system

Electrodeposition of Sm is not possible in aqueous media due to its negative reduction potential.

1

General Introduction: Ionic Liquids

ELECTROCHEMISTRY Department of Applied Chemistry Faculty of Science and Technology KEIO UNIVERSITY

Ionic liquids that are liquids at or below room temperature are known as room temperature ionic liquids.

- ✓ Replace toxic and volatile organic media
- ✓ No stabilizers
- ✓ Preparation of metal and its alloy nanoparticles
- ✓ Catalysis
- ✓ Stabilization by electrostatic and/or steric repulsion

This study

(1-butyl-1-methyl pyrrolidinium) BMP^+

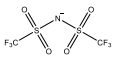

bis(trifluoromethyl sulfonyl)amide $TFSA^-$

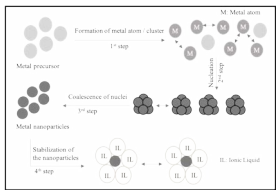

A schematic representation of the formation and stabilization processes of nanoparticles.

- ✓ Wide electrochemical potential window
- ✓ Acceptable ionic conductivity
- ✓ Dispersion and stabilization capability of the nanoparticles

2

General Introduction

ELECTROCHEMISTRY Department of Applied Chemistry Faculty of Science and Technology KEIO UNIVERSITY

Previous studies

- ✓ Electrochemical behavior of Sm(III)/Sm(II) in BMPTFSA at 25 °C[1]
- ✓ Electrodeposition of Co in BMPTFSA at 25-200 °C[2]
- ✓ Attempt on the electrodeposition of Sm-Co in BMPTFSA[3]
- ✓ Preparation of Sm and Sm-Co nanoparticles and their reaction mechanism was not clarified

Objectives of this study

- ✓ The electrochemical preparation of Sm and Sm-Co alloy nanoparticles in BMPTFSA

Co and Sm species

- ✓ $CoCO_3 + 2HTFSA \rightarrow Co(TFSA)_2 + H_2O + CO_2$[1]
- ✓ $Sm_2O_3 + 6HTFSA \rightarrow 2Sm(TFSA)_3 + 3H_2O$[2]
- ✓ Vacuum drying of $Co(TFSA)_2$ and $Sm(TFSA)_3$
- ✓ The purity was estimated to be 98%

1. M. Yamagata et al., *J. Electrochem. Soc.*, **153**, E5 (2006).
2. Y. Katayama et al., J. Electrochem. Soc., 154, D534 (2007).
3. A. Ispas et al., *ECS Trans.*, **16**, 119 (2009).

3

Experimental

ELECTROCHEMISTRY Department of Applied Chemistry Faculty of Science and Technology KEIO UNIVERSITY

Electrodes

Working electrode (WE):
Glassy carbon (GC) disk or plate
Reference electrode (RE):
Ag wire immersed in BMPTFSA containing 0.1 M $AgCF_3SO_3$
Counter electrode (CE):
Pt or Co wire

Characterization techniques

- ✓ Scanning electron microscopy (SEM)
- ✓ Energy dispersive X-ray (EDX) spectroscopy
- ✓ X-ray diffraction (XRD)
- ✓ Transmission electron microscopy (TEM)
- ✓ Fourier transform-infrared (FT-IR) spectroscopy
- ✓ X-ray photoelectron spectroscopy (XPS)

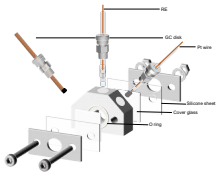

A one-compartment electrochemical cell.

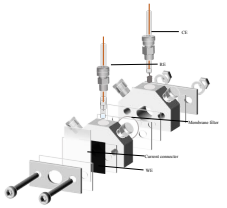

A two-compartment electrochemical cell.

4

Electrochemical Formation of Sm Nanoparticles in BMPTFSA at Different Temperatures

5

Electrochemical Measurements of Sm(III) in BMPTFSA

ELECTROCHEMISTRY Department of Applied Chemistry Faculty of Science and Technology KEIO UNIVERSITY

Cyclic voltammograms at different temperatures

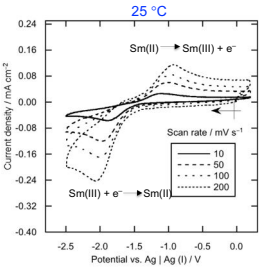

Cyclic voltammograms of a GC electrode (3 mmϕ) in BMPTFSA containing 10 mM $Sm(TFSA)_3$ with various scan rates at 25 °C. Printed in the Journal of The Electrochemical Society.[5]

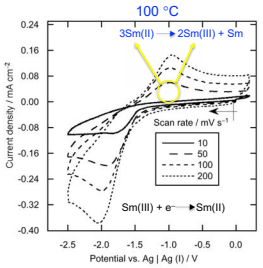

Cyclic voltammograms of a GC electrode (3 mmϕ) in BMPTFSA containing 10 mM $Sm(TFSA)_3$ with various scan rates at 100 °C. Printed in the Journal of The Electrochemical Society.[5]

- ✓ Sm(III) was reduced to Sm(II)
- ✓ No deposits were obtained at 25 °C after electrodepostion[4,5]

- ✓ Anodic peak of Sm(II) was found to disappear at 10 mVs^{-1}
- ✓ Disproportionation of Sm(II) occured[4,5]

4. Y.-F. Pan et al., *Inorg. Chem.*, **52**, 3241 (2013).
5. M. Manjum et al., *J. Electrochem. Soc.*, **166**, D483 (2019).

Electrochemical Formation of Sm Nanoparticles

ELECTROCHEMISTRY Department of Applied Chemistry Faculty of Science and Technology KEIO UNIVERSITY

Deposits on a GC electrode

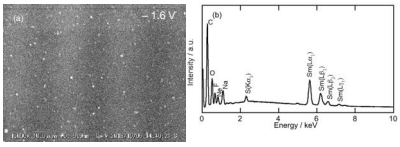

(a) SEM image and (b) EDX spectrum of the deposits obtained on a GC electrode after potentiostatic cathodic reduction at –1.6 V in BMPTFSA containing 10 mM $Sm(TFSA)_3$. Temperature: 100 °C. Electric charge: 3 C. Printed in the Journal of The Electrochemical Society.[5]

- ✓ Granular deposits
- ✓ Sm, F, and S in EDX spectrum
- ✓ No diffraction pattern for Sm in XRD
- ✓ Deposits were the aggregated nanoparticles

Nanoparticles dispersed in BMPTFSA

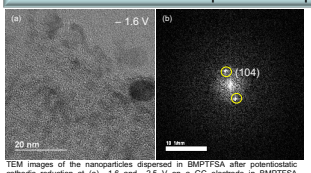

TEM images of the nanoparticles dispersed in BMPTFSA after potentiostatic cathodic reduction at (a) –1.6 and –2.5 V on a GC electrode in BMPTFSA containing 10 mM $Sm(TFSA)_3$. Temperature: 100 °C. Electric charge: 3 C. The insets show the electron diffraction diagrams of the nanoparticles.

- ✓ Nanoparticles with lattice fringes
- ✓ (104) plane of Sm
- ✓ Aggregates of the nanoparticles
- ✓ (104) plane was observed in the deposits

Reactions at 100 °C (EC' reaction):

$Sm(III) + e^- \rightleftharpoons Sm(II)$

$3Sm(II) \rightleftharpoons 2Sm(III) + Sm$; Disproportionation

5. M. Manjum et al., *J. Electrochem. Soc.*, **166**, D483 (2019).

Proportionation Reaction between Sm(III) and Sm Metal

ELECTROCHEMISTRY Department of Applied Chemistry Faculty of Science and Technology KEIO UNIVERSITY

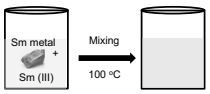

A scheme of a proportionation reaction between Sm(III) and Sm metal.

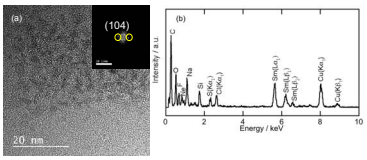

(a) TEM image and (b) EDX spectrum of the nanoparticles dispersed in BMPTFSA after immersion of Sm metal in BMPTFSA containing 10 mM $Sm(TFSA)_3$at 100 °C. Time: 3 hours. The inset shows the electron diffraction diagram of the nanoparticles. Printed in the Journal of The Electrochemical Society.[5]

Proportionation reaction:

At 25 °C, No nanopartitcles

At 100 °C,

$2Sm(III) + Sm\ (metal) \rightleftharpoons 3Sm(II)$

$3Sm(II) \rightleftharpoons 2Sm(III) + Sm$

- ✓ Formation of Sm nanoparticles
- ✓ Sm, F, S, and O were detected in EDX

- ✓ Sm nanoparticles were found to be formed by the disproportionation and proportionation reaction.
- ✓ Similar results were observed without exposing the sample to air.
- ✓ Stabilization of Sm in air was possible due to the enclosure with BMP^+ and/or $TFSA^-$.

5. M. Manjum et al., *J. Electrochem. Soc.*, **166**, D483 (2019).

Electrochemical Formation of Sm-Co Nanoparticles in BMPTFSA at 25 °C

Electrochemical Behavior of Co and Sm Species

ELECTROCHEMISTRY Department of Applied Chemistry Faculty of Science and Technology KEIO UNIVERSITY

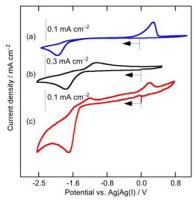

Cyclic voltammograms of a GC electrode (3 mmϕ) in BMPTFSA containing (a) 30 mM $Co(TFSA)_2$, (b) 5 mM $Sm(TFSA)_3$, and (c) 30 mM $Co(TFSA)_2$ and 5 mM $Sm(TFSA)_3$ at 25 °C. Scan rate: 10 mV s^{-1}. Printed in the Journal of The Electrochemical Society.[6]

At (a),

$Co(II) + 2e^- \longrightarrow Co$ (cathodic peak)[1]

$Co \longrightarrow Co(II)$ (anodic peak) + $2e^-$

At (b),

$Sm(III) + e^- \longrightarrow Sm(II)$ (cathodic peak)[2,3]

$Sm(II) \longrightarrow Sm(III)$ (anodic peak) + e^-

At (c), disappearance of the anodic peak of Sm (II)

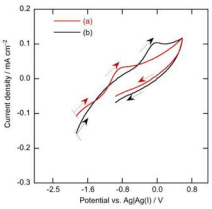

Cyclic voltammograms of a GC electrode (3 mmϕ) in BMPTFSA containing (a) 5 mM $Sm(TFSA)_3$ and (b) 30 mM $Co(TFSA)_2$ and 5 mM $Sm(TFSA)_3$ at 25 °C. The potential was held at –1.9 V for 60 s before the measurements. Scan rate: 10 mV s^{-1}. Printed in the Journal of The Electrochemical Society.[6]

- ✓ At (a), the anodic peak of Sm(II) was observed without Co(II).
- ✓ At (b), the disappearance of the anodic peak of Sm(II) by Co(II).
- ✓ The electrochemical behavior of Sm(II) was affected by the presence of Co(II).

1. Y. Katayama et al., *J. Electrochem. Soc.*, **154**, D534 (2007).
2. M. Yamagata et al., *J. Electrochem. Soc.*, **153**, E5 (2006).
3. M. Manjum et al., *J. Electrochem. Soc.*, **166**, D483 (2019).
6. M. Manjum et al., *J. Electrochem. Soc.*, **167**, 042205 (2020).

Potentiostatic Cathodic Reduction

ELECTROCHEMISTRY Department of Applied Chemistry Faculty of Science and Technology KEIO UNIVERSITY

Electrodeposition at –1.6 V

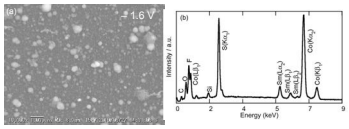

(a) SEM image and (b) EDX spectrum of the deposits obtained on a GC electrode after potentiostatic cathodic reduction at –1.6 V in BMPTFSA containing 30 mM $Co(TFSA)_2$ and 5 mM $Sm(TFSA)_3$. Temperature: 25 °C. Electric charge: 1.2 C. Printed in the Journal of The Electrochemical Society.[6]

- ✓ Granular deposits
- ✓ Co, Sm, F, and S in EDX
- ✓ No diffraction peak for Sm-Co alloy in XRD
- ✓ Color of the electrolyte: Pink to black opaque pink

- ✓ Nanoparticles with lattice fringes
- ✓ Interplanar spacings were 0.244 and 0.210 nm
- ✓ Two planes, (110) and (111) of $SmCo_7$[7]
- ✓ Phase angle between (110) and (111): 30°

1. Y. Katayama et al., *J. Electrochem. Soc.*, **154**, D534 (2007).
6. M. Manjum et al., *J. Electrochem. Soc.*, **167**, 042205 (2020).
7. Z. X. Zhang et al., *Scripta Materialia*, **62**, 594 (2010).

Non-electrochemical reduction of Co

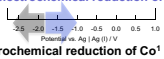

Electrochemical reduction of Co[1]

TEM: Deposits

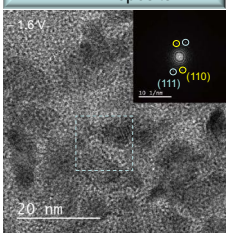

TEM image of the deposits rubbed from a GC electrode after potentiostatic cathodic reduction at –1.6 V in BMPTFSA containing 30 mM $Co(TFSA)_2$ and 5 mM $Sm(TFSA)_3$. Temperature: 25 °C. Electric charge: 1.2 C. The inset displays the electron diffraction diagram obtained on the rectangular area. Printed in the Journal of The Electrochemical Society.[6]

Nanoparticles Dispersed in BMPTFSA and Reaction Mechanism

ELECTROCHEMISTRY
Department of Applied Chemistry
Faculty of Science and Technology
KEIO UNIVERSITY

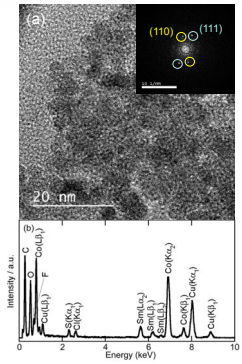

(a) TEM image and (b) EDX spectrum of the nanoparticles dispersed in BMPTFSA after potentiostatic cathodic reduction on a GC electrode at –1.6 V in BMPTFSA containing 30 mM $Co(TFSA)_2$ and 5 mM $Sm(TFSA)_3$. Temperature: 25 °C. Electric charge: 1.2 C. The inset displays the electron diffraction diagram of the nanoparticles. Printed in the Journal of The Electrochemical Society.[6]

- ✓ $SmCo_7$ nanoparticles
- ✓ Sm, Co, S, and F in EDX spectrum
- ✓ Formation of $SmCo_7$ in BMPTFSA at –1.6 V indicates the reaction between Sm(II) and Co(II).

$Sm(III) + e^- \rightleftharpoons Sm(II)$

$2Sm(II) + Co(II) \rightleftharpoons 2Sm(III) + Co$

$3Sm(II) + 7Co \rightleftharpoons 2Sm(III) + SmCo_7$

$\boxed{17Sm(II) + 7Co(II) \rightleftharpoons 16Sm(III) + SmCo_7}$

The total electrode reaction at –1.6 V,

$Sm(III) + 17e^- + 7Co(II) \rightleftharpoons SmCo_7$

In the presence of Co(II) at 25 °C:

- ✓ Disproportionation reaction of Sm(II) to Sm(III) and Sm is not favorable.
- ✓ Formation of $SmCo_7$ seems to be promoted.

6. M. Manjum et al., *J. Electrochem. Soc.*, **167**, 042205 (2020).

Electrochemical Preparation of Sm(II) at 25 °C and Mixing with Co(II)

ELECTROCHEMISTRY
Department of Applied Chemistry
Faculty of Science and Technology
KEIO UNIVERSITY

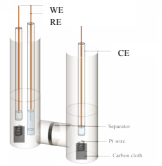

A schematic representation of a two-compartment glass cell for the preparation of BMPTFSA containing Sm(II).

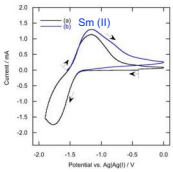

Cyclic voltammograms of a carbon cloth electrode (a) before and (b) after bulk electrolysis at –1.6 V in BMPTFSA containing 10 mM $Sm(TFSA)_3$. Temperature: 25 °C. Scan rate: 10 mV s^{-1}. Printed in the Journal of The Electrochemical Society.[6]

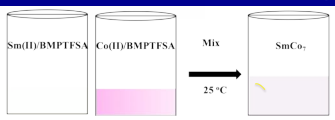

Mixing of Sm(II)/BMPTFSA and Co(II)/BMPTFSA at 25 °C for 16 hours.

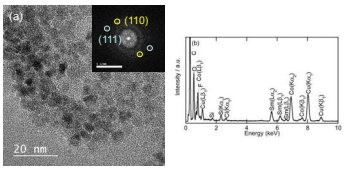

(a) TEM image and (b) EDX spectrum of the nanoparticles dispersed in BMPTFSA after mixing Sm(II)/BMPTFSA and Co(II)/BMPTFSA at 25 °C for 16 hours. The inset displays the electron diffraction diagram of the nanoparticles. Printed in the Journal of The Electrochemical Society.[6]

- ✓ The reduction of Co(II) was promoted by Sm(II).
- ✓ The formation of $SmCo_7$ was found during the non-electrochemical reaction between Co(II) and Sm(II).

6. M. Manjum et al., *J. Electrochem. Soc.*, **167**, 042205 (2020).

IR and XPS Spectra of Sm-Co Nanoparticles

ELECTROCHEMISTRY
Department of Applied Chemistry
Faculty of Science and Technology
KEIO UNIVERSITY

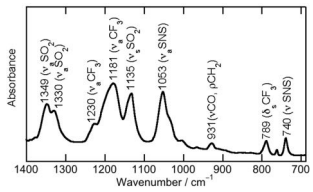

ATR-FT-IR spectrum of the aggregates of the nanoparticles collected after potentiostatic cathodic reduction at –1.6 V in BMPTFSA containing 30 mM $Co(TFSA)_2$ and 5 mM $Sm(TFSA)_3$. Temperature: 25 °C. Electric charge: 1.2 C.

- ✓ Peaks assignable to $TFSA^-$
- ✓ The inclusion of BMP^+ and/or $TFSA^-$ in the aggregates of the nanoparticles

A photograph of nanoparticles collected on a magnet.

XPS: Aggregates

Before Ar^+ etching,

- ✓ No peaks corresponding to Co and Sm were found in the aggregates
- ✓ But peaks of F, S, and O were found in the aggregates
- ✓ Ar^+ etching is not suitable for powder sample

Aggregated nanoparticles were considered to be covered by the layer of BMPTFSA.

Electrodeposition with a Magnet

ELECTROCHEMISTRY
Department of Applied Chemistry
Faculty of Science and Technology
KEIO UNIVERSITY

Sufficient amount of the nanoparticles was collected on a GC by placing a magnet during electrodeposition

SEM and TEM images: Deposits

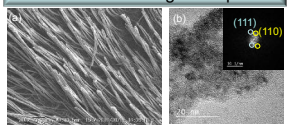

(a) SEM and (b) TEM images of the deposits obtained on the center region of the GC electrode after potentiostatic cathodic reduction at –1.6 V in BMPTFSA containing 30 mM $Co(TFSA)_2$ and 5 mM $Sm(TFSA)_3$ with a magnet. Temperature: 25 °C. Electric charge: 1.2 C. The inset shows the electron diffraction diagram of the nanoparticles.

- ✓ $SmCo_7$ nanowires were obtained with a magnet
- ✓ The slight shift of the binding energies indicated the formation of $SmCo_7$[8]
- ✓ Decomposition of $TFSA^-$ occurred by Ar^+ etching
- ✓ $TFSA^-$ in the sample interacts with the nanoparticles
- ✓ $SmCo_7$ nanoparticles were stable by the protecting shell of BMPTFSA

8. E. Herrera et al., *J. Electrochem. Soc.*, **166**, D460 (2019).

XPS analysis: After Ar^+ etching

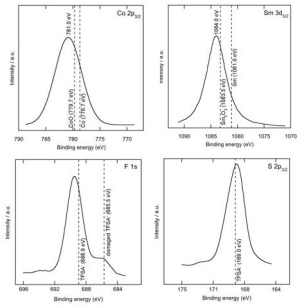

XPS spectra of the deposits obtained on a GC electrode with a NdFeB magnet after potentiostatic cathodic reduction at –1.6 V in BMPTFSA containing 30 mM $Co(TFSA)_2$ and 5 mM $Sm(TFSA)_3$. Temperature: 25 °C. Electric charge: 1.2 C. Printed in the Journal of The Electrochemical Society.[6]

6. M. Manjum et al., *J. Electrochem. Soc.*, **167**, 042205 (2020).

Conclusions

ELECTROCHEMISTRY
Department of Applied Chemistry
Faculty of Science and Technology
KEIO UNIVERSITY

(a) The electrochemical formation of Sm nanoparticles was obtained in BMPTFSA by the disproportionation and proportionation equilibrium among Sm(II), Sm(III), and Sm at high temperatures.

(b) The electrochemical preparation of Sm-Co alloy nanoparticles was achieved in BMPTFSA by the reduction of Co(II) and the disproportionation of Sm(II) in the presence of Co(II) even at room temperature.

(c) Sm and Sm-Co nanoparticles were considered to be stable in air because of the enclosure of the ionic liquid layer.

Thank you for your kind attention

3.16 T. Nomoto（Tokyo Inst. Tech.）

Drug delivery using functional polymer-conjugates

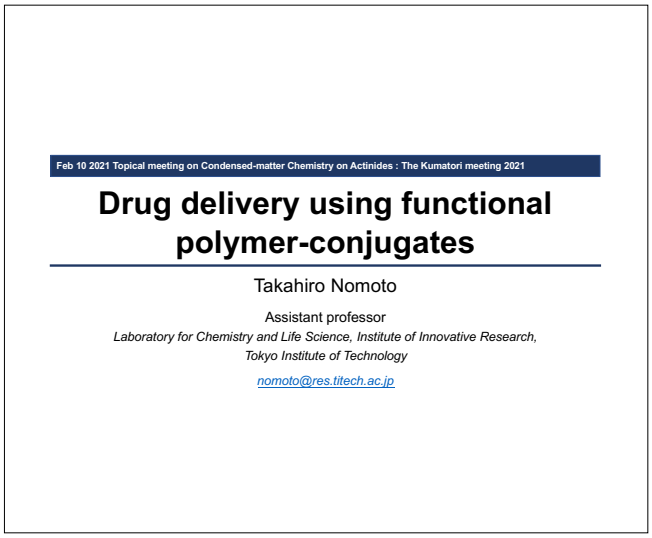

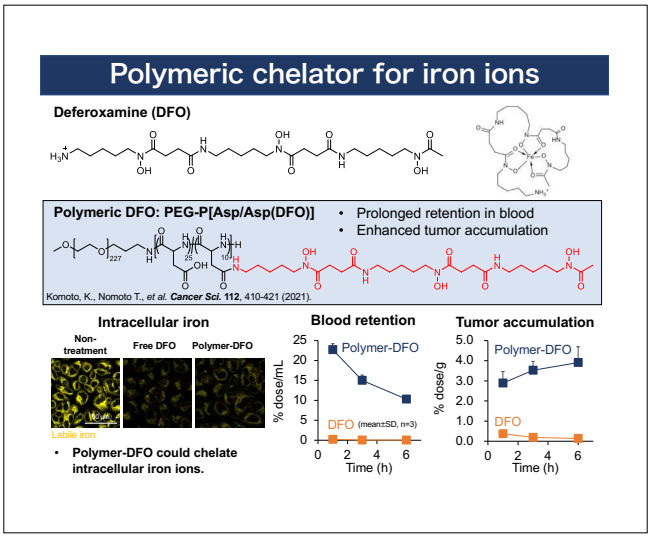

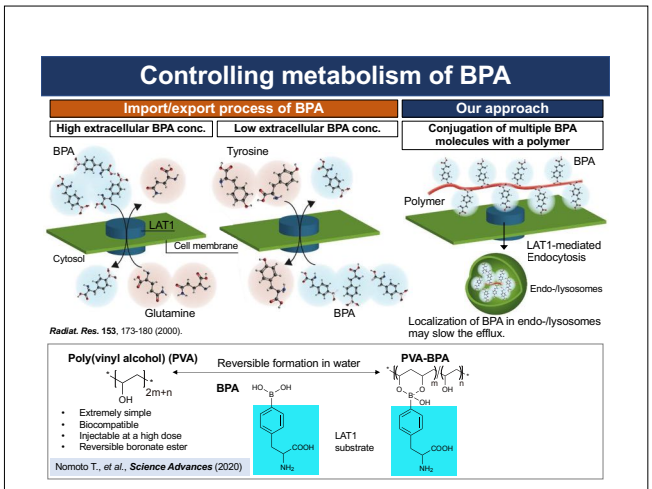

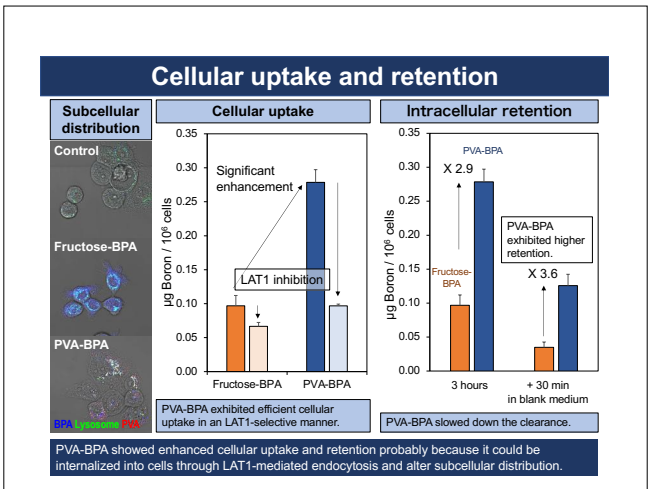

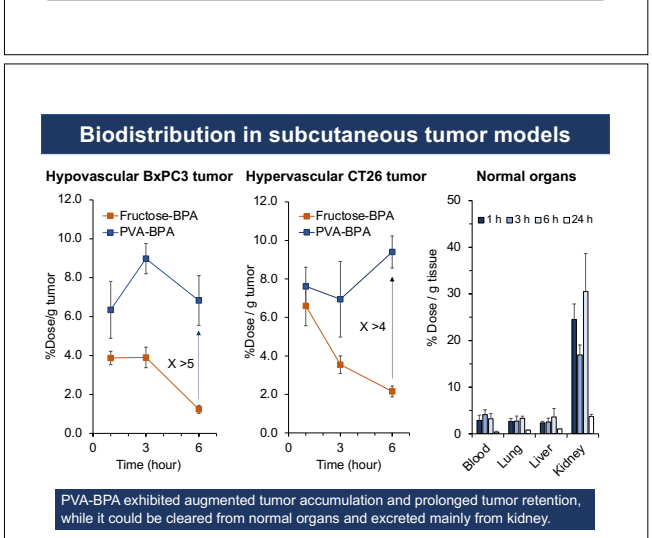

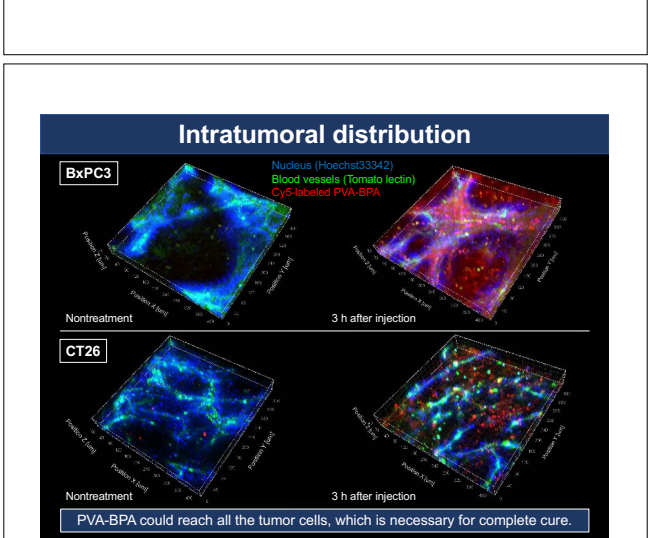

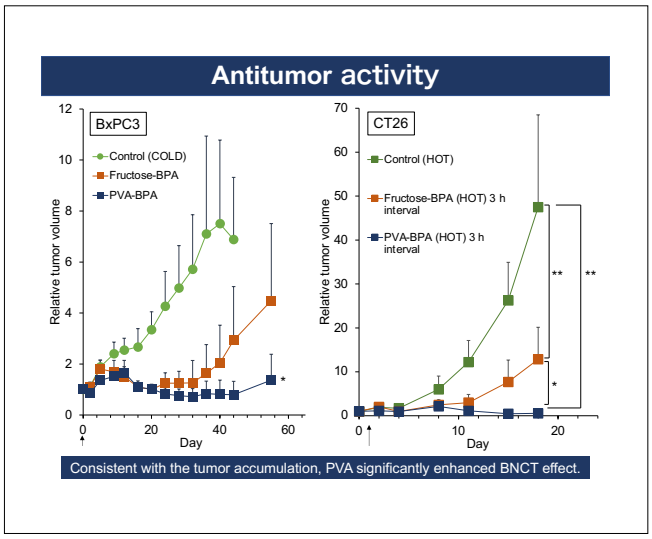
Antitumor activity
BxPC3
Control (COLD)
Fructose-BPA
PVA-BPA
Relative tumor volume
Day
CT26
Control (HOT)
Fructose-BPA (HOT) 3 h interval
PVA-BPA (HOT) 3 h interval
Relative tumor volume
Day
Consistent with the tumor accumulation, PVA significantly enhanced BNCT effect.

3.17 A. P. Goncalves（Universidade Lisboa, Portugal）

On the U-Fe-Ge system and its compounds

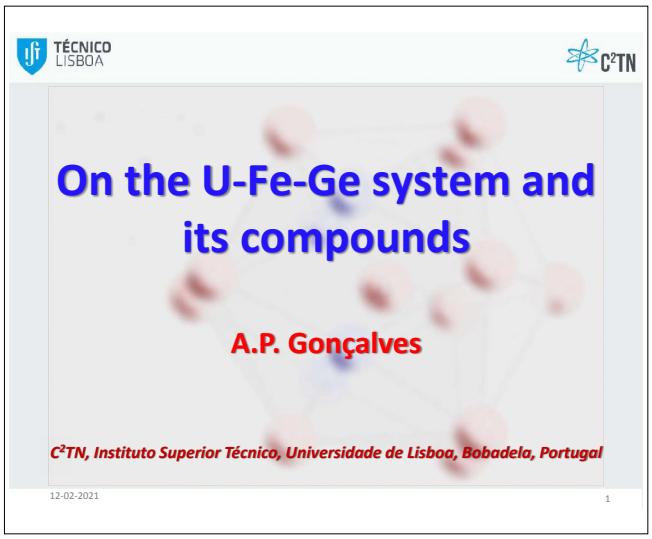

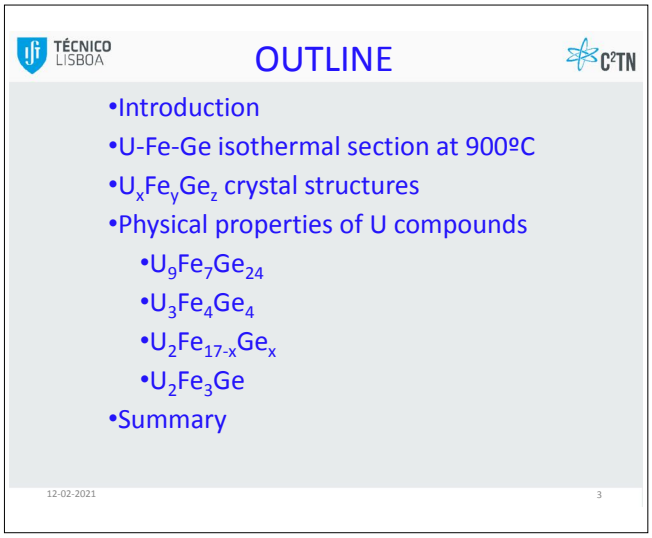

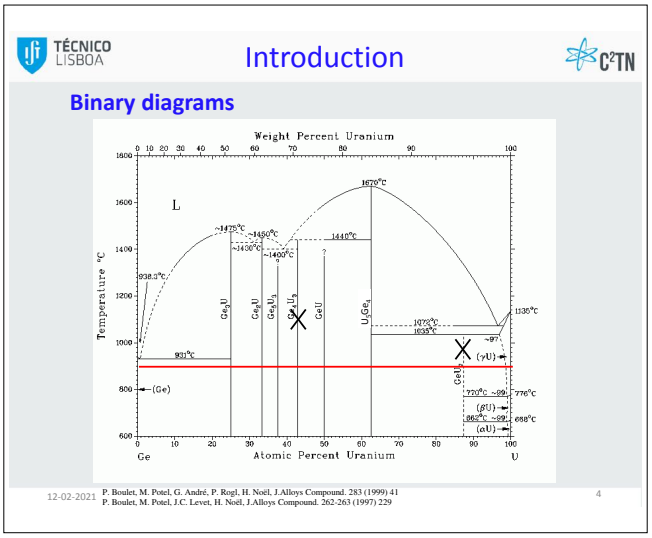

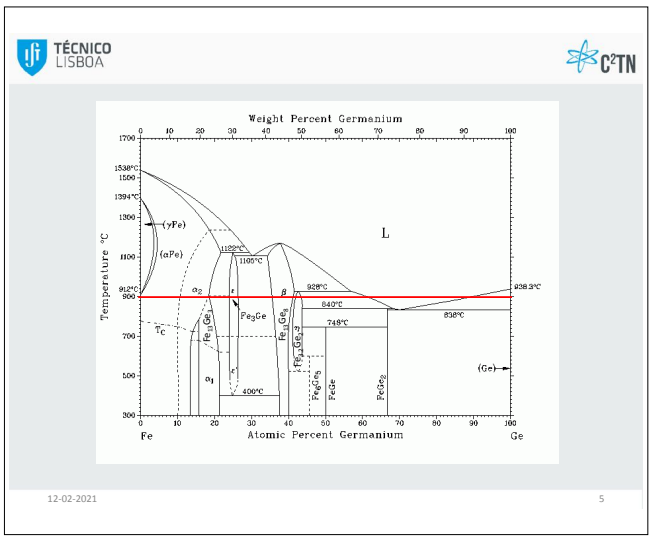

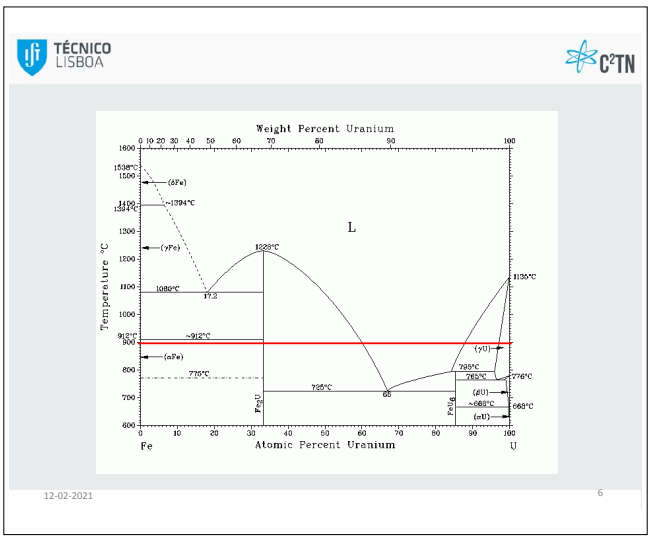

TÉCNICO LISBOA

C²TN

Data for the unary and binary phases taken from the U-Fe, U-Ge, and Fe-Ge sytems.

Phase	Transformation temperature (°C)	Structure type	Space group	Lattice parameters (Å)		
				a	*b*	*c*
U (α)	662, t	U	*Cmcm*	2.8537	5.8695	4.9548
U (β)	772, t	CrFe	*P4₂/mnm*	10.7589	--	5.6531
U (γ)	1132, f	W	*Im-3m*	3.5335	--	--
Fe (α)	910, t	W	*Im-3m*	2.8665	--	--
Fe (γ)	1390, t	Cu	*Fm-3m*	3.6599	--	--
Fe (δ)	1535, f	W	*Im-3m*	2.9315	--	--
Ge	938, f	C diamond	*Fd-3m*	5.621		
UFe_2	1235, f	$MgCu_2$	*Fd-3m*	7.055	--	--
U_6Fe	805, p	U_6Mn	*I4/mcm*	10.3022	--	5.2386
UGe_3	1475, f	$AuCu_3$	*Pm-3m*	4.196	--	--
UGe_2	1450, f	$ZrGa_2$	*Cmmm*	4.036	14.928	4.116
U_3Ge_5		AlB_2	*P6/mmm*	3.954	--	4.125
UGe		ThIn	*Pbcm*	9.827	8.932	5.841
U_3Ge_4	1670, f	Ti_3Ga_4	*P6₃/mcm*	8.744	--	5.863
$Fe_{11}Ge_8$		$Fe_{11}Ge_8$	*Pm-3m*	5.763	--	--
$Fe_{3.2}Ge_2$	1130, f	$Fe_{3.2}Ge_2$	*P6₃/mcm*	3.998	--	5.010
$Fe_{11}Ge_8$	928, p	$Fe_{11}Ge_8$	*P6₃/mcm*	7.976	--	4.993
Fe_3Ge	1122, p	Ni_3Sn	*P6/mmc*	5.162	--	4.207

t- solid state transition; m- melting point; p- peritectic reaction

TÉCNICO LISBOA

Ternary phases @ 900ºC (literature)

C²TN

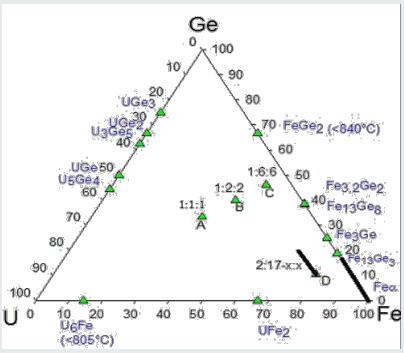

F. Canepa, P. Manfrinetti, M. Pani, A. Palenzona, J. Alloys Compd. 234 (1996) 225
L. Havela, A. Kolomiets, V. Sechovský, M. Diviš, M. Richter, A.V. Andreev, J. Magn. Magn. Mater. 177-181 (1998) 47
R.Marazza, R. Ferro, G. Rambaldi, G. Zanicchi, J. Less-Common Met. 53 (1977) 193
A. J. Dirkmaat, T. Endstra, E. A. Knetsch, A. A. Menovsky, G. J. Niewenhuys, J. A. Mydosh, J. Magn. Magn. Mater. 84 (1990) 143
A.P. Gonçalves, J.C. Waerenborgh, G. Bonfait, A. Amaro, M.M. Godinho, M. Almeida, J.C. Spirlet, J. Alloys Compd. 204 (1994) 59
T. Berlureau, B. Chevalier, L. Fournès, J. Etorneau, Materials Letters 9 (1989) 21

TÉCNICO LISBOA

C²TN

Isothermal section @900ºC

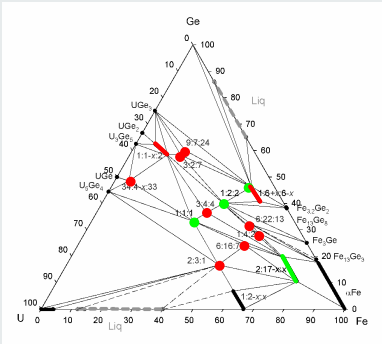

A:UFeGe

B:UFe_2Ge_2

C:$UFe_{6+x}Ge_{6-x}$ (x<0.7)

D:$U_2Fe_{17-x}Ge_x$ (2<x<3.7)

E: $U_{34}Fe_{4-x}Ge_{33}$ (x=1.36)

F: $UFe_{1-x}Ge_2$

G: $U_3Fe_2Ge_7$

H: $U_9Fe_7Ge_{24}$

I : U_2Fe_3Ge

J: $U_6Fe_{16}Ge_7$

K: $U_3Fe_4Ge_4$

L: UFe_4Ge_2

M: $U_6Fe_{22}Ge_{13}$

M. S. Henriques, David Berthebaud, A. Lignie, Z. El Sayah, C. Moussa, O.Tougait, L. Havela, A. P Gonçalves, J. Alloys Compnd. 639 (2015) 224

TÉCNICO LISBOA

C²TN

$UFe_{1-x}Ge_2$

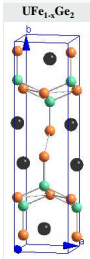

Structure type-$CeNiSi_2$
Space group-*Cmcm*
a (Å) - 4.083(5)
b (Å) - 15.805(5)
c (Å) - 4.030(5)

$U_6Fe_{16}Ge_7$

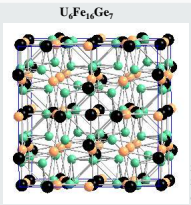

Structure type-$Mg_6Cu_{16}Si_7$
Space group-*Fm-3m*
a = *b* = *c* (Å) - 11.923(3)

$U_3Fe_4Ge_4$

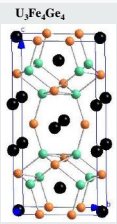

Structure type-$Gd_3Cu_4Ge_4$
Space group-*Immm*
a (Å) - 13.686(5)
b (Å) - 6.640(5)
c (Å) - 4.086(5)

UFe_4Ge_2

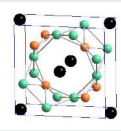

Structure type-$ZrFe_2Si_2$
Space group-*P4₂/mmm*
a = *b* (Å) - 7.28(1)
c (Å) - 3.85(1)

U_2Fe_3Ge

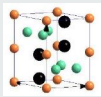

Structure type-Mg_2Cu_3Si
Space group-*P6₃/mmc*
a = *b* (Å) - 5.1870(3)
c (Å) - 7.8501(5)

$U_3Fe_2Ge_7$

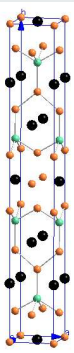

Structure type-$La_3Co_2Ge_7$
Space group-*Cmmm*
a (Å) - 4.15(1)
b (Å) - 24.92(1)
c (Å) - 4.14(1)

TÉCNICO LISBOA

C²TN

$U_{34}Fe_{4-x}Ge_{33}$

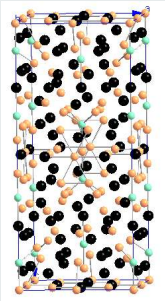

Structure type-$U_{34}Fe_{4-x}Ge_{13}$
Space group-*I4/mmm*
a = *b* (Å) - 10.875(5)
c (Å) - 25.250(5)
142 atoms

$U_9Fe_7Ge_{24}$

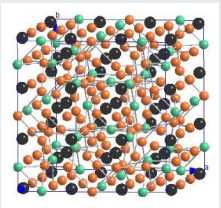

Structure type-$U_9Fe_7Ge_{24}$
Space group-*I4/mmm*
a = *b* (Å) - 12.365(1)
c (Å) - 18.256(3)
160 atoms

$U_6Fe_{22}Ge_{13}$

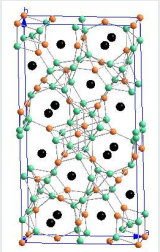

Structure type-$U_6Fe_{22}Ge_{13}$
Space group-*Pbam*
a (Å) - 12.674(5)
b (Å) - 24.196(5)
c (Å) - 4.005(5)
82 atoms

TÉCNICO LISBOA

C²TN

UGe_3

Structure type-$AuCu_3$
Space group-*Pm-3m*
a (Å) - 4.20

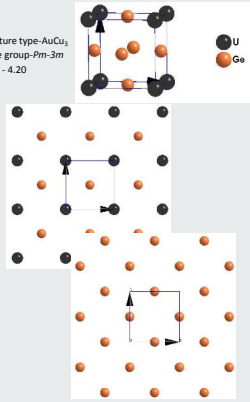

UGe_2

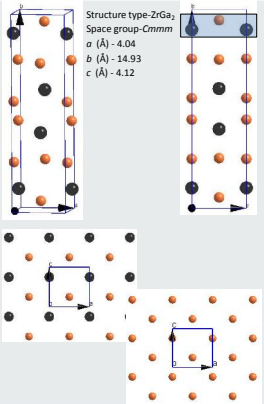

Structure type-$ZrGa_2$
Space group-*Cmmm*
a (Å) - 4.04
b (Å) - 14.93
c (Å) - 4.12

TÉCNICO LISBOA

C²TN

$UFe_{1-x}Ge_2$

Structure type-$CeNiSi_2$
Space group-*Cmcm*
a (Å) - 4.083(5)
b (Å) - 15.805(5)
c (Å) - 4.030(5)

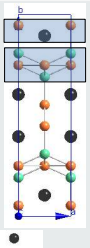

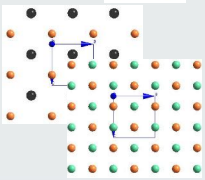

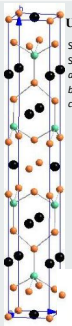

$U_3Fe_2Ge_7$

Structure type-$La_3Co_2Ge_7$
Space group-*Cmmm*
a (Å) - 4.15(1)
b (Å) - 24.92(1)
c (Å) - 4.14(1)

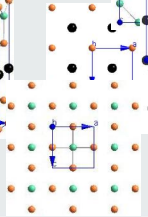

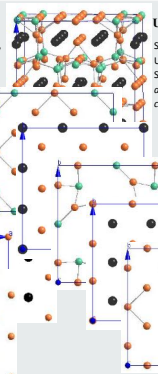

$U_9Fe_7Ge_{24}$

Structure type
$U_9Fe_7Ge_{24}$
Space group-*I4/mmm*
a = *b* (Å) - 12.365(1)
c (Å) - 18.256(3)

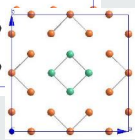

12-02-2021 13

TÉCNICO LISBOA

C²TN

$U_{34}Fe_{4-x}Ge_{33}$

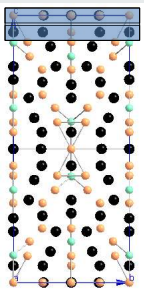

Structure type-$U_{34}Fe_{4-x}Ge_{33}$
Space group-*I4/mmm*
a = *b* (Å) - 10.875(5)
c (Å) - 25.250(5)

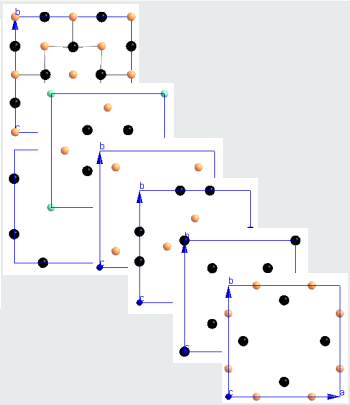

12-02-2021 14

TÉCNICO LISBOA

C²TN

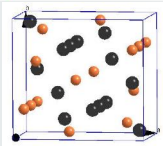

UGe

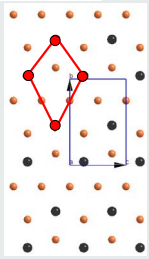

U_5Ge_4

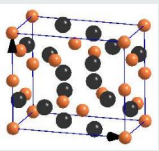

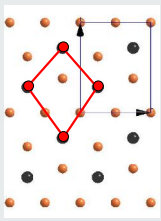

UFeGe

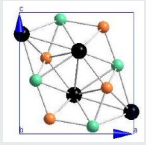

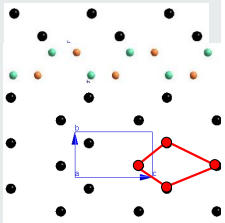

12-02-2021 15

TÉCNICO LISBOA

C²TN

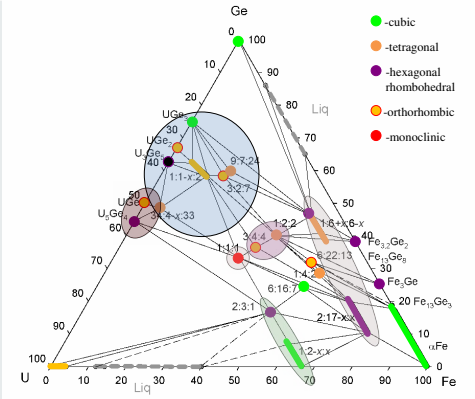

12-02-2021 16

TÉCNICO LISBOA

C²TN

Copyright protected content

Light actinides
- Pauli paramagnets
(exchange enhanced)

Heavy actinides
- ionic magnetism; "Hund's rules"
- but strong s-o coupling leads to *j-j* coupling

12-02-2021

Albers, R. C., 2001, Nature London 410, 759.
Boring, A. M., and J. L. Smith, 2000, in *Challenges in Plutonium Science, Vol. I*, No. 26, p. 91.

17

TÉCNICO LISBOA

U compounds…

C²TN

Copyright protected content

12-02-2021

Hill H. H., 1970, in *Plutonium 1970 and Other Actinides, edited* by W. N. Miner The Metallurgical Society of the AIME, New York.

18

TÉCNICO LISBOA

C²TN

U_5Ge_4

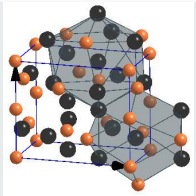

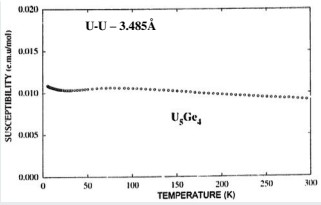

UGe_2

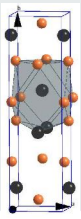

U-U – 3.667Å

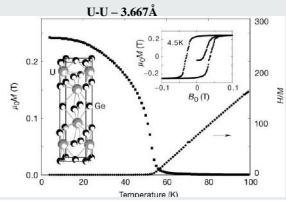

UGe_3

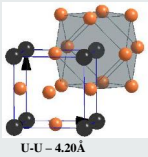

U-U – 4.20Å

12-02-2021 19

TÉCNICO LISBOA

C²TN

$U_9Fe_7Ge_{24}$

U1

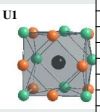

	NN	Atoms	d (Å)		NN	Atoms	d (Å)
U1(*4e*)	4	Ge1(*16m*)	2.894	**U2(*16m*)**	1	Ge3(*4e*)	2.968
	4	Fe3(*8i*)	3.116		2	Ge4(*16n*)	2.984
	4	Ge5(*16n*)	3.140		2	Ge6(*16l*)	3.001
	4	Fe1(16m)	3.436		2	Ge7(*8j*)	3.012
					2	Ge5(*16n*)	3.055
					1	Ge1(*16m*)	3.094
U3(*16n*)	2	Ge4(*16n*)	2.888		1	Fe1(*16m*)	3.116
	2	Ge6(*16l*)	2.942		1	Fe1(*16m*)	3.172
	2	Ge1(*16m*)	2.957		2	Ge2(*16k*)	3.374
	1	Ge8(*4c*)	2.997				
	1	Fe3(*8i*)	3.016				
	2	Ge2(*16k*)	3.018	**Fe2(*4d*)**	4	Ge2(*16k*)	2.482
	1	Fe2(*4d*)	3.211		4	Ge4(*16n*)	2.985
	1	Ge5(*16n*)	3.291		4	U3(*16n*)	3.211
	2	Fe1(*16m*)	3.376				
Fe1(*16m*)	1	Ge1(*16m*)	2.349	**Fe1(*16m*)**	4	Ge1(*16m*)	2.489
	2	Ge5(*16n*)	2.378		2	Fe3(*8i*)	2.783
	2	Ge2(*16k*)	2.383		2	Ge6(*16l*)	2.980
	1	Fe1(*16m*)	2.892		2	U3(*16n*)	3.016
	1	U2(*16m*)	3.120		2	U1(*4e*)	3.135
	1	U2(*16m*)	3.172				
	2	U3(*16n*)	3.376				
	1	U1(*4e*)	3.436				

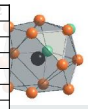

U3

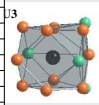

Fe1

12-02-2021 20

TÉCNICO LISBOA

C²TN

$U_9Fe_7Ge_{24}$

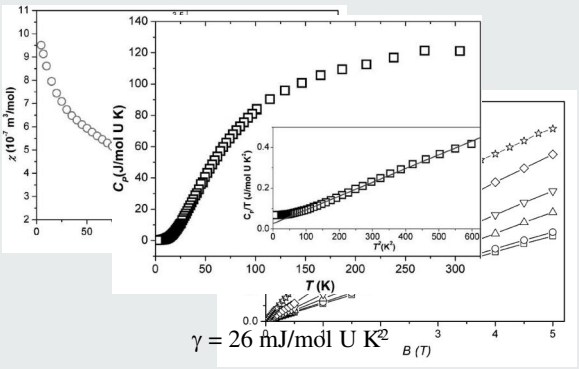

γ = 26 mJ/mol U K^2

12-02-2021 M.S. Henriques, D. Berthebaud, L.C.J. Pereira, E.B. Lopes, M.B.C. Branco H. Noël, O. Tougait, E. Santavá, L. Havela, P.A. Carvalho, A.P. Gonçalves, Intermetallics 19 (2011) 841-847 21

TÉCNICO LISBOA

C²TN

$U_3Fe_4Ge_4$

U1

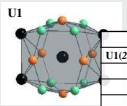

U2

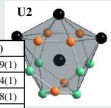

	NN	Atoms	d (Å)		NN	Atoms	d (Å)
U1(*2a*)	4	Ge2(*4g*)	2.888(1)	**U2(*4j*)**	4	Fe(*8l*)	2.909(1)
	2	Ge1(*4i*)	2.911(1)		2	Ge1(*4i*)	2.944(1)
	8	Fe(*8l*)	3.402(1)		2	Fe(*8l*)	2.968(1)
	4	U2(*4j*)	3.787(1)		4	Ge2(*4g*)	3.023(1)
					2	Ge1(*4i*)	3.494(1)
					1	U2(*4j*)	3.643(1)
Fe(*8l*)	1	Ge2(*4g*)	2.479(1)		2	U1(*2a*)	3.787(1)
	2	Ge1(*4i*)	2.496(1)				
	1	Ge1(*4i*)	2.536(1)				
	1	Fe(*8l*)	2.651(2)				
	2	U2(*4j*)	2.909(1)				
	1	U2(*4j*)	2.968(1)				
	2	Fe(*8l*)	3.009(1)				
	2	U1(*2a*)	3.402(1)				

Fe

12-02-2021 D. Berthebaud, O. Tougait, M. Potel, E.B. Lopes, J.C. Waerenborgh, A.P. Gonçalves, H. Noël, J. Alloys Compnd. 554 (2013) 408 22

TÉCNICO LISBOA

C²TN

$U_3Fe_4Ge_4$

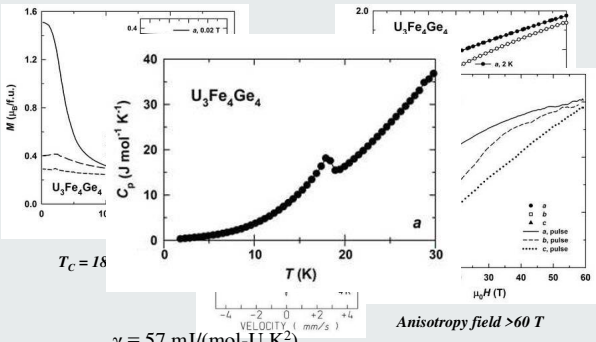

T_C = 18

Anisotropy field >60 T

γ = 57 mJ/(mol-U K^2)

Fe atoms → no ordered magnetic moments

→magnetism originates from U

12-02-2021 M.S. Henriques, D.I. Gorbunov, J.C. Waerenborgh, L. Havela, A.V. Andreev, Y. Skourski, A.P. Gonçalves, J. Alloys Compnd. 555 (2013) 304 23

TÉCNICO LISBOA

C²TN

$U_2Fe_{17-x}Ge_x$

U1

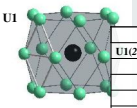

U2

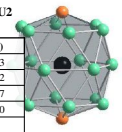

	NN	Atoms	d (Å)		NN	Atoms	d (Å)
U1(*2b*)	6	Fe2(*12j*)	2.809	**U2(*2d*)**	6	Fe2(*12j*)	2.813
	12	Fe3(*12k*)	3.214		2	Ge(*4f*)	3.012
					6	Fe3(*12k*)	3.207
					6	Fe1(*6g*)	3.210
Fe1(*6g*)	4	Fe3(*12k*)	2.433				
	4	Fe2(*12j*)	2.522	**Fe2(*12j*)**	4	Fe3(*12k*)	2.520
	2	Ge(*4f*)	2.603		2	Fe1(*6g*)	2.522
	2	U2(*2d*)	3.210		2	Fe2(*12j*)	2.809
					1	U1(*2b*)	2.809
					1	U2(*2d*)	2.813
Fe3(*6g*)	2	Fe1(*6g*)	2.433		1	Fe2(*12j*)	2.817
	2	Fe3(*12k*)	2.440		2	Ge(*4f*)	3.047
	4	Fe2(*12j*)	2.520				
	1	Ge(*4f*)	2.598				
	1	U2(*2d*)	3.206				
	2	U1(*2b*)	3.214				

Fe1

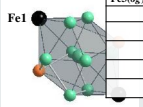

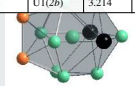

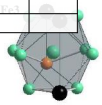

12-02-2021 24

TÉCNICO LISBOA — C²TN

$U_2Fe_{17-x}Ge_x$

Copyright protected content

T. Berlureau, B. Chevalier, L. Fournès, J. Etorneau, *Materials Letters* 9 (1989) 21
B. Chevalier. P. Gravereau. T. Berlureau. L. Fournès. J. Etorneau. *J. Alloys Compound.* 233 (1996) 174

TÉCNICO LISBOA — C²TN

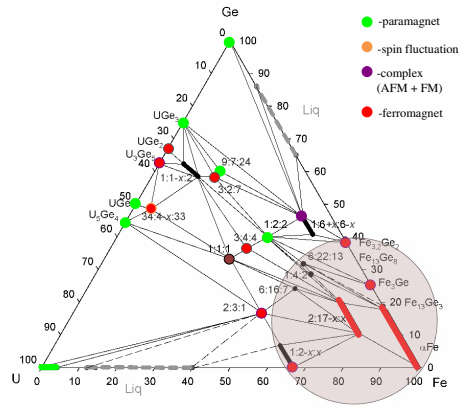

TÉCNICO LISBOA — C²TN

U_2Fe_3Ge

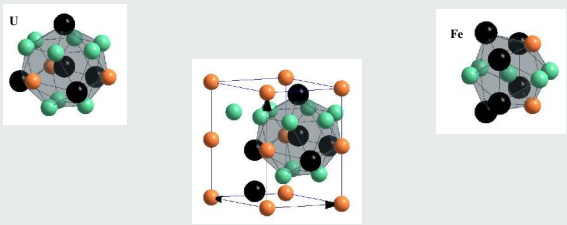

	NN	Atoms	d (Å)		NN	Atoms	d (Å)
U(4f)	1	U(4f)	2.751(2)	Fe(6h)	2	Ge(2a)	2.485(2)
	3	Fe(6h)	2.930(1)		2	Fe(6h)	2.527(4)
	6	Fe(6h)	2.9320(6)		2	Fe(6h)	2.651(4)
	3	Ge(2a)	3.0458(6)		2	U(4f)	2.930(1)
	3	U(4f)	3.209(1)		4	U(4f)	2.2320(6)

TÉCNICO LISBOA — C²TN

U_2Fe_3Ge

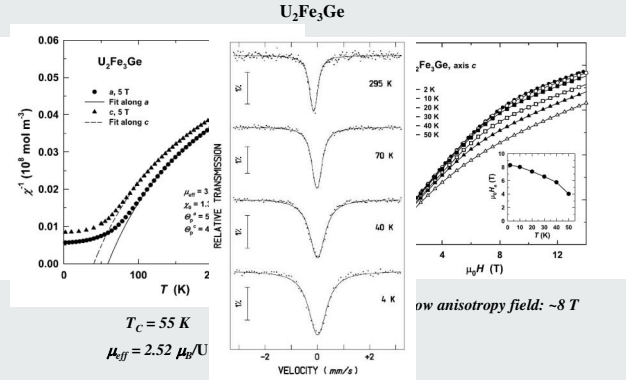

$T_C = 55$ K

$\mu_{eff} = 2.52\ \mu_B$/U

ow anisotropy field: ~8 T

M.S. Henriques, O. Tougait, H. Noel, L.C.J. Pereira, J.C. Waerenborgh, A.P. Gonçalves, Solid State Commun.148 (2008) 159
M S Henriques, D I Gorbunov, J C Waerenborgh, L Havela, A B Shick, M Divis, A V Andreev, A P Gonçalves, J. Phys.: Condens. Matter 25 (2013) 066010

TÉCNICO LISBOA — C²TN

U_2Fe_3Ge

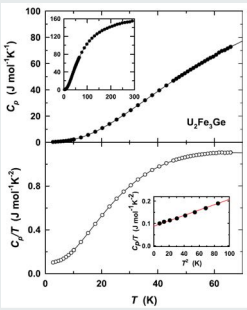

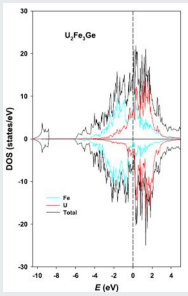

U_2Fe_3Ge=>γ~ 46 mJ mol^{-1} U K^{-2}
θ_D=217K

UNi_2: γ~65 mJmol^{-1} K^{-2}
θ_D=248K

Method	FP-LAPW				FPLO			
Atom	U		Fe		U		Fe	
Magnetic moments	M_s	M_L	M_s	M_L	M_s	M_L	M_s	M_L
LSDA	0.827	−0.545	−0.993	−0.080	0.835	−0.473	−0.938	−0.080
LSDA+U = 1 eV	1.062	−1.405	−1.163	−0.143				
LSDA+U = 2 eV	1.204	−1.904	−1.237	−0.164				

M S Henriques, D I Gorbunov, J C Waerenborgh, L Havela, A B Shick, M Divis, A V Andreev, A P Gonçalves, J. Phys.: Condens. Matter 25 (2013) 066010

TÉCNICO LISBOA — C²TN

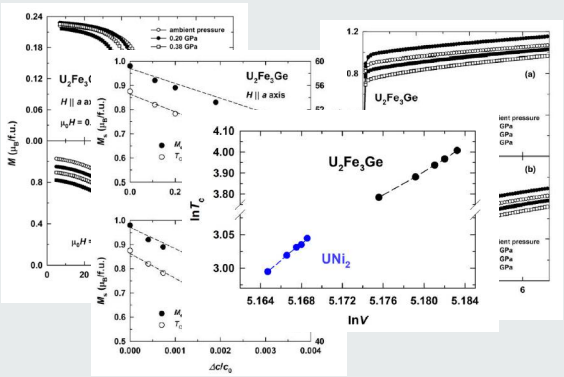

M.S. Henriques, D. I. Gorbunov, A.V. Andreev, Z. Arnold, S. Surblé, S. Heathman, J.-C. Griveau, E.B. Lopes, J. Prchal, L. Havela, A.P. Gonçalves, Phys. Rev. B, 89 (2014) 054407

TÉCNICO LISBOA

Summary

C²TN

- U-Fe-Ge system at 900ºC is very rich, with 13 ternary solid phases;
- 4 (3 + 1) ternary solid solutions, 3 new structure types;
- A rich crystallography, with common trends, are seen;
- Different ground states are observed;
- Hill rule is partially followed;
- Magnetism of high Fe-content phases dominated by Fe;
- Hybridization leads to a decrease of the magnetic moments and magnetic ordering temperature;
- U_2Fe_3Ge an unique compound;

12-02-2021 31

TÉCNICO LISBOA

C²TN

12-02-2021 32

3.18 A. S. P. Gomes（Universite de Lille, France）

Electronic structure of actinide systems from relativistic correlated and quantum embedding approaches

Electronic structure of actinide systems from relativistic correlated and quantum embedding approaches

www.cnrs.fr

André Severo Pereira Gomes
andre.gomes@univ-lille.fr

Laboratoire de Physique des Lasers, Atomes et Molécules (PhLAM), CNRS UMR8523
Université de Lille
http://phlam.univ-lille.fr

Acknowledgements

- PCMT @ PhLAM (Lille)
  - Yassine Bouchafra, Loic Halbert, **Florent Réal, Valérie Vallet**
- (relativistic) Embedding + electronic structure
  - Malgorzata Olejniczak (Warsaw), Radovan Bast (Tromso), **Christoph Jacob (Braunschweig)**, Pawel Tecmer (Torun), **Lucas Visscher (Amsterdam)**, Trond Saue (Toulouse), Avijit Shee (Ann Arbor)
- Support

http://diracprogram.org
@DIRACprogram

Actinides in condensed phase

- Understanding the behavior of actinides in condensed phase a key technological issue
  - Nuclear fuel cycle: optimization of separation processes
  - waste disposal: interaction with clays in geological repositories, environment

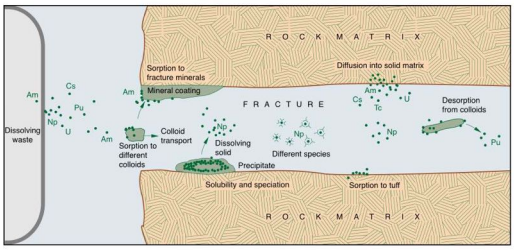

Los Alamos Science, 26 (2006)

The complexity of An electronic structure

- Properties based on filling the 5f orbitals: 5f/6d/7p/7s orbitals have similar energies from U to Am
  - Competition between $5f^N7s^2$ and $5f^{N-1}6d7s^2$ configurations, resulting in many quasi-degenerate states
- Relativistic effects due to the high atomic charge of heavy nuclei
- Virtually all compounds measured in solution or in the solid state
  - many oxidation states possible, different species are most stable
    - atomic ions: oxidation states II-VI
    - oxo (Pa) and dioxo (AnO_2^{n+}, or actinyl) ions: oxidation states V, VI
  - Variable number of ligands in first coordination sphere
    - typically 8-9 ligands for atoms, up to five for actinyls

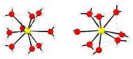

Electronic structure of Ln/An: environment effects (=ligands)

Los Alamos Science, 26 (2006)

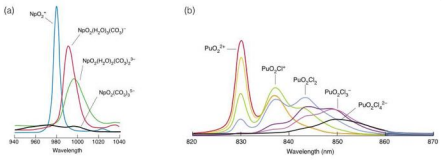

Los Alamos Science, 26 (2006)

Actinyl (AnO_2^{n+}) MO Diagram: understanding low-lying spectra

- U(VI): transitions from σ_u (blue box) to unoccupied (δ, φ orange box) orbitals
- U(V)/U(IV), Np, Pu,…: transitions between partially filled orbitals (δ, φ orange box)

Copyright protected content

Denning JPCA 2007, 111, 4125

www.cnrs.fr

relativistic correlated electronic structure and quantum embedding methods

Relativistic effects

- Mass increase effect: contraction of *s*, *p* and expansion of *d*, *f* orbitals/spinors
- Spin-orbit coupling (SOC): ***J*** (not ***L***, ***S***) good quantum number
- Dirac equation: set of four coupled differential equations
  - H-like atoms $\begin{pmatrix} V-E & c(\boldsymbol{\sigma}\cdot\mathbf{p}) \\ c(\boldsymbol{\sigma}\cdot\mathbf{p}) & V-E-2mc^2 \end{pmatrix}\begin{pmatrix} \psi^{\mathrm{L}} \\ \psi^{\mathrm{S}} \end{pmatrix} = 0$
    with $V = -Z/r$ and $\boldsymbol{\alpha} = \begin{pmatrix} \mathbf{0} & \boldsymbol{\sigma} \\ \boldsymbol{\sigma} & \mathbf{0} \end{pmatrix}$
  - Molecular systems $\hat{H} = \sum_i \hat{h}_i + \frac{1}{2}\sum_{i\neq j} \hat{g}_{ij} + V_{NN}$
    - One-electron operator: $\hat{h}_i \equiv \hat{h}_D(i) = c\boldsymbol{\alpha}\cdot\mathbf{p}(i) + \boldsymbol{\beta}' mc^2 + v_{nuc}$ $\quad \boldsymbol{\beta}' \rightarrow \boldsymbol{\beta} - \mathbf{I}_{4\times4}$
    - Two-electron operator: charge-charge and current-current interactions
      $\hat{g}_{ij} = \left[\frac{\mathbf{I}_{4\times4}}{r_{ij}}\right] - \left[\frac{\boldsymbol{\alpha}_i\cdot\boldsymbol{\alpha}_j}{2r_{ij}}\right] - \left[\frac{(\boldsymbol{\alpha}_i\cdot\mathbf{r}_{ij})(\boldsymbol{\alpha}_j\cdot\mathbf{r}_{ij})}{r_{ij}^2}\right] = \hat{g}_{ij}^{\mathrm{Coulomb}} + \hat{g}_{ij}^{\mathrm{Gaunt}} + \hat{g}_{ij}^{\mathrm{gauge}}$
- Dirac equation can be taken from 4-component to 2-component form by block diagonalization

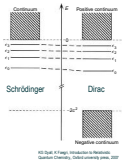

KG Dyall, K Fægri, Introduction to Relativistic Quantum Chemistry, Oxford university press, 2007

see e.g. Saue ChemPhysChem 2011, **12**, 3077 for further references

Electron correlation : coupled cluster approaches

- Single-reference coupled-cluster (SR-CC) : ground state wave functions (WFs), accurate scheme, solved by projection, truncated (CCSD)
  $|\Psi_0\rangle = \exp(\hat{T})|\Phi_{\mathrm{HF}}\rangle \qquad \hat{T} = \hat{T}_1 + \hat{T}_2 + \ldots = \sum_{\mu_1} t_{\mu_1}\hat{\tau}_{\mu_1} + \sum_{\mu_2} t_{\mu_2}\hat{\tau}_{\mu_2} + \ldots$
- Fock-space coupled cluster (FS-CCSD) : multi reference approach
  - Effective Hamiltonian $\hat{H}|\Psi_m\rangle = E_m|\Psi_m\rangle \longrightarrow \hat{H}_{\mathrm{eff}}|\varphi_m\rangle = \hat{\Omega}^{-1}\hat{H}\hat{\Omega}|\varphi_m\rangle = E_m|\varphi_m\rangle$
  - WFs obtained within a model spaces (P) $\{|\varphi_k\rangle\}$ ($|\Psi_k\rangle = \hat{\Omega}|\varphi_k\rangle$) in different sectors of Fock space (FS) denoted by different in (h,p) to closed shell reference
    $\mathrm{M}(0,0) \rightarrow \mathrm{M}^{+}(1,0) \rightarrow \mathrm{M}^{-}(0,1) \rightarrow \mathrm{M}^{(*)}(1,1)$
  - Intermediate Hamiltonian (IH) : P = P_m + P_i largely eliminates intruder states, first used on actinides for PuO_2^{2+}, NpO_2^{2+} (Infante *et al.* JCP 2006, **125**, 074301)
- Equation of motion (EOM-CCSD): WFs linear parametrization of SRCC
  $|\Psi_k\rangle = \hat{C}_k\exp(\hat{T})|\Phi_{\mathrm{HF}}\rangle \qquad \hat{C}_k = \hat{C}_1^{(k)} + \hat{C}_2^{(k)} + \ldots = \sum_{\mu_1} C_{\mu_1}^{(k)}\hat{\tau}_{\mu_1} + \sum_{\mu_2} C_{\mu_2}^{(k)}\hat{\tau}_{\mu_2} + \ldots$
  $\langle\tilde{\Psi}_l| = \langle\Phi_{\mathrm{HF}}|(1+\hat{\tilde{C}}_l\exp(-\hat{T}))$

  expansion coefficients obtained from diagonalization of $H_{ij} = \langle\tilde{\Psi}_i|\hat{H}|\Psi_j\rangle = \mathbf{C}_i^T\mathbf{H}\mathbf{C}_j$

UO_2^{2+}, isoelectronic species' (NUO^+, NUN) excitation energies

- IHFSCC as reference — Tecmer *et al.* PCCP 2011, **13**, 6249
- TD(DFT) often unreliable
  - CAMB3LYP, PBE0 seem the best for actinies
  - ALDA, full derivative close but not equivalent
- CASPT2: good average, large spread
- EOM-CC (not shown): origin shifted but very reproducible spacings

Copyright protected content

ThF⁺	Denis *et al.*, New J Phys 2015, **17**, 043005
PuO_2^{2+}	Kervazo *et al.*, Inorg. Chem. 2019, **58**, 14507
Actinyls	Real *et al.*, JPCA, 2009, **113**, 12504
	Tecmer, *et al*, JCP 2014, **141**, 041107

Embedding approaches : quantum embedding

- Spectra with accurate (costly) methods for species of interest (red)
- Environment (blue) with more approximate methods

All with accurate: ~months

All with approximate: ~weeks

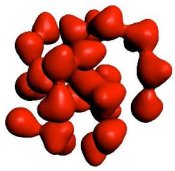

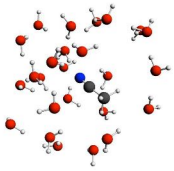

Embedding: ~weeks

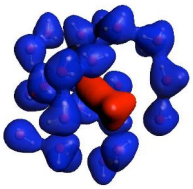

- In QM/QM (quantum) embedding, electronic structure in all fragments available

Frozen density embedding: DFT-in-DFT

- Partition into subsystems (SS) (Wesolowski, Warshel, JPC 1993, **97**, 8050)
  $n(\boldsymbol{r}) = n_{\mathrm{I}}(\boldsymbol{r}) + n_{\mathrm{II}}(\boldsymbol{r}) \longrightarrow E[n] = E_{\mathrm{I}}[n_{\mathrm{I}}] + E_{\mathrm{II}}[n_{\mathrm{II}}] + E_{\mathrm{int,}}[n_{\mathrm{I}}, n_{\mathrm{II}}]$
  $E_{\mathrm{int,}}[n_{\mathrm{I}}, n_{\mathrm{II}}] = E_{\mathrm{nuc}}^{\mathrm{I,II}} + \iint \frac{n_{\mathrm{I}}(\boldsymbol{r})n_{\mathrm{II}}(\boldsymbol{r}')}{|\boldsymbol{r}-\boldsymbol{r}'|}d\boldsymbol{r}d\boldsymbol{r}'$
  $+ \int\left[n_{\mathrm{I}}(\boldsymbol{r})v_{\mathrm{nuc}}^{\mathrm{II}}(\boldsymbol{r}) + n_{\mathrm{II}}(\boldsymbol{r})v_{\mathrm{nuc}}^{\mathrm{I}}(\boldsymbol{r})\right]d\boldsymbol{r} + E_{\mathrm{xck}}^{\mathrm{nadd}}[n_{\mathrm{I}}, n_{\mathrm{II}}]$

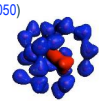

- Non-additive terms
  $E_{\mathrm{xck}}^{\mathrm{nadd}}[n^{\mathrm{I}}, n^{\mathrm{II}}] = E_{\mathrm{xc}}^{\mathrm{nadd}}[n^{\mathrm{I}}, n^{\mathrm{II}}] + T_{\mathrm{s}}^{\mathrm{nadd}}[n^{\mathrm{I}}, n^{\mathrm{II}}]$
  $= E_{\mathrm{xc}}[n^{\mathrm{I}} + n^{\mathrm{II}}] - E_{\mathrm{xc}}[n^{\mathrm{I}}] - E_{\mathrm{xc}}[n^{\mathrm{II}}] + T_{\mathrm{s}}[n^{\mathrm{I}} + n^{\mathrm{II}}] - T_{\mathrm{s}}[n^{\mathrm{I}}] - T_{\mathrm{s}}[n^{\mathrm{II}}]$
- Minimization of total energy: KS-like equations including the embedding potential
  $\left[T_{\mathrm{s}}(i) + v_{\mathrm{KS}}[n_{\mathrm{I}}] + v_{\mathrm{int}}^{\mathrm{I}}[n_{\mathrm{I}}, n_{\mathrm{II}}] - \varepsilon_i\right]\phi_i^{\mathrm{I}}(\boldsymbol{r}) = 0$
  $v_{\mathrm{int}}^{\mathrm{I}}(\boldsymbol{r}) = v_{\mathrm{xc}}^{\mathrm{nadd}}(\boldsymbol{r}) + \left.\frac{\delta T_{\mathrm{s}}^{\mathrm{nadd}}}{\delta n}\right|_{n_{\mathrm{I}}} + v_{\mathrm{nuc}}^{\mathrm{II}}(\boldsymbol{r}) + \int\frac{n_{\mathrm{II}}(\boldsymbol{r}')}{|\boldsymbol{r}-\boldsymbol{r}'|}d\boldsymbol{r}'$
- Molecular properties : response theory (see e.g. Gomes and Jacob, Annu. Rep. Prog. Chem. Sect. C: Phys. Chem. 2012, **108**, 222 and references therein)

Frozen density embedding: CC-in-DFT

- WFT-in-DFT (e.g. Huang and Carter, JCP 2006, **125**, 084102, Wesolowski PRA 2008, **77**, 012504)
  - $E_I[n_I] = \langle \Psi_I | \hat{H}_I | \Psi_I \rangle$, minimize total energy wrt variations of $n^I(\boldsymbol{r}) \leftarrow \Psi_I^\dagger \Psi_I$
  - embedding potential costly (several WFT calculations)
  - Simple WFT-in-DFT scheme (Gomes *et al.*, PCCP 2008, **10**, 5353): DFT-in-DFT potential a local, 1-body operator. Useful with CC (IHFSCC, EOM)

    $v^I_{\text{int}}(\boldsymbol{r}) \implies F_{pq} \leftarrow \langle p | v^I_{\text{int}}(\boldsymbol{r}) | q \rangle$
- **Common framework** for DFT-in-DFT, WFT-in-DFT or WFT-in-WFT (Höfener *et al.* JCP 2012, **136**, 044104;JCP 2013, **139**, 104106) for **time-(in)dependent molecular properties**
  - Straightforward definition of CC-in-DFT ground-state, response
    - Simple CC-in-DFT scheme: good approximation also in the response case
  - Black-box handling of SOC in heavy elements (Shee *et al.*, JCP 2018, **149**, 174113): 4C-EOM-IP/EE/EA-CCSD

www.cnrs.fr

Determining the properties of actinide species in the presence of an environment

Benchmarking systems for actinyl species

- Crystalline materials ($Cs_2UO_2Cl_4$, etc): know structure, accurate data
  - molecular ions (actinyls chlorides, nitrates, carbonates, …)

Copyright protected content

Single-crystal polarized absorption spectrum of $Cs_2UO_2Cl_4$ at 4.2 K (R. G. Denning, Structure and Bonding 79, 1992)

- This talk: valence excitation and ionization energies (work in progress: core ionization and excitation energies)
  - Goal: arrive at embedded models with lowest computational cost possible but still accurate results w.r.t. the original complex (= actinyl + equatorial ligands)

Actinyls (NpO_2^{2+} and UO_2^{2+}) in $Cs_2UO_2Cl_4$

- Structural models: $AnO_2Cl_4^{2-}$ without (D_{4h}) and with (C_{2h}) the crystal environment
  - active subsystem: WFT/DFT; environment, near: DFT, far: point charges

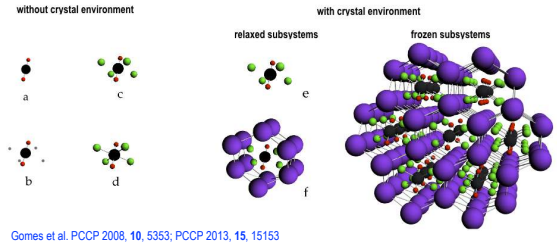

Gomes et al. PCCP 2008, **10**, 5353; PCCP 2013, **15**, 15153

Actinyls as active subsystems in $AnO_2Cl_4^{2-}$: what changes ?

- Actinyl (here uranyl) embedded onto the equatorial field of chlorides (SF-ZORA, TZ2P, SAOP model potential)

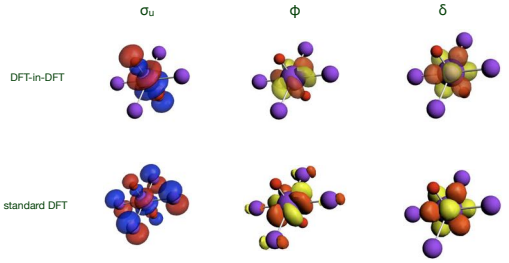

$NpO_2Cl_4^{2-}$ in $Cs_2UO_2Cl_4$: f-f spectrum

embedded neptunyl a good model (discrepancy between models c-FnT, d often around 300 cm^{-1})

need to have a good starting density for Cl_4^{4-} group (FnT)

large long-range effects for Π states

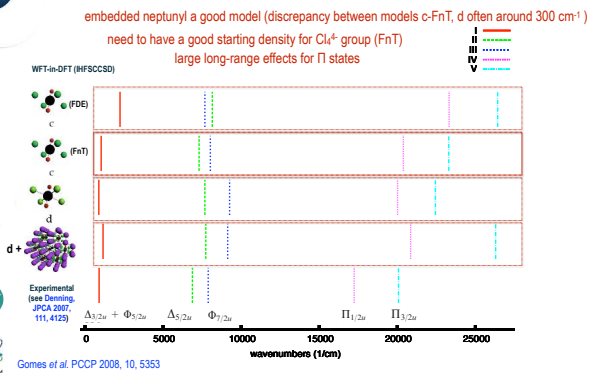

Gomes *et al.* PCCP 2008, 10, 5353

$UO_2Cl_4^{2-}$ in $Cs_2UO_2Cl_4$: "σ-f" spectrum, relative to state VII ($\sigma_u\delta$)

embedded uranyl a pretty good model (1000 cm^{-1} discrepancy between models c, d)
small effects due to crystal: all states stabilized

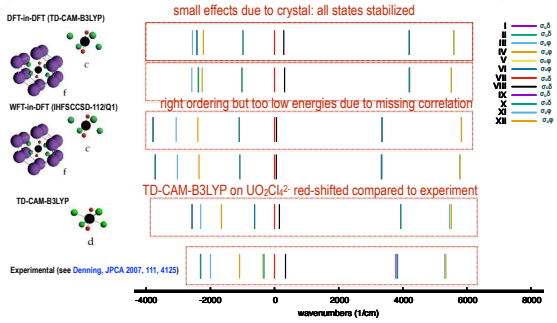

Gomes *et al.*, PCCP 2013, **15**, 15153

$UO_2Cl_4^{2-}$: DFT-in-DFT, CC-in-DFT ionization energies

embedded uranyl a good mode in gas phase and in the crystal

uranyl

9.32 eV (CAM-B3LYP)
10.61 eV (IHFSCC/Q_1)

~9.4 eV (Exp.)

Copyright protected content

Dau *et al.*, JCP 2012, 137, 064315

Copyright protected content

Denning, JPC A 2007, 111, 4125

Gomes *et al.*, PCCP 2013, **15**, 15153

Towards systems in aqueous solution: Polarizable force fields

- Many-body polarizable force-fields (TCPE)

$$U_{int} = \sum_i U_i^{pair} + \sum_j U_{pol}^{Many-Body} + \sum_i U_{sp}^{pair} + \sum_j U_{sp}^{Many-Body}$$

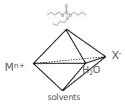

- Parametrization from QM cluster calculations
- Actinide (Th(IV) to Bk(IV))-water, H-bonding, solute-solvent-counter-ion interactions, halogen-water interactions
- Accurate for large range of temperatures and pressure (water liquid at 298.15 K)

Masella, Cuniasse, JCP 2003, **119**, 1866
Real *et al.* JCP 2013, **139**, 114502
Real *et al.* JPCB 2010, **114**, 15913
Real *et al.* J. Comput. Chem. 2013, **34**, 707
Real *et al.*, JCP 2016, **144**, 124513
Acher *et al.* PCCP 2020, **22**, 2343

Copyright protected content

Exp.: Soper, CPL 2000, **258**, 121

Acher *et al.* PCCP 2020, **22**, 2343

Conclusions

- DFT functionals are often unreliable for energetics and properties of actinide species
  - IHFS-CCSD, EOM-CCSD or CASPT2 to be preferred
- Quantum embedding methods (DFT-in-DFT and WFT-in-DFT) very useful for molecular species in complex environments
  - Full QM treatment retained : access to properties for all subsystem
    - other molecular properties (NMR shielding etc) can be investigated
  - Simple CC-in-DFT approach works well for electronic spectra and ionizations
    - Not easy to describe excitation spectra of uranyl in $Cs_2UO_2Cl_4$ (differential correlation in ground and excited states)
- Classical polarizable force fields provide a reliable way to incorporate temperature and sampling for (highly) charged heavy element systems

www.cnrs.fr

supplementary slides

Valence electron binding energies in water droplets

- Comparisons for iodide
  - WFT-in-DFT over 100 classical MD snapshots (TCPE2016)
  - Subsystem A: WFT (EOM-IP-CCSD)
    - absolute energy differences and $^2P_{3/2}$ - $^2P_{1/2}$ separation are quite good
  - Subsystem B: DFT (SAOP)

State	Experiment / eV	Theory / eV
$^2P_{3/2}$	8.03(6)	8.0(3)
$^2P_{1/2}$	8.96(7)	9.0(3)
b_1	11.31(4)	10.4(5)
a_1	13.78(7)	12.5(4)

- Competitive in accuracy with state of the art band structure calculations (G_0W_0/sc-hybrid Gaiduk *et al.*, JACS 2016, **138**, 6912)

Copyright protected content

Kurahashi *et al.*, JCP 2014, **140**, 174506

Copyright protected content

Bouchafra *et al.*, PRL 2018, **121**, 266001

DFT-in-DFT for magnetic perturbations

- Static magnetic fields induce changes in the total energy

$$E(\varepsilon) = E_0 + \frac{1}{2}\frac{d^2E}{d\varepsilon_A d\varepsilon_B}\varepsilon_A\varepsilon_B + \frac{1}{4!}\frac{d^4E}{d\varepsilon_A\ldots d\varepsilon_4}\varepsilon_A\ldots\varepsilon_4 + \ldots$$

- NMR spectroscopy: external magnetic field (**B**), nuclear magnetic moment (m_K)
  - NMR Shielding tensor $\sigma^K_{\alpha\beta} = \left.\frac{d^2E}{dB_\alpha dm_{K;\beta}}\right|_{\vec{B},\{\vec{m}_K\}=0}$,
  - Indirect spin-spin coupling tensor

$$K^{KL}_{\alpha\beta} = \left.\frac{d^2E}{dm_{K;\alpha}dm_{L;\beta}}\right|_{\{\vec{m}_K\}=0} \qquad K^{KL}_{\alpha\beta} = 2\pi/(\hbar\gamma_K\gamma_L)J^{KL}_{\alpha\beta}.$$

- Magnetizability tensor: external magnetic field (**B**)

$$\xi_{\alpha\beta} = -\left.\frac{d^2E}{dB_\alpha dB_\beta}\right|_{\vec{B}=0}$$

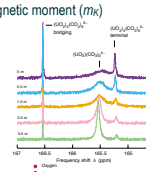

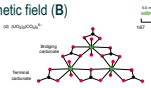

Los Alamos Science, 26 (2006)

- 1C/2C FDE description for *J*, σ (Jacob, Visscher JCP 2006, **125**, 194104; Götz *et al.* JCP 2014, **140**, 104107), 4C FDE formulation for all three tensors (Olejniczak *et al.*, PCCP 2017, **19**, 8400) but still unexplored for actinides

Need for better kinetic energy DFs: CUO-noble gas complexes

- CUO (isoelectronic to uranyl): shifts in vibrational frequencies when changing from neon to argon matrix due to change in ground-state (singlet to triplet)?

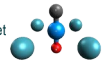

- Kinetic energy density functionals found not to be accurate enough for WFT-in-DFT to address this question (Tecmer *et al.* JCP 2012, **137**, 084308)

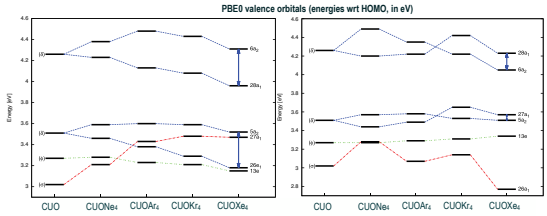

full complex

FDE (PW91k): CUO active subsystem

3.19 R. Caciuffo（EU JRC, Karlsruhe, Ger- many）

Radioisotopes for medical applications

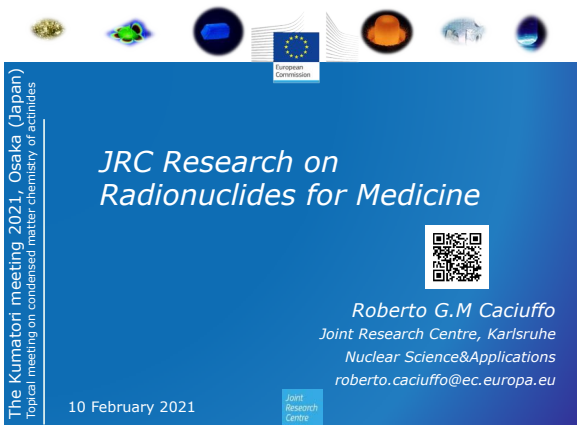

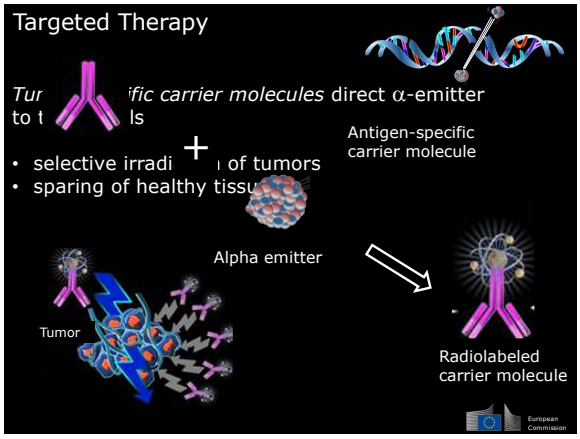

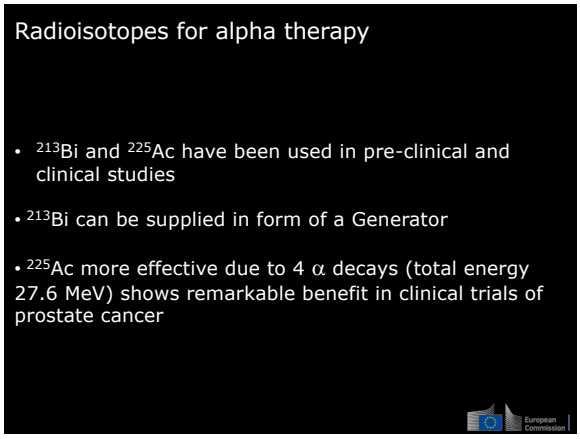

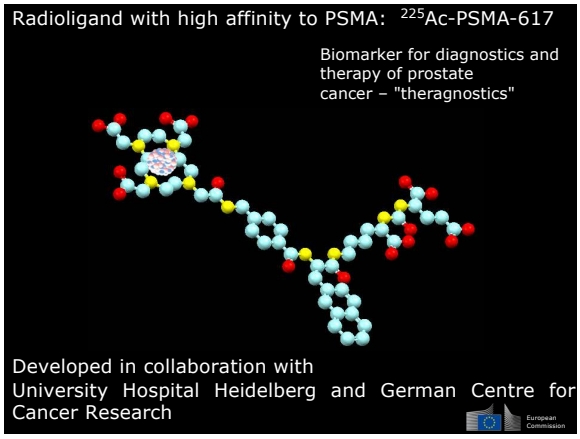

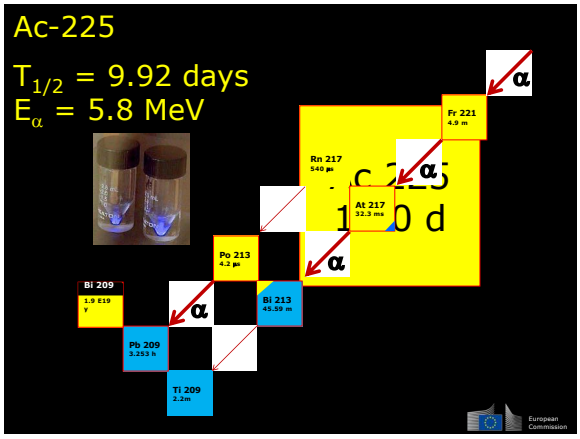

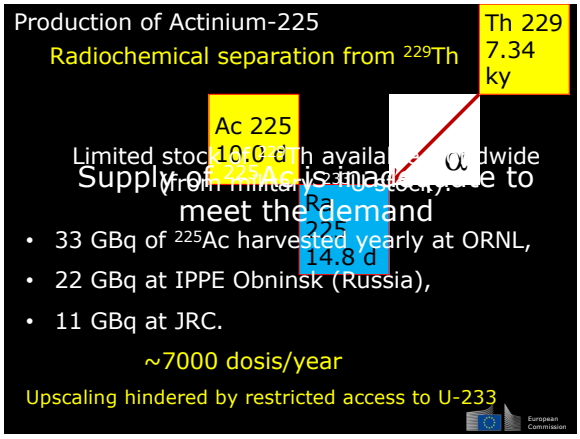

Production through the $^{229}Th/^{225}Ra/^{225}Ac$ generator

^{229}Th stock (~ 1 g) absorbed on ion exchange resin.

Ingrowth of ^{225}Ra and ^{225}Ac through ^{229}Th alpha decay

^{225}Ra and ^{225}Ac are eluted and split into separate fractions.

^{225}Ac can be collected from the ^{225}Ra fraction as well

^{229}Th is strongly absorbed on an ion exchanger

European Commission

Transmutation of ^{226}Ra to ^{229}Th by (n,γ) reactions

(n,γ) → Th 229 7.34 ky

Potential production of ^{229}Th at a high flux reactor:

~0.5 GBq/g ^{226}Ra / year

- Very large Radium targets needed
- Radon management is a severe challenge
- Almost 1000 more ^{228}Th co-produced

European Commission

Transmutation of Ra-226 by (n, 2n) reaction

Favored for fast neutrons

Ac 225 10.0 d

Ra 225 14.8 d

(n, 2n)

Target

Ra 226 1600 y

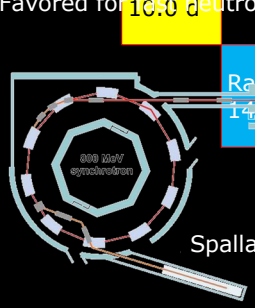

Spallation Neutron Sources

European Commission

Proton irradiation of Ra-226 $^{226}Ra(p,2n)^{225}Ac$

σ = 710 mb at 16.8 MeV

-100 µA proton current

-50 mg Ra target:

500 doses/day

Ac 225 10.0 d

Ac 227 21.8 y

Ra 226 1600 y

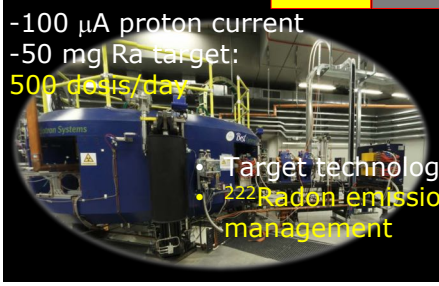

- Target technology
- $^{222}Radon$ emission management

European Commission

Excitation function $^{226}Ra(p, 2n)^{225}Ac$

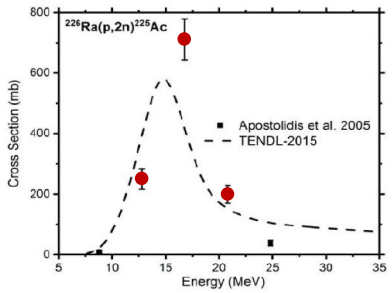

European Commission

Production process

Common steps for most methods are:

- From ^{226}Ra a target is manufactured
  - Pellet pressing
  - Electrodeposition
  - Evaporation
  - precipitation
- Welding or sealing the ^{226}Ra in the target
- Cyclotron irradiation
- ^{226}Ra target opening and dissolution
- ^{225}Ac recovery and purification
- ^{226}Ra recovery and preparation/ conversion for re-use

Example invention: method for producing Ac-225... (EP 0 962 942 A1)

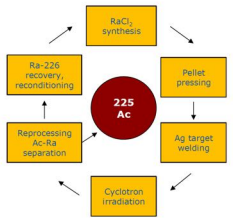

European Commission

Managing the ^{222}Rn emission is a problem

In the process macro amounts (mg to g) of ^{226}Ra will be at least partly openly handled.

- All process steps requires tight Rn control
- Special Rn filters
- Extended radioprotection
- Makes the handling very difficult

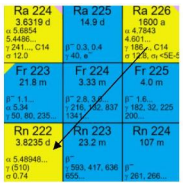

A(^{226}Ra) = A(^{222}Rn)
secular equilibrium

^{222}Rn constantly produced from ^{226}Ra

•chemical inert
•difficult to contain
•diffuses through plastics
•Requires under-pressure and gas-tight conditions

Liquid target with closed loop

Maximise Ra concentration in the liquid target to optimise production rate

Circulation - solution composition optimised for stability and solubility

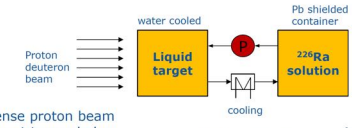

No target dissolution, allows direct chemical separation between Ac and Ra

Intense proton beam current to maximise production rate

Efficient liquid cooling (heat removal)

As less aggressive as possible (acidity)

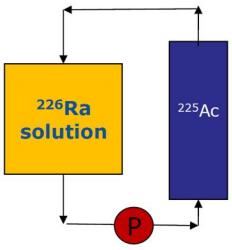

Closed recirculation over extraction chromatography columns

^{225}Ac stays on the column

^{226}Ra + daughters remains in solution

Closed ^{225}Ac Recovery and purification

Principles

- Ra with daughters and impurities are kept in the recirculation liquid target solution.
- Actinium is purified on extraction chromatography columns (the concentration of actinium is so small that problems of high metal loading is avoided)
- Actinium is moved from column to column by changing acidity
- The solutions are recirculated in closed loops (movement of acidity is limited as the resin capacity for acid extraction is limited).
- Rn is managed by columns filled with powdered activated carbon / granulated activated carbon.
- Ra losses (if any) in the first separation are directed towards a Ra recovery with Rn filters (low volume stream)

^{225}Ac production rates in a liquid loop

Example : T_{irr} = 1 week, Tcool = 0 days, ^{226}Ra concentration = 0.10 M, σ = 0.5 b

Current	^{225}Ac activity		Heat tot
uA	Bq	mCi	W
10	3.64E+08	9.8	300
20	7.27E+08	19.7	600
30	1.09E+09	29.5	900
40	1.45E+09	39.3	1200
50	1.82E+09	49.1	1500
60	2.18E+09	59.0	1800
70	2.54E+09	68.8	2100

Current Dir G site Karlsruhe production every 8 weeks

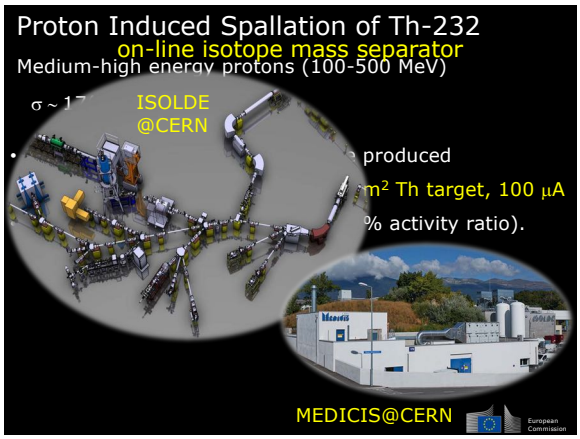

ISOL production

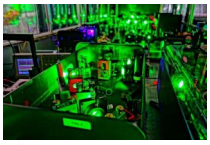

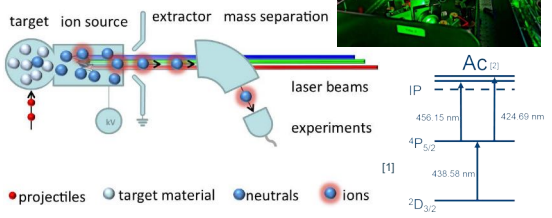

➔ Chemical and mass selectivity for pure beam

Courtesy K. Dockx (Leuven University)

[1] [CERN. (n.d.). RILIS. Retrieved November 28, 2016, from cern.ch
[2] Ferrer, R., et al. Nature communications 8 (2017): 1452; Reader, S., et al. Hyperfine Interactions 216(2013): 33
[3]http://rilis.web.cern.ch/

γ irradiation of Ra-226

$^{226}Ra(\gamma,n)^{225}Ra(\beta)^{225}Ac$

Investigated in Karlsruhe about 20 years ago.

Feasible, but cross-section and yields are largely unknown

It could be of interest as today LINACs are more available as well advanced light sources *e.g.* FLASH, LCLS

The potential of this method will be investigated at GELINA in Geel

Acknowledgement

TAT has been developed at JRC-Karlsruhe over more than 30 years.
The idea was first developed by
L. Koch, M. W. Geerlings, and C. Apostolidis.

The program is currently run by
Alfred Morgenstern and Frank Bruchertseifer.

The effort on radionuclide production is coordinated by:
Rikard Malmbeck and Alban Kellerbauer

Chapter 4 Break Session

4.1 Break Session 1

4.1.1 H. Shishido（Tohoku Univ.）

Proposals for the advanced nuclear fuel cycle by introducing a fusion reactor

Proposal for the advanced nuclear fuel cycle by introducing a fusion reactor

Hiroki Shishido

Department of Quantum Energy Engineering,
Graduate School of Engineering,
Tohoku University

1

1. Introduction
1.1 Severe problems on fusion reactor development

Controlled fusion reaction will be achieved by the ITER project.

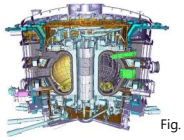

Fig. ITER[1]

Demo design is not fixed due to remaining engineering issues

1) the divertor system loaded by extremely high heat flux
2) maintenance of components loaded by neutrons

Even after the Demo construction, , ,

DEMO reactors → Scaling up → Commercial reactors

The power increase brings **more severe heat load** to the divertor.

As one of the options,
Transmutation of minor actinides (MA) and fission product generated from nuclear power plants.

[1] https://www.iter.org/

2

1. Introduction
1.2 Closed nuclear fuel cycle with a fusion reactor [2]

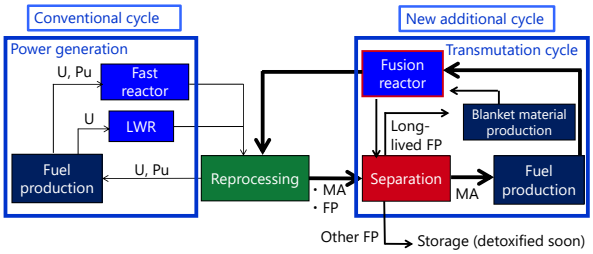

To contribute to "Geological repository"

[2] H. Hashizume et al., presented at the 14th International Symposium on Fusion Nuclear Technology, 2019 Budapest, Hungary.

3

1. Introduction
1.3 The concepts of this study

Copyright protected content

Today's topic

Minor actinides transmutation [4]

- Solid fuels (Oxides or Nitrides)
- Underneath the null points
  Large neutron load
  and small heat load
- Very limited region

Minimization of the influences on the latest design

Fission products transmutation

- Liquid fuels
  (dissolved in molten salts)
- Very limited region in the blanket

Evaluation of the ^{135}Cs transmutation[5]

Development of the molten salts for specialized transmutation[6]

[3] A. Sagara et al., Fusion Eng. Des. 89 (2014) 2114.
[4] Y. Furudate, H. Shishido et al., Prog. Nucl. Energy 103 (208) 28.
[5] T. Kitasaka, H. Shishido et al., Fusion Eng. Des., submitted.
[6] T. Kitasaka, H. Shishido et al., Plasma and Fusion Research 15 (2020) 2405077.

1. Introduction
1.4 MA transmutation in a fusion reactor

Copyright protected content

Fig. Helical fusion reactor FFHR-d1[3]

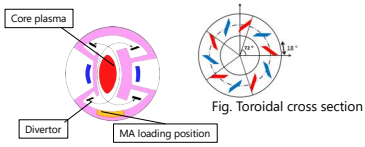

Fig. Toroidal cross section

Fig. Poloidal cross section

Table Summary of the burn-up characteristics [4]

Loaded MA [ton]	80	
Fusion power [MW]	1,000	
Heat generation rate in fuel[W/cm³]	119	58
In reactor core [W/cm³]	55.7	13.6
Support factor [-]	28.3	22.6

*support factor = Transmuted MA/year in a fusion reactor / Generated MA/year from a 1GWe PWR

[3] A. Sagara et al., Fusion Engineering and Design 89 (2014) 2114-2120.
[4] Y. Furudate, H. Shishido et al., Prog. Nucl. Energy 103 (208) 28.

5

1. Introduction
1.4 MA transmutation in a fusion reactor

Copyright protected content

Fig. Helical fusion reactor FFHR-d1[3]

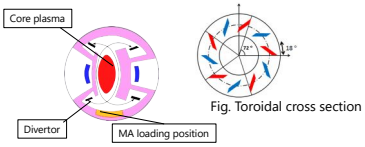

Fig. Toroidal cross section

Fig. Poloidal cross section

Table Comparison of support factors between fusion reactors and ADS

	Under construction			Next system	
	Name	Main parameter		Main parameter	Support factor
ADS	MYRRHA (Belgium)	Proton beam 2.4 MW	12.5 times →	Proton beam 30 MW	10
Fusion reactor	ITER (France)	Fusion power 500 MW	2–3.6 times →	Fusion power 1000–1800 MW	**22–40**

1. Introduction
1.5 Pu transmuted from MA

Copyright protected content

$^{237}Np \xrightarrow{(n,\gamma)} {}^{238}Np \rightarrow {}^{238}Pu$

β decay
$T_{1/2}$ = 2.4 d

[7] A. Sasahara et al., Journal of Nuclear Science and Technology 41 (2004) 448-456.

7

1. Introduction
1.5 Pu transmuted from MA (Cont'd)

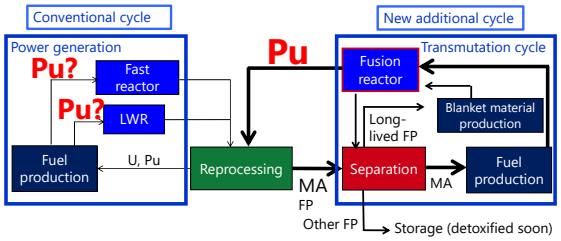

Is it possible to re-utilize the transmuted Pu in a fission reactor?
High level **waste** → Energy **resource**?

8

2. Today's presentation contents

The presentation provides:

1) Fast reactor core characteristics loaded the transmuted Pu,
2) MOX BWR core characteristics with the transmuted Pu to evaluate the controllability of reactivity,
3) Thermodynamics evaluation of the actinide oxides using density functional calculations.

9

3. Fast reactor core characteristics
3.1 Simulation conditions

JSFR: Japan Sodium-cooled Fast Reactor

Table Specification of JSFR core[12]

Thermal power output	3570 MWth
Number of subassemblies	150/495
Number of fuel pins per subassembly	331/331
Fuel composition	U-TRU-Zr
Fuel density	11.85 g/cm^3
Pu enrichment	12.4 wt%
Zr content rate	10.0/6.0 wt%
Total amount of loading Pu	5.5 ton

Calculation code : MVP-2.0 , MVP-Burn
Cross section data library : JENDL-4.0

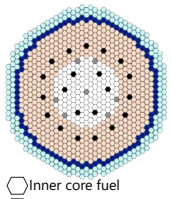

Inner core fuel
Outer core fuel
Radial reflector (SUS)
Radial shielding(ZrH)
Primary control rod
Secondary control rod

Fig. JSFR core design[1]

[12] S. Ohki et al., JAEA 77 (2006)

10

3. Fast reactor core characteristics
3.1 Simulation conditions

Loading amount of transmuted Pu into the fast reactor

Operational cycle length : 800 days (26.3 months)
Amount of transmuted Pu from a fusion reactor : 66.6 kg/year

Loading amount : 150 kg
(1)Heterogeneous(14 subassemblies)
(2)Homogeneous

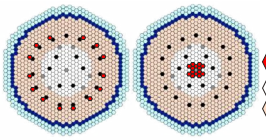

Fuel containing transmuted Pu
Inner core fuel
Outer core fuel
Radial reflector (SUS)
Radial shielding (ZrH)
Primary control rod
Secondary control rod

Fig. Samples of the core design in the simulations

Table Pu isotopic vectors of the fuels

	^{238}Pu	^{239}Pu	^{240}Pu	^{241}Pu	^{242}Pu
JSFR	1.0	68.0	26.0	2.5	2.5
Transmuted Pu	81.2	4.8	2.7	0.6	10.0

11

3. Fast reactor core characteristics
3.2 Simulation results

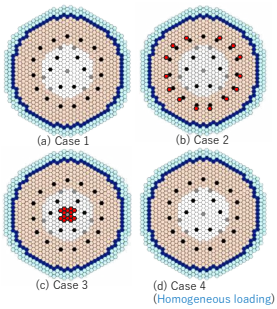

Fuel containing Pu from fusion reactor

Fig. Core design in the simulation

Initial value k_{eff} =1.023 (Case1)
Reference k_{eff} =1.02[12]

Data have not been published.

Fig. k_{eff} changes with burn-up during operation cycle

12

[12] S. Ohki et al., JAEA 77 (2006)

3. Fast reactor core characteristics
3.2 Simulation results

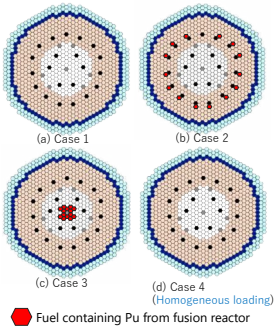

Fuel containing Pu from fusion reactor

Fig. Core design in the simulation

Data have not been published.

Fig. Total amount of ^{238}Pu with burn-up during operation cycle

4. BWR core with the transmuted Pu

	a	b	c	d	e	f	g	h	i	j
1	2.7	3.9	5.2	5.2	5.2	6.7	5.2	5.2	3.9	2.7
2	3.9	6.7	6.7	7.6	6.7	10.6	10.6	6.7	6.7	3.9
3	5.2	6.7	10.6	10.6	10.6	10.6	10.6	10.6	6.7	5.2
4	5.2	7.6	10.6	10.6	10.6	Gd	10.6	10.6	10.6	5.2
5	5.2	6.7	10.6	10.6	Water channel			7.6	6.7	6.7
6	6.7	10.6	10.6	Gd				Gd	6.7	5.2
7	5.2	10.6	10.6	10.6				Gd	7.6	5.2
8	5.2	6.7	10.6	10.6	7.6	Gd	Gd	6.7	6.7	5.2
9	3.9	6.7	6.7	10.6	6.7	6.7	7.6	6.7	6.7	3.9
10	2.7	3.9	5.2	5.2	6.7	5.2	5.2	5.2	3.9	2.7

Fig. Core design in the simulation
The numbers represent plutonium enrichments and Gd means UO_2/Gd_2O_3 rod.

$^{238}Pu \xrightarrow[(n,\gamma)]{} {}^{239}Pu$

Is it possible to control the reactivity with the transmuted Pu??

- MOX BWR core characteristics with the transmuted Pu
- OECD/NEA Benchmark for MOX BWR (10×10 BWR fuel assemblies)
- Eigenvalue problem (The power density = 25 W/gHM)

Table Pu isotopic vectors of the fuels

	^{238}Pu	^{239}Pu	^{240}Pu	^{241}Pu	^{242}Pu
Present MOX	2.2	46.2	29.4	13.4	8.8
Transmuted Pu	**79.8**	5.2	2.9	0.4	11.7

[9] K. V. Walters, *Nuclear Fuel Management II, Vol. 10.* 1997.
[10] OECD/NEA. *Plutonium Physics, Vol.7.* pp.15, 2003

4. BWR core with the transmuted Pu

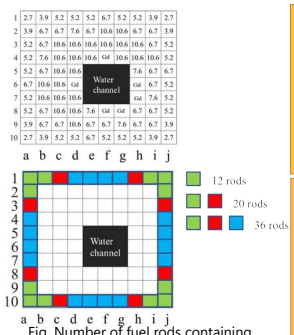

Fig. Number of fuel rods containing the transmuted plutonium.

Data have not been published.

The transmuted Pu makes k_{eff} low and flat.

Data have not been published.

k_{eff} is almost constant for 400 days operation.

5. Thermodynamic evaluation

- We have begun thermodynamic evaluation of actinide oxides using density functional calculation.
- The objective is to predict the phase diagram of the actinide oxides for designing of the transmutation system.
- All electron calculation (WIEN2k) and phonon calculations at harmonic and quasi-harmonic levels (Phonopy).

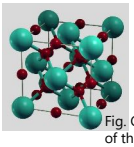

Fig. Calculation structure of the actinide dioxide (AnO2) crystal structure (Fm3¯m symmetry)

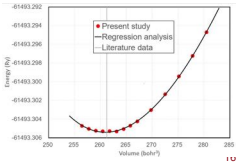

6. Summary

Proposal for the advanced nuclear fuel cycle by introducing a fusion reactor

- Fusion system is very attractive to solve the most important problem **"how to close nuclear fuel cycle"**.
- We evaluated a possibility of **effective utilization of the plutonium transmuted** from MA as fertile fuel in BWR.
- A fuel assembly loaded the transmuted plutonium can keep its **effective multiplication factor almost constant** for 400 days operation.
- We also demonstrated all-electron calculation to evaluate thermodynamic properties of actinide for further discussion of the design of the transmutation system.

4.1.2 M. Nakase（Tokyo Inst. Tech.）

Development and characterization of phthalocyanine derivatized ligands for recognition and complexation of light Actinide elements

Topical meeting on Condensed-matter Chemistry on Actinides : The Kumatori meeting

Development and characterization of phthalocyanine derivatized ligands for recognition and complexation of light Actinide elements

Masahiko Nakase
Research Institute of Innovation, Tokyo Institute of Technology

- To recognize and complexation of f-block elements by **phthalocyanine (Pc)** framework for many purposes, the **synthetic and purification scheme of derivatized Pc is studied**.
- The prepared derivatized-Pc will be used for the following purposes;
  1. Convert into Pc-metal complex for characterization
  2. Use as extractant for metal separation
  3. Study on coordination chemistry of Pc and An in solution (or soft materials)

Joint research with KURNS

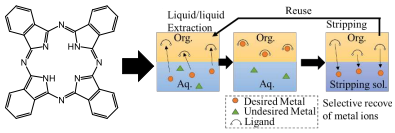

- Modification of Pc to extractants selective for f-element
- I am interested in the chemical characteristics of Pc-metal complex in solution (and soft materials)

Synthesis

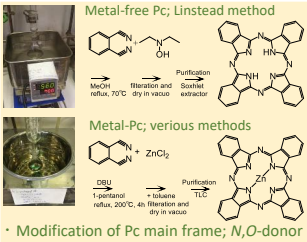

・Modification of Pc main frame; *N,O*-donor
Addition of functional groups; alkyl-chain

Purification

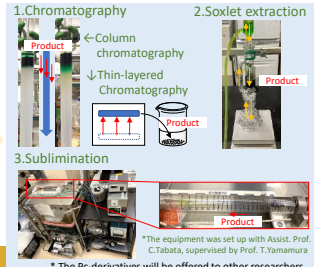

*The equipment was set up with Assist. Prof. C.Tabata, supervised by Prof. T.Yamamura

* The Pc-derivatives will be offered to other researchers

2

Background

Separation and recognition of f-elements in Nuclear Engineering Field

Nuclear Waste Treatment

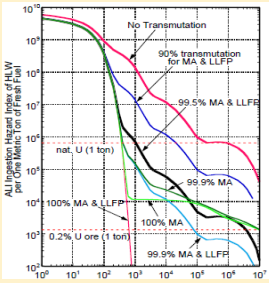

Separation of MA can reduce the long-term radiotoxicity and minimize the burden on final disposal

Resources

[24]S.Koyama, T.Suzuki, M.Ozawa, From waste to resource, nuclear rare metals as a dream of modern alchemists, *Energy convers Manage.* Vol.51, pp.1799-1805 (2010)

Copyright protected content

Medical purpose

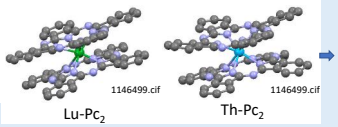

3

Property of f-elements and ion recognition

For treatment of High Level Liquid Waste(HLLW), Am(III)/Eu(III), Am(III)/Cm(III) separations are important but difficult due to similar chemical properties.

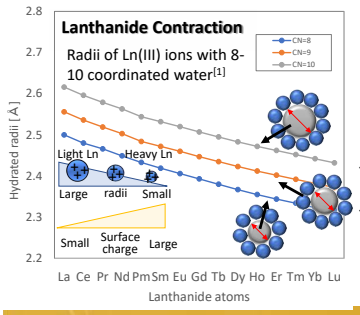

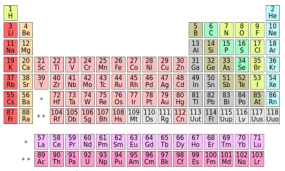

- Trivalent f-elements are chemically similar which makes separation difficult
- Recognize slight difference in ionic radius

N,O-hybrid donor ligands

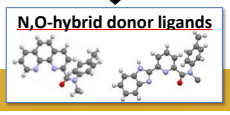

[1] I.D. Brown and R.D. Shannon, Acta Cryst., A29, pp.266-282(1973)

4

Separation Methods in Nuclear Reprocessing Field

< Solvent Extraction (SX) >

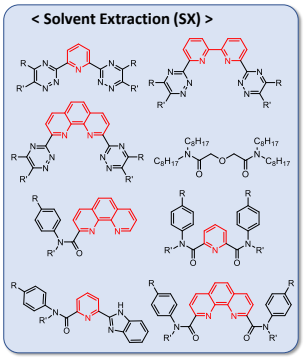

<SX with synergists, complexants>
- ✓ TALSPEAK - Combination of phosphate and DTPA (masking agent) with existence of buffer
- ✓ Combination of DGA and masking agents
- ✓ Ionic liquid ✓ Reverse micelle extraction

<Adsorption>
- ✓ Extraction chromatography
- ✓ Sold/liquid extraction
- ✓ Gel/liquid extraction - ligand immobilized gel, pH, temperature swing separation

<Pyro reprocessing>
- Electrochemical approach

<Other Methods>
- ✓ Crystallization ✓ Precipitation

I have never tried cyclic compounds yet!!

5

My Separation Approach

1. Development of extractant

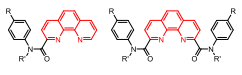

- ✓ Extractant, Complexsant, Synergist
- ✓ Solvent Extraction, Structural study
- ✓ Solution and coordination chemistry

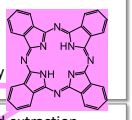

2. Control of complexation in soft matter

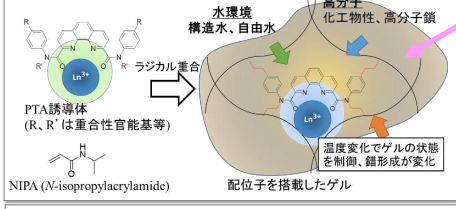

- ✓ Gel/liquid extraction
- ✓ Extraction chromatography
- ✓ More fundamental study

Polymer chemistry
+
Coordination chemistry

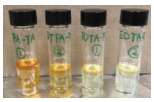

3. Valence control of An and extraction

4. Application study ; Contactors, Separation Process analysis

6

Phthalocyanine derivatized extractant

Pc is one of the most famous ligands to form complexes with various kind metal ions

→ Make Pc extractant applicable to solvent extraction

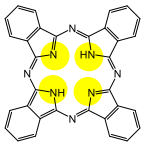

1. Make Pc compatible to solvent extraction method
   - Addition of alkylchain and functional groups
2. Modification of central Pc structure
   - *N,O*-hybrid donor, asymmetric Pc etc…

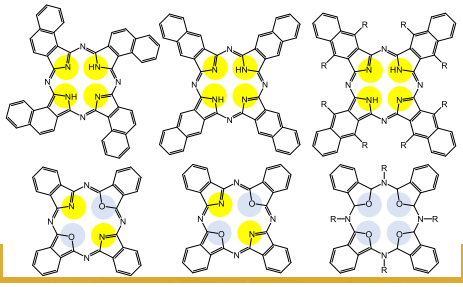

Synthesis

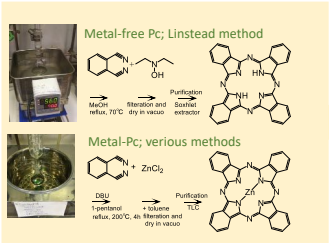

Various kinds of building blocks are commercially available

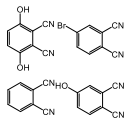

etc…

Replacement of functional groups such as –OH and –Br into other functional groups or addition of other fragment via such joint points are easy task

- Various kinds of *N*-Pc can be synthesized by the same method
  → There are plenty of methods to synthesized Pc derivatives
- Purification method will be changed due to the nature of the ligands
  → Typical Pc does not dissolve into many solvents. Also, purification should not produce huge amount of waste since actinide will be used

Synthesis of Zn-Pc by Linstead method

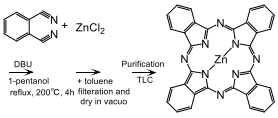

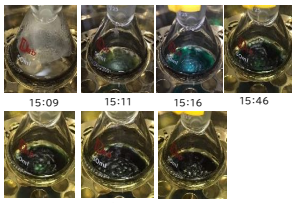

- Zn will be removed and replace into other metals
- Optimization of the synthesis and other synthetic route will be tested

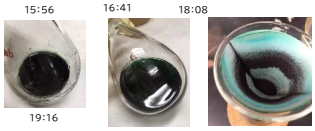

Purification

1.Chromatography

Column chromatography

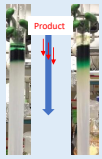

Thin-layered Chromatography

2.Soxlet extraction

3.Sublimination

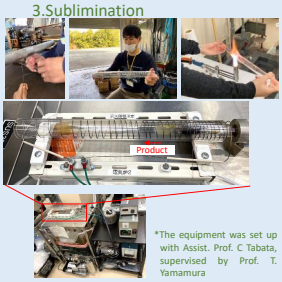

*The equipment was set up with Assist. Prof. C Tabata, supervised by Prof. T. Yamamura

- Purification is dependent on many aspects;
  - Physco-chemical property of product; solubility into solvent, solid or liquid …
  - Amount of the products - Co-existed impurity - Target yield and purity
  - Accepted amount of waste → rad materials or not, etc …

We are now trying many methods to find out the appropriate purification method

Sublimination

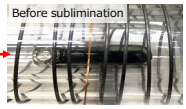

- Residual solvent was perfectly removed
- Sublimination is not yet completed

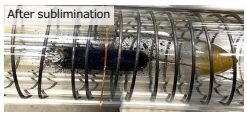

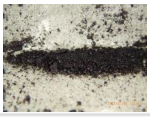

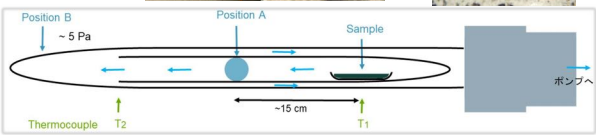

Conclusion

- Some of the Pc-derivatives were synthesized
- Some purification scheme were tested

Plan

- Synthesis and purification will be upgraded
  - catch up with the latest researches
- Target Pc-derivatives will be decided and select the best synthetic and purification scheme.
- Synthesized Pc-derivatives will be offered to collaborators and try solvent extraction

4.1.3 H. Nakai（Kindai Univ.）

Development of ligands for new actinide complexes

Topical meeting on Condensed-matter Chemistry on Actinides, Feb. 10, 2021.

Development of ligands for new actinide complexes

Hidetaka Nakai
Kindai University (Dept. of Applied Chemistry)

Macrocyclic Polyamines 1

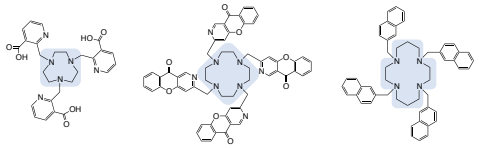

T. J. Meade et al., *Chem. Rev.* **2014**, *114*, 4496.
E. Tondello et al., *Coord. Chem. Rev.* **2010**, *254*, 487.

Macrocyclic Polyamines 2

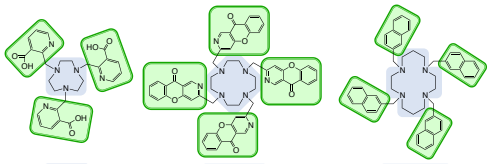

T. J. Meade et al., *Chem. Rev.* **2014**, *114*, 4496.
E. Tondello et al., *Coord. Chem. Rev.* **2010**, *254*, 487.

Aryloxide Ligands 3

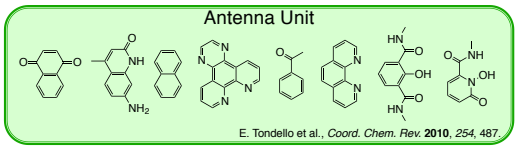

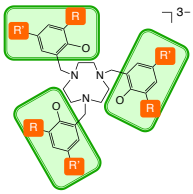

- ✓ Utilized in f-element Chemistry
- ✓ Luminescent Ln/Ac Complexes have not been Investigated

Our Ligands 4

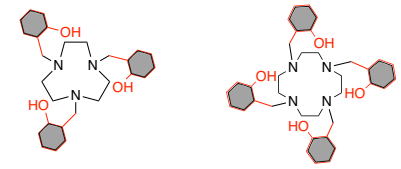

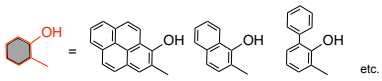

Our Ligands 5

Achiral Ligand

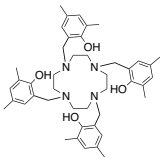

Enantiomers (in the crystal)

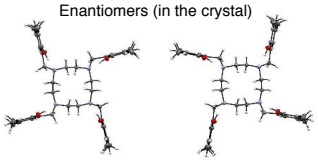

Tb Complex as actinide analogues

6

Chem. Commun. **2014**, *50*, 13737.

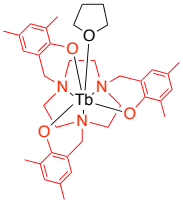

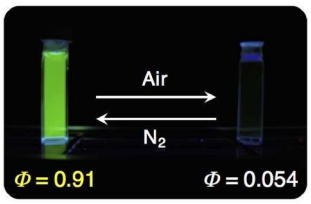

✓ Highly Luminescent
✓ Highly Oxygen-responsive

The Highest Φ (0.91) Among
the Oxygen-responsive Lanthanide Complexes

Tb Complex as actinide analogues

7

Dalton Trans. **2016**, *45*, 9492.

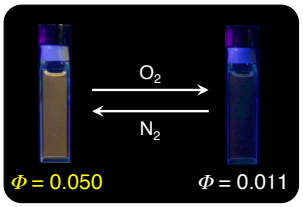

The First Dysprosium(III) Complex that Shows
Oxygen-responsive Luminescence

Tacn → Cyclen

8

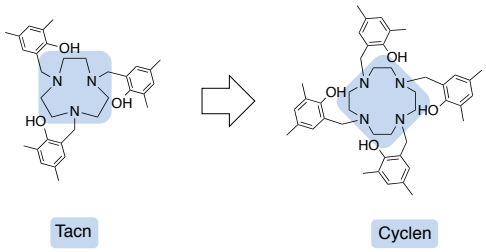

Extendable Phenol Pendant Arm

9

Dalton Trans. **2015**, *44*, 10923.

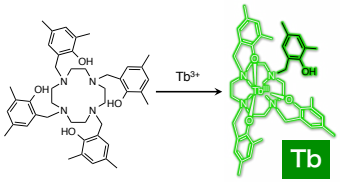

Φ = 91% (N_2)
Φ = 3% (Air)

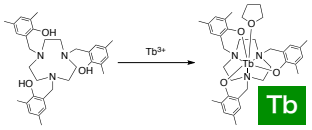

Φ = 91% (N_2)
Φ = 5% (Air)

Me → tBu

10

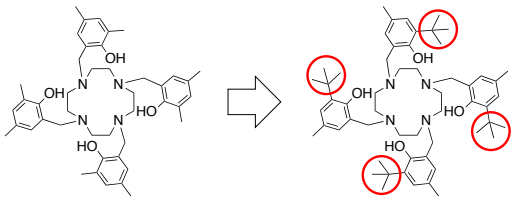

Control of Coordination Environment

11

Inorg. Chem. **2016**, *55*, 6609.

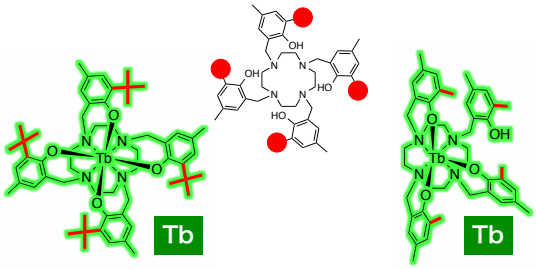

CN = 8 (N_4O_4)

CN = 7 (N_4O_3)

Control of Coordination Environment

12

Inorg. Chem. **2016**, *55*, 6609.

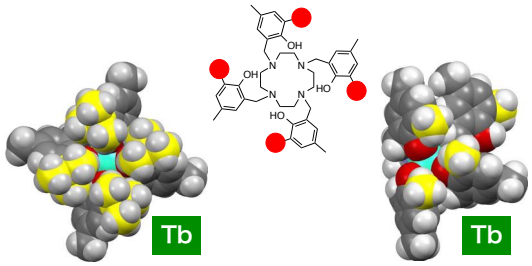

CN = 8 (N_4O_4) CN = 7 (N_4O_3)

Control of Coordination Environment

13

Inorg. Chem. **2016**, *55*, 6609.

	8 Coordinated Structure	7 Coordinated Structure
ε($M^{-1}cm^{-1}$)	12000	15000
λ_{max} (nm)	301	299
Φ_{N_2} (%)	68	91
Φ_{Air} (%)	1.9	3.1
τ_{N_2} (μs)	1180	1070
τ_{Air} (μs)	40	40
K_{sv}(M^{-1})	17600	12600

Control of Coordination Environment

14

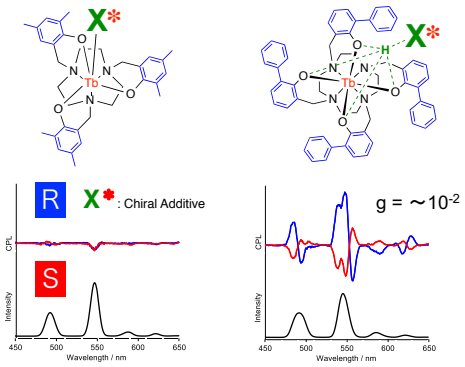

Development of ligands for new actinide complexes

- Various ligands for new actinide complexes (especially, for U^{III} and U^{IV}) have been synthesized.

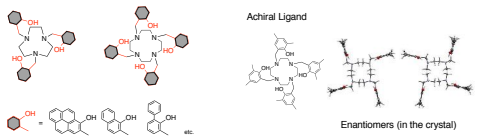

- Lanthanide(III) complexes have been synthesized as actinide analogues.

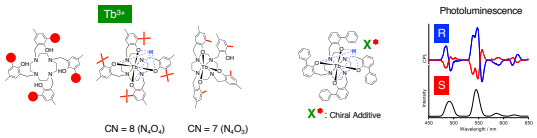

4.1.4 C. Tabata（Kyoto Univ.）

Crystal structure and magnetic property of uranium phthalocyanine complexes

Topical meeting on Condensed-matter Chemistry on Actinides, Feb. 10, 2021.

Crystal structure and magnetic properties of uranium phthalocyanine complexes

Chihiro Tabata
Institute for Integrated Nuclear and Radiation Science, Kyoto University

1

Collaborators

IMR, Tohoku University	H. Watanabe, D.X. Li, and K. Shirasaki
Graduate School of Science, Osaka University	T. Fukuda and N. Ishikawa
KURNS, Kyoto University	A. Sunaga and T. Yamamura

2

Phthalocyanine complexes

Phthalocyanine (Pc)

- Highly stable *n*-conjugated molecule
- Forms complexes with various metallic ions
- Characteristic optical absorption of the visible light

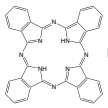

Pc molecule

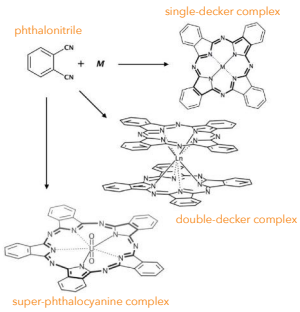

3

Applications of Phthalocyanine complexes

- High chemical and thermal stability
  - Typical dyes material
    - CuPc → "Phthalocyanine blue"
    - $CuHPc_4Cl_{15}$ → "Phthalocyanine green"
  - Target of radiation irradiation for producing ^{64}Cu isotope
- Redox activity
  - Electrochromic devices
  - Photomemory
  - Solar cell
- Magnetism of central metal ion
  - Single molecular magnet

4

Research of Pc complexes to date

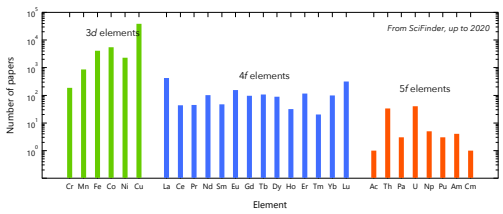

- Pc complexes of 5*f* elements have much fewer reports than those of 3*d* and 4*f* elements.
- Conventional synthesis of UPc_2 have been mol-scale synthesis (~70s).
  ➡ Synthesis with smaller scale is required because of highly toxic and radioactive properties of 5*f* elements.

5

Aim of study

- Development of microscale synthesis of $AnPc_2$ (An: actinides).
- Exploring novel Pc complexes of actinides with characteristic electronic properties.
- Elucidation of those properties via structural, magnetic and transport aspects.

First we did…

- Microscale synthesis and single crystal growth of UPc_2
- Crystal structural analysis and magnetization measurements of UPc_2
- Electrosynthesis of cationic salts of UPc_2

6

Microscale synthesis of UPc_2

Mixture of UCl_4 and $C_6H_4(CN)_2$

230~270°C, 3h

Blue-green powder was obtained.

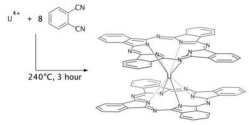

Characterization with UV-Vis spectra

Copyright protected content

Purification of UPc_2

- Sublimation in the furnace with temperature gradient

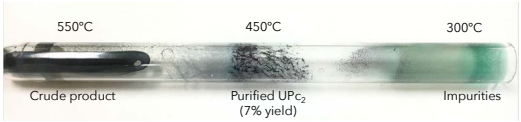

- Single crystal growth

450°C, 1h in vacuum

Cool down by 10°C/h

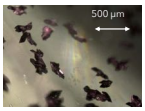

Characterization with UV-Vis spectra

Copyright protected content

Structural analysis of UPc_2

- Single crystal X-ray diffraction measurement
  - R-AXIS Rapid II (Rigaku)
  - Mo K-alpha radiation
  - T_{meas} = 150 K (N_2 flow cooling)
- Structural analysis
  - Direct method (SIR2014)
  - Least-square refinement (Shelxl)

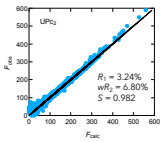

Unpublished data

➡ Consistent with the literatures.

[1] A. Gieren and W. Hoppe, J. Chem. Soc., Chem. Commun. D **8** (1971) 413.
[2] I. S. Kirin et al., Zh. Struk. Khim. **15** (1973) 486.

Copyright protected content

Magnetization of UPc_2

- Magnetization measurements of powdered UPc_2 by ACMS using PPMS

Unpublished data

Curie-Weiss fit of magnetic susceptibility

Unpublished data

< 3.58 μ_B (Expected for U^{4+} ion)

Synthesis of cationic UPc_2: $[UPc_2][BF_4]$

Electrolyzation by 1 μA for 1 week

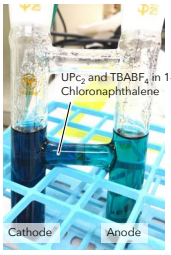

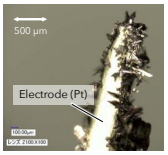

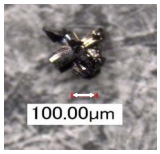

Dark blue crystals were grown on the anode electrode.

Copyright protected content

Structural analysis of $[UPc_2][BF_4]$

Unpublished data

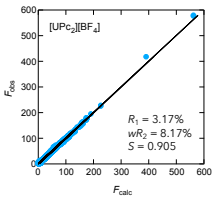

Unpublished data

13

Disordered structure of $[UPc_2][BF_4]$

Unpublished data

14

Disordered structure of $[UPc_2][BF_4]$

Unpublished data

15

Theoretical Calculations: Preliminary Work

Calculation by A. Sunaga

Input molecular structures:

UPc_2 UPc_2^+

Unpublished data

Theoretical Calculations: Preliminary Work

Calculation by A. Sunaga

Notation:
- ✓ In this analysis, we cannot separate the contribution from 5s, 6s and 7s. All of them are summarized to "s" orbital.
- ✓ Mulliken population analysis and BLYP calculation are poor methodology. It is a preliminary calculation.
- ✓ In this table, the values represent the difference between the ground state $7s^2 6d^1 5f^3$ and the uranium in UPc_2 or UPc_2^+. For example,
  - ✓ + 0.75 of the p orbital implies that 0.75 of 6p is removed.
  - ✓ -1.49 of the d orbital implies that the occupation of 6d is 2.49

Charge of Uranium and decomposition to each orbital by using Mulliken population analysis

Unpublished data

Computational detail

・Method：BLYP (DFT)
・Program：Gaussian16
・Basis set: Stuttgart-Dresden's ECP for U; D95 for H, C, and N

17

Developments of sublimation purification equips. at Hot Lab. in Kumatori

1st try with $U(acac)_4$

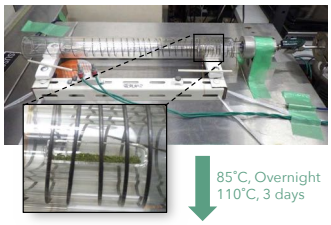

85˚C, Overnight
110˚C, 3 days

Crystals with 0.1~0.3 mm of diameter

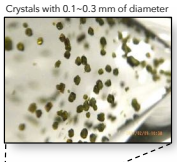

18

Summary

- A microscale synthesis of uranium phthalocyanine complex UPc_2 was successfully performed in Laboratory of Alpha-Ray Emitters, IMR.
- The crystal structure was determined to be a monoclinic structure belonging the space group of *C*2/*c*, which is consistent with the previous reports.
- Magnetization of the powder sample indicates the paramagnetic state down to 2 K. The effective moment evaluated from the Curie-Weiss behavior was ~2.3 μ_B, which is smaller than that expected for a free U^{4+} ion.
- A cation salt $UPc_2[BF_4]$ was synthesized by electrolysis, and the crystal structure was determined to be a tetragonal (*P*4*nc*) structure.
- Future work:
  - Growth of larger single crystals and detailed measurement of magnetic and transport properties
  - Investigation of structural and electronic properties by quantum chemical calculations

19

4.1.5 Y. Kasamatsu（Osaka Univ.）

Co-precipitation experiment of group 2 elements with barium hydrosulfate toward chemical study of No

Topical meeting on Condensed-matter Chemistry on Actinides, Feb. 10, 2021.

Co-precipitation experiment of group 2 elements with barium hydrosulfate toward chemical study of No

Graduate School of Science, Osaka University
Yoshitaka Kasamatsu

S. Hayami, E. Watanabe, R. Nakanishi, K. Tonai, K. Takamiya,[KURNS] A. Shinohara

1

Introduction -Heavy elements-

Heavy elements：Atomic number (Z) > 100 (beyond Fm)

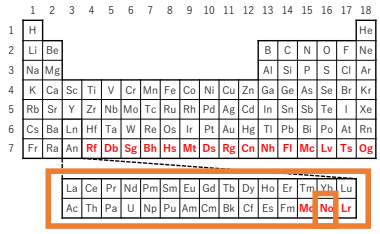

Relativistic effect

- Inner (s,p) shells → contraction
- Outer (d,f) shells → expansion
- Split of spin orbit

Deviation of chemical behavior of heavy elements from that expected from tendency in the lighter homologues in the periodic table

Experimental and theoretical approaches

Currently, these properties are largely unknown because heavy elements can be produced only by nuclear reactions and have short half-lives.

2

Introduction -Nobelium-

Nobelium (No)

- Z = 102、member of f block element
- Stable oxidation state of No in aqueous solution is +2, whereas those of other heavy actinides and all lanthanides are all +3!

Most stable oxidation state of f block elements in aq

La +3	Ce +3	Pr +3	Nd +3	Pm +3	Sm +3	Eu +3	Gd +3	Tb +3	Dy +3	Ho +3	Er +3	Tm +3	Yb +3	Lu +3
Ac +3	Th +4	Pa +5	U +6	Np +5	Pu +4	Am +3	Cm +3	Bk +3	Cf +3	Es +3	Fm +3	Md +3	No +2	Lr +3

copyright protected content

[1] J. Maly, T. Sikkeland, R. Silva, A. Ghiorso, Science 160, 1114-1115 (1963).

3

Introduction -Nobelium-

Solvent extraction in TOA/HCl[1]

copyright protected content

Solvent extraction[1]

Different from d block elements but similar to Ba (group 2 element)

Ion exchange[1]

Compared with Be, Mg, Ca, Sr, Ba, and Ra (group 2), behavior of No is similar to that of Ca and Sr having similar ionic radii to that of No

So far, mainly limited to HCl system (not coordinated)

Observation for behavior in the other reaction systems and coordination to No is desired.

Is there difference from group 2 elements (characteristic behavior as f block element)? Can influence of relativistic effects be observed?

Electron configuration

		5f	7s	7p
Fm	[Rn]	12	2	
Md	[Rn]	13	2	
No	[Rn]	14	2	
Lr	[Rn]	14	2	1

4

[1] R. J. Silva, W. J. Mcdowell, O. L. Keller, et al. J. Inorg. Nucl. Chem. 38, 1207-1210 (1976).

Our previous studies -Coprecipitation with $Sm(OH)_3$-

One atom never forms precipitate → Coprecipitation with $Sm(OH)_3$ [1]

- Rapid and simple procedure
- High energy resolution in α spectrometry

Coprecipitation yields for various elements[2]

	Added basic solution				
	dil.NH_3	conc.NH_3	0.1 M NaOH	1 M NaOH	6 M NaOH
Na, K, Rb(+1)	0	0	0	0	0
Zn(+2)	80	0	60	40	20
Ce, Eu, Gd, Tb(+3)	100	100	100	100	100
Dy, Er, Tm, Lu(+3)	100	100	100	80	40

Precipitation behavior	Hydroxide ppt	No complexation	Ammine complex ion (NH_3)	Hydroxide complex ion

Coprecipitation behavior qualitatively reflects hydroxide precipitation properties

Hydroxide and ammine complexation can be studied based on coprecipitation behavior

5

[1] H. Kikunaga et al. Appl. Radiat. Isot. 67, 539 (2008). [2] Y. Kasamatsu et al. Appl. Radiat. Isot. 118, 105-116 (2016).

Our previous studies –Coprecipitation of No and Rf

We succeeded in investigating hydroxide precipitation properties of $_{102}$No[1] and $_{104}$Rf[2] through their coprecipitation behavior

However, problem is suggested for hydroxide coprecipitation of No:
Polymer formation of group 2 elements in hydroxide precipitates

6

[1] 二宮秀美　大阪大学大学院理学研究科修士論文 (2019).　[2] Y. Kasamatsu et al., Nature Chemistry in press (2021).

Present study –Sulfate complex-

Characteristic reactions for group 2 elements

Formation of **sulfate**・carbonate complexes and precipitate

Difference in solubility products (effect of ionic radius) → No？（influence of relativistic effects）

Concentration of sulfuric acid can be easily adjusted. → Sulfate coprecipitation method

Problems

- Precipitation properties can be studied from coprecipitation behavior?
- Applicable to No experiment?（Carrier element? Amount?・resolution in α spectrum）
- Electronic configuration in chemical bonds can be discussed?（Calculation）

Purpose

To develop experimental method and determine suitable conditions to investigate sulfate precipitation properties of No using group 2 elements

Contents

- Determination of carrier element
- Check of energy resolution of α spectrum using ^{228}Ra
- Comparison of behavior between macro and micro amounts
- Coprecipitation behavior of group 2 elements with $BaSO_4$
- Theoretical calculation for sulfate complexes of group 2 elements and No

8

Experiment and Results -carrier and α spectrum-

Requirements for carrier element

- 100％precipitation under wide concentration range of H_2SO_4
- High α resolution（<20 μg）

→ **Carrier：Ba**
Amounts：5～10 μg

Yields of Sr and Ba when using 20 μg

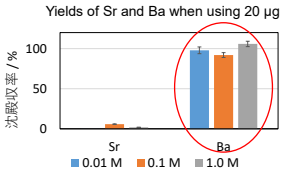

Yield vs. Ba carrier amount

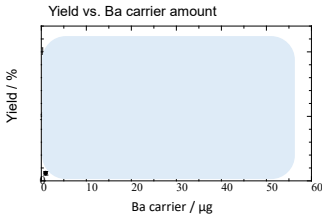

Energy resolution vs. carrier amount

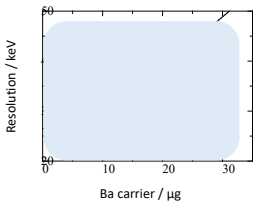

To develop experimental method and determine suitable conditions to investigate sulfate precipitation properties of No using group 2 elements

Contents

- Determination of carrier element
- Check of energy resolution of α spectrum using ^{228}Ra
- Comparison of behavior between macro and micro amounts
- Coprecipitation behavior of group 2 elements with $BaSO_4$
- Theoretical calculation for sulfate complexes of group 2 elements and No

10

Experiment –Precipitation and Co-ppt-

Experiment

^{47}Ca: Produced by neutron irradiation at KURNS
^{85}Sr, ^{133}Ba: Produced by proton irradiation at RCNP

RI tracer in 0.01 M HCl 10 μL

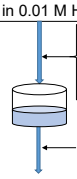

- 0.01 M HCl 20 μL
- Carrier or metal 10 μL
- 200 μL water

Ammonium sulfate solution（0.001 M～2.0 M: 8 concentrations）

Amount of carrier or metal

RI	Co-ppt carrier	ppt macro amount
^{47}Ca	Ba 20 μg	Ca 1 mg
^{85}Sr	Ba 20 μg	Sr 1 mg
^{133}Ba	Ba 20 μg	Ba 1 mg
^{226}Ra	Ba 20 μg	

Stirring (5 min)

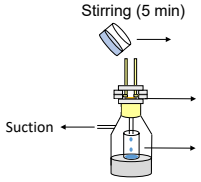

γ-ray measurement with Ge detector

ppt or co-ppt yield (%)

$$= \frac{A_{ppt}+A_{cup}}{A_{ppt}+A_{cup}+A_{fil}} \times 100$$

11

Results –Precipitation and Co-ppt-

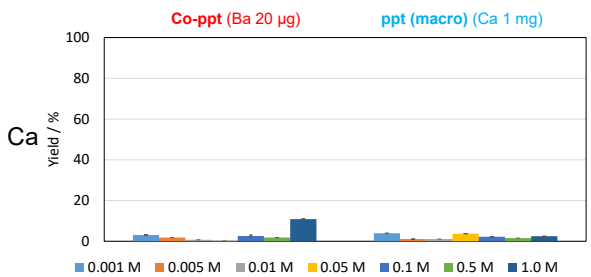

Not precipitated in both co-ppt and ppt

12

[1]大木道則ら, 化学大辞典第1版, 東京化学同人 (1989).

Results –Precipitation and Co-ppt-

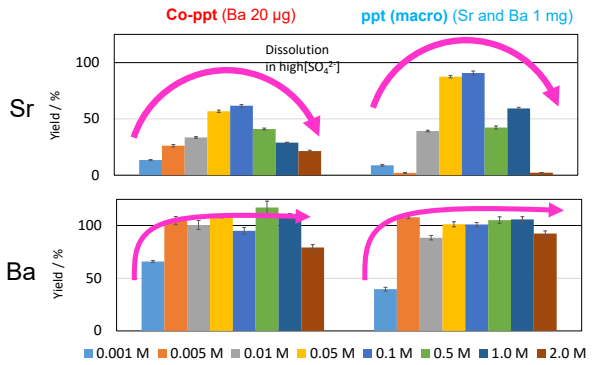

$Y_{co\text{-}ppt} = Y_{ppt}$

Qualitatively precipitation properties can be investigated based on the coprecipitation behavior

Results and Discussion –co-ppt behavior-

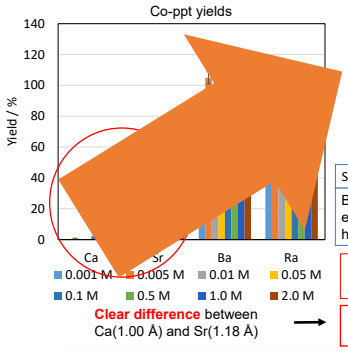

	Solubility product ($\log K_{sp}$)	M^{2+} ionic radius, CN=6 (Å)
$CaSO_4$	-4.63	1.00 (CN=6)
$SrSO_4$	-6.53	1.18 (CN=6)
$BaSO_4$	-10.00	1.35 (CN=6)
$RaSO_4$	-14.38	1.48 (CN=8)

Solubility of MSO_4

Based on large SO_4^{2-} (2.30 Å), group 2 elements with longer radius tend not to be hydrated ⇒ low solubility

Order in yield = order in ionic radius
Ca < Sr < Ba < Ra

Clear difference between Ca(1.00 Å) and Sr(1.18 Å) → Suitable condition for observing the behavior of No (1.10 Å calc.)

Tendency for complexation cannot be discussed ⇒ Calculation

[1] L. G. Sillén, A. E. Martell. (Eds.) *Stability constants of metal-ion complexes*. London: The Chemical Society (1964).
[2] R. D. Shannon., Acta Cryst. A 32, 751 (1976)

14

To develop experimental method and determine suitable conditions to investigate sulfate precipitation properties of No using group 2 elements

Contents

- Determination of carrier element
- Check of energy resolution of α spectrum using ^{228}Ra
- Comparison of behavior between macro and micro amounts
- Coprecipitation behavior of group 2 elements with $BaSO_4$
- Theoretical calculation for sulfate complexes of group 2 elements and No

15

Calculation -Ionic radius & bond distance-

Check: Comparison with experimental data for bond distance

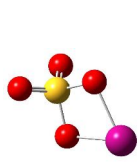

Geometry optimized $NoSO_4$

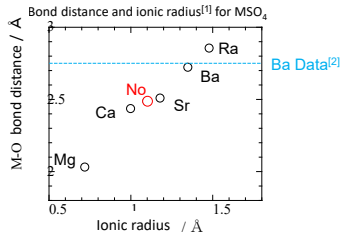

Software：Gaussian 16 rev. C.01
Function：B3LYP/6-31G* for Mg, Ca, S, O
SDD for Sr, Ba, Ra, No
Solvent effect：PCM

Basically, bond distance ∝ ionic radius

[1] R. D. Shannon., Acta Cryst. A 32, 751 (1976). [2] R. J. Hill., Canadian Mineralogist, 15 522-526 (1977).

16

Calculation -Electron configuration-

Results in NBO analysis

$_3SO_4$

Higher yield of $NoSO_4$ coppt than expected? (Ca<No<Sr)

Relativistic calculation -Enthalpy-

Relativistic caulculation: Reaction enthalpy for $M^{2+} + SO_4^{2-} \rightarrow MSO_4$

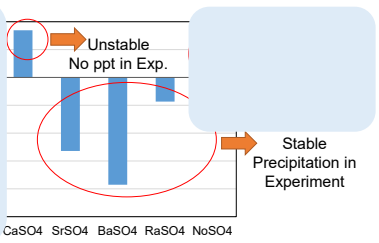

Software：ADF 2019.105
Function ：PW91/QZ4P Solvent effect：SM12
Spin-Orbit ZORA

Probability of non-precipitation of No

18

Discussion -Expectation for No behavior-

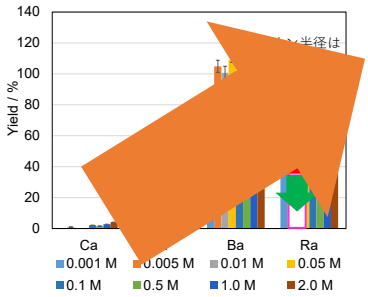

For No
- Simple extrapolation (ionic radius; solubility): Ca<No<Sr
- Higher yield?
- Unstable $NoSO_4$?: 0% yield?

Importance of experiment of No

[1] R. D. Shannon., Acta Cryst. A 32, 751 (1976).

Summary

- We developed coprecipitation method with barium sulfate to investigate chemical properties of No and determined suitable conditions.

  Determination of carrier element to be Ba
  High energy resolution of precipitated sample in α spectroscopy
  Coprecipitation behavior reflects precipitation properties in MSO_4

  ⇒ It is intriguing to determine the coprecipitation yield of No with barium sulfate.

- We calculated electron configuration, charge, and stability of MSO_4 complex for group 2 elements.

20

Acknowledgement

Deeply thanks for collaboration

○Production of ^{47}Ca
Operators in KURNS

○Production of ^{85}Sr and ^{133}Ba
Operators in RCNP

○Calculation
RIKEN supercomputer system
HOKUSAI BigWaterfall

21

4.1.6 K. Shirasaki（Tohoku Univ.）

Extraction of strontium from aqueous solutions into HFC using dicyclohexano-18-crown-6 and perfluorinated polyethylene glycol derivative

Topical meeting on Condensed-matter Chemistry on Actinides, Feb. 10, 2021.

Extraction of strontium from aqueous solutions into HFC using dicyclohexano-18-crown-6 and perfluorinated polyethylene glycol derivative

Kenji Shirasaki
Institute for Materials Research, Tohoku University

Abstract

- The extraction of Sr^{2+} and some other alkaline earth metal and alkaline metal from aqueous nitric media by HFC mixed solvents as diluent with DCH18C6 was studied.
- In the aqueous conditions of 10 mM Sr^{2+}, slops of almost unity for $\log D_{Sr}$ were obtained from 5 to 20 mM for [DCH18C6] and were consistent with an extracted complex containing a single DCH18C6 molecule.
- Attention to the effect of H_2PFTOUD, slopes of almost 2 for $\log D_{Sr}$ are obtained form 5 to 50 mM for log[H_2PFTOUD] and are consistent with an extracted complex double extractant molecules.

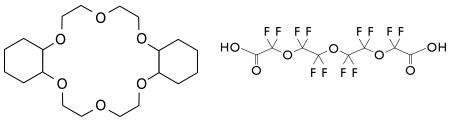

DCH18C6 H_2PFTOUD

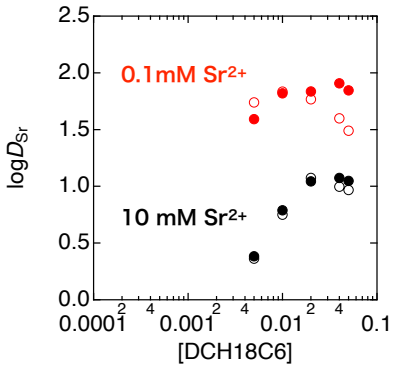

Fig. Dependence of D_{Sr} on DCH18C6 concentration

Collaborators

Mitsuie Nagai (IMR, Tohoku Univ.)
Chihiro Tabata, Tomoo Yamamura (IINRS, Kyoto Univ.)
Masahiko Nakase (Tokyo Institute for Technology)
Tsuyoshi Yaita (JAEA)

4.1.7 Y. Sekiguchi（CRIEPI）

Thermodynamic estimation of vaporization of CsI dissolved in LiF-NaF-KF molten salt

Thermodynamic Estimation of Vaporization of CsI Dissolved in LiF-NaF-KF Molten Salt

Nuclear Technology Research Laboratory
Central Research Institute of Electric Power Industry
Yuma Sekiguchi

Topical meeting on Condensed-matter Chemistry on Actinides
2021/Feb/10th Online (ZOOM)

 1 CRIEPI

Background

Molten salt reactor (MSR)
- Liquid fuel design
- Thorium utilization
- Transmutation of Minor actinide(MA)
- Advanced safety

Solvent salt
- Molten fluoride salt for thermal spectrum reactors

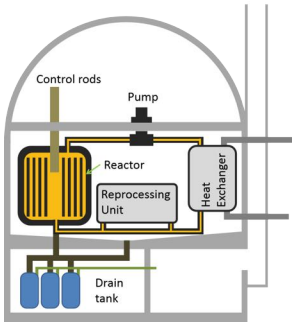

 2 CRIEPI

Accident analysis on MSR

- RIA
  - Calculated in several cases
- LOCA
  - Calculated as troubles on salt circulation
- Salt leakage
  - Possibility of vaporization of fissile materials and fission products.
  - Only a simplified calculation

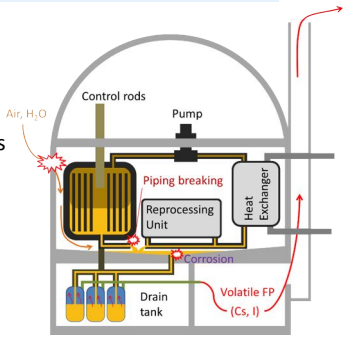

 3 CRIEPI

Purpose of Study

- To clarify the behavior of the volatile FP in the molten alkali fluorides from the view point of safety analysis on MSR.
  - Solvent salt: FLiNaK(LiF-NaF-KF: 46.5-11.5-42.0mol%)
  - Focus on Cs and I

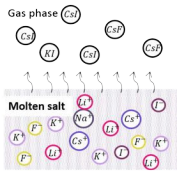

Vapor:
Anion and cation were combined

Liquid:
Anion and cation were separately

 4 CRIEPI

Contents

- Vapor pressure measurement
- Molecular Dynamics (MD) simulation

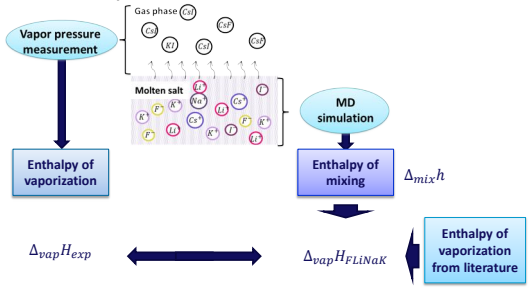

 5 CRIEPI

Contents

- Vapor pressure measurement
- Molecular Dynamics (MD) simulation

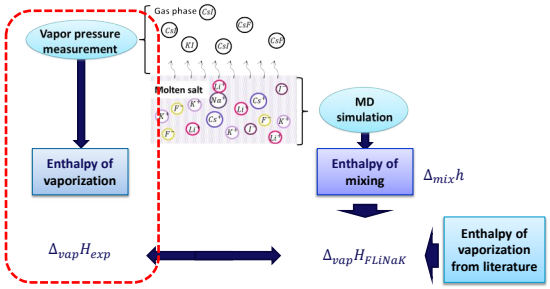

 6 CRIEPI

TG-DTA-MS

◆Equipment : Thermo mass photo/H (Rigaku)

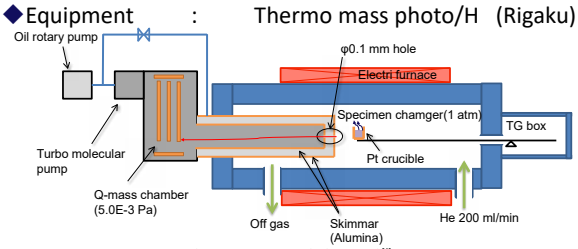

Schematic diagram of TG-DTA-MS[1]

◆High temperature vapors under atmospheric pressure were directly analyzed by quadrupole-mass spectrometry(Q-mass)

[1] Y. Sekiguchi et al, *Proc. of GLOBAL 2019*, Seattle, WA, U.S.A., Sep 22-26 (2019)

Measurement conditions

Summary of the conditions[1]

Temperature (K)	923, 973, 1023, 1073
Holding time (min)	60 (923, 973K) 30 (1023, 1073K)
Ionization energy (eV)	24
SEM Voltage (V)	1600
Gas flow rate (cm³/min) (Specimen chamber)	100

Composition of Specimens[1] (mol%)

Specimen (Cs-I)	LiF	NaF	KF	CsI	KI	CsF
0-1	46.0	11.4	41.6	-	1.00	-
1-1	46.1	11.4	41.5	0.997	-	-
1-2	45.8	11.2	41.0	0.997	0.997	-
1-5	44.2	10.9	39.9	1.00	4.00	-
1-0	46.1	11.4	41.5	-	-	1.00
2-1	45.6	11.3	41.2	1.00	-	0.997
5-1	43.7	10.8	39.5	-	1.00	5.00
2-2	44.7	11.0	40.3	-	2.00	2.00
5-5	41.8	10.4	37.8	-	5.00	5.00

[1] Y. Sekiguchi et al, *Proc. of GLOBAL 2019*, Seattle, WA, U.S.A., Sep 22-26 (2019)

Measured Vapor Pressure

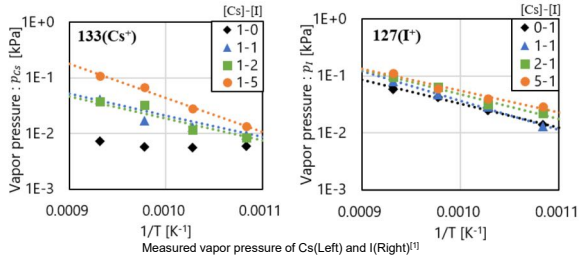

Measured vapor pressure of Cs(Left) and I(Right)[1]

◆No evaporation of Cs from the specimen without I.

◆CsI and KI evaporated from FLiNaK containing Cs and I.

[1] Y. Sekiguchi et al, *Proc. of GLOBAL 2019*, Seattle, WA, U.S.A., Sep 22-26 (2019)

Enthalpy of Vaporization

◆From vapor pressure data at different temperature, enthalpy of vaporization : $\Delta_{vap}H$ was obtained with Clausius-Clapeyron equation.

$$\ln\frac{p_2}{p_1} = -\frac{\Delta_{vap}H}{R}\left(\frac{1}{T_2}-\frac{1}{T_1}\right)$$

◆ $\Delta_{vap}H$ was obtained in this study from the gradient of 4 plots in former slide.

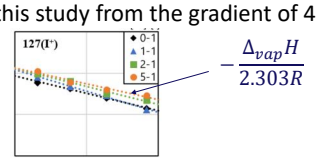

Measured vapor pressure of I(repost)[1]

[1] Y. Sekiguchi et al, *Proc. of GLOBAL 2019*, Seattle, WA, U.S.A., Sep 22-26 (2019)

Contents

◆Vapor pressure measurement

◆Molecular Dynamics (MD) simulation

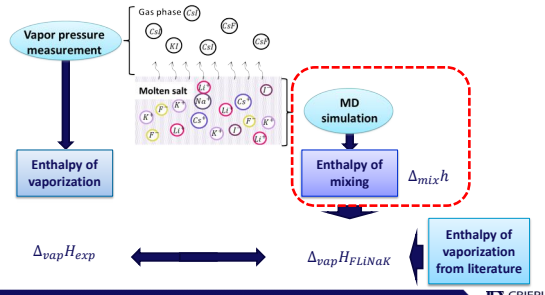

Molecular Dynamics

◆ Classical Moclecular Dynamics

➢ Solving the equation of motion about lots of atoms

➢ Attractive or repulsive force by interatomic potential equation

$$u_{ij}(r_{ij}) = \underbrace{\frac{z_i z_j e^2}{4\pi\epsilon_0 r_{ij}}}_{\text{Coulomb term}} - \underbrace{\frac{c_i c_j}{r_{ij}^6}}_{\text{van der Waarls term}} + \underbrace{f_0(b_i+b_j)\exp\left(\frac{a_i+a_j-r_{ij}}{b_i+b_j}\right)}_{\text{Short-range repulsive force term}}$$

◆ MD software

➢ **MXDORTO**

➢ Performed in inorganic crystal, glass and liquid

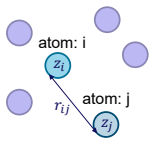

◆ **Purpose of Calculation**

➢ Enthalpy of mixing on FLiNaK-CsI/KI/CsF system

Potential parameters

◆Potential parameter determines the atoms behavior.

$$u_{ij}(r_{ij}) = \underbrace{\frac{z_i z_j e^2}{4\pi\epsilon_0 r_{ij}}}_{\text{Coulomb term}} - \underbrace{\frac{c_i c_j}{r_{ij}^6}}_{\text{van der Waarls term}} + \underbrace{f_0(b_i + b_j)\exp\left(\frac{a_i + a_j - r_{ij}}{b_i + b_j}\right)}_{\text{Short-range repulsive force term}}$$

Interatomic potential parameters[1]

atom	Parameter				
	Atomic weight	charge	a (nm)	b (nm)	c (kJ$^{0.5}$ nm^3 mol$^{-0.5}$)
Li	6.941	1.0	0.1070	0.0047	0.01227
Na	22.990	1.0	0.1493	0.0120	0.01841
K	39.098	1.0	0.1781	0.0120	0.03273
Cs	132.905	1.0	0.1969	0.0098	0.04296
F	19.000	-1.0	0.1733	0.0196	0.04091
I	126.905	-1.0	0.2386	0.0215	0.06136

[1] Y. Sekiguchi et al, *Proc. of GLOBAL 2019*, Seattle, WA, U.S.A., Sep 22-26 (2019)

Enthalpy of Mixing

◆Enthalpy of mixing:$\Delta_{mix}h$ of pseudo-binary systems(FLiNaK-CsI, FLiNaK-KI, FLiNaK-CsF)

- Calculation conditions
  - Number of atoms:6000
  - Temperature :1000K
  - Pressure :0.1MPa
  - Time step :2fs/step
- Average of 5×10^5 steps calculation after the equilibrium

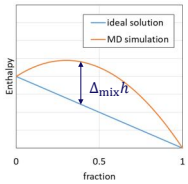

$$h_{AB} = x_A h_A + x_B h_B + \Delta_{mix}h$$

h_{AB}:molar enthalpy of mixture

h_i: molar enthalpy of pure *i*

x_i: molar fraction of *i*

Enthalpy of Mixing

◆$\Delta_{mix}h$ of FLiNaK-CsF system were negative values.

➢ Mixture was stabilized by perturbation of cations.

◆$\Delta_{mix}h$ of FLiNaK-CsI, FLiNaK-KI were positive.

➢ Caused by exchange reaction between FLiNaK and CsI/KI

$$LiF + CsI \leftrightarrows LiI + CsF$$
$$\Delta G = 113.4\ kJ/mol$$

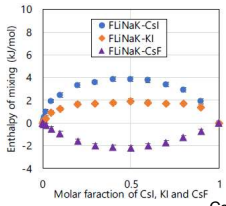

Molar enthalpy of mixing of the pseudo-binary systems by MD[1]

[1] Y. Sekiguchi et al, *Proc. of GLOBAL 2019*, Seattle, WA, U.S.A., Sep 22-26 (2019)

Phase separation

◆Snapshots of pseudo-binary systems at $x = 0.5$

◆Two phases were observed in FLiNaK-CsI/KI systems, on the other hand FLiNaK-CsF system was uniform.

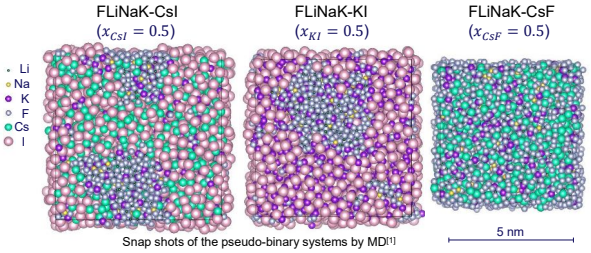

Snap shots of the pseudo-binary systems by MD[1]

[1] Y. Sekiguchi et al, *Proc. of GLOBAL 2019*, Seattle, WA, U.S.A., Sep 22-26 (2019)

Interaction parameter

◆Interaction parameter: ω_{AB} is derived from $\Delta_{mix}h$.

$$\Delta_{mix}h = x_A x_B \omega_{AB}$$

- Interaction parameter was constant on the composition for the uniform mixture.
- The differential heat of solution: Δh_A was obtained from ω_{AB}.

$$\Delta h_A = \frac{\partial(n_A + n_B)\Delta_{\text{mix}}h}{\partial n_A}$$
$$= x_B^2 \omega_{AB}$$

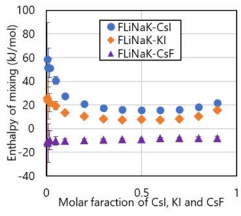

Interaction parameters (ω_{AB}) of the pseudo-binary systems by MD[1]

[1] Y. Sekiguchi et al, *Proc. of GLOBAL 2019*, Seattle, WA, U.S.A., Sep 22-26 (2019)

Contents

◆Vapor pressure measurement

◆Molecular Dynamics (MD) simulation

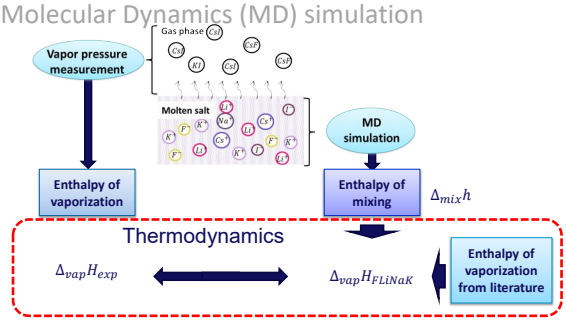

Thermodynamics

- The relation $\Delta_{vap}H_{exp}$ by TG-DTA-MS and Δh_A by MD
- Vaporization of pure CsI

$$\mu^*_{CsI(g)} - \mu^*_{CsI(l)} = \Delta_{vap}H^* - T\Delta_{vap}S^*$$

- Chemical potential of CsI in gas phase

$$\mu_{CsI(g)\ from\ FLiNaK} = \mu^*_{CsI(g)} + \mathrm{RT}\ln\frac{p_{CsI}}{p^*_{CsI}}$$

- Chemical potential of CsI dissolved in FLiNaK

$$\mu_{CsI(l),inFLiNaK} = \mu^*_{CsI(l)} + RT\ln x_A + \Delta h_A$$

Thermodynamics

- Chemical potential change on the vaporization of CsI from FLiNaK[1]

$$\mu_{CsI(g)\ from\ FLiNaK} - \mu_{CsI(l),inFLiNaK}$$
$$= -RT\ln x_A - x_B^2\omega_{AB} + RT\ln\frac{p_{CsI}}{p^*_{CsI}} + \Delta_{\mathrm{vap}}H^* - T\Delta_{vap}S^*$$

- Entropy terms

$$-\Delta_{vap}S_{FLiNaK} = -R\ln x_A - \Delta_{vap}S^* + R\ln\frac{p_{CsI}}{p^*_{CsI}}$$

- Enthalpy terms

$$\Delta_{\mathrm{vap}}H_{FLiNaK} = \Delta_{\mathrm{vap}}H^* - x_B^2\omega_{AB}$$

[1] Y. Sekiguchi et al, *Proc. of GLOBAL 2019*, Seattle, WA, U.S.A., Sep 22-26 (2019)

Thermodynamics

- $\Delta_{vap}H_{FLiNaK}(CsI)$ agreed well with $\Delta_{vap}H_{exp}(CsI)$.

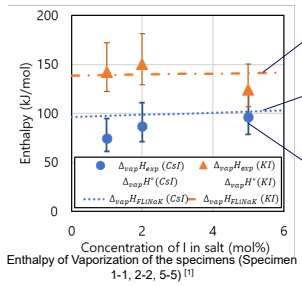

Enthalpy of Vaporization of the specimens (Specimen 1-1, 2-2, 5-5) [1]

$\Delta_{vap}H^*(CsI)$: Enthalpy of vaporization of pure CsI

$\Delta_{vap}H_{FLiNaK}(CsI)$: Enthalpy of vaporization of CsI from FLiNaK by MD

$\Delta_{vap}H_{exp}(CsI)$: Enthalpy of vaporization of CsI from FLiNaK by experiment

[1] Y. Sekiguchi et al, *Proc. of GLOBAL 2019*, Seattle, WA, U.S.A., Sep 22-26 (2019)

Conclusion

- Vapor pressure of CsI and KI evaporated from FLiNaK containing Cs and I were measured, and enthalpy of vaporization were obtained.
- Enthalpy of mixing of the pseudo-binary systems (FLiNaK-CsI, FLiNaK-KI, FLiNaK-CsF) were calculated by Molecular Dynamics, and dissolving CsI and KI into FLiNaK was difficult.
- The results of experiments and calculations were consistent thermodynamically, and it indicates the MD has capability to assist the vapor pressure estimation.

4.1.8 F. Kon（Hokkaido Univ.）

Observation of Antiferromagnetic Order in the Heavy-Fermion Compound UIr_2Ge_2 - Resonant X-ray Scat-tering

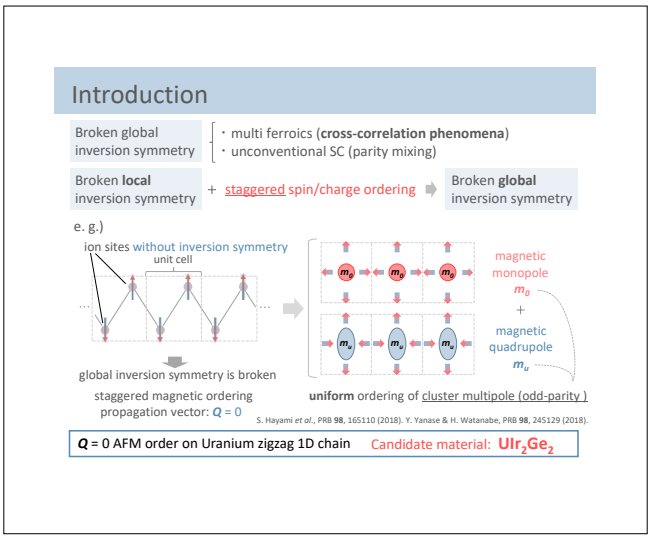

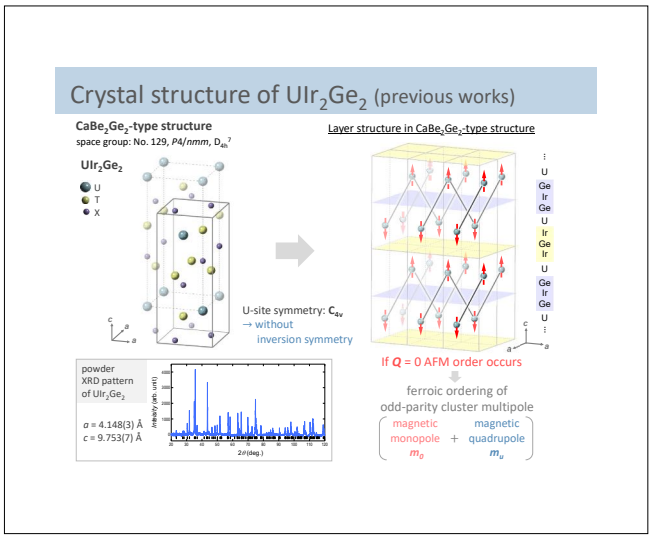

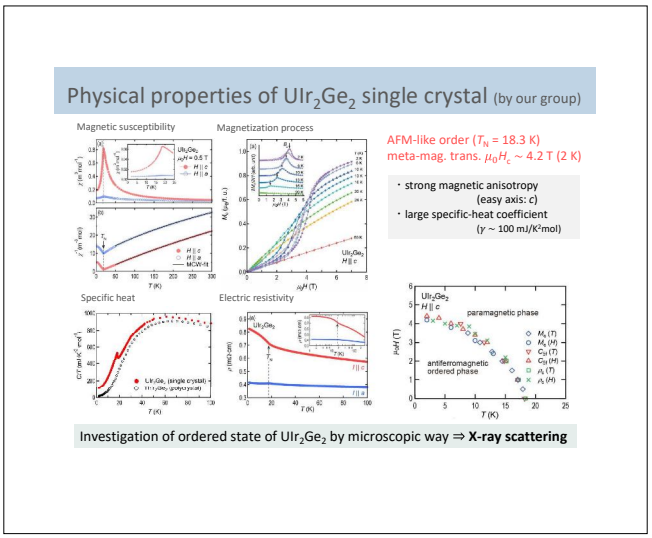

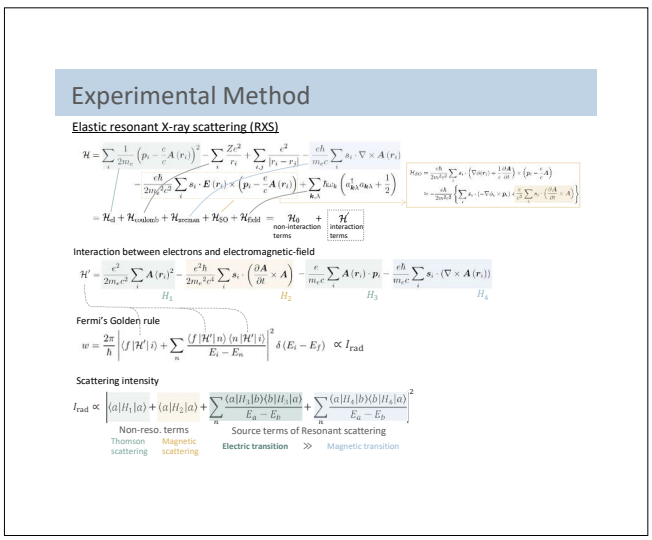

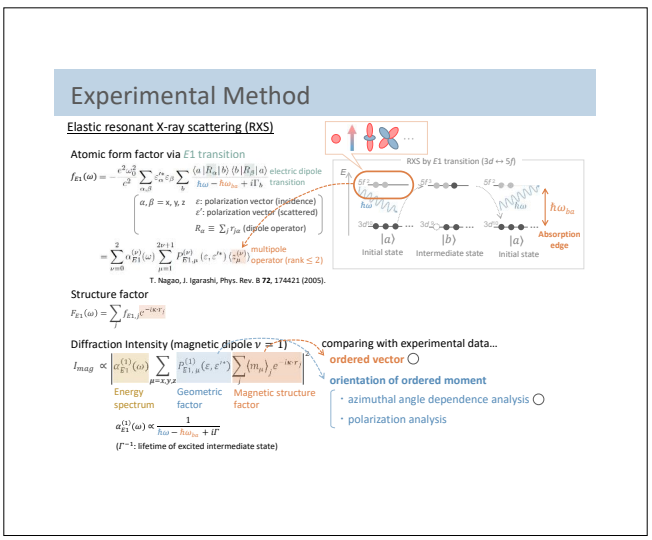

Experimental Procedure

KEK PF BL-11B Versatile two-circle diffractometer

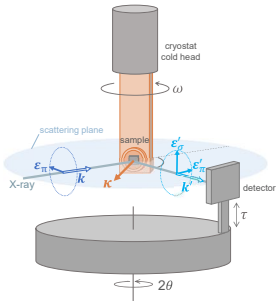

Chamber
- vacuum chamber (10^{-5} ~ 10^{-6} Pa)

Cooling system
- ^{4}He-flow cryostat (6 ~ 300 K)

Incident X-ray
- Energy: 3.7-3.75 keV (M_4-edge of U, $E1$)
- Polarization: holizontal (π-pol.)

Detector
- silicone drift detector (SDD)

Samples
- sample1 (scattering plane: ***c***-(110))
- sample2 (scattering plane: ***a***-***c***)

grown by Czochralski method (IMR Tohoku Univ.)

Experimental Result

Line scans in ***c****-(1, 1, 0)* plane

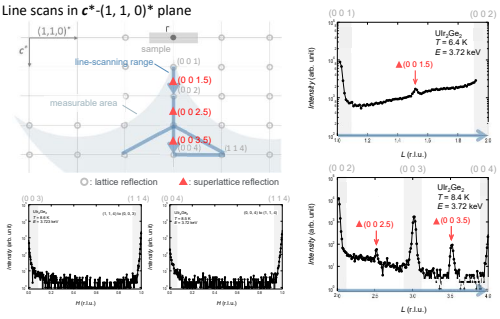

Experimental Result

Line scans in ***a****-***c****plane

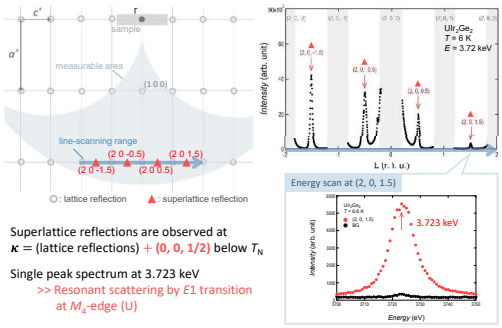

Superlattice reflections are observed at
$\boldsymbol{\kappa}$ = (lattice reflections) + **(0, 0, 1/2)** below T_N

Single peak spectrum at 3.723 keV
>> Resonant scattering by $E1$ transition at M_4-edge (U)

Experimental Result

Temperature profile

Superlattice reflection

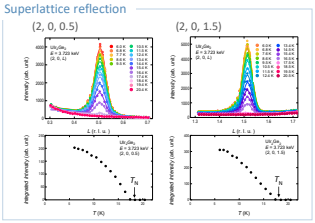

Test for Q = 0 ordering

Lattice reflection

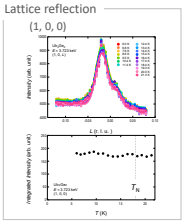

Superlattice reflections are observed at
$\boldsymbol{\kappa}$ = (lattice reflections) + **(0, 0, 1/2)** below T_N

Single peak spectrum at 3.723 keV
>> Resonant scattering by $E1$ transition at M_4-edge (U)

Conclusion

Not $\boldsymbol{Q}$ = 0, but

$\boldsymbol{Q}$ = (0, 0, 1/2) AFM order by uranium 5*f*-electron under T_N

Magnetic structure analysis

based on Landau theory for 2nd order transition

Crystal structure
Space group: *P*4/*nmm* (No. 129) + **propagation vector *Q* = (0, 0, 1/2)** non-zero magnetic moment at U-site

Maximal magnetic space groups

(1) $P_{2c}4/nm'm'$ (No. 129.13.1087) (2) $C_{2c}m'ma$ (No. 67.11.587) (3) $P_{2c}nm'm'$ (No. 59.9.486)

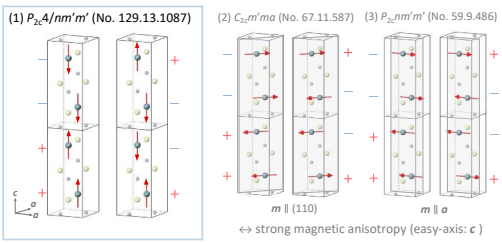

↔ strong magnetic anisotropy (easy-axis: ***c***)

AFM ordering with magnetic moment along *c*-axis ($P_{2c}4/nm'm'$) ?

Experimental Procedure

azimuthal angle dependence of superlattice intensity

$$F_{\mathrm{resO}}(\omega) = \sum_{\nu=0}^{2} \alpha_{E1}^{(\nu)}(\omega) \sum_{\mu=1}^{2\nu+1} P_{E1,\mu}^{(\nu)}(\varepsilon, \varepsilon'^*) \, Z_{\mu}^{(\nu)}$$

Multipole structure factor

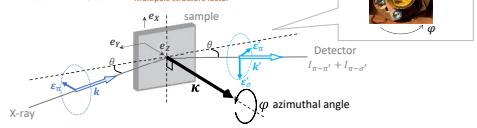

e. g.)

In the case of AFM order (magnetic dipole $\boldsymbol{m}$ (ν = 1))

$$F_{E1,\mu}^{(1)} \propto \sum_{\mu} (\boldsymbol{\varepsilon}'^* \times \boldsymbol{\varepsilon})_{\mu} m_{\mu} \quad (\mu = X, Y, Z)$$

$$\langle \varepsilon_{\pi}'^* \times \varepsilon_{\pi} \rangle_X = (-2\sin\theta\cos\theta)\cos\varphi, \quad \langle \varepsilon_{\sigma}'^* \times \varepsilon_{\pi} \rangle_X = \cos\theta\sin\varphi$$
$$\langle \varepsilon_{\pi}'^* \times \varepsilon_{\pi} \rangle_Y = (2\sin\theta\cos\theta)\sin\varphi, \quad \langle \varepsilon_{\sigma}'^* \times \varepsilon_{\pi} \rangle_Y = \cos\theta\cos\varphi$$
$$\langle \varepsilon_{\pi}'^* \times \varepsilon_{\pi} \rangle_Z = 0, \quad \langle \varepsilon_{\sigma}'^* \times \varepsilon_{\pi} \rangle_Z = -\sin\theta$$

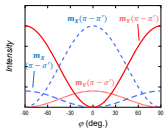

$\boldsymbol{m} \parallel \boldsymbol{e}_X \cdots I_{\pi-\pi'} \propto (1 + \cos 2\varphi)$ $\boldsymbol{m} \parallel \boldsymbol{e}_Y \cdots I_{\pi-\pi'} \propto (1 - \cos 2\varphi)$

Experimental Result

azimuthal angle dependence of superlattice intensity

$-90° < \varphi < 0$

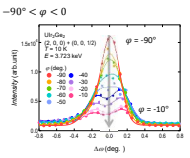

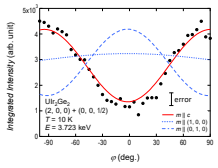

$0 < \varphi < 90°$

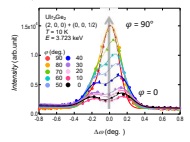

In the case of $\boldsymbol{m} \parallel \boldsymbol{c}$

$\varphi = 0 \quad \boldsymbol{m} = (m_x, m_y, m_z) = m(0, 0.998, 0.0565)$

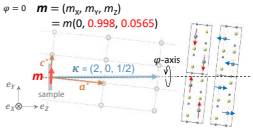

Summary for magnetic structure

- Super lattice reflections are observed at (lattice reflection) + (0, 0, 1/2) below T_N
- Azimuthal dependent of super lattice reflection intensity shows a good agreement with the calculations for magnetic moment parallel to the *c* axis.

- UIr_2Ge_2 undergoes AFM order below T_N with "**uudd structure**".
  → a rare example of magnetic order

Magnetic structure of UIr_2Ge_2

AFM order with $\boldsymbol{Q}$ = (0, 0, ½)
→"**uudd structure**"

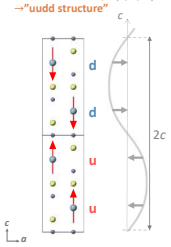

uudd-type magnetic structure

Example 1: ^{3}He AFM order at ultra-low temperature

M. Roger and J. H. Hetherington, Phys. Rev. B, **41**, 200 (1990).

bcc crystal structure

Copyright protected content

$$H_{ex} = \frac{J_1}{2}\sum_{i<j}^{(1)} \boldsymbol{\sigma}_i \cdot \boldsymbol{\sigma}_j + \frac{J_2}{2}\sum_{i<j}^{(2)} \boldsymbol{\sigma}_i \cdot \boldsymbol{\sigma}_j + \frac{J_3}{2}\sum_{i<j}^{(3)} \boldsymbol{\sigma}_i \cdot \boldsymbol{\sigma}_j$$

Nearest neighbor(NN) Second NN Third NN

$$+ \frac{K_P}{4}\sum_{i<j<k<l}^{(P1)} \left(\sum_{\alpha<\beta} \sigma_{i\alpha} \cdot \sigma_{j\beta} + g_{ijkl} \right) + E_P$$

Four-body interaction

$$g_{ijkl} = (\boldsymbol{\sigma}_i \cdot \boldsymbol{\sigma}_j)(\boldsymbol{\sigma}_k \cdot \boldsymbol{\sigma}_l) + (\boldsymbol{\sigma}_j \cdot \boldsymbol{\sigma}_k)(\boldsymbol{\sigma}_i \cdot \boldsymbol{\sigma}_l) - (\boldsymbol{\sigma}_i \cdot \boldsymbol{\sigma}_k)(\boldsymbol{\sigma}_j \cdot \boldsymbol{\sigma}_l)$$

Example 2: 1D spin chain ($TlCoCl_3$)

Y. Nishiwaki et al., J. Phys. Soc. Jpn., 75, 034707 (2006).

Copyright protected content

- the axial next-nearest-neighbor Ising (ANNNI) model

frustration is relevant

Magnetic Interaction

Magnetic interaction model of UIr_2Ge_2

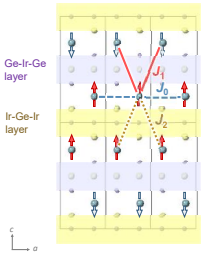

J_0: in-plane FM interaction
J_1: inter layer AFM interaction
J_2: inter layer FM interaction

uudd-type AFM order emerge naturally in UIr_2Ge_2 without
- complex magnetic interaction
- geometric frustration

CW-fitting for magnetization

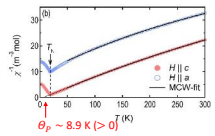

θ_p ~ 8.9 K (> 0)
→ Ferromagnetic interaction

Cluster multipole ordering

Description by using the concept of **Cluster multipole**

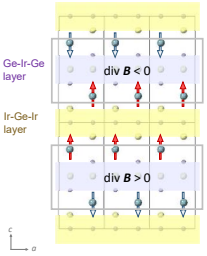

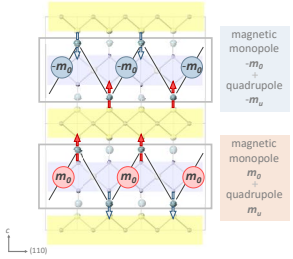

Alternatively stacked odd-parity multipole layered structure

Conclusion

- UIr_2Ge_2 undergoes "uudd"-type AFM order by magnetic moments parallel to c-axis under T_N.
- Magnetic structure in UIr_2Ge_2 is regarded as antiferroic-stacking of layers of odd-parity cluster magnetic multipole.
- From our critical behavior analysis, it is suggested that UIr_2Ge_2 behave like 2D-Ising model under magnetic field.

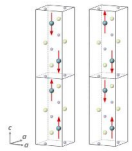

Future works

- Studies of the relationship between dimensional crossover and bulk properties.
  - RXS experiments under weak field
  - Measurements of physical properties under 1.2 K
- Quantitative analysis of magnetic interactions.
- Detailed investigation of magnetic interactions
  - study of spin wave excitation by inelastic scattering (X-ray/neutron)

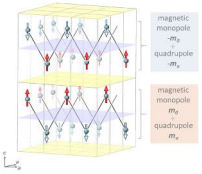

4.1.9 A. Sato（Tokyo Met. Univ.）

Theoretical study on isotope fractionation in uraninite

TOKYO METROPOLITAN UNIVERSITY
東京都立大学

Theoretical study on isotope fractionation in uraninite

○Ataru Sato,[1] Eri Ichikawa,[2] Minori Abe,[1,2] Masahiko Hada[1,2]
[1]Department of Chemistry, Tokyo Metropolitan University,
[2]Faculty of Science, Tokyo Metropolitan University

1

Background: Uranium isotope fractionation during reduction

Stylo *et al. Proc. Natl. Acad. Sci. USA.* **112**, 5619 (2015)

$^{235}U(VI) \rightarrow {}^{235}U(IV)$, $^{238}U(VI) \rightarrow {}^{238}U(IV)$

Biotic reduction by *S.oneidensis* strain MR-1

Abiotic reduction by FeS, $[HS^-]_{aq}$, $[Fe^{(II)}]_{aq}$ etc...

Copyright protected content

Change in isotope ratio of U(VI)

$$\delta^{238}U(VI) \equiv \left[\frac{\left(\left[^{238}U\right]/\left[^{235}U\right]\right)_{sample}}{\left(\left[^{238}U\right]/\left[^{235}U\right]\right)_{standard}} - 1\right] \times 1000$$

C/C_0 Progress of reaction

$\delta^{238}U(VI) < 0$

^{238}U is enriched in U(IV).

C/C_0 C/C_0 Progress of reaction

$\delta^{238}U(VI) \geq 0$

^{238}U is not enriched in U(IV).

Biotic & abiotic reductions show the different tendency.

⇒May give an insight into paleo-redox conditions in the earth's history

2

Background: Speciation of initial substance

Stylo *et al. Proc. Natl. Acad. Sci. USA.* **112**, 5619 (2015)

pH6.8 (Abiotic reduction)

pH7.3 (Biotic reduction)

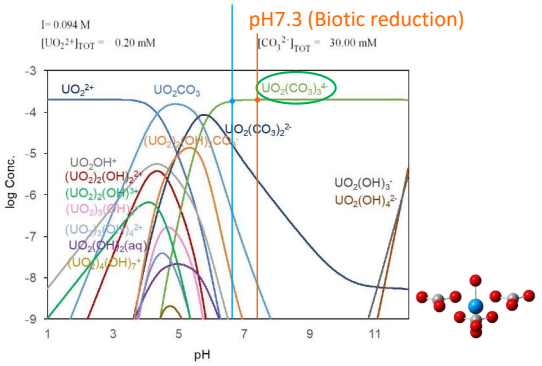

Both biotic & abiotic reduction: $UO_2(CO_3)_3^{4-}$ is the dominant species.

3

Background: Prediction of product by EXAFS

Stylo *et al. Proc. Natl. Acad. Sci. USA.* **112**, 5619 (2015)

Copyright protected content

U(VI)
UO_2 crystal (Uraninite)
Non-crystalline U(IV)

$[HS^-]_{aq}$
Peat
Chemogenic magnetite
1mM chemogenic FeS
5mM chemogenic FeS
Biogenic FeS

S.oneidensis(BP)
S.oneidensis(WLP)

References
Only uraninite shows a peak around 4 Å.

Abiotic
A peak around 4 Å is observed.➔Uraninite

Biotic (WLP)
A peak around 4 Å isn't observed.
➔Non-crystalline U(IV)

Abiotic reduction: Uraninite is the final product.

WLP: Widdel Low Phosphate medium, BP: Bicarbonate-Pipes medium

4

Theoretical basis of isotope fractionation in equilibrium

Isotope exchange reaction

$$AX + A'Y = A'X + AY$$

A: Heavy isotope
A': Light isotope

Isotope fractionation coefficient

$$\varepsilon \equiv \frac{[AY]/[A'Y]}{[AX]/[A'X]} - 1$$

$$\approx \ln K_{nm} + \ln K_{nv}$$

Nuclear mass term — Dominant for heavy elements

Nuclear volume term — Dominant for light elements

$\varepsilon > 0$ ⇒ A is enriched in AY.

5

Nuclear mass term $\ln K_{nm}$

Bigeleisen and Mayer, *JCP.* **15**, 261 (1947)

Different reduced mass (μ) of isotopologues
➔ Difference in harmonic frequencies (ν)

$$\nu = \frac{1}{2\pi}\sqrt{\frac{k}{\mu}}$$

$$\ln K_{nm} = \ln \beta(AY) - \ln \beta(AX)$$

$$\ln \beta = \ln\left[\prod_i \frac{u_i}{u_i'} \frac{e^{-u_i/2}/(1-e^{-u_i})}{e^{-u_i'/2}/(1-e^{-u_i'})}\right], \quad u_i = \frac{h\nu_i}{k_B T}$$

β: Reduced partition function ratio
ν : Harmonic frequency

Vibrational energy of AX

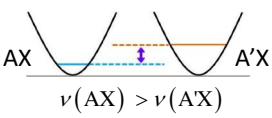

$\nu(AX) > \nu(A'X)$

Heavy isotope is more enriched in the system with tightly bound.

6

Nuclear volume term $\ln K_{nv}$

Nomura *et al. JACS.* **118**, 9127 (1996) & Bigeleisen, *JACS.* **118**, 3676 (1996)

Different nuclear size and shape of isotopes
➔ Difference in electronic energy

$$\ln K_{nv} = \left[\Delta E_{nv}(\mathrm{AX}) - \Delta E_{nv}(\mathrm{AY})\right]/k_B T$$

ΔE_{nv}: Electronic energy difference between isotopic species

$$\Delta E_{nv} \propto \rho(0)$$

$\rho(0)$: Electron density at the nucleus

Electronic energy of AX

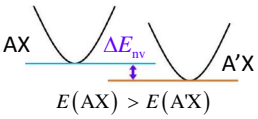

$$E(\mathrm{AX}) > E(\mathrm{A'X})$$

- ✓ Heavy isotope is more enriched in the system with small ΔE_{nv}.
- ✓ Electronic state around the nucleus is important.
  ⇒Relativistic method based on Dirac equation is essential.

Schauble, *GCA.* **71**, 2170 (2007) & Abe *et al. JCP.* **129**, 164309 (2008)

7

Theoretical basis of kinetic isotope fractionation

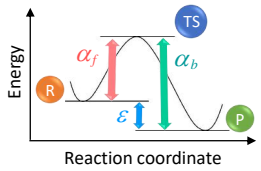

R Reactant
P Product
TS Transition state

α for the forward reaction (α_f)

R ⇌ TS, R' ⇌ TS'

$$\alpha_f \equiv \frac{[\mathrm{R'}]/[\mathrm{R}]}{[\mathrm{TS'}]/[\mathrm{TS}]} - 1$$

Equal to ε between R and TS

α for the backward reaction (α_b)

P ⇌ TS, P' ⇌ TS'

$$\alpha_b \equiv \frac{[\mathrm{P'}]/[\mathrm{P}]}{[\mathrm{TS'}]/[\mathrm{TS}]} - 1$$

Equal to ε between P and TS

It is impossible to obtain TS for reaction involving crystal.
⇒This study: We calculate ε assuming equilibrium between R & P.

8

Motivation

Biotic reduction

- ^{238}U enriches in U(IV)
- Reactant: $UO_2(CO_3)_3^{4-}$
- Product: Non-crystalline U(IV)

Abiotic reduction

- ^{238}U does not enrich in U(IV)
- Reactant: $UO_2(CO_3)_3^{4-}$
- Product: Uraninite

Stylo *et al. PNAS.* **112**, 5619 (2015)

Isotope fractionation difference may be caused by the difference of product.

Objective
- ✓ Calculate $\ln K_{nv}$ for uraninite
- ✓ Calculate ε between $UO_2(CO_3)_3^{4-}$ & uraninite assuming equilibrium and compare it to biotic reduction*

Biotic reduction

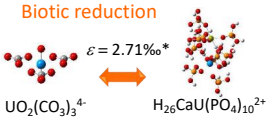

*Sato et al. submitted.

Abiotic reduction

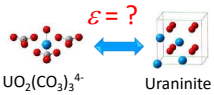

9

Problem in calculation of $\ln K_{nv}$ for crystal

Calculation of $\ln K_{nv}$
requires accurate relativistic methods.
(e.g., 4cmp-Dirac, IODKH, X2C)

Accurate relativistic method
For molecule → ○
For crystal → ×

An alternative calculation method for $\ln K_{nv}$ in crystal
by Schauble, *PNAS.* **110**, 17714 (2013)

✓ $\ln K_{nv}$ can be determined by $\rho(0)$.

$$\left(\because \ln K_{nv} = \left[\Delta E_{nv}(\mathrm{AX}) - \Delta E_{nv}(\mathrm{AY})\right]/k_B T,\ \Delta E_{nv} \propto \rho(0)\right)$$

⬇

✓ First-principles calculation (DFT) can deal with crystal.

⬇

✓ If $\rho(0)$ by the first-principle and accurate relativistic method shows good correlation, we may be able to estimate $\ln K_{nv}$ for crystal.

This method worked well for Sn, Cd, & Hg system.

10

Computational way of $\ln K_{nv}$ for crystal

Schauble, *Proc. Natl. Acad. Sci. USA.* **110**, 17714 (2013)

1. Calculate $\rho(0)$ of some molecules by first-principles & relativistic calcs. & We get relationship (1).
2. Calculate ΔE_{nv} of some molecules by relativistic calc. & We get relationship (2).
3. Calculate $\rho(0)$ of crystal by first-principles calc.
4. Convert $\rho(0)$ of crystal to ΔE_{nv} using relationships (1) & (2)
5. Calculate $\ln K_{nv}$ of crystal

Relationship (1)
$\rho(0)$ obtained by first-principles calc. vs $\rho(0)$ obtained by relativistic calc.

Relationship (2)
$\rho(0)$ vs ΔE_{nv} obtained by relativistic calc.

11

Computational details

➢ Geometry optimization & Calculation of $\ln K_{nm}$

■ Uraninite
Program: VASP5.4.1 & PHONOPY2.8.1
Method: DFT calc. (Functional: PBE)
Pseudopotential: PAW
Cut-off energy: 1750eV
K-points: 6 × 6 × 6

■ $UO_2(CO_3)_3^{4-}$
Program: Gaussian16
Method: DFT calc. (Functional: CAM-B3LYP)
Basis sets: SDD small core (U)
6-31++G** (remaining atoms)
Solvation effect: PCM (water)

➢ Calculation of $\ln K_{nv}$

✓ First-principles calc.
Program: ABINIT8.8.3
Method: DFT calc. (Functional: PBE)
Pseudopotential: PAW
Cut-off energy: 20 a.u. (544.23eV)
K-points: 4 × 4 × 4

✓ Relativistic calc.
Program: DIRAC16
Method: X2C-HF
Basis sets: Dyall.cv2z (U)
6-31++G** (remaining atoms)

In the calculation of $\ln K_{nv}$ & $\ln K_{nm}$, temperature is assumed to be 298K.

12

$\ln K_{nm}$ between $UO_2(CO_3)_3^{4-}$ & Uraninite

✓ $\ln\beta$ is calculated from harmonic frequencies of all atoms

$$\ln\beta = \ln\left[\prod_i \frac{u_i}{u_i'} \frac{e^{-u_i/2}/(1-e^{-u_i})}{e^{-u_i'/2}/(1-e^{-u_i'})}\right],\quad u_i = \frac{h\nu_i}{k_B T}$$

✓ Computational result of $\ln K_{nm}$

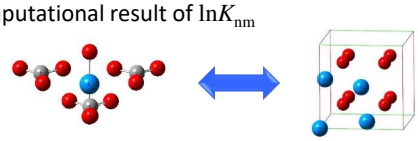

$UO_2(CO_3)_3^{4-}$ Uraninite

$\ln\beta$: Unpublished data

$\ln K_{nm} = \ln\beta(\text{Uraninite}) - \ln\beta(UO_2(CO_3)_3^{4-}) =$

13

Relationship (1): $\rho(0)$ obtained by ABINIT & DIRAC

Unpublished data

- U(VI)
- U(V)
- U(VI)

→ Good correlation!

$\rho(0)$ obtained by the first-principles calculation (ABINIT) can be converted to $\rho(0)$ by the relativistic calculation (DIRAC).

14

Relationship (2): $\rho(0)$ vs ΔE_{nv} obtained by DIRAC

Unpublished data

- U(VI)
- U(V)
- U(VI)

→ Good correlation!

Confirmed that ΔE_{nv} is proportional to $\rho(0)$

$$\Delta E_{nv} \propto \rho(0)$$

15

$\ln K_{nv}$ between $UO_2(CO_3)_3^{4-}$ & Uraninite

Relationship (1) Relationship (2)

Unpublished data

$\rho(0)$ of uraninite by ABINIT is converted to $\rho(0)$ of uraninite by DIRAC

$\rho(0)$ of uraninite by DIRAC is converted to ΔE_{nv} of uraninite by DIRAC

$\ln K_{nv} = [\Delta E_{nv}(UO_2(CO_3)_3^{4-}) - \Delta E_{nv}(\text{Uraninite})]/k_B T =$

✓

✓

Unpublished data

16

Dependence of ε on product

Abiotic reduction (This study) Biotic reduction* (Previous study)

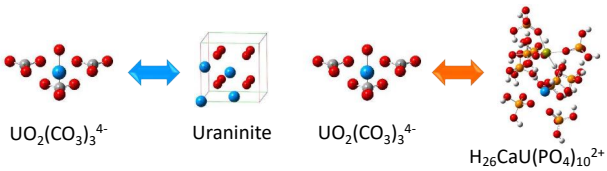

$UO_2(CO_3)_3^{4-}$ Uraninite $UO_2(CO_3)_3^{4-}$ $H_{26}CaU(PO_4)_{10}^{2+}$

Unpublished data ⟷ $\varepsilon = 2.71‰$

Same tendency

Direction of isotope fractionation does not depend on electronic state of product.

*A. Sato, R. Bernier-Latmani, M. Hada, and M. Abe, submitted.

17

Conclusion

✓ We calculated ε assuming equilibrium between $UO_2(CO_3)_3^{4-}$ & uraninite

Unpublished data

$UO_2(CO_3)_3^{4-}$ Uraninite

✓ We succeeded in calculating $\ln K_{nv}$ for uraninite

✓ ε obtained in our calculation has the same sign as that for the biotic reduction (2.71‰).*

➡Difference in electronic state of product does not affect the direction of isotope fractionation.

*A. Sato, R. Bernier-Latmani, M. Hada, and M. Abe, submitted.

18

4.1.10 Y. Kitawaki（Kyoto Sangyo Univ.）

Orbital magnetization in many-electron systems described by spin-orbital-polarized coupled Dirac equation

Topical meeting on Condensed-matter Chemistry on Actinides, Feb. 10, 2021.

Orbital magnetization in many-electron systems described by spin-orbital-polarized coupled Dirac equation

Yohei Kitawaki
(Division of Science, Graduate School, Kyoto Sangyo University)

Abstract

- SOPCD (spin-orbital-polarized coupled Dirac) equation was derived as an ab-initio theory to describe orbital magnetization, by adding orbital-genetic current density to SPCD (spin-polarized coupled Dirac) equation based on spin-polarized relativistic density functional theory.
- Numerical calculations of SOPCD equation for actinide trivalent ions yielded an orbital-polarization of 5f energies, which is different from that of SPCD equation.

Collaborators

H. Yamagami (Dept. of Phys. Kyoto Sangyo Univ.)

1

Outline

- Introduction
- SPCD equation (previous research)
- SOPCD equation
- Results of numerical calculations
- Summary

2

Introduction

- Orbital magnetization is significant in magnetism of heavy element materials.
- ex.) Magnetic moment of actinide compounds AFe_2

	$\mu_{\rm exp}$	μ_S^B	μ_L^B	μ_L^B	μ_S	μ_L	μ_T
UFe_2	0.06	-0.58	0.47	-0.11	-0.83	0.88	0.05
$NpFe_2$	1.09	-1.17	0.70	-0.47	-2.29	3.49	1.20
$PuFe_2$	0.45	-3.48	1.45	-2.03	-3.19	3.52	0.33

Experiments by neutron scattering (Lander et al. ,1977)

Normal band calculations (Eriksson et al. ,1990)

Orbital polarized band calculations with a parameter (Eriksson et al. ,1990)

- We need <u>an ab-initio relativistic theory</u> that can describe orbital magnetization <u>without the parameter</u>.

3

SPCD equation

Spin-Polarized Relativistic Density Functional Theory (SPRDFT)

- Charge density $n(\boldsymbol{r})$ and Spin magnetization density $\boldsymbol{m}(\boldsymbol{r})$
- Local Spin Density Approximation (LSDA)
- Kohn-Sham-Dirac equation

$$\left[c\boldsymbol{\alpha}\cdot\boldsymbol{p}+(\beta-I)mc^2+V(\boldsymbol{r})+\beta\boldsymbol{\Sigma}\cdot\boldsymbol{B}(\boldsymbol{r})\right]\Phi_i(\boldsymbol{r})=\varepsilon_i\Phi_i(\boldsymbol{r})$$

- Expand $\Phi_i(\boldsymbol{r})$ by two different relativistic atomic orbitals for $j = l \pm 1/2$
- Derive a radial equation with spherical symmetry approximation

Spin-Polarized Coupled Dirac (SPCD) equation

$$\left(\frac{d}{dr}+\frac{\kappa_\pm}{r}\right)G_i^\pm-\left[2+\frac{\varepsilon_i-V(r)\mp B(r)u_{l\pm1,\mu}}{c^2}\right]cF_i^\pm=0$$

$$\left(\frac{d}{dr}-\frac{\kappa_\pm}{r}\right)cF_i^\pm+\left[\varepsilon_i-V(r)\mp B(r)u_{l\mu}\right]G_i^\pm+B(r)\sqrt{1-u_{l\mu}^2}G_i^\mp=0$$

H. Yamagami et al. (1997) J. phys. : Condens. Matter **9** 10881

4

SPCD equation

- LSDA exchange-correlation energy

$$E_{\rm xc}[n,m]=\int d\boldsymbol{r}n(\boldsymbol{r})\epsilon_{\rm xc}\left(n(\boldsymbol{r}),m(\boldsymbol{r})\right)$$

- Approximation for interaction energy

$$\langle\Psi|H_{\rm int}|\Psi\rangle=\int d\boldsymbol{r}J^\mu(\boldsymbol{r})A_\mu(\boldsymbol{r})$$
$$\approx\int d\boldsymbol{r}\left[en(\boldsymbol{r})V(\boldsymbol{r})-\mu_B\boldsymbol{m}(\boldsymbol{r})\cdot\boldsymbol{B}(\boldsymbol{r})\right]$$

described by $n(\boldsymbol{r})$ and $\boldsymbol{m}(\boldsymbol{r})$

- There is a possibility of <u>overlooking interactions that are important for orbital magnetism</u>.

5

SOPCD equation

- Orbital-genetic current density

$$\boldsymbol{j}(\boldsymbol{r})=\langle\Psi|\psi^\dagger(\boldsymbol{r})c\boldsymbol{\alpha}\psi(\boldsymbol{r})|\Psi\rangle$$

$$\langle\Psi|H_{\rm int}|\Psi\rangle\approx\int d\boldsymbol{r}\left[en(\boldsymbol{r})V(\boldsymbol{r})-e\boldsymbol{j}(\boldsymbol{r})\cdot\boldsymbol{A}(\boldsymbol{r})-\mu_B\boldsymbol{m}(\boldsymbol{r})\cdot\boldsymbol{B}(\boldsymbol{r})\right]$$

described by $n(\boldsymbol{r})$, $\boldsymbol{m}(\boldsymbol{r})$ and $\boldsymbol{j}(\boldsymbol{r})$

- Vector potential $\boldsymbol{A}(\boldsymbol{r})$ in Coulomb gauge $\nabla\cdot\boldsymbol{A}(\boldsymbol{r})=0$
- Kohn-Sham-Dirac equation with orbital-genetic current density

$$\left[c\boldsymbol{\alpha}\cdot\boldsymbol{p}+(\beta-I)mc^2+V(\boldsymbol{r})-e\boldsymbol{\alpha}\cdot\boldsymbol{A}(\boldsymbol{r})+\beta\boldsymbol{\Sigma}\cdot\boldsymbol{B}(\boldsymbol{r})\right]\Phi_i(\boldsymbol{r})=\varepsilon_i\Phi_i(\boldsymbol{r})$$

$$V(\boldsymbol{r})=V_{\rm ext}(\boldsymbol{r})+\int d\boldsymbol{r}'\frac{e^2n(\boldsymbol{r}')}{4\pi\varepsilon_0|\boldsymbol{r}-\boldsymbol{r}'|}+V_{\rm xc}(\boldsymbol{r})$$
$$\boldsymbol{A}(\boldsymbol{r})=\boldsymbol{A}_{\rm ext}(\boldsymbol{r})+\frac{2}{c^2}\int d\boldsymbol{r}'\frac{e^2\boldsymbol{j}(\boldsymbol{r}')}{4\pi\varepsilon_0|\boldsymbol{r}-\boldsymbol{r}'|}$$
$$\boldsymbol{B}(\boldsymbol{r})=\boldsymbol{B}_{\rm ext}(\boldsymbol{r})+\boldsymbol{B}_{\rm xc}(\boldsymbol{r})$$

6

SOPCD equation

- Spin-Orbital-Polarized Coupled Dirac (SOPCD) equation

$$\left[\left(\frac{d}{dr}+\frac{\kappa_\pm}{r}\right)-\frac{1}{c}A^{\pm}_{1l\mu}\right]G^{\pm}_i-\left[2+\frac{\varepsilon_i-V(r)\mp B(r)u_{l+1,\mu}}{c^2}\right]cF^{\pm}_i-\frac{1}{c}A^{\pm}_{2l\mu}G^{\pm}_i=0$$

$$\left[\left(\frac{d}{dr}-\frac{\kappa_\pm}{r}\right)+\frac{1}{c}A^{\pm}_{1l\mu}\right]cF^{\pm}_i+\left[\varepsilon_i-V(r)\pm B(r)u_{l\mu}\right]G^{\pm}_i+B(r)\sqrt{1-u^2_{l\mu}}G^{\pm}_i+\frac{1}{c}A^{\pm}_{2l\mu}cF^{\pm}_i=0$$

- Effective potentials

$$V(r)=-\frac{Z}{r}+\left(\frac{1}{r}\int_0^r dr'+\int_r^\infty dr'\frac{1}{r'}\right)n(r')+V_{xc}[n(r),m(r)]$$

$$B(r)=B_{xc}[n(r),m(r)]$$

$$A^{\pm}_{q l\mu}(r)=\sum_{k=1}^{2l+1}A^k(r)C^{\pm}_q(l\mu;k)\qquad(q=1,2)$$

$$A^k(r)=\left(\frac{1}{r^{k+1}}\int_0^r dr' r'^k+r^k\int_r^\infty dr'\frac{1}{r'^{k+1}}\right)n^k(r')$$

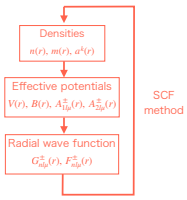

- Densities

Charge $\quad n(r)=\sum_i W_i\left[G_i^{+\,2}+G_i^{-\,2}+F_i^{+\,2}+F_i^{-\,2}\right]$

Spin magnetization $\quad m(r)=\sum_i W_i\left[u_{l\mu}G_i^{+\,2}-u_{l\mu}G_i^{-\,2}+u_{l+1,\mu}F_i^{+\,2}-u_{l-1,\mu}F_i^{-\,2}-2\sqrt{1-u^2_{l\mu}}G_i^+G_i^-\right]$

Orbital current $\quad a^k(r)=\sum_i W_i\left[G_i^+F_i^+C_1^+(l\mu;k)+G_i^-F_i^-C_1^-(l\mu;k)+G_i^+F_i^-C_2^-(l\mu;k)+G_i^-F_i^+C_2^+(l\mu;k)\right]$

7

Summary

- SOPCD equation leads to spin-orbital polarization in lanthanide $4f$ and actinide $5f$ energies.
- SOPCD calculation is novel in terms of self-consistent calculation that includes orbital current density as one of the fundamental variables.
- This theory can be useful for describing localized orbital magnetism.

Future work

- Application to relativistic band theory
- Linear augmented-Slater-type-orbital (LASTO) method

8

4.2 Break Session 2

4.2.1 T. Fukuda（JAEA）

Present status of the study on energy conversion using actinides in radioactive wastes

アクチノイドのα線等を利用した放射線発電の現状

Present status of the study on energy conversion into electricity using actinides in radioactive wastes

Tatsuo Fukuda, Kenji Yoshii and Tsuyoshi Yaita

Materials Sciences Research Center
Japan Atomic Energy Agency (JAEA)

Nuclear wastes as energy resources

Nuclear wastes

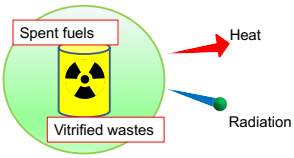

- Long lifetime: longer than 50 years
- Continuous energy emission
- CO_2 emission free

Energy resource

Research thus far

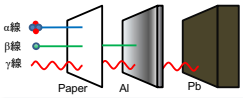

Mainly on α and β particles
α：Thermoelectrics
β：Thermoelectrics and direct energy conversion

Heat Space use (NASA)

Radioisotope thermoelectric generator (RTG)

Direct conversion

^{14}C battery
Bristol (2016)

Gammavoltaics: Energy conversion using SiC

Silicon carbide (SiC)
Tolerant to radiation: space usage
Without hazardous elements

- Sample: QST Takasaki
  Ni(80 nm)/SiC Schottky diode
  (n-type single-crystalline SiC;
  1.7mm^2, t=0.37mm)

- Energy conversion measurement
  SPring-8 BL22XU: 60 keV, 30keV (^{241}Am,^{237}Np): $10^{9\text{-}12}$ photons/s/mm^2
  X-ray apparatus：8keV(Cu $K\alpha$):$10^{9\text{-}10}$photons/s

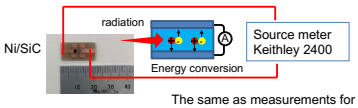

The same as measurements for solar batteries.

K. Yoshii, T. Fukuda, T. Yaita *et al.*, Meeting of Atomic Energy Society of Japan (2019)

Commercially available Si battery

Measurement on low-cost Si solar battery

Amorphous Si solar battery (¥200)
0.5V 250mA：about 2-3 dollars（20mm × 100mm）
Goldmaster & Everstep Development Limited

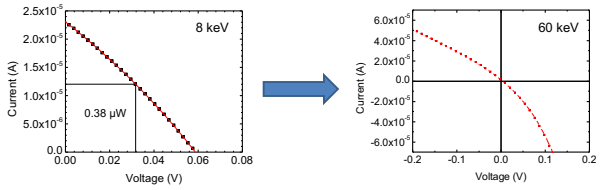

- Low output voltages：Band gap of Si, 1.1eV; 3.3 eV for SiC
- No detectable electrical power for 60 keV：Transparent
  ⇒ SiC is more suitable.

Waste heat recovery: Spintronics

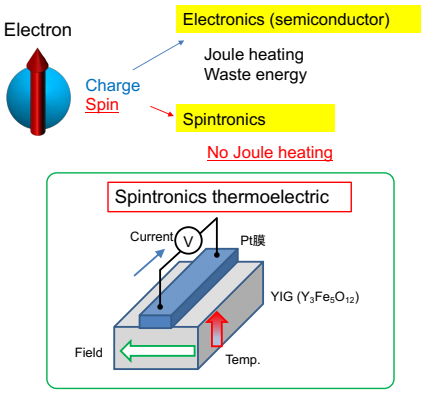

Advanced Science Research Center, JAEA
K. Uchida et al., J. Appl. Phys. **111**, 103903 (2012)

Tolerance for gamma rays

Electronics (semiconductor)
Secondary electrons
Lattice defect

Spintronics
Tolerant of gamma rays

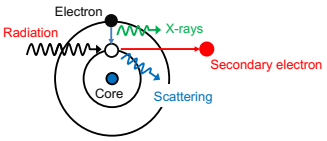

A. Yagmur *et al.*, Appl.Phys.Lett. **109**, 243902 (2016)

Possible usage of nuclear waste as energy resource

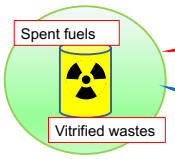

Gamma rays

Particles (α, β, neutrons)

Effect on spintronics?

Tolerance for gamma rays

Au irradiation

Tandem accelerator @JAEA Tokai

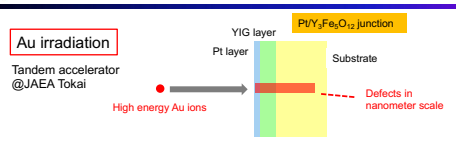

Extremely long life

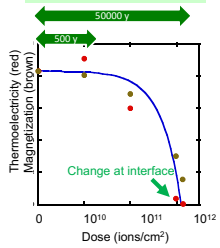

S. Okayasu et al., J. Appl. Phys. **128**, 083902 (2020).

https://www.jaea.go.jp/02/press2020/p20082802/

Origin of decrease in thermoelectriciry

High energy X-ray photoelectron spectroscopy (HAXPES)@BL22XU of SPring-8 (JAEA bemline)

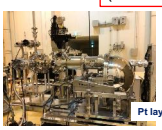

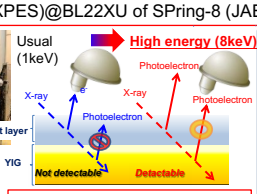

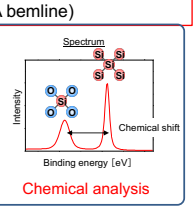

Chemical analysis

HAXPES spectra of oxygen

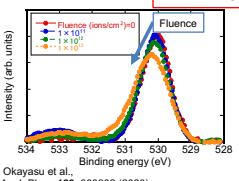

S. Okayasu et al., J. Appl. Phys. **128**, 083902 (2020).

- Valence of oxygen at Pt/YIG interface changes from 2-
- Chemical reaction at interface

To be done
More stable substrate
Heavier element than oxygen?

Collaboration with Kyoto Univ.

Collaborative works among Hot Labs.

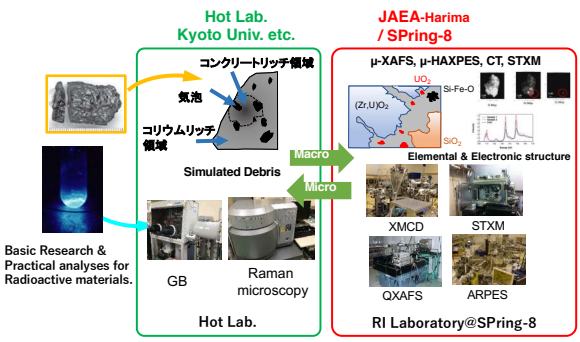

Summary and future studies

1. Gammavoltaics using semiconductors
   - Dark current measurement
     Nearly an ideal diode
   - Electrical power of 0.1-1μW/cm²
     Efficiencies about 0.2%
     Radiation monitor, rather than energy resource?
   - Efficiency should be increased.
     Heavy elements
     Stacking of thin films
2. Spitronics: Fe/YIG films
   -Tolerant against gamma rays
   - Electronic state observation using synchrotron radiation
   - Energy conversion of radiation damaged samples (in progress)

Collaborators

Gammavoltaics

JAEA Spring-8

T. Fukuda, T. Shobu, M. Kobata, H. Tanida, T. Kobayashi, H. Shiwaku

JAEA Tokai

J. Kamiya, Y. Iwamoto

QST Takasaki

T. Makino, Y. Yamazaki, T. Ohshima

Spintronics: JAEA Tokai, Tohoku Univ., Univ. of Tokyo

J. Ieda, K. Harii, S. Okayasu, E. Saitoh
T. Kikkawa, T. Hioki

4.2.2 T. Oda（Kyoto Univ.）

Slow dynamics study by neutron resonance spin echo spectrometer

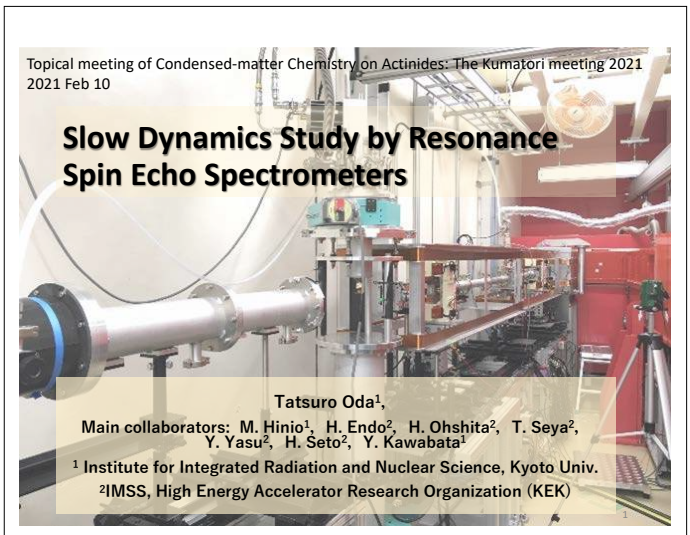

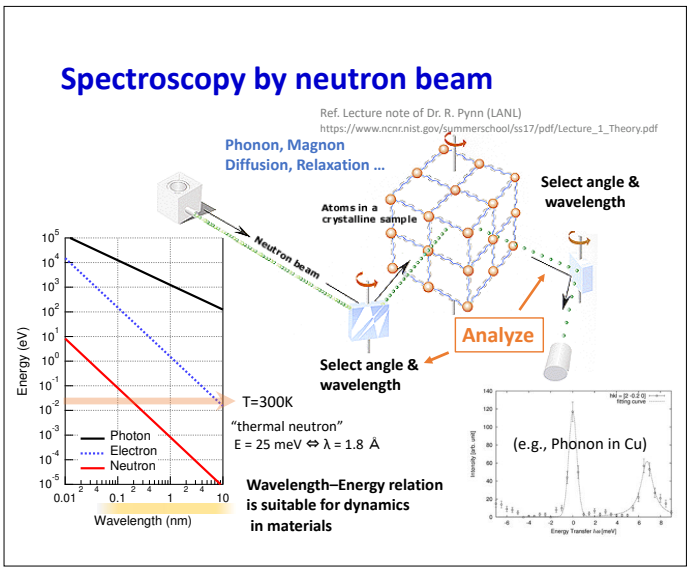

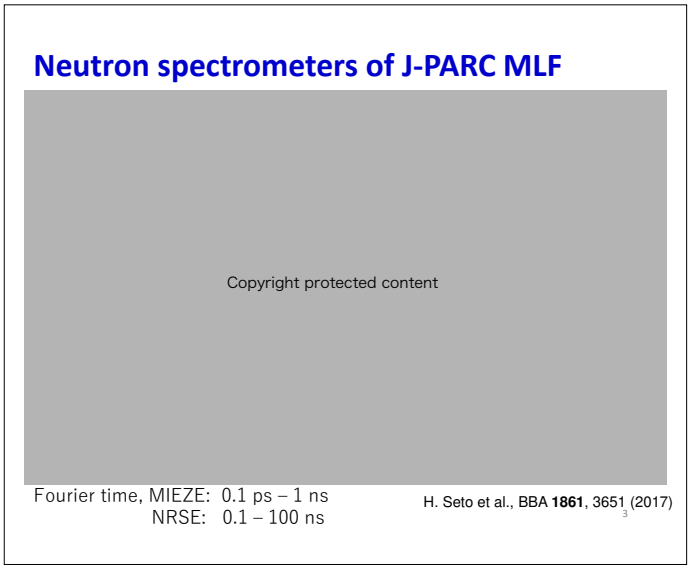

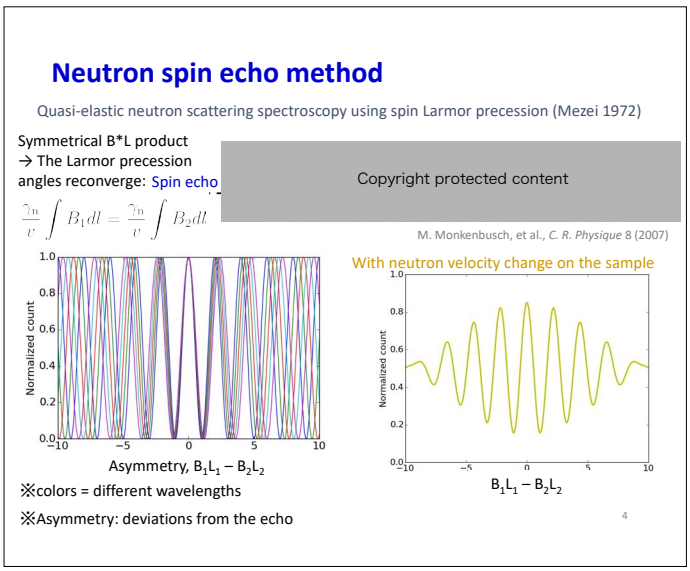

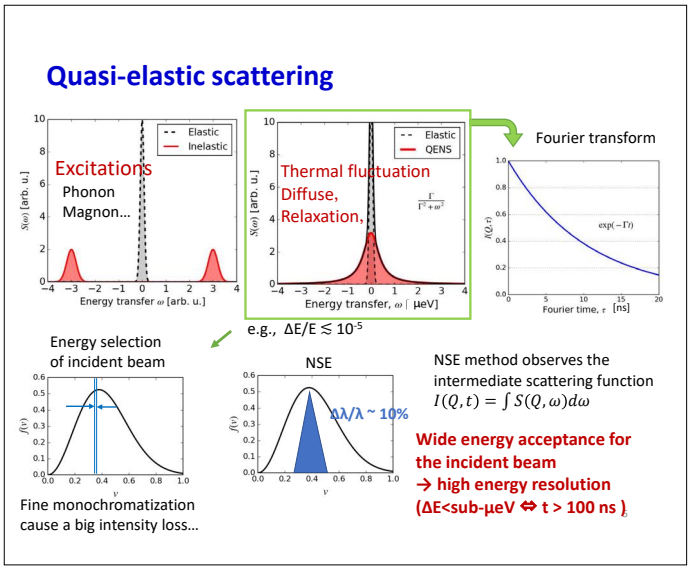

Village of neutron resonance spin echo spectrometers (VIN ROSE)

Copyright protected content

- NRSE (Neutron resonance spin echo)

  Aim for high energy resolution (～100 ns)

- MIEZE
  (Modulation of intensity with zero effort)

  Study of magnetic dynamics under a high magnetic field

Copyright protected content

NRSE: R. Gähler and R. Golub, Z. Phys. B **65**, 269-273 (1987)
MIEZE: R. Gähler et al., Physica B 180&181, 899-902 (1992)

MIEZE-type spin echo spectroscopy

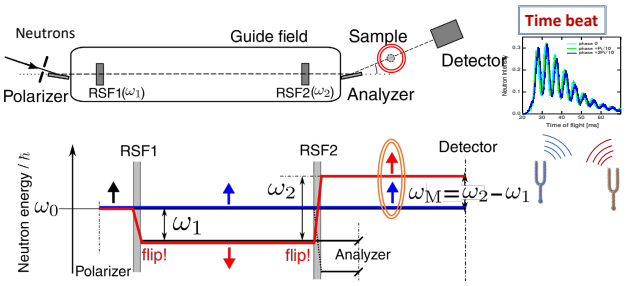

Quantum superposed state with different energies
→ **time beat of neutron intensity**

MIEZE: R. Gähler et al., Physica B 180&181, 899-902 (1992)
Features of TOF-MIEZE: T. Oda et al., Phys. Rev. Applied **14**, 054032 (2020)

8

Features of MIEZE-type spin echo

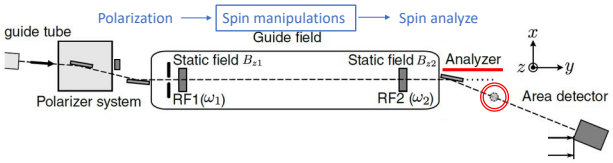

1. **The incident neutrons to the sample are in spin-up state only.**
   => The echo signal is robust to the magnetic field.
2. **Additional spin analyzer is applicable after the sample**

⇩

Suitable for the study of spin dynamics

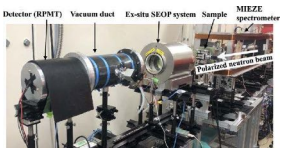

Test of ^{3}He spin filter as the 2nd analyzer
T. Okudaira et al., Nucl. Instrum. Methods A 977, 164301 (2020)

Towards wide dynamic range

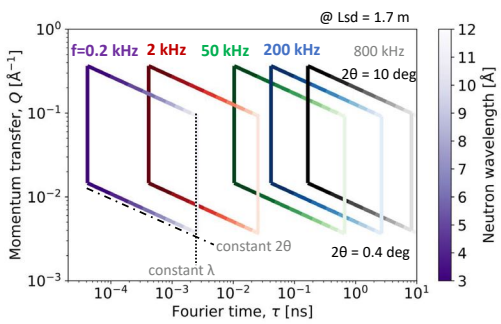

* Fast dynamics region (< sub ps) need fast neutrons such that δv << v

10

Recent application of MIEZE spin echo spectroscopy

Magnetic Skyrmion

Copyright protected content

Muhlbauer *et al.*, Science **323**, 915 (2009)

Copyright protected content

MIEZE spectroscopy by continuous beam

Kindervater et al., Phys. Rev. X **9**, 041059 (2019)

MIEZE spin echo measurement with cryostat and magnetic field at BL06

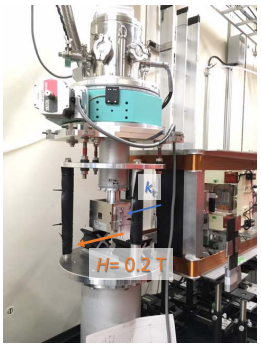

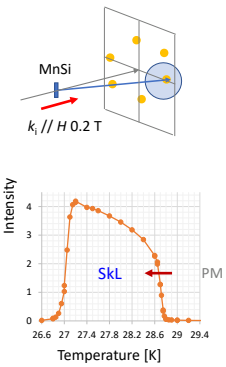

PI: T. Nakajima (ISSP, Univ. Tokyo)

12

Spin dynamics at phase boundary of Skyrmion phase

Copyright protected content

Analysis of dynamical information, I (Q,t) in resolved Qx-Qy space

Nakajima, et al., Phys. Rev. Res. **2**, 043393 (2020)

13

Acknowledgements

- KEK IMSS Neutron Scattering Program Advisory Committee Proposals No. 2019S07, No. 2014S07, No. 2009S07
- Program of the Development of System and Technology for Advanced Measurement Analysis (SENTAN), JST
- The Photon and Quantum Basic Research Coordinated Development Program, MEXT Japan
- JSPS KAKENHI Grants No. 19K20601 and No. 19H01856.

14

4.2.3 A. Sunaga（Kyoto Univ.）

Theoretical study of the linearity of uranyl molecule based on relativistic correlation method

京都大学

京都大学複合原子力科学研究所

Theoretical study of the linearity of uranyl molecule based on relativistic correlation method

Ayaki Sunaga

Institute for Integrated Radiation and Nuclear Science, Kyoto University

1/12

Background

Orbital energy (a.u.)

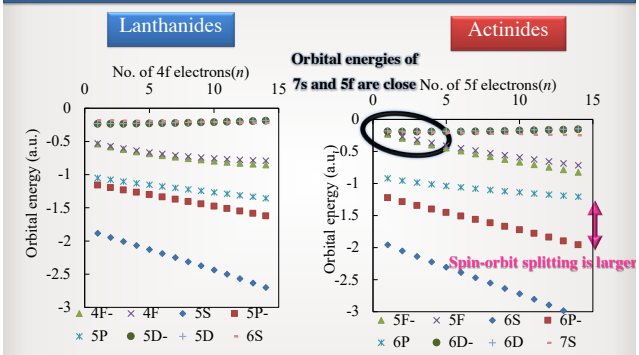

Method：4c-mutli component SCF/Numerical basis set; configuration：$4f^n5d^1 6s^2$, or $5f^n6d^1 7s^2$

2/12

Background

Orbital radius <r> (a.u.)

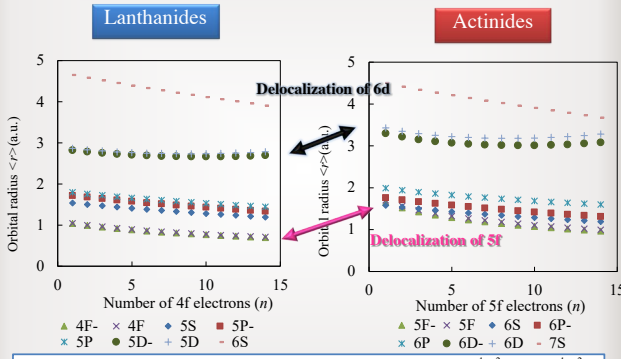

Method：4c-mutli component SCF/Numerical basis set; configuration：$4f^n5d^1 6s^2$, or $5f^n6d^1 7s^2$

3/12

Previous work

Electronic structure of actinide compounds

- **Review on oxides (AnO, AnO_2 and cations)**
  "Quantum Chemical Calculations and Experimental Investigations of Molecular Actinide Oxides"[1]
- **Ground state of uranium dioxide (UO_2) [1]**
  Initial calculation：$^3S_g^-$[2], ^3H_g[3]
  Recent calculation：$^3F_{2u}$(4c-CI [4], 4c-MRCC[5])
- **Derivatives of UO_2^{2+} and their properties**
  Gibbs free energy of $UO_2^{2+}(H_2O)_n^{2+}$ [6]
  Electronic population of $UO_2(NO_3)^+ \cdot (H_2O)$ [7]

[1] A. Kovács, R. J. M. Konings, J. K. Gibson, I. Infante, and L. Gagliardi, Chem. Rev. **115**, 1725 (2015).
[2] J. H. Wood, M. Boring, and S. B. Woodruff, J. Chem. Phys. **74**, 5225 (1981).
[3] G. C. Allen, E. J. Baerends, P. Vernooijs, J. M. Dyke, A. M. Ellis, M. Fehér, and A. Morris, J. Chem. Phys. **89**, 5363 (1988).
[4] T. Fleig, H. J. A. Jensen, J. Olsen, and L. Visscher, J. Chem. Phys. **124**, (2006).
[5] F. Real, A. S. P. Gomes, L. Visscher, V. Vallete, and E. Eliav, J. Phys. Chem. A **113**, 12504 (2009).
[6] S. Tsushima, T. Yang, and A. Suzuki, Chem. Phys. Lett. **334**, 365 (2001).
[7] M. Hirata, R. Sekine, J. Onoe, H. Nakamatsu, T. Mukoyama, K. Takeuchi, and S. Tachimori, J. Alloys Compd. 271, **128** (1998).

4/12

Previous work 1/2

Linearity of UO_2^{2+}

[1]

[1]

- ✓ From Figure 2, **the potential favors the linear form** by adding the 6p orbital [1].
- ✓ From Figure 3, σ_u^+ orbital is stabilized mainly by 5f orbital [1]

Which is more stabilized, $b_1 + a_1$ in the bend one, or $\sigma_u^+ + \sigma_g^+$ in the linear one?

[1] K. Tatsumi and R. Hoffmann, Inorg. Chem. **19**, 2656 (1980).

5/12

Previous work 2/2

Linearity of UO_2^{2+}

- ✓ As the molecule becomes bend (from 180° to 120°), the **MO #10** is destabilized. (Finally the destabilization is 0.9 eV)
- ✓ The ratio of 6p(U)-2p(O) anti-bonding π orbitals is increased by the bend structure.

Some orbitals look stabilized in the bend structure…

[1] P. Pyykkö and L. L. Lohr, Inorg. Chem. **20**, 1950 (1981).
[2] P. Pyykko and L. Laaksonen, J. Phys. Chem. **88**, 4892 (1984).

6/12

Objective

Analysis of the linearity of UO_2^{2+}
based on the relativistic quantum chemical calculations

i) Clarification of the origin of the linearity of the UO_2^{2+} by calculating the various structures of UO_2^{2+}

ii) Clarification of the contributions from the atomic orbitals of U and O to the molecular orbitals of UO_2^{2+}

7/12

Result

Molecular orbital energy of UO_2^{2+}

✓ Total electron of UO_2^{2+} : 106
Orb. 53 (HOMO)…Elec. 105,106
Orb. 52 (HOMO-1)…Elec. 103,104
✓ The O=U=O angle is changed from 90° to 180°

Relativistic effect: exact two-component;
Method: Hartree-Fock; Basis set: dyall.2zp

The result has been unpublished

8/12

Result

Orbital energy at 120 and 180 degrees

From the comparison between the sums of the orbital energies (from #53 to #43),

The result has been unpublished

9/12

Result

Comparison between H_2O and UO_2^{+2}

The result has been unpublished

10/12

Result

Contribution of correlation effects

The result has been unpublished

Relativistic effect:
DCG-X2Cmmf
Method: CCSD(T)
Basis set: dyall.cv3z

11/12

Conclusion

◆Linearity of UO_2^{2+} has been clarified?

The result has been unpublished

[1] P. Pyykkö and L. L. Lohr, Inorg. Chem. **20**, 1950 (1981).
[2] P. Pyykko and L. Laaksonen, J. Phys. Chem. **88**, 4892 (1984).

12/12

4.2.4 M. Nogami（Kindai Univ.）

Change in precipitation ability of treated cyclic urea compounds for selective precipitation of U(VI) species

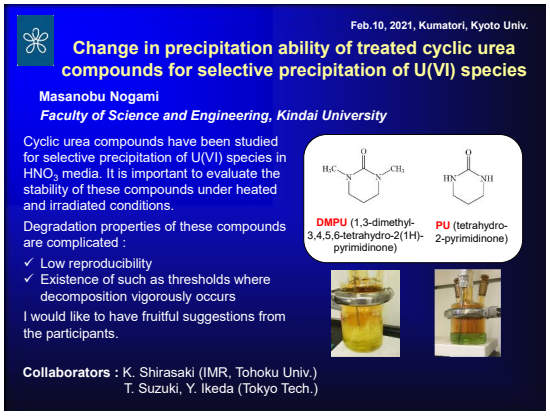

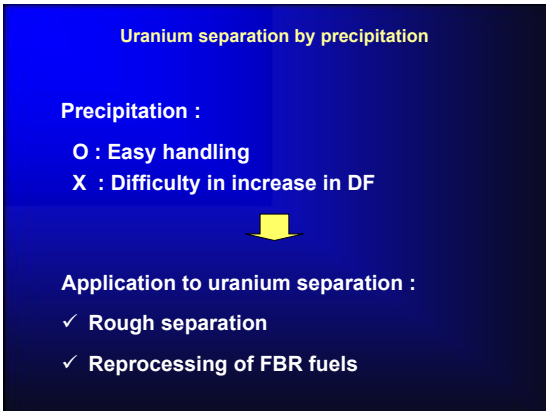

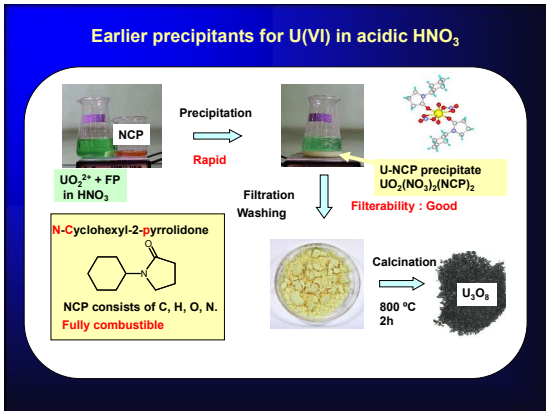

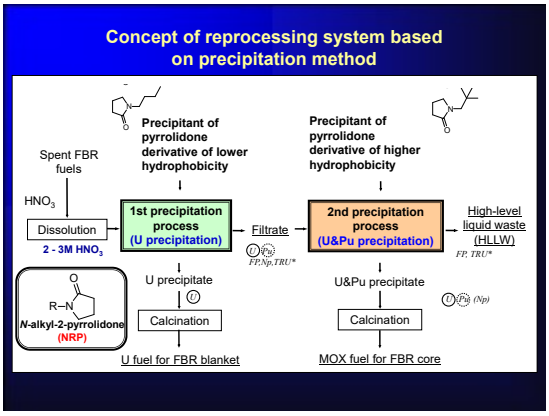

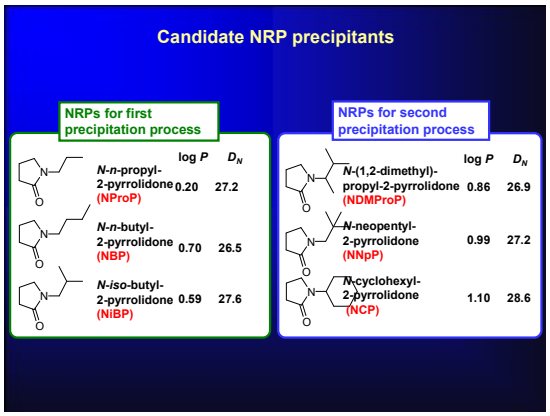

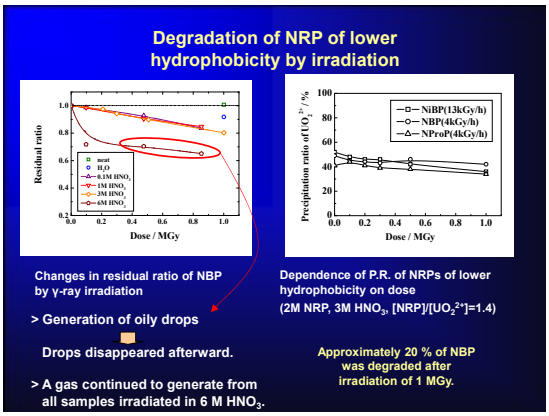

Degradation of NRP of higher hydrophobicity by irradiation

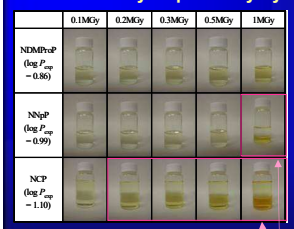

Appearance of irradiated samples (13kGy/h, R.T. : 2M NRP, 3M HNO_3)

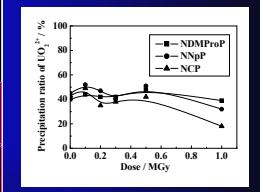

Dependence of P.R. of NRPs of higher hydrophobicity on dose (2M NRP, 3M HNO_3, $[NRP]/[UO_2^{2+}]$=1.4)

Split into 2 phases

Expected major degraded mechanism of NBP

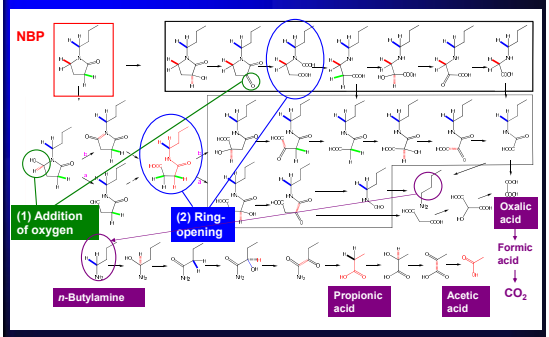

Urea compounds for selective precipitation of U(VI) in HNO_3

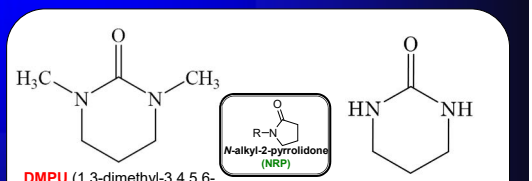

DMPU (1,3-dimethyl-3,4,5,6-tetrahydro-2(1H)-pyrimidinone)

PU (tetrahydro-2-pyrimidinone)

Comparison of urea compounds with NRP :

O : Expectation of higher selectivity to U(VI) than Pu(IV)

X : Less chemical stability

Stability experiments

Heating experiments

- Test solutions : HNO_3 containing 0.5 M (=mol/dm³) DMPU or PU
- HNO_3 conc. : max. 8 M
- Heating time : 360 min
- Heating temp. : 90 °C

γ–Ray irradiation experiments

- Test solutions : HNO_3 containing 0.5 M DMPU or PU
- HNO_3 conc. : 3, 4 M
- Irradiation source : ^{60}Co
- Irradiation time : ca. 140 h
- Dose : max. ca. 0.63 MGy

Evaluation of residual ratio by ^1H NMR

Utilization of change in area of each signal to that of standard material for evaluation of residual ratio

Solvent : D_2O
Standard material : Formic acid

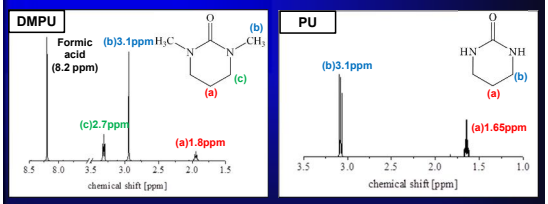

^1H NMR spectra of DMPU (left) and PU (right)

Appearance of sample solution of heated DMPU

- 1 M HNO_3 : kept colorless transparent
- 2 M HNO_3 : turned pink (after 90 min) and pale yellow (after 360 min)
- 4 M HNO_3 : generated vigorous NOx gas with turning yellow

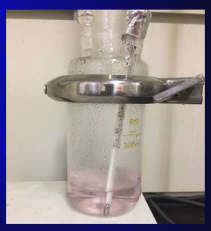

Appearance of sample solution of heated DMPU

- 1 M HNO_3 :
  kept colorless transparent
- 2 M HNO_3 :
  turned pink (after 90 min)
  and pale yellow (after 360 min)
- 4 M HNO_3 :
  generated vigorous NOx gas
  with turning yellow

Appearance of sample solution of heated DMPU

- 1 M HNO_3 :
  kept colorless transparent
- 2 M HNO_3 :
  turned pink (after 90 min)
  and pale yellow (after 360 min)
- 4 M HNO_3 :
  generated vigorous NOx gas
  with turning yellow

Appearance of sample solution of heated PU

- 1 to 6 M HNO_3 :
  kept colorless transparent
- 8 M HNO_3 :
  turned pale yellow
  (after 120 min)
  and generated vigorous
  NOx gas with turning green
  (after 330 min)

Appearance of sample solution of heated PU

- 1 to 6 M HNO_3 :
  kept colorless transparent
- 8 M HNO_3 :
  turned pale yellow
  (after 120 min)
  and generated vigorous
  NOx gas with turning green
  (after 330 min)

Changes in residual ratio depending on heating time

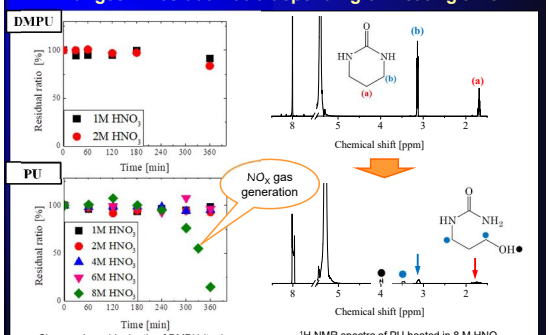

Changes in residual ratio of DMPU (top) and PU (bottom) versus time

^{1}H NMR spectra of PU heated in 8 M HNO_3 for 0 min (top) and 360 min (bottom)

Appearance of irradiated sample solutions

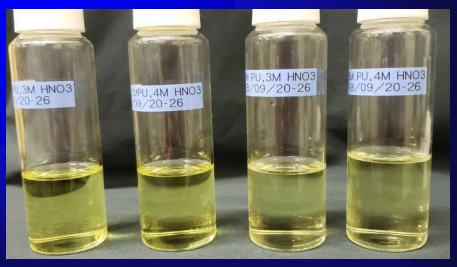

DMPU, 3M HNO_3 DMPU, 4M HNO_3 PU, 3M HNO_3 PU, 4M HNO_3

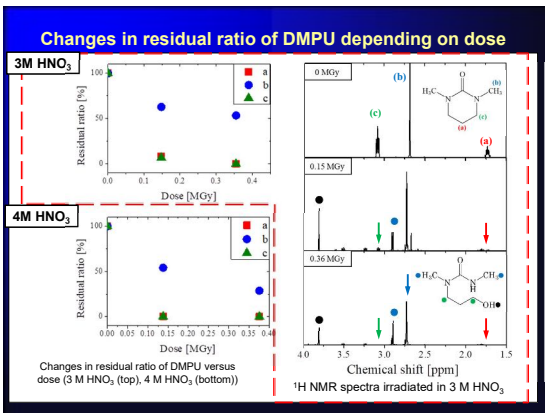

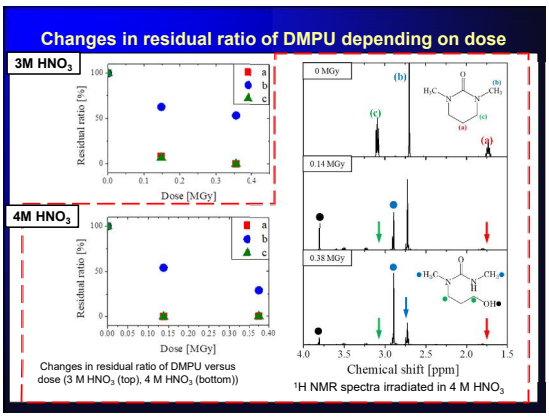

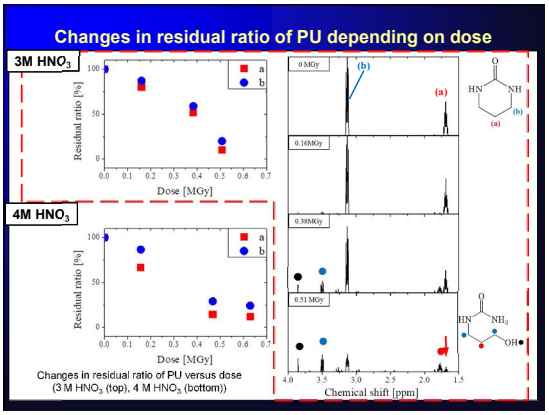

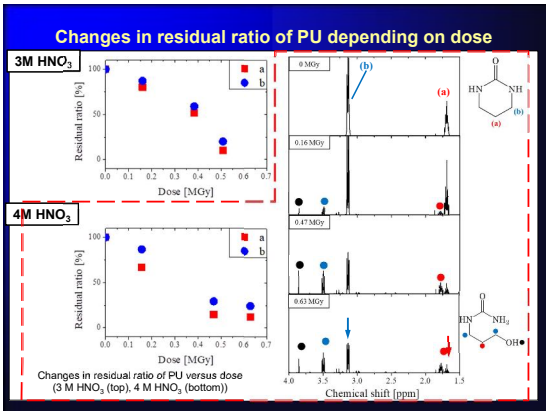

Precipitation experiments

Precipitant sample

1. Neat DMPU and PU
2. Heated or irradiated DMPU
3. Irradiated PU

Solutions of U(VI) and FP ions

FP ions

Zr(IV), Nd(III), Mo(VI), Fe(III), Re(VII), Pd(II)

Mixing at 1 (v/v)

Measurement of metal ion concentration of supernatant by ICP-OES

- R.T.
- HNO_3 conc. : 3, 4 M
- Precipitant conc. : 0.5 M each
- Metal ion conc. : U(VI) 0.5 M, FP 2 mM each
- Mixing time : U(VI) 1 h, FP 0.5 h

Evaluation of precipitation ratio (*P. R.*)

$$P.R. = \frac{M_{ini} - M_{sup}}{M_{ini}} \times 100\ [\%]$$

M_{ini} : Initial conc. of metal ion
M_{sup} : Metal ion conc. of supernatant

Change in P.R. of treated precipitants

		P.R. [%]													
		Zr(IV)		Nd(III)		Mo(VI)		Fe(III)		Re(VII)		Pd(II)		U(VI)	
	HNO_3 conc.	3M	4M	3M	4M	3M	4M	3M	4M	3M	4M	3M	4M	3M	4M
DMPU	Neat	~ 0	6.8	~ 0	~ 0	~ 0	~ 0	~ 0	~ 0	~ 0	~ 0	18.2	8.8	44.0	30.6
	Heated	~ 0	~ 0	2.7	~ 0	~ 0	2.0	~ 0	0.2	1.4	0.4	10.5	12.0	6.3	8.1
	Irradiated	2.3	~ 0	~ 0	~ 0	1.8	~ 0	0.2	~ 0	~ 0	~ 0	18.1	18.1	6.6	6.8
PU	Neat	~ 0	1.9	~ 0	~ 0	~ 0	~ 0	7.9	3.3	2.6	0.0	0.8	~ 0	~ 0	5.1
	Irradiated	2.7	~ 0	~ 0	4.6	~ 0	~ 0	~ 0	0.2	~ 0	~ 0	17.6	25.8	2.0	3.1

- Precipitate was not observed for samples of P.R. < 10 %.
- P.R. of treated DMPU for U(VI) were decreased.
- For PU, U(VI) precipitate was observed only for neat samples after mixing for ca. 12 h.

Change in P.R. of treated precipitants

		P.R. [%]													
		Zr(IV)		Nd(III)		Mo(VI)		Fe(III)		Re(VII)		Pd(II)		U(VI)	
	HNO_3 conc.	3M	4M	3M	4M	3M	4M	3M	4M	3M	4M	3M	4M	3M	4M
DMPU	Neat	~ 0	6.8	~ 0	~ 0	~ 0	~ 0	~ 0	~ 0	~ 0	~ 0	18.2	8.8	44.0	30.6
	Heated	~ 0	~ 0	2.7	~ 0	~ 0	2.0	~ 0	0.2	1.4	0.4	10.5	12.0	6.3	8.1
	Irradiated	2.3	~ 0	~ 0	~ 0	1.8	~ 0	0.2	~ 0	~ 0	~ 0	18.1	18.1	6.6	6.8
PU	Neat	~ 0	1.9	~ 0	~ 0	~ 0	~ 0	7.9	3.3	2.6	0.0	0.8	~ 0	~ 0	5.1
	Irradiated	2.7	~ 0	~ 0	4.6	~ 0	~ 0	~ 0	0.2	~ 0	~ 0	17.6	25.8	2.0	3.1

- Precipitate was not observed for samples of P.R. < 10 %.
- P.R. of treated DMPU for U(VI) were decreased.
- For PU, U(VI) precipitate was observed only for neat samples after mixing for ca. 12 h.

Conclusions

Stability

- PU was found more stable than DMPU.
- Both precipitants seem to have thresholds where decomposition vigorously occurs during heating.

Expected applicable solution conditions	DMPU : HNO_3 conc. max. 2 M PU : max. 6 M

Precipitation ability

- P.R. of treated DMPU and PU for U(VI) were decreased to extent that no U(VI) precipitates were observed.
- Precipitation ability of treated DMPU for U(VI) was found higher than that of PU.

4.2.5 Y. Homma（Tohoku Univ.）

Mossbaure spectroscopy of the Eu-based skyrmion compounds EuPtSi and $EuAl_4$

Topical meeting on Condensed-matter Chemistry on Actinides:
The Kumatori meeting 2021 (Online)

Mössbauer Spectroscopy of Eu-based Skyrmion Compounds EuPtSi and $EuAl_4$

IMR, Tohoku University
Yoshiya HOMMA

Research

Collaborator

A. Nakamura[1], M. Kakihana[2,3], Y. Tokunaga[4], Y. Shimizu[1], D.X. Li[1], A. Maurya[1], Y.J. Sato[6],1, F. Honda[1], D. Aoki[1], M. Hedo[5], T. Nakama[5], Y. Ōnuki[5,7]

[1]IMR, Tohoku Univ., [2]Grad. School Eng. & Sci., Univ. Ryukyus, [3]Acrorad Co. Ltd., [4]ASR, JAEA, [5]Fac. Sci., Uni. Ryukyus, [6]Grad. School Eng., Tohoku Univ., [7]CEMS, RIKEN

Research　University of the Ryukyus　ASR　RIKEN

① A-Phase induced by magnetic field

Dzyalosinkii-Morita Interaction

➡Magnetic skyrmion in f-electron system

Copyright protected content

Copyright protected content

Copyright protected content

S. Mühlbauer *et al.* Science. **323**, 915 (2009)

M. Kakihana *et.al*, *J. PSJ*, **87**, 023701 (2018)

M. Kakihana *et.al*, *J. PSJ*, **88**, 094705 (2019)
T. Takeuchi *et.al*, *J. PSJ*, **88**, 053703 (2019)

EuPtSi
Stable A-Phase
in wide temperature range

② 1st Order Transition at T_N=4 K EuPtSi with trillium lattice

Antiferromagnetic (helimagnetic) transition at T_N=4 K
First-order-like

Copyright protected content

Sharp Peak at 4 K

Kakihana, Onuki *et.al*, *J. Elec. Mater*, 46, 3572 (2017)

M. Kakihana *et.al*, *J. PSJ*, **87**, 023701 (2018)

Hysteresis at around 4 K

Sakakibara, Nakamura *et al.* JPSJ 88, 093701(2019)

Reach to R*ln*8 at 15～20K

D.G. Franco et al. PRB 96 014401 (2017)

EuPtSi → 4Kで不完全な1次転移

③ Connected Triangles in the Trillium lattice

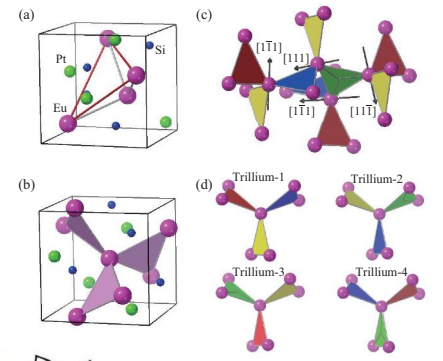

- B20型立方晶 $P2_13$(#198)
- 2-fold screw:[100]
- lost 4-fold rotation
- 3-fold rotation C_3 [111]

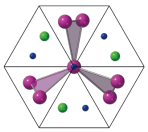

- 4 sites

トリリウム格子 → 単純にして複雑

Monte-Carlo simulation of FM ising model for Eu Trillium lattice

T.E Redpath & J.M. Hopkinson
Phys. Rev. B ***82****, 014410 (2010)*

Trillium lattice

Ontario Trillium Foundation

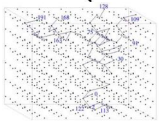

Spin-Ice

Specific heat of trillium spin lattice
Soft peak with broad Tail

Copyright protected content

Inverse magnetic susceptibility
Deviation from C-W law

Copyright protected content

^{151}Eu Mössbauer Spectroscopy

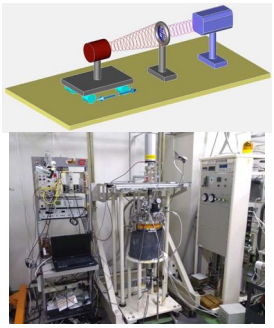

Transmission
^{151}Sm source 3.7GBq
Vel. Calib ; Laser Interferometer
Source Temp. ; keen at 4 – 5 K
Crushed Powder from single crystal

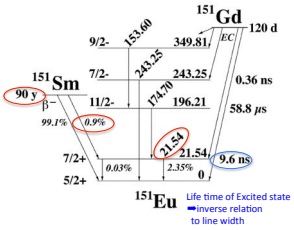

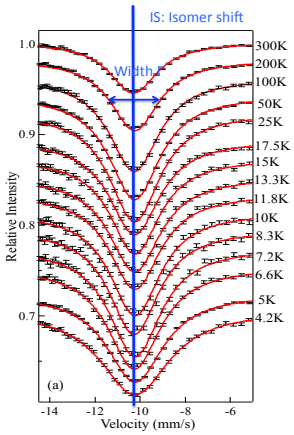

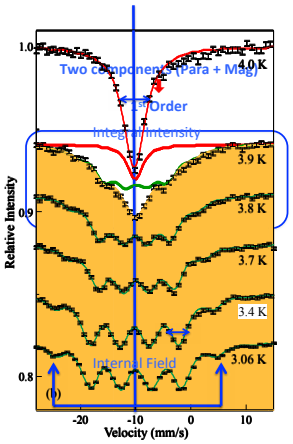

Hyperfine Field at Eu sites

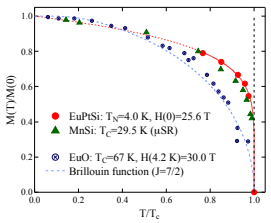

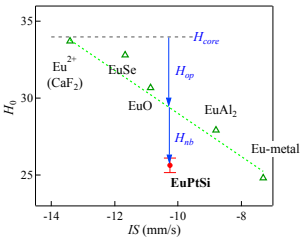

$H_0 = H_{core} + H_{op} + H_{nb} = 25.6 \pm 0.4$ T

as $H_{core} = 34$ T (for localized Eu^{2+} with $7\mu_B$)

Alloying effect : $H_{op} = -4.6 \pm 0.8$ T

Coordination effect : $H_{nb} = -3.8 \pm 0.8$ T

Temperature dependence of the intensity of Mössbauer spectra and specific heat

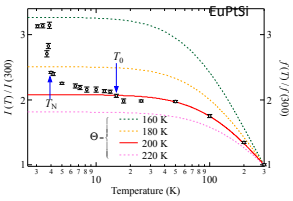

Recoilless fraction

$$I \propto f(T)$$

$$= \exp\left[-\frac{3E_R}{2k_B\Theta}\left\{1+4\left(\frac{T}{\Theta}\right)^2\int_0^{\Theta/T}\frac{x}{e^x-1}dx\right\}\right]$$

$$E_R = 1.6151\times10^{-3}\,\text{eV}$$

Copyright protected content

Debye phonon

$$C_{ph} = 9Nk_B\left(\frac{T}{\Theta}\right)\int_0^{\Theta/T}\frac{x^4e^x}{(e^x-1)^2}dx$$

Line Width Γ reflecting Magnetic fluctuation

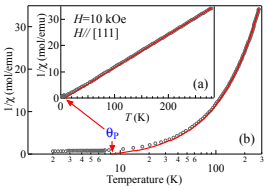

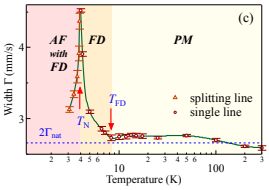

Induced below 8K

Remaining magnetic fluctuation Below T_N<4K ?

Relaxation rate Observed by μSR

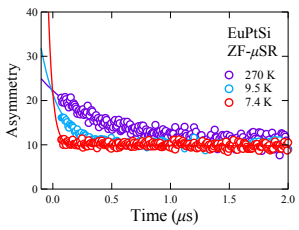

$A(t) = A0\exp(\lambda(t-T0)) + C$

The relaxation rate

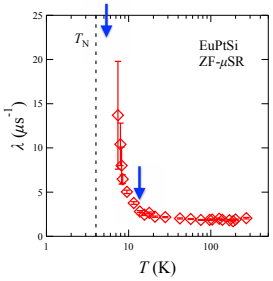

Enhancement of relaxation ratebelow 15 K

Diverged below 9 K

Fluctuation-induced first-order
Brazovskii Theory
Precursor of the helical magnetic order

Copyright protected content

M. Janoschek et al.
PRB 87 134407 (2013)

T^*: Precursor of 1-st order (Vollhardt Invariance) $T^* \sim T_C + 1$

T_{MF}: based on Mean field (Weiss temperature) $T_{MF} \sim q_p$

FD (Fluctuation Disorder)
IM (Intermediate)
SRO (Short range order)

Copyright protected content

Bauer & C. Pfleiderer
PRB 85 214418 (2017)

MnSi (Pfleiderer's group of TUM)

Fluctuation-induced first-order transition is realized between PM and HM

"DM-HM is at the heart of problems such as topological magnetic order"

Brazovskii Theory For liquid crystal

The "blue phase" between a chiral cholesteric phase & anisotropic phase

Copyright protected content

S.Meiboom et al.
Phys. Rev. Lett. 46, 1216 (1981).

Dispute about the Fluctuation induced 1st order

Neutron diffraction of MnSi under magnetic field
Incoinsidence of the magnetic field point between 1st order & magnetic fluctuation

C. Pappas *et al.*
PRL **119**, 047203 (2017)

Thermal expansion of MnSi under magnetic field
Non-observation of tricrutical point

A.E. Petrova & S. M. Stishov
PRB **94**, 020410(R) (2016)

We need
Mössbauer spectroscopy
under magnetic field

Thermal stability of A-phase and FD-phase

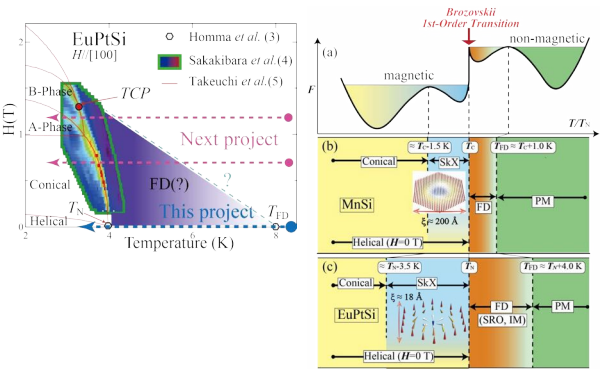

centrosymmetric tetragonal structure Of $EuAl_4$

Copyright protected content

A. Nakamura *et al.* J. Phys. Soc. Jpn. 84 (2015), 124711.

Successive four transitions and anomalous resistivity of $EuAl_4$

Copyright protected content

T. Shang *et al.* Phys. Rev. B103 (2020), L020405.

Mössbauer Spectra of $EuGa_4$

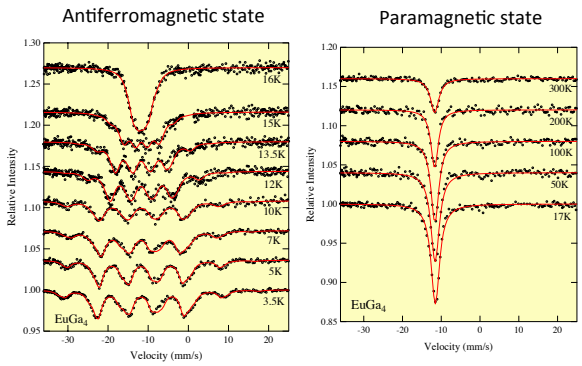

Mössbauer Spectra of $EuAl_4$

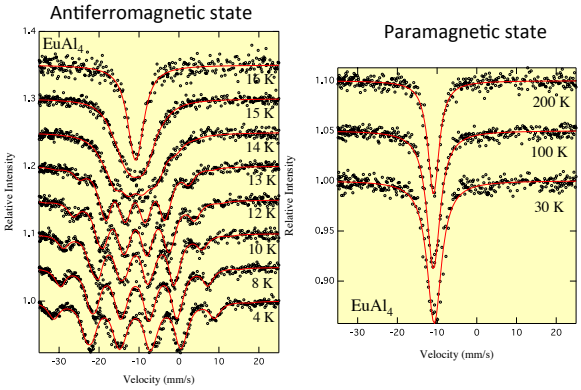

Hyperfine Fields of EuGa4 & EuAl4

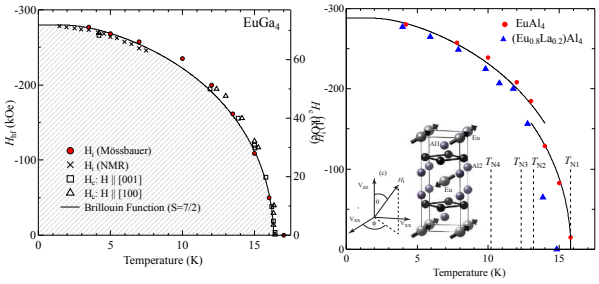

Magnetic structure of EuX_4

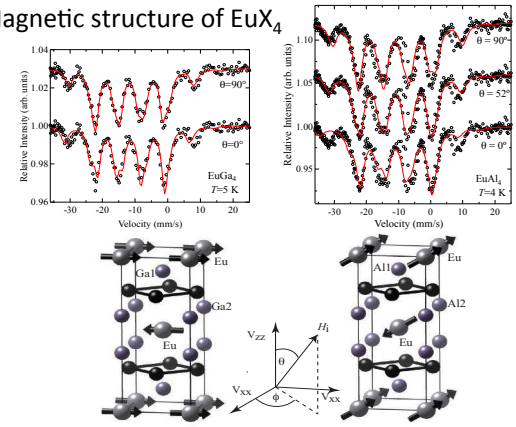

4.2.6 K. Nagata（Osaka Univ.）

Synthesis of Actinium Complex with a Macrocycle Having Pyridine Phosphonate Pendant Arms

Synthesis of Actinium Complex with a Macrocycle Having Pyridine Phosphonate Pendant Arms

Kojiro Nagata,[1] Kazuaki Baba,[1] Atsushi Toyoshima,[2] Tatsuo Yajima,[3] Takashi Yoshimura[1]

[1]RadioIsotope research Center, Institute for Radiation sciences, Osaka University
[2]Division of Science, Institute for Radiation sciences, Osaka University
[3]Faculty of Chemistry, Materials and Bioengineering, Kansai University

- In the field of nuclear medicine, the development of a new chelator suitable for stabilizing actinides and lanthanides complex is important for drug discovery.

- We succeeded in the synthesis of a novel macrocycle chelator, macropp, H_4L, and the La complex with the ligand. It was characterized by ^1H NMR spectra, IR spectra and X-ray analysis.

- The crystal structure of $[LaHL(H_2O)]$ shows the coordination site of La^{3+} are occupied by HL^{3-} and H_2O as displayed in Fig. 1.

- The stability constant of the La complex was determined in 0.1 M KNO_3(aq.) by means of potentiometric titration. The obtained K_{ML} value is 11.2 M^{-1}.

- In higher concentration of [L] = 10^{-6} M, quantitative radiolabeling of H_4L with ^{225}Ac (Radiolabeling Chemical Yield > 95%) was achieved under ambient conditions as shown in Fig. 2.

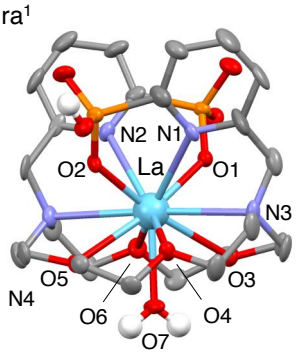

Fig.1. Crystal structure of $[LaHL(H_2O)]$

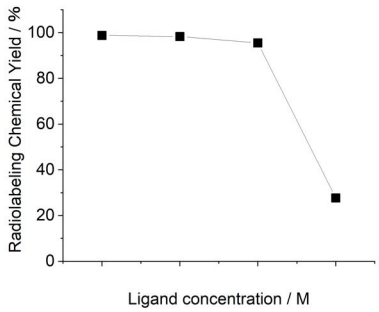

Fig. 2. Radiolabeling of H_4L with $^{225}Ac^{3+}$

4.2.7 T. Yamane（Nagaoka Univ. Tech.）

Electrochemical method of minor actinide recovery from nitric acid solution using Ga liquid electrode and ionic liquid

Topical meeting on Condensed-matter Chemistry on Actinides, Feb.10, 2021

Electrochemical method of minor actinide recovery from nitric acid solution using Ga liquid electrode and ionic liquid

Tomoya Yamane[1], Tatsuya Suzuki[1], Chikage Abe[2], Kenji Konashi[2]
[1] Nagaoka University of Technology , [2] Tohoku University

Break Session 2
16:00 – 17:00

Introduction 1

Currently, spent fuel is reprocessed by PUREX method.
The minor actinides(MA) and fission products(FP) removed by PUREX method

It is being considered for geological disposal by vitrifying it as high-level radioactive waste (HLW).

Wet reprocessing(PUREX method)

- ✓ The Purex method is one of the solvent extraction methods that uses a nitric acid solution as an aqueous solution and TBP as an extractant. The process of separating U and Pu by reducing Pu after simultaneous extraction of U and Pu.
- ✓ Since a large amount of water is used, the process becomes complicated and the amount of waste generated increases.

Introduction 2

Potential radiotoxicity of spent fuel

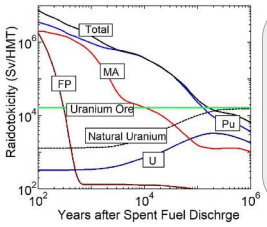

Spent fuel has a potential radiotoxicity, which continue approximately 100,000 years until this radiotoxicity reduce under natural level of original uranium ore.

This time is reduced to hundreds of years by removing MA from spent fuel.

- ✓ Separation of MA from lanthanides is difficult in the aqueous solution, because of the valence and ionic radii of MA and lanthanides.

Introduction 3

Dry reprocessing(Molten salt electrolysis method)

- ✓ One of the dry reprocessing techniques, can separate MA from lanthanides relatively easily.
- ✓ LiCl-KCL is used as the molten salt at high temperature and in an argon gas atmosphere, and the liquid Cd metal electrode is used as a cathode. MA is recovered in this Cd electrode with nuclear fuel materials.
- ✓ Molten salt is not easily deteriorated by radiation, so it can be applied to fuels with a short cooling period and fuels with high burnup.
- ✓ The operating temperature is high and the decontamination factor is low.

Research is being conducted using Ga as an alternative electrode material for Cd.

Introduction 4

In this study

Proposing a new MA recovery method that can be bonded to the PUREX method by taking advantage of the molten salt electrolysis method

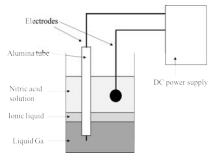

- ✓ The ionic liquids are used as molten salt, and the liquid Ga electrode is used as an electrode for MA recovery.
- ✓ The ionic liquid (BMIMPF6), was sandwiched between the liquid Ga electrode and the nitic acid solution.

A constant voltage is applied to recover MA, and the concentrations of Am and lanthanoids in the nitrate solution before and after the voltage application are measured using an inductively coupled plasma mass spectrometer (ICP-MS) and a Ge semiconductor detector.
→ Evaluate the separation performance of MA and lanthanoids

Experiment 5

Selection of electrode material

New MA recovery method proposed in this study

- ✓ It can be joined with the PUREX method by taking advantage of the molten salt electrolysis method.
- ✓ Operates at a much lower temperature (about 40~60℃) than the molten salt electrolysis method

【MA recovery electrode】
Adopt Ga, which is a low melting point metal, in consideration of the assumed temperature range (about 40~60℃).

【Counter electrode】
Select a material with high acid resistance to put it in a nitric acid solution.
Pt is used because it is chemically stable and has excellent heat resistance.

Experiment 6

Selection of ionic liquids

- ✓ Used as a molten salt in the process proposed in this study
- ✓ Prevents the reaction between nitric acid and Ga by sandwiching it between the nitric acid solution and liquid Ga.

Uses BMIMPF6, an ionic liquid that is hydrophobic and has a heavier specific gravity than water.

Preparation of cell

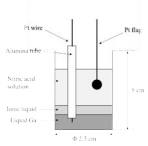

- ✓ Add liquid Ga, ionic liquid, and nitric acid solution to the sample vial.
- ✓ Connect Pt flag electrode to nitric acid solution and Pt wire to liquid Ga

Experiment 7

Cyclic voltammetry (CV) measurement

- ✓ Nitric acid solution(Concentration ：3 M)
  Dissolve Ce, Gd, Eu, Nd, Yb to 1000 ppm
- ✓ To make a cell and stabilize the solution temperature, leave it in a low temperature constant temperature bath (40.0℃) for 1 hour.
- ✓ Connect FUNCTION GENERATOR and POTENTIOSTAS / GALVANOSTAT to the cell.
- ✓ Uses Ag/AgCl electrode as reference electrode.
- ✓ Potential sweep：-2.5~1.5 V vs. Ag/AgCl,100 mV/s
- ✓ The CV of a nitric acid solution containing no rare earth elements is used as the background CV(BGCV).
- ✓ Comparison of CV of nitric acid solution in which rare earth elements are dissolved and BGCV

Experiment 8

Extraction test by applying constant voltage

- ✓ Nitric acid solution using only rare earth elements
  Concentration ：3 M
  Dissolve Ce, Gd, Eu, Nd, Yb to 1 ppm
- ✓ Nitric acid solution with Am
  Concentration ：3 M
  Dissolve Am-241 at 0.592 kBq and Eu-152 at 1.48 kBq

【Nitric acid solution using only rare earth elements】

- ✓ Make a cell and leave it in a low temperature constant temperature bath (40.0℃, 50.0℃, 60.0℃) for 1 hour.
- ✓ Connect DC power supply to cell
- ✓ Apply voltage of 2.5,2.2,1.9 V vs. CE (Application time :10,30 min)

【Nitric acid solution with Am】

- ✓ Make a cell and leave it in a low temperature constant temperature bath (40.0℃) for 1 hour.
- ✓ Connect DC power supply to cell
- ✓ Apply voltage of 2.5,2.2,1.9 V vs. CE (Application time :30 min)

Experiment 9

Extraction test by applying constant voltage

Measurement of MA and rare earth element concentrations in nitric acid solution before and after voltage application with ICP-MS and Ge semiconductor detectors.

Calculate the decrease rate(D) of rare earth element concentration from the measurement result of ICP-MS

$$D = \frac{\text{Rare earth element concentration in sampled nitric acid solution}}{\text{Rare earth element concentration in nitric acid solution before applying voltage}}$$

Calculate the following from the measurement results of the Ge semiconductor detector

- ✓ Ratio of Am and Eu counts(Am/Eu)
- ✓ Separation factor for nitric acid solution (Original HNO3) before voltage application(SF)
- ✓ Sample counts/Original HNO_3 counts ratio

$$SF = \frac{\text{Sample Am / Eu ratio}}{\text{Origimal } HNO_3 \text{Am / Eu ratio}}$$

Results and discussion 10

Extraction test by applying constant voltage(only rare earth elements)

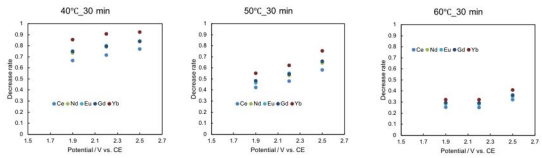

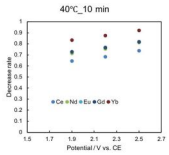

- ✓ There is almost no change in the decrease rate depending on the voltage application time.
- ✓ decrease rate decreases as the temperature of low temperature bath rises.

- ✓ Rare earth elements move to ionic liquids or liquid Ga by electrophoresis rather than redox reaction on the electrode surface.

Results and discussion 11

Extraction test by applying constant voltage(With Am)

Measurement result of Ge semiconductor detector

Sample	Counts 59.83 keV Am-241	Counts 121.98 keV Eu-152	Am/Eu	SF	Sample counts/Original HNO_3 counts 59.83 keV Am-241	Sample counts/Original HNO_3 counts 121.98 keV Eu-152
Original HNO_3	6817	9117	0.748	1.00	-	-
HNO_3 (2.5 V after)	6071	5513	1.10	1.47	0.891	0.605
HNO_3 (2.2 V after)	6224	5246	1.19	1.59	0.913	0.575
HNO_3 (1.9 V after)	6169	5425	1.14	1.52	0.905	0.595
Ionic liquid (2.5 V after)	157	782	0.201	0.269	-	-
Ionic liquid (2.2 V after)	164	1233	0.133	0.178	-	-
Ionic liquid (1.9 V after)	216	1554	0.139	0.186	-	-
Ga (After the experiment)	102	2149	0.047	0.063	-	-

- ✓ Sample counts/Original HNO_3 counts ratio does not change much due to the applied voltage
- ✓ Eu has a lower Sample counts/Original HNO_3 counts ratio than Am
  → Suggested that Eu is easier to move to ionic liquids or liquid Ga than Am
- ✓ Separation factor exceeds 1 for nitric acid solution and 1 or less for ionic liquid and liquid Ga
  → It is suggested that Am is difficult to move to ionic liquid or liquid Ga and remains on the nitric acid solution side.

Results and discussion 12

Extraction test by applying constant voltage(With Am)

Measurement result of Ge semiconductor detector

Sample	Counts		Am/Eu	SF	Sample counts/Original HNO_3 counts	
	59.83 keV Am-241	121.98 keV Eu-152			59.83 keV Am-241	121.98 keV Eu-152
Original HNO_3	6817	9117	0.748	1.00	-	-
HNO_3 (2.5 V after)	6071	5513	1.10	1.47	0.891	0.605
HNO_3 (2.2 V after)	6224	5246	1.19	1.59	0.913	0.575
HNO_3 (1.9 V after)	6169	5425	1.14	1.52	0.905	0.595
Ionic liquid (2.5 V after)	157	782	0.201	0.269	-	-
Ionic liquid (2.2 V after)	164	1233	0.133	0.178	-	-
Ionic liquid (1.9 V after)	216	1554	0.139	0.186	-	-
Ga (After the experiment)	102	2149	0.047	0.063	-	-

- ✓ The ratio of the mobility of Am and Eu calculated from the mass of Am and Eu is 1.26.
  → The maximum separation effect of Am and Eu due to mobility is 1.26.
- ✓ The separation factor of the nitric acid solution is greater than 1.26

It is suggested that the transfer of Eu from nitric acid solution to ionic liquid or liquid Ga has effects other than electrophoresis.

Results and discussion 13

Extraction test by applying constant voltage(With Am)

Measurement result of Ge semiconductor detector

Sample	Counts		Am/Eu	SF	Sample counts/Original HNO_3 counts	
	59.83 keV Am-241	121.98 keV Eu-152			59.83 keV Am-241	121.98 keV Eu-152
Original HNO_3	6817	9117	0.748	1.00	-	-
HNO_3 (2.5 V after)	6071	5513	1.10	1.47	0.891	0.605
HNO_3 (2.2 V after)	6224	5246	1.19	1.59	0.913	0.575
HNO_3 (1.9 V after)	6169	5425	1.14	1.52	0.905	0.595
Ionic liquid (2.5 V after)	157	782	0.201	0.269	-	-
Ionic liquid (2.2 V after)	164	1233	0.133	0.178	-	-
Ionic liquid (1.9 V after)	216	1554	0.139	0.186	-	-
Ga (After the experiment)	102	2149	0.047	0.063	-	-

- ✓ The ratio of the mobility of Eu and Am is 0.794.
- ✓ Separation factor of ionic liquid and Ga is smaller than 0.794
  → Suggested that Am does not move much to ionic liquids and liquid Ga

Assume that the γ-ray attenuation coefficient of Ga is 10 times different between 59.83 keV and 121.98 keV.
→ Since the separation factor is smaller than 0.794, it is suggested that Am does not move much to ionic liquid or liquid Ga.

Results and discussion 14

Cyclic voltammetry (CV) measurement

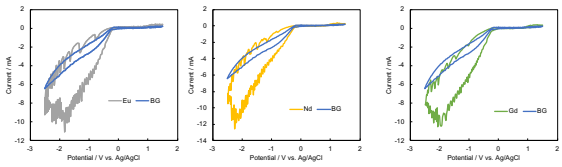

Eu,Nd,Gd
- ✓ The current larger than BG
- ✓ The current is maximum near -2 V vs. Ag/AgCl
- ✓ Suggested movement to the ionic liquid and liquid Ga side by applying voltage

The change in the current value is almost the same as the result of the decrease rate of rare earth elements in the constant voltage application test.

Results and discussion 15

Cyclic voltammetry (CV) measurement

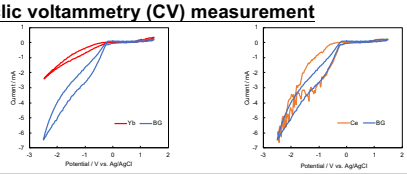

Yb
- ✓ The current is less than the BG
- ✓ Suggests less migration to ionic liquids and liquid Ga than other rare earth elements.

Ce
- ✓ Almost the same current as BG
- ✓ The change in current value differs from the result of the decrease rate of rare earth elements in the constant voltage application test.
  → Suggested by other reactions

Conclusion 16

- ✓ As a result of the constant voltage test, it was confirmed that MA was concentrated in the nitric acid solution and lanthanoid was concentrated in the Ga electrode.
- ✓ The change in the decrease rate of rare earth elements due to the applied voltage was slight, but the decrease rate of rare earth elements increased as the constant temperature bath temperature increased.
- ✓ As a result of CV measurement, no peak of redox current was observed, but the change in current value was almost in agreement with the result of the decrease rate of rare earth elements by the constant voltage application test.

4.2.8 M. Yokota（Kindai Univ.）

Adsorptivity of monoamide polymer adsorbent impregnated with PPTPT to metal ions in neutral aqueous solutions for recovery of uranium in seawater

Adsorptivity of monoamide polymer adsorbent impregnated with PPTPT to metal ions in neutral aqueous solutions for recovery of uranium in seawater

Kindai University

○Masayoshi YOKOTA, Masanobu NOGAMI, Kazuki HASHIMOTO , and Hiroki SATOU

Introduction(1)

- In Japan, light water reactors are used as commercial nuclear reactors, and uranium is used as fuel. However, uranium resources rely on imports from overseas.
- Uranium is dissolved in seawater. The concentration is quite low(3μg/dm^3), but the total amount reaches 4.5 billion tons ⇒About 1000 times as much as that of mine uranium resources.
- Adsorbents to recover uranium in seawater has not been put into practical use.

Introduction(2)

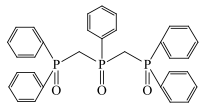

1,1,3,5,5-pentaphenyl-1,3,5-triphosphapentanetrioxide(PPTPT)

One of polyphosphine polyoxides

Adsorbent studied in our research group

Silicas-supported adsorbent impregnated with PPTPT

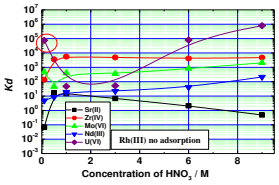

Adsorptivity of PPTPT adsorbent to various metal in HNO_3 solutions

M.Nogami, et al., *J. Radioanal. Nucl. Chem.*, 284, 195-199 (2010).

Unusual high selectivity for U(VI) in HNO_3 of very low concentrations.

It was expected from this property that the PPTPT adsorbent might be applied for uranium recovery from seawater.

Introduction(3)

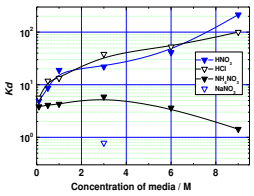

Adsorptivity of PPTPT to Nd(III) in media (5cm^3 / 0.25g-ads, 298K, 24h)

M.Nogami, et al., *J. Radioanal. Nucl. Chem.*, 284, 195-199 (2010)

PPTPT adsorbent has exhibited a low adsorptivity to U(VI).

Little salting-out effect, i.e., a poor wetting property of PPTPT.

Introduction(4)-earlier studies

PPTPT with selectivity for U(VI)

＋

Polar polymer support (RCSPO, AER)

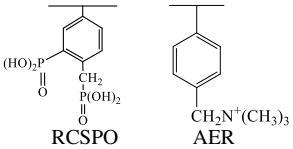

Adsorbents impregnated with PPTPT

Development of adsorbents with two characteristics

Monoamide compounds

- It has one amide bond in the structure.
- It is well-known to exhibit coordination to tetravalent and hexavalent actinide.

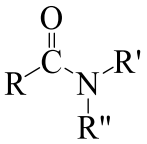

(R, R', R'' : hydrocarbon groups)

Structure of monoamides

Purpose

A silica-supported DMAA impregnated with PPTPT (PPTPT-DMAA) was newly prepared and the adsorptivity to various metal ions was investigated in neutral aqueous solutions.

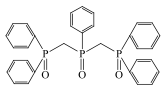

PPTPT

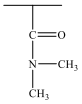

DMAA

Preparation of adsorbent

Silica supported DMAA adsorbent

DMAA
m/p-divinylbenzene(DVB)
m-xylene
heptane
1,1'-Azobis(cyclohexane-1-carbonitrile)(ACCN)
2,2'-Azobis(isobutyronitrile)(AIBN)
Porous silica

↓

Polymerization for about 17h (～90°C)

↓

Washing with water and aceton,and drying

↓

Silica supported DMAA resin

PPTPT-DMAA

PPTPT dissolved in CH_2Cl_2

＋

Impregnation in DMAA

↓

Removal of CH_2Cl_2 at 50°C

↓

Drying at 50°C

↓

PPTPT-DMAA

Adsorption experiments by batch method

Various metal ions in max 1.71M various aqueous solutions (10mM, 3cm³)

Resins (0.15g)

↓

Mixing and shaking(298K,24h)

↓

Measurement of concentration of metal ion in solution after contact (ICP-OES)

↓

Calculation of distribution coefficient (K_d)

Adsorptivity in NaCl solutions(1)

NaCl concentration in seawater

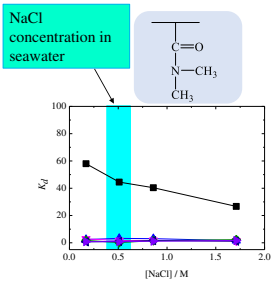

DMAA

Fe(III) was adsorbed.
The K_d values for Fe(III) decrease with increasing NaCl concentration.

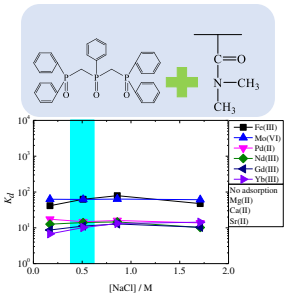

PPTPT-DMAA

Wetting property improved, judging from the appearance of the adsorbents.
It was expected that contribution of PPTPT to adsorption is distinguished.

Adsorptivity in NaCl solutions(2)

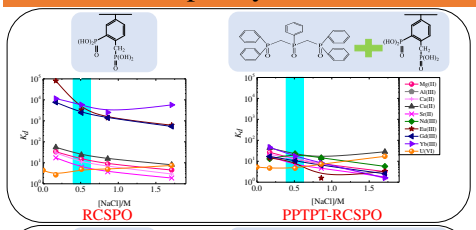

RCSPO　　PPTPT-RCSPO

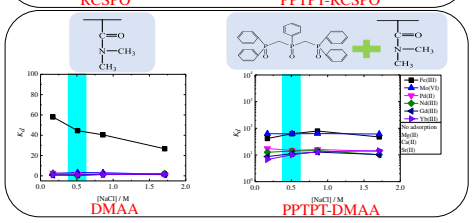

DMAA　　PPTPT-DMAA

PPTPT-RCSPO

- Impregnation of PPTPT reduced K_d values for trivalent metal ions.
- Dependency on NaCl concentration is similar compared with those of RCSPO.

PPTPT-DMAA

- Dependency on NaCl concentration is different compared with those of DMAA
- It is expected that DMAA take on a role bringing metal ions closer to PPTPT.

Adsorptivity in chloride solutions

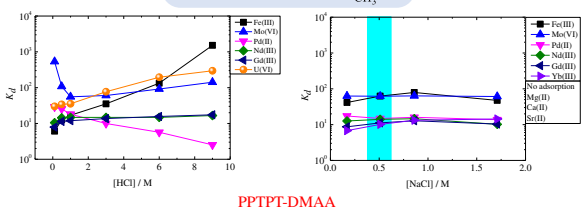

PPTPT-DMAA

U(VI) was absorbed and the K_d increase with increasing HCl concentration.
Fe(III) showed similar behavior.
It is expected that PPTPT-DMAA adsorps U(VI) in NaCl solution.

Adsorptivity in chloride solutions

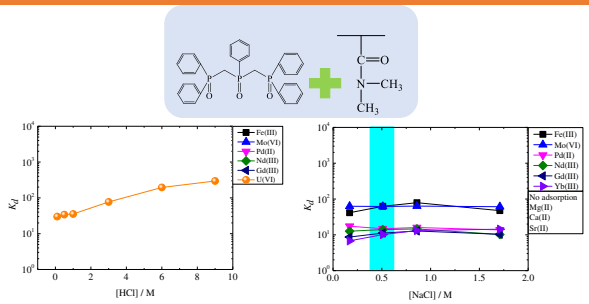

PPTPT-DMAA

U(VI) was absorbed and the K_d increase with increasing HCl concentration.
Fe(III) showed similar behavior.
It is expected that PPTPT-DMAA adsorps U(VI) in NaCl solution.

Adsorptivity in chloride solutions

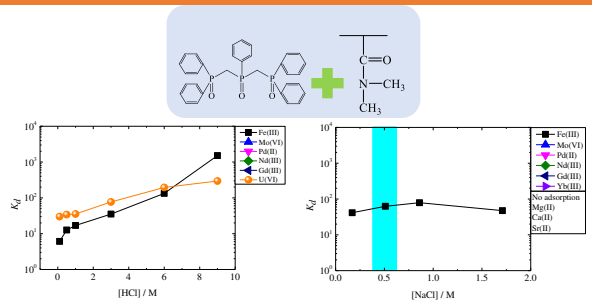

PPTPT-DMAA

U(VI) was absorbed and the K_d increase with increasing HCl concentration.
Fe(III) showed similar behavior.
It is expected that PPTPT-DMAA adsorps U(VI) in NaCl solution.

Adsorptivity in $NaNO_3$ solutions

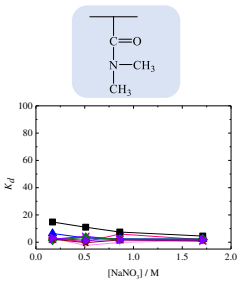

DMAA

All metal ions was not adsorbed.

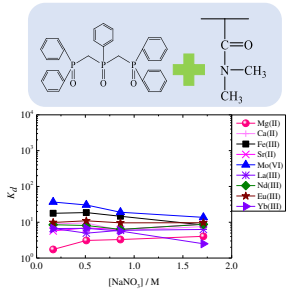

PPTPT-DMAA

Wetting property improved, judging from the appearance of the adsorbents. It was expected that contribution of PPTPT to adsorption is distinguished.

Summary and future prospects

- Wetting property improved by using silica-supported DMAA adsorbent as the polar support for PPTPT impregnation.
- It is expected that PPTPT-DMAA adsorbs U(VI) in NaCl solutions.
- We will investigate adsorption mechanism of DMAA and PPTPT-DMAA.

Thank you
for your kind attention

4.2.9 K. Mori（Kyoto Univ.）

Introduction of Versatile Compact Neutron Diffractometer (VCND) at B-3 Beam Port of KUR

Topical meeting on Condensed-matter Chemistry on Actinides, Feb. 10, 2021.

Introduction of Versatile Compact Neutron Diffractometer (VCND) at B-3 Beam Port of KUR

Kazuhiro Mori, Ryo Okumura, Masaya Kanayama, and Hirofumi Yoshino
Institute for Integrated Radiation and Nuclear Science, Kyoto University

Abstract

- Versatile compact neutron diffractometer (VCND) with a detector bank including 25 ^{3}He gas-filled tube detectors (0.5-in diameter) has been built at the B–3 beam port of KUR [1].
- The resolution of the VCND, $\Delta d/d$, is ≈1%. The beam flux, ϕ, is 1.3 × 10^5 n/s/cm^2 for operation at the power of 5 MW on KUR.
- We show the first results of the VCND for various materials: strontium fluoride (SrF_2), lanthanum-nickel intermetallic alloy ($LaNi_5$), an austenitic-ferritic stainless steel, etc.

VCND (B–3)

Detector bank

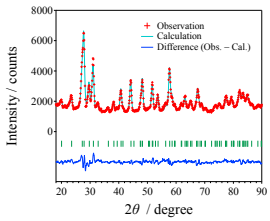

$LaNi_5$

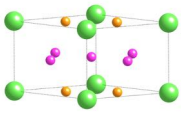

[1] K. Mori *et al.*, JPS Conference Proceedings, in press.

4.2.10 T. Kobayashi（SPring-8, JAEA）

XAFS study on the the aged deterioration of a simulated fuel debris

Topical meeting on Condensed-matter Chemistry on Actinides, 2021.

XAFS study on the aged deterioration of a simulated fuel debris

Tohru Kobayashi
Actinide chemistry group
Materials Sciences research center
Japan Atomic Energy Agency

1/21

Background and purpose of this study

For safe and reliable decommissioning the Fukushima-Daiichi Nuclear Power Plant, it is necessary to understand the following points.

- Composition, element distribution, chemical state and structure of fuel debris.
- Aged deterioration of fuel debris in actual environment (in the reactor).
- Characteristic changes with change in environmental conditions caused by removing the debris from reactor.

In this study….

- Prepare a simulated fuel debris.
- Reproduce the environment in and out of the reactor
- Investigate changes in chemical state and structure by XAFS method.

2/21

Contents

- Example of XAFS analysis
- XAFS study on simulated debris ①
  By using UO_2 @ KEK-PF BL27B
- XAFS study on simulated debris ②
  By using $UZrO_2$ @ SPring-8 BL22XU

3/21

XAFS measurement @ BL22XU

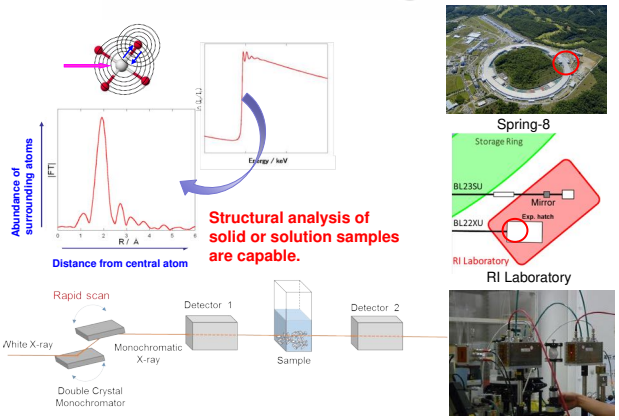

4/21

In-situ observation of uranium Photoreduction

XAFS spectra of UO_2 solution were measured while UV irradiating

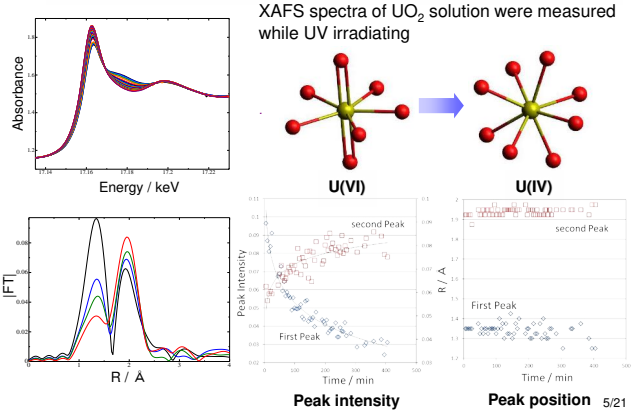

5/21

In-situ observation of selective Ln precipitation

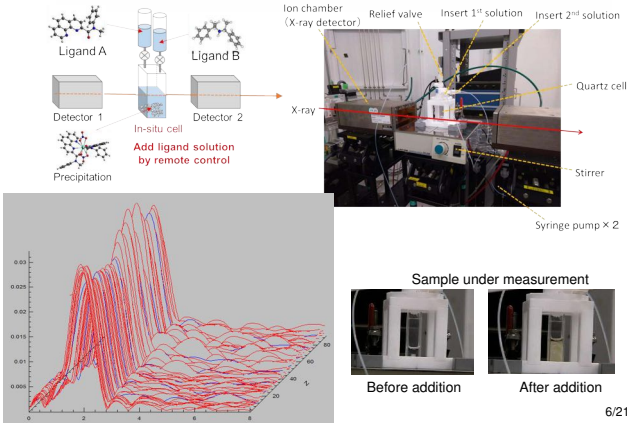

6/21

XAFS investigation of debris using UO_2 (@ KEK-PF BL27B, U-L_{III} edge, Fluorescence mode)

【Simulated conditions】

- The Fuel debris in the reactor is immerged in water.
  ⇒ UO_2 pellet immersed in water
- Inside of reactor is under reductive and high radiation condition.
  ⇒ chemical treatment with reductant ($NaBH_4$)
- Debris will be exposed to oxidative atmosphere in removal process.
  ⇒ pick up the pellet from water and expose to air

【Sample preparation】

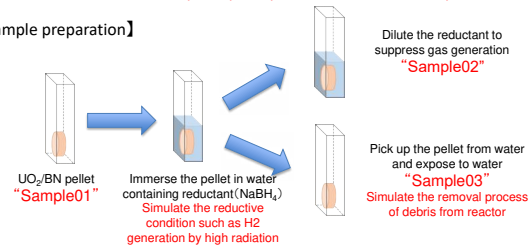

Appearance of sample

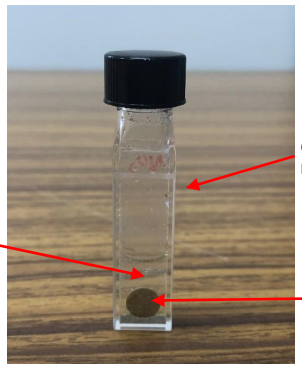

XRD of sample before reduction

同定された結晶相

結晶相名	式	信頼度(FOM)	結晶相登録詳細情報	空間群	DBカード番号
Uraninite	O2 U	0.491	サーチマッチ(COD)	225 : Fm-3m	9009049
alpha	U O2 (O H)2	0.850	サーチマッチ(RCSI)	64 : Cmca	114159
Schoepite	H18 O21 U4	1.132	サーチマッチ(COD)	29 : P21ca	9004444

結晶相データビュー

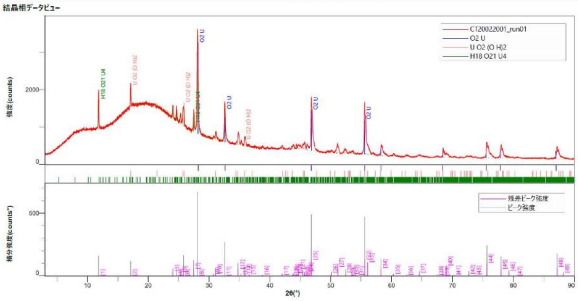

In addition to UO_2, hexavalent U suchas $UO_2(OH)_2$ are also included.

U L_{III}-edge XANES spectra

XANES analysis

Comparison of peak position

Summary

13/21

XAFS investigation of debris using $UZrO_2$ (@ SRring-8 BL22XU, U-L_{III} edge, Fluorescence and transmission mode)

【Simulated conditions】

- The fuel debris in the reactor is immersed in water
  ⇒ Sintered $U_{0.7}Zr_{0.3}O_2$ immersed in water.
- Inside of reactor is under reductive and high radiation condition.
  ⇒ γ-ray irradiation
- Debris will be exposed to oxidative atmosphere in removal process.
  ⇒ pick up the pellet from water and expose to air

【Sample preparation】

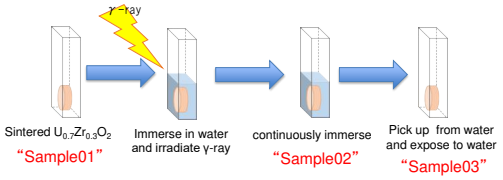

14/21

XANES spectra of water immersion samples (Fluorescence mode)

15/21

EXAFS analysis of water immersion samples (Fluorescence mode)

16/21

XANES spectra of water immersion samples (Transmission mode)

EXAFS analysis of water immersion samples (Transmission mode)

17/21

XANES spectra of air exposure samples (Fluorescence mode)

EXAFS analysis of air exposure samples (Fluorescence mode)

Summary

Chapter 5 Concluding Remarks

5.1 S. Kambe（ASRC, JAEA）

Concluding Remarks 1

Concluding Remarks

JAEA/ASRC

S. Kambe

Current situation

1) The community of basic actinide science (Physics, Chemistry, Medical science, Materials science etc) is small.
2) In contrast, this field becomes more important as many new subjects appear, presented in this workshop.
3) Considering the current situation, it is quite important to promote the collaborations between actinide researchers of different fields over the world.

Future perspectives

1) We need young researcher who can act as an intermediary between basic research and nuclear engineering, which are rather separated at present.
2) If possible, it is useful to organize a new international collaboration system for wide actinide research by the young researchers mentioned in 1). For example, I think that the former Actinet is still of narrow scope.
3) It is quite useful to organize international workshops such as the present one for the above purposes. The next JDA may be a good occasion.

5.2 H. Yamagami（Kyoto Sangyo Univ.）

Concluding Remarks 2

10 February, 2021 ZOOM meeting

Topical meeting of Condensed-matter Chemistry on Actinides : The Kumatori Meeting 2021

Concluding Remarks2 : Theoretical side

- Department pf Physics, Faculty of Science, Kyoto-Sangyo University, JAPAN
- Electronic-Structure Research Group, JAEA, Harima, JAPAN

Hiroshi Yamagami

Concluding Remark2: Theoretical Side

A. Sato, Theoretical study on isotope fractionation in uraninite
Y. Kitawaki, Orbital magnetization in many-electron systems described by spin—orbital-polarized coupled Dirac equation.
A. Sunaga, Theoretical study of the linearity of uranyl molecule based on relativistic correction method.
A. S. P. Gomes, Electronic structure of actinide systems from relativistic correlated and quantum embedding approaches.

key point and common sense in this meeting:

- 5f electrons in Actinides:

  Solid-State physics : Superconductivity and Magnetism
  Crystal growth, Multipole, Cross-correlation
  Spring-8, JAEA : ARPES Electronic structure, XMCD Magnetisim
  Multiple photon excitation
  Coordination chemistry : LUMO, HOMO, Excited state
  Dissolution : valence, valence bonding
  isotope fractionation : ρ(0) of s-state, phonon frequency

- Basic character of 5f electrons:
  - Actinide contraction
  - Relativistic effect
  - occupation number and valence (common in physics and chemistry) electron configuration

Finally

Thank you for your attention!

See you again next year!

Chapter 6 Summary of Discussion

Active discussions were held on the fundamentals and applications of actinide property chemistry. The interests and issues raised by the speakers can be found in their respective presentation materials. The community of basic actinide science (physics, chemistry, medical science, materials science, etc.) is small. In contrast, this field becomes more important as many new subjects appear, presented in this workshop. Considering the current situation, it is quite important to promote the collaborations between actinide researchers of different fields over the world.

The importance of the emerging young researcher who can act as an intermediary between basic research and nuclear engineering was strongly pointed out. For the purpose, the organization of a new international collaboration system for wide actinide research by the young researchers was mentioned of.

Concluding remark was also given from the theoretical side. Key points in this meeting are (1) 5f electrons in actinides and (2) basic character of 5f electrons. The latter include actinide contraction, relativistic effect, and occupation number and valence (common in physics and chemistry) electron configuration.

Chapter 7 List of Participants

The following people participated in the meeting. Thank you very much.

Participants	affiliations
Fusako Kon	Graduate School of Science, Hokkaido University
Hiroshi Amitsuka	Graduate School of Science, Hokkaido University
Tatsuya Yanagisawa	Graduate School of Science, Hokkaido University
Kenji Shirasaki	IMR, Tohoku University
Yoshiya Homma	IMR, Tohoku University
Hiroki Shishido	Tohoku University
Kohshin Washiyama	Advanced Clinical Research Center, Fukushima Global Medical Science Center, Fukushima Medical University
Takahiro Nomoto	Institute of Innovative Research, Tokyo Institute of Technology
Masahiko Nakase	Tokyo Institute of Technology
Tatsuya Suzuki	Nagaoka University of Technology
Tomoya Yamane	Nagaoka University of Technology
Minoru Suzuki	Institute for Integrated Radiation and Nuclear Science, Kyoto University
Tomoo Yamamura	Institute for Integrated Radiation and Nuclear Science, Kyoto University
Tomoo Yamamura	Institute for Integrated Radiation and Nuclear Science, Kyoto University
Masahiro Hino	Institute for Integrated Radiation and Nuclear Science, Kyoto University
Tatsuro Oda	Institute for Integrated Radiation and Nuclear Science, Kyoto University
Ayaki Sunaga	Institute for Integrated Radiation and Nuclear Science, Kyoto University
Chihiro Tabata	Institute for Integrated Radiation and Nuclear Science, Kyoto University
Kazuhiro Mori	Institute for Integrated Radiation and Nuclear Science, Kyoto University
Hiroki Tanaka	Institute for Integrated Radiation and Nuclear Science, Kyoto University
Kenji Ishida	Kyoto University
Akio Kawaguchi	Institute for Integrated Radiation and Nuclear Science, Kyoto University
Takashi Yoshimura	Radioisotope Research Center, Institute for Radiation Sciences, Osaka University
Kojiro Nagata	Radioisotope research center, Osaka University
Atsushi Toyoshima	Osaka University
Naoto Ishikawa	Osaka University
Yoshitaka Kasamatsu	Graduate School of Science, Osaka University
Minori Abe	Tokyo Metropolitan University
Yasushi Katayama	Keio University
Marjanul Manjum	Keio University
Takafumi Kitazawa	Department of Chemistry, Faculty of Science, Toho University

Participants	affiliations
Masayoshi Yokota	Kindai University
Masanobu Nogami	Kindai University
Hidetaka Nakai	Kindai University
Yoshinori Haga	Advanced Science Research Center, Japan Atomic Energy Agency
Shinsaku Kambe	Advanced Science Research Center, Japan Atomic Energy Agency
Koji Maeda	Japan Atomic Energy Agency
Tohru Kobayashi	Actinide chemistry group, Materials Sciences research center, Japan Atomic Energy Agency
Kenji Yoshii	Japan Atomic Energy Agency
Tatsuo Fukuda	Materials Sciences Research Center, Japan Atomic Energy Agency
Tsuyoshi Yaita	Japan Atomic Energy Agency
Masatoshi Iizuka	Central Research Institute of Electric Power Industry
Yuma Sekiguchi	Central Research Institute of Electric Power Industry
Mitsuyoshi Yoshimoto	National Cancer Center
Takahiro Tadokoro	Hitachi, Ltd. Research & Development Group
Mamoru Kamoshida	Hitachi-GE Nuclear Energy, Ltd.
Daisuke Watanabe	Hitachi-GE Nuclear Energy, Ltd.
Takashi Shimada	Mitsubishi Heavy Industries, Ltd.
Koichi Kakinoki	Mitsubishi Heavy Industries, Ltd.
Valérie Vallet	CNRS
Roberto Caciuffo	EU JRC
António Pereira Gonçalves	Instituto Superior Técnico, Universidade Lisboa
Andre Severo Pereira Gomes	Universite de Lille
Yohei Kitawaki	Kyoto Sangyo University
Hiroshi Yamagami	Kyoto Sangyo University
Hiroshi Takeuchi	Metal Technology Co. Ltd.
Eri Ichikawa	Tokyo Metropolitan University
Sumika Iwamuro	Tokyo Metropolitan University
Ataru Sato	Graduate School of Science, Tokyo Metropolitan University
Masahiko Hada	Tokyo Metropolitan University
Akira Yoshida	Tokyo Metropolitan University

Chapter 8 Photos of the workshop

Photos of the lectures are shown in the order of the program.

Fig. 8.1: Tomoo Yamamura, Kyoto University

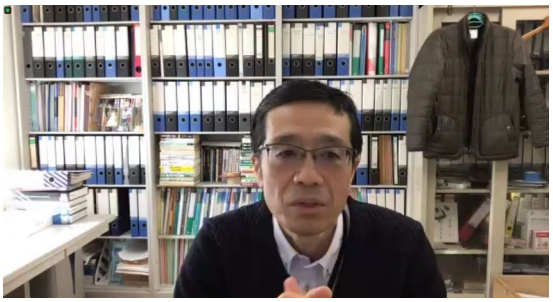

Fig. 8.2: Hiroshi Yamagami, Kyoto Sangyo University

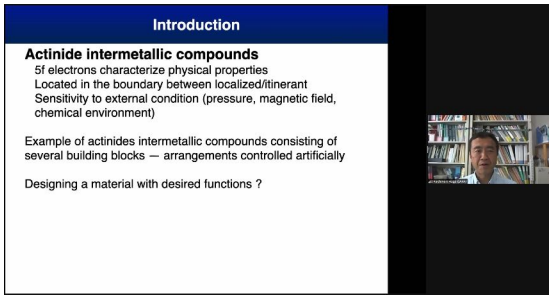

Fig. 8.3: Yoshinori Haga, JAEA

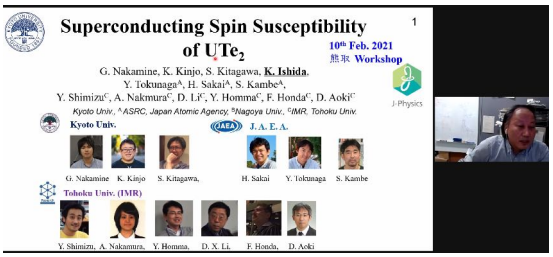

Fig. 8.4: Kenji Ishida, Kyoto University

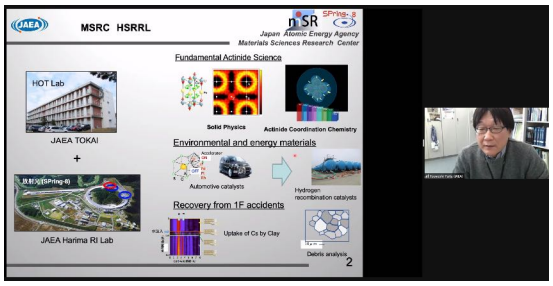

Fig. 8.5: Tsuyoshi Yaita, JAEA

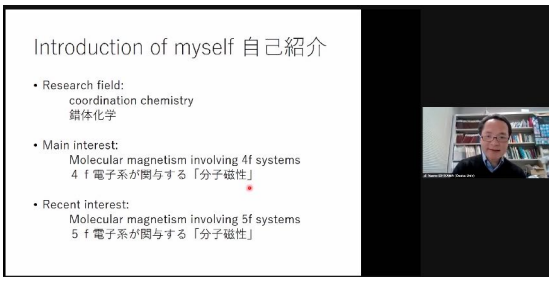

Fig. 8.6: Naoto Ishikawa, Osaka University

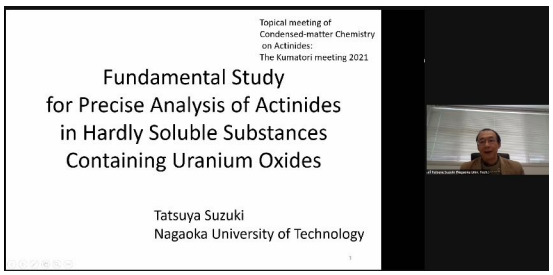

Fig. 8.7: Tatsuya Suzuki, Nagaoka University of Technology

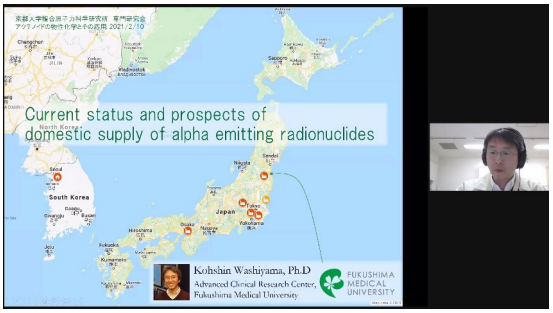

Fig. 8.8: Koshin Washiyama, Fukushima Medical University

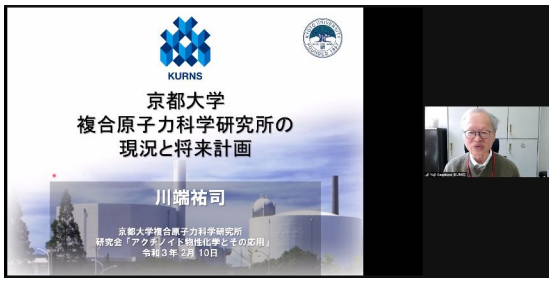

Fig. 8.9: Yuji Kawabata, Kyoto Univertisy

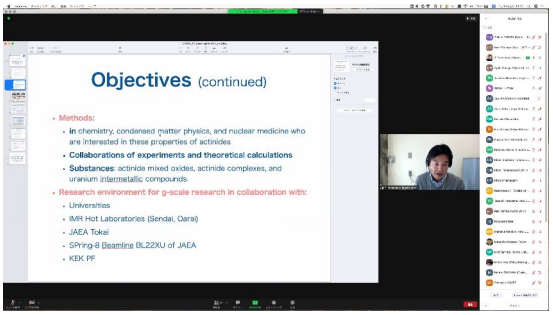

Fig. 8.10: Tomoo Yamamura, Kyoto University

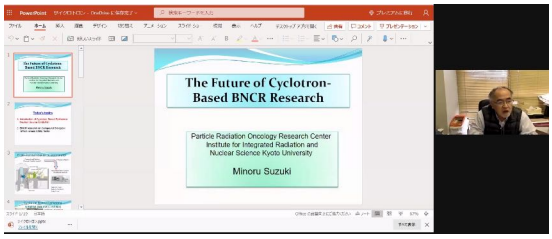

Fig. 8.11: Minoru Suzuki, Kyoto University

Fig. 8.12: Takashi Kitazawa, Toho University

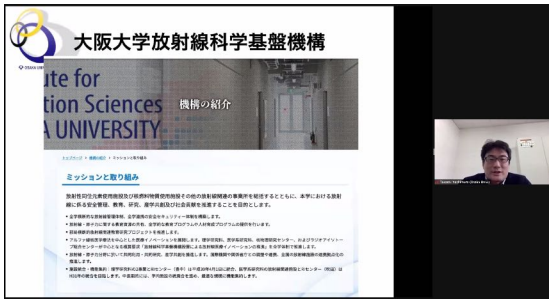

Fig. 8.13: Takashi Yoshimura, Osaka University

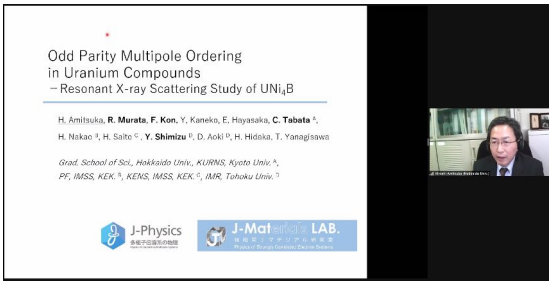

Fig. 8.14: Hiroshi Amitsuka, Hokkaido University

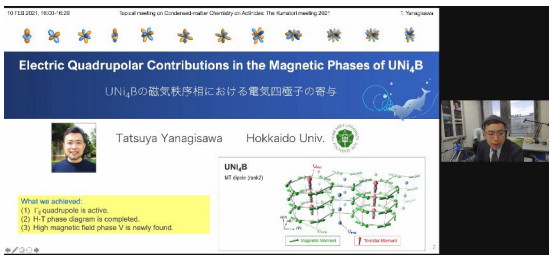

Fig. 8.15: Tatsuya Yanagisawa, Hokkaido University

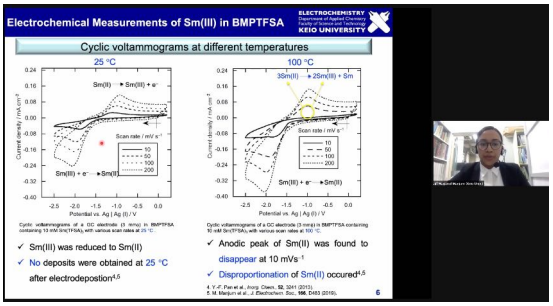

Fig. 8.16: Marjanul Manjum, Keio University

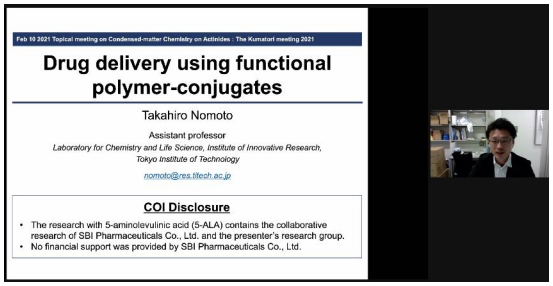

Fig. 8.17: Takahiro Nomoto, Tokyo Institute of Technology

Fig. 8.18: Antonio Pereira Goncalves, Universidade Lisboa

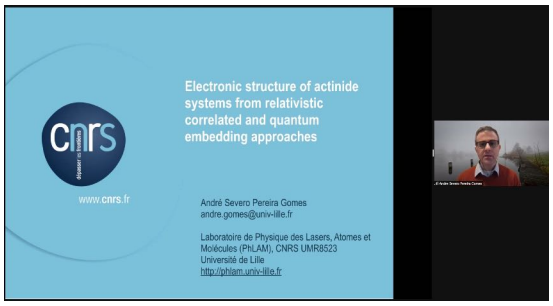

Fig. 8.19: Andre Severo Pereira Gomes, Universite de Lille

Fig. 8.20: Roberto Caciuffo, EU JRC

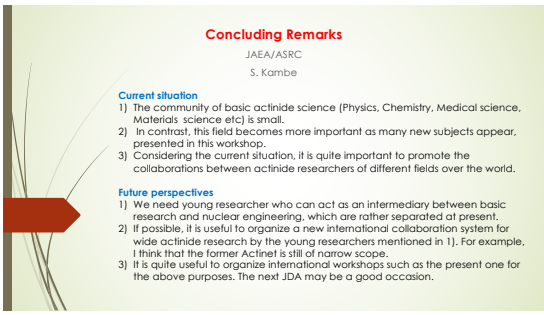

Fig. 8.21: Shinsaku Kambe, JAEA

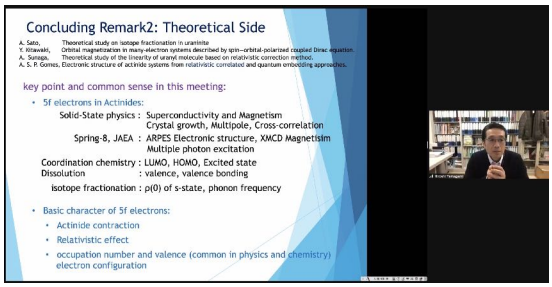

Fig. 8.22: Hiroshi Yamagami, Kyoto Sangyo University

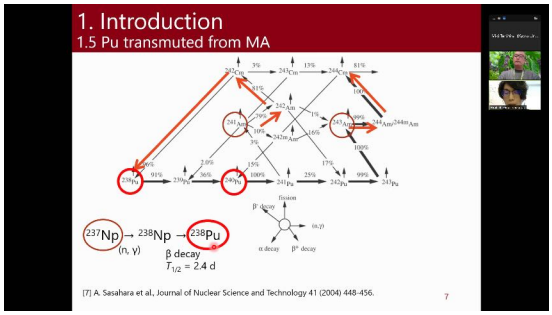

Fig. 8.23: Hiroki Shishido, Tohoku University

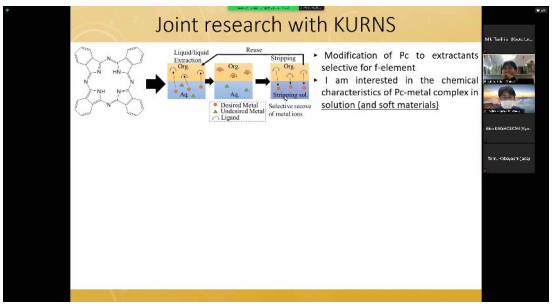

Fig. 8.24: Masahiko Nakase, Tokyo Institute of Technology

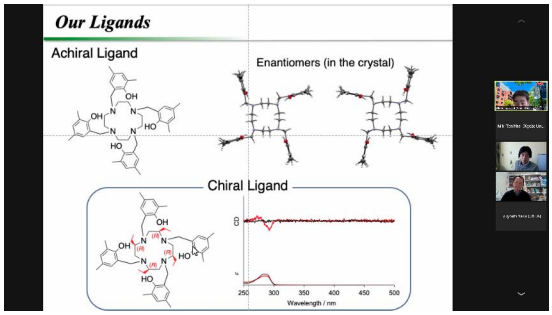

Fig. 8.25: Hidetaka Nakai, Kindai University

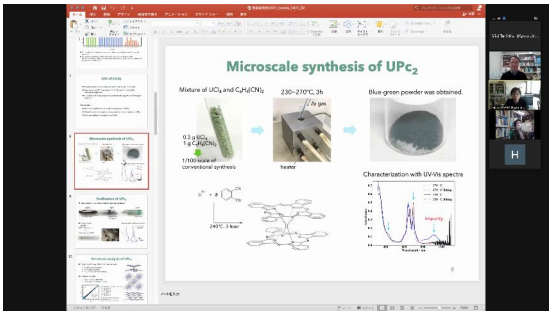

Fig. 8.26: Chihiro Tabata, Kyoto University

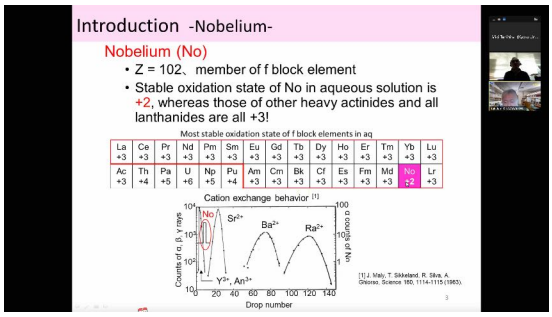

Fig. 8.27: Yoshitaka Kasamatsu, Osaka University

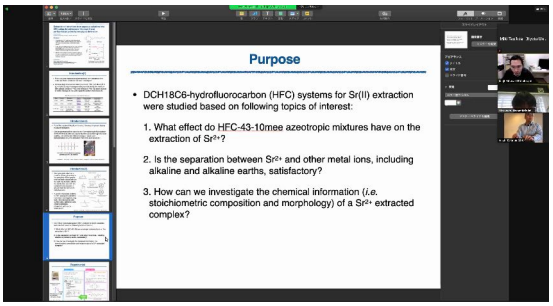

Fig. 8.28: Kenji Shirasaki, Tohoku University

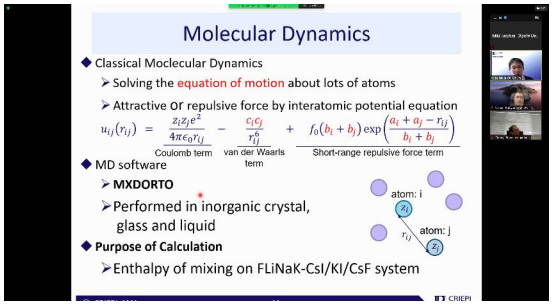

Fig. 8.29: Yuma Sekiguchi, Central Research Institute of Electric Power Industry

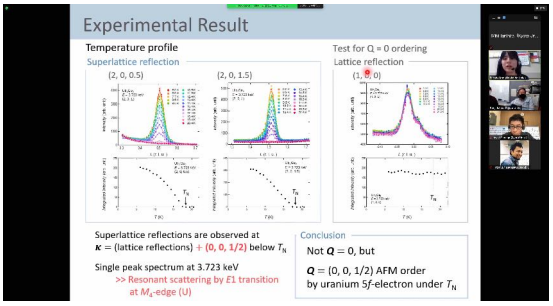

Fig. 8.30: Fusako Kon, Hokkaido University

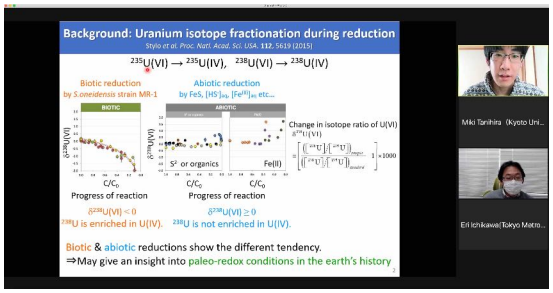

Fig. 8.31: Ataru Sato, Tokyo Metropolitan University

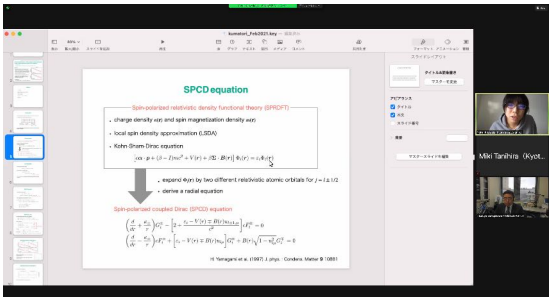

Fig. 8.32: Yohei Kitazawa, Kyoto Sangyo University

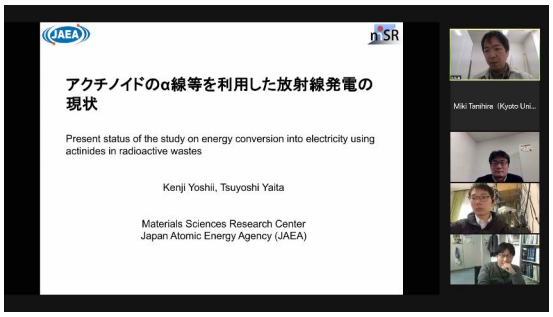

Fig. 8.33: Tatsuo Fukuda, JAEA

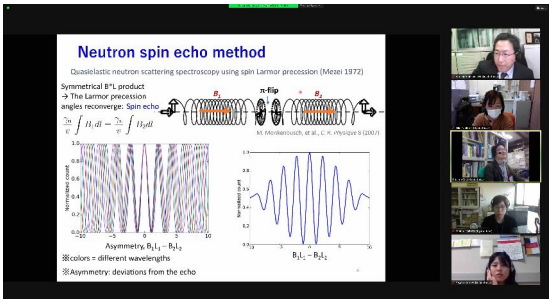

Fig. 8.34: Tatsuro Oda, Kyoto University

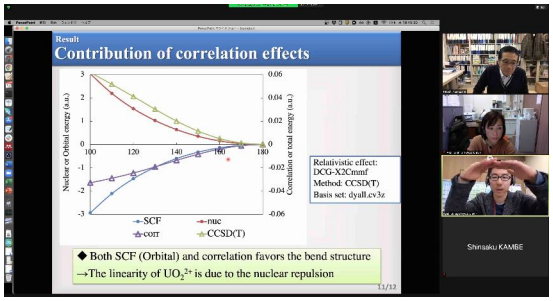

Fig. 8.35: Ayaki Sunaga, Kyoto University

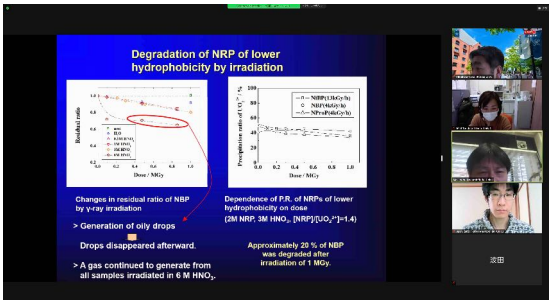

Fig. 8.36: Masanobu Nogami, Kindai University

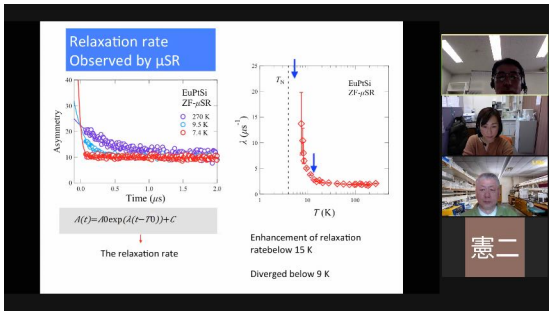

Fig. 8.37: Yoshiya Honma, Tohoku University

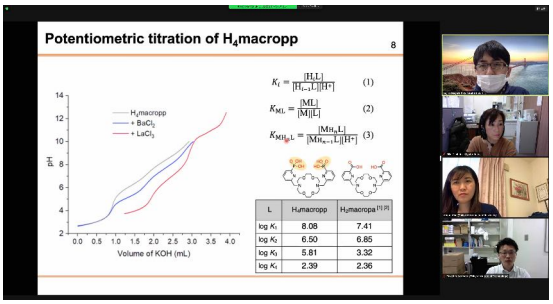

Fig. 8.38: Kojiro Nagat, Osaka University

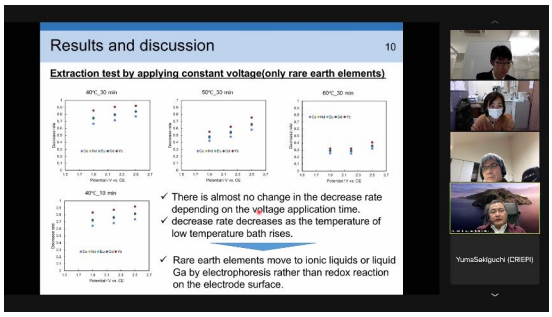

Fig. 8.39: Tomoya Yamane, Nagaoka University of Technology

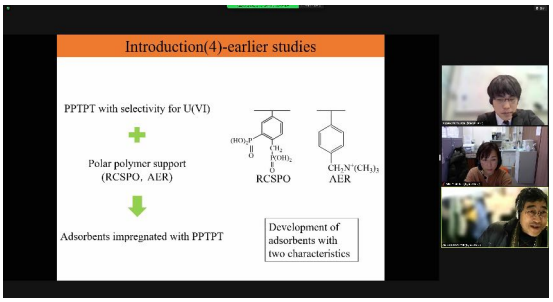

Fig. 8.40: Masayoshi Yokota, Kindai University

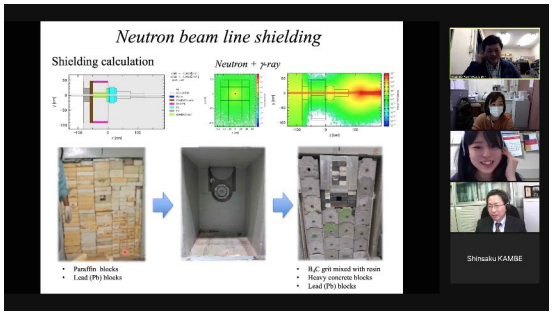

Fig. 8.41: Kazuhiro Mori, Kyoto University

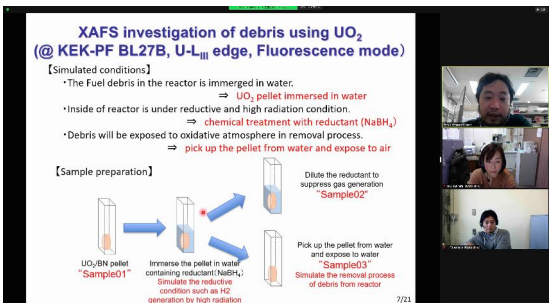

Fig. 8.42: Tohru Kobayashi, JAEA